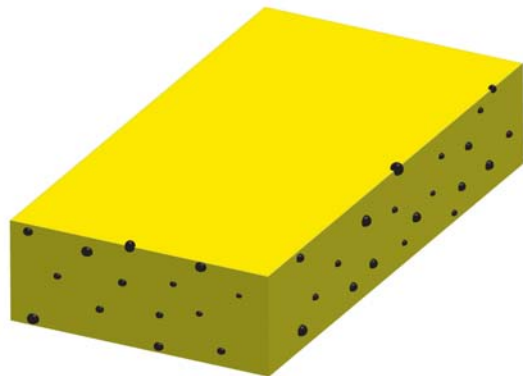


Photodeposition of platinum nanoparticles on well-defined tungsten oxide

Controlling oxidation state, particle size and geometrical distribution



Kasper
Wenderich

**PHOTODEPOSITION OF PLATINUM
NANOPARTICLES ON WELL-DEFINED
TUNGSTEN OXIDE**

*CONTROLLING OXIDATION STATE, PARTICLE SIZE
AND GEOMETRICAL DISTRIBUTION*

PROMOTIECOMMISSIE

Voorzitter

Prof. dr. ir. J. W. M. Hilgenkamp University of Twente

Promotor

Prof. dr. G. Mul University of Twente

Leden

Prof. dr. F. G. Mugele	University of Twente
Prof. dr. ir. G. Koster	University of Twente
Prof. dr. P. E. de Jongh	Utrecht University
Prof. dr. P. Fornasiero	University of Trieste
Dr. A. Trunschke	Fritz Haber Institute of the Max Planck Society

The research reported in this thesis was carried out at the Photocatalytic Synthesis (PCS) Group within the Faculty of Science and Technology and the MESA+ Institute for Nanotechnology at the University of Twente. A part of the research was performed at the Reactivity Group within the Department of Inorganic Chemistry at the Fritz Haber Institute of the Max Planck Society (Berlin, Germany). This work was funded by the Dutch National Research School Combination Catalysis Controlled by Chemical Design (NRSC-Catalysis).

Cover. Front: artistic impression of an ideal situation of structure-directed photodeposition of Pt nanoparticles on a WO₃ nanoplate. Back: adjusted photograph of the LED used in photocatalytic propane oxidation measurements.

Photodeposition of platinum nanoparticles on well-defined tungsten oxide: controlling oxidation state, particle size and geometrical distribution

PhD thesis, University of Twente, Enschede, The Netherlands

Printed by Gildeprint, Enschede, The Netherlands

Copyright © 2016, Kasper Wenderich

DOI: 10.3990/1.9789036540582

ISBN: 978-90-365-4058-2

**PHOTODEPOSITION OF PLATINUM
NANOPARTICLES ON WELL-DEFINED
TUNGSTEN OXIDE**
*CONTROLLING OXIDATION STATE, PARTICLE SIZE
AND GEOMETRICAL DISTRIBUTION*

PROEFSCHRIFT

ter verkrijging van
de graad van doctor aan de Universiteit Twente,
op gezag van de rector magnificus,
Prof. dr. H. Brinksma,
volgens besluit van het College voor Promoties
in het openbaar te verdedigen
op vrijdag 18 maart 2016 om 14.45 uur

door

Kasper Wenderich
geboren op 11 november 1987
te Hengelo, Nederland

Dit proefschrift is goedgekeurd door de promotor:

Prof. dr. G. Mul

“Learn from yesterday, live for today, hope for tomorrow. The important thing is not to stop questioning.”

– Albert Einstein

Table of contents

Chapter 1 - General introduction	1
1.1 The promise of photocatalysis	2
1.2 Heterogeneous photocatalysis	3
1.2.1 <i>Fundamentals of heterogeneous photocatalysis</i>	3
1.2.2 <i>Photocatalytic materials</i>	5
1.3 Tungsten trioxide (WO ₃) as a photocatalyst	6
1.4 Cocatalytic nanoparticles	7
1.4.1 <i>Fundamentals of cocatalytic nanoparticles</i>	7
1.4.2 <i>Pt-loaded WO₃</i>	9
1.5 Crystal facet engineering	10
1.5.1 <i>Basics of crystal facet engineering</i>	10
1.5.2 <i>Crystal facet engineering of WO₃</i>	11
1.6 Aims and thesis outline	13
1.7 Bibliography	15
Chapter 2 - Principles, mechanism, and applications of photodeposition in (photo)catalysis	21
2.1 Introduction to photodeposition	22
2.2 Photodeposition of particles on TiO ₂	25
2.3 Photodeposition of Ag on ZnO	31
2.4 Photodeposition of particles on WO ₃	36
2.4.1 <i>Photodeposition of Pt on WO₃</i>	37
2.4.2 <i>Photodeposition of other metals on WO₃</i>	42
2.4.3 <i>Photodeposition of Ag/AgX (X = Cl or Br) particles on WO₃</i>	44
2.4.4 <i>Photodeposition on composite photocatalysts containing WO₃</i>	45
2.5 Structure-directed photodeposition	45
2.6 Points for improvement in photodeposition studies	53
2.6.1 <i>Loading vs. doping</i>	53
2.6.2 <i>Verification of the valence state of as-deposited particles</i>	54
2.6.3 <i>Verification of wt loading</i>	54
2.6.4 <i>Measuring of the photon flux</i>	54
2.6.5 <i>Conclusions about bandgap change</i>	54
2.6.6 <i>Conclusions on favored reductive and oxidative sites</i>	55

2.6.7 High temperature treatment	55
2.7 Summary and future perspectives of photodeposition	55
2.8 Bibliography	56
Chapter 3 - Towards temperature-dependent crystal facet engineering of hydrate-free WO₃ with plate-like morphology	73
3.1 Introduction	74
3.2 Materials and methods	75
3.3 Results and discussion	77
3.3.1 Characterization of as-synthesized WO ₃ samples	77
3.3.2 Photocatalytic performance of synthesized WO ₃ samples	81
3.4 Conclusions	85
3.5 Bibliography	85
3.6 Appendix	90
Chapter 4 - Phase transformations in citric acid-assisted hydrothermal growth of WO₃ and implications for photocatalytic performance	93
4.1 Introduction	94
4.2 Materials and methods	94
4.3 Results and discussion	97
4.3.1 <i>In situ</i> Raman spectroscopy of crystal phases during hydrothermal synthesis of WO ₃	97
4.3.2 Microwave-assisted hydrothermal synthesis experiments	100
4.3.3 Photocatalytic activity tests	103
4.4 Conclusions	105
4.5 Bibliography	106
4.6 Appendix	110
Chapter 5 - Photodeposition mechanism of platinum on tungsten oxide and its corresponding stability upon aqueous phase illumination	115
5.1 Introduction	116
5.2 Materials and methods	118
5.2.1 Photodeposition	118
5.2.2 Characterization	119
5.3 Results and discussion	120
5.3.1 Kinetics of photodeposition	120
5.3.2 Oxidation state of Pt after photodeposition	121
5.3.3 Additional illumination experiments	123
5.3.4 Additional photodeposition experiments	126
5.3.5 HR-TEM studies	128
5.3.6 Discussion on photodeposition mechanism	130
5.4 Conclusions	134
5.5 Bibliography	134

5.6 Appendix	139
Chapter 6 - Sorption-determined deposition of platinum on well-defined plate-like WO₃	143
6.1 Introduction	144
6.2 Materials and methods	145
6.3 Results and discussion	147
6.4 Conclusions	155
6.5 Bibliography	155
6.6 Appendix	159
6.7 Appendix – particle counting	163
<i>Photodeposition sample 1</i>	166
<i>Photodeposition sample 2</i>	170
<i>Impregnation sample</i>	174
Chapter 7 - Photocatalytic propane oxidation over platinum-loaded tungsten oxide nanoplates	179
7.1 Introduction	180
7.2 Materials and methods	181
7.3 Results and discussion	183
7.3.1 <i>Characterization of as-synthesized Pt/WO₃</i>	183
7.3.2 <i>Photocatalytic propane oxidation measurements</i>	186
7.3.3 <i>Discussion</i>	189
7.4 Conclusions	194
7.5 Bibliography	195
7.6 Appendix	198
Chapter 8 - Outlook	199
8.1 Crystal facet engineering	200
8.1.1 <i>Crystal facet engineering of WO₃ nanoplates</i>	200
8.1.2 <i>Crystal facet engineering on a broader perspective</i>	201
8.2 Photodeposition	201
8.2.1 <i>Photodeposition of platinum on WO₃</i>	201
8.2.2 <i>Future usage of photodeposition</i>	201
8.3 Structure-directed photodeposition	202
8.4 Bibliography	204
Summary	207
Samenvatting	213
Acknowledgements	219
List of publications	225
Curriculum Vitae	227

Chapter 1

General introduction

1.1 The promise of photocatalysis

Over the recent centuries, science has formed the foundation of bringing mankind a high level of economic prosperity and increased human lifetimes. As a result, the world population and corresponding human demands are increasing rapidly, and are expected to increase only further. Therefore, science is faced with multiple challenges to provide a continuation of the high level of human wealth. For example, world-wide energy demands are increasing, while at the same time we are starting to run out of fossil fuels. Ideally, a clean energy source should be employed for replacing fossil fuels. Options which arise are the utilization of for instance wind and hydraulic energy. However, while the amount of energy provided could sustain a fraction of the required energy production, wind or hydraulic energy alone would not be able to cover the full energy demand.^[1, 2] Solar energy, on the other hand, has the potential of becoming the dominant energy source used in society. Theoretically, all energy demands could be met merely by the utilization of solar energy.^[1, 2] Two routes can be employed for solar energy harvesting: first, photo-voltaics could be used to directly provide electricity for human society.^[3] However, a major disadvantage is that in this case, the energy (in the form of electricity) has to be used immediately or indirectly stored in *e.g.* batteries or capacitors; otherwise it will be forfeit. Therefore, direct storage of solar energy should be a promising solution to counter the drawbacks related to photo-voltaics. In such a case, photocatalysis provides an outcome, where the solar energy is stored through the synthesis of a fuel. Here, the solar energy can be stored in hydrogen by the splitting of water,^[1, 4, 5] or in the form of hydrocarbons by the reduction of CO₂.^[6, 7]

The relevance of photocatalysis for as-described societal challenges exceeds merely the storage of solar energy. Photocatalysis also provides an extremely important basis for the degradation of harmful compounds in the gas phase.^[8, 9] Due to the nature of our wealth, many people spent time in indoor areas. However, volatile organic compounds (VOCs) could be present in such spaces, causing symptoms related to the sick building syndrome (such as headaches). Photocatalytic oxidation can be used to degrade these VOCs. In underdeveloped countries, photocatalysis might provide a solution in providing people clean drinking water. In such a case, a photocatalytic material is used to degrade harmful compounds in wastewater, such as dyes, bacteria or metal ions.^[10, 11] Lastly, a huge advantage of photocatalysis is that high selectivities can be obtained through a green process.^[7, 12]

Despite the promise that photocatalysis holds, it is a relatively new field of research, only gaining attention over the past couple of decades. The activities of the photocatalysts reported are often relatively low, and there is still room for a lot of improvement. Understanding and exploiting the very fundamentals of (heterogeneous) photocatalysis will contribute in obtaining higher photocatalytic activities and/or selectivities in all applications described.

1.2 Heterogeneous photocatalysis

1.2.1 Fundamentals of heterogeneous photocatalysis

In heterogeneous photocatalysis, a semiconductor crystal is used as a catalyst which is activated by the input of energy in the form of light.^[4, 13] When photons with an energy equal or larger than the bandgap ($E_p \geq E_g$) are incident on the semiconductor, the photons may be absorbed by the material. The photon energy is then used to excite electrons from the valence band to the conduction band (Figure 1.1). The electron vacancies left in the valence band are called holes. Ideally, in photocatalysis, the electrons and holes are separated and migrate to the surface. There, the excited electrons are used to reduce chemical compounds adsorbed on the surface of the photocatalyst, provided that the edge of the conduction band is more negative than the corresponding reduction potential. The holes are used to oxidize other adsorbed compounds, which is possible if the edge of the valence band is more positive than the corresponding oxidation potential. Generally, in water splitting the electrons are used for the reduction of protons to hydrogen, whereas the holes are used for the oxidation of water.^[1, 4] In the degradation of pollutants, the electrons are used to reduce O_2 (forming *e.g.* $O_2^{\cdot-}$ radicals) and the holes are used either for direct oxidation or for the production of hydroxyl radicals (OH^{\cdot}) from water (vapor).^[8, 14, 15] The formed radicals can then be used for the degradation of the pollutants. Another possible pathway of electrons and holes is the recombination of these charge carriers. In such a case, the energy provided by the incident photon will be lost (in the form of heat). Carrier recombination should be suppressed to obtain increased photocatalytic activities. A method to do so is loading a photocatalyst with a cocatalyst, which will be touched upon later in this chapter.

The optimal energetic location of the conduction and valence band and the corresponding bandgap is dependent on the application of the photocatalyst. According to equation 1.1, the wavelength λ of a photon is inversely related to its energy E_p :

$$E_p = h\nu = \frac{hc}{\lambda} \quad (1.1)$$

where h is Planck's constant, ν is the photon frequency and c is the photon speed.^[16] Theoretically, in the most beneficial case, the photocatalyst has a bandgap as small as possible, so that harvesting of photons with high wavelengths can take place. However, the edges of the valence and conduction band should not be at an unfavorable position for one of the redox reactions. For instance, in solar water splitting, the bandgap should be as small as possible, whereas the conduction band edge should be more negative than the proton reduction potential (0 V vs. NHE at pH = 0) and the valence band edge should be more positive than the water oxidation potential (1.23 V vs. NHE at pH = 0).^[1,4] This means that theoretically a bandgap of 1.23 V should be sufficient for the splitting of water. Practically however, there will be energy losses (for instance due to electron/hole transfer) before the charge carriers can be used in the photocatalytic reaction. Therefore, the practical minimum size of the bandgap is estimated to be in the range of 2.0 to 2.2 eV.^[1]

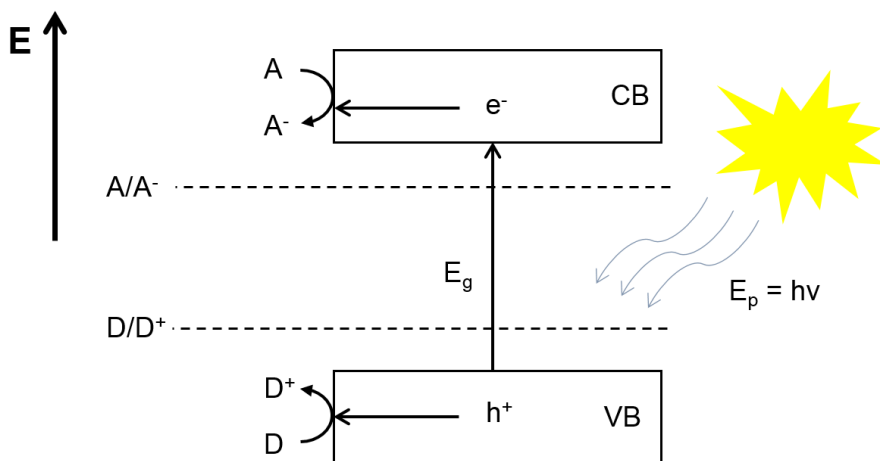


Figure 1.1. Basic concept of heterogeneous photocatalysis. Excited electrons (e^-) are used for the reduction of an electron acceptor A , whereas holes (h^+) are used to oxidize an electron donor D .

1.2.2 Photocatalytic materials

Many semiconductors are candidates to be used in photocatalysis. Some examples of photocatalytic materials which can be used for *e.g.* the splitting of water are displayed in Figure 1.2. An ideal photocatalyst needs to meet the following requirements:^[1, 17, 18]

- A suited location of the edges of the conduction and valence band compared to the reduction and oxidation potentials related to the photocatalytic reaction
- A small bandgap
- Efficient electron/hole separation and migration, resulting in a low charge carrier recombination rate
- The ability to provide sufficient active sites
- Availability/low production costs
- Non-toxicity
- Stability

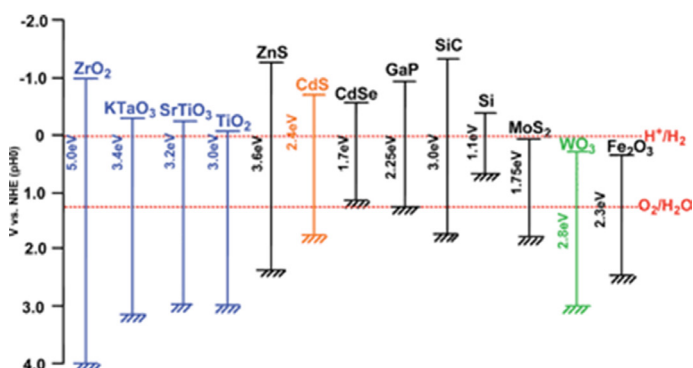


Figure 1.2. Examples of different photocatalysts, depicting their conduction and valence band position as a function of V vs. NHE at $\text{pH} = 0$. The redox potentials corresponding to water splitting are shown as well. Reproduced from Ref. [5] with permission from The Royal Society of Chemistry.

In Figure 1.2, cadmium sulfide (CdS) seems to be the most suitable material for solar water splitting. However, the material is not photo-stable, as the generated holes will oxidize the material:^[5]



From the other materials shown, titanium dioxide (TiO_2) is by far the most studied photocatalyst.^[7, 8, 11] This makes sense, as TiO_2 meets most of the mentioned requirements. However, the bandgap is relatively large, making photocatalysis only possible up to a wavelength of approximately 413 nm. Only a small fraction of the solar spectrum can thus be harvested using this material. For solar applications TiO_2 is therefore not a good photocatalyst. Two possibilities arise to solve this problem: doping the TiO_2 to introduce new energy levels, or simply looking for an alternative for TiO_2 . Doping, especially cationic doping, can have negative consequences for the photocatalytic activity of a sample due to the introduction of new charge carrier recombination sites.^[1, 19] Therefore research should be conducted on other photocatalysts with a smaller bandgap than TiO_2 , which may have promise in future applications. Tungsten trioxide (WO_3) is such a material.

1.3 Tungsten trioxide (WO_3) as a photocatalyst

Tungsten trioxide (WO_3) is considered to be a promising photocatalyst, despite the edge of the conduction band not being at a favorable position for proton and single-electron oxygen reduction.^[17, 18, 20-22] WO_3 has this reputation due to amongst others its chemical stability in acidic media and non-toxicity. Very importantly, the bandgap of WO_3 is relatively small compared to TiO_2 (2.5 to 2.8 eV), making absorption of visible light up to a wavelength of almost 500 nm possible. This would mean that WO_3 should be able to harvest approximately 12% of the solar spectrum. Another advantage is that WO_3 exhibits a good electron transport. Within the field of photocatalysis, tungsten oxide has been used for the degradation of organic compounds,^[23-25] NO degradation,^[26] the reduction of CO_2 ^[27] and the oxidation of water, either in a photoelectrochemical^[28, 29] or in a photocatalytic application.^[27, 30-32] In the latter case, WO_3 can be used for full water splitting if it is incorporated in a Z-scheme.^[33, 34]

Tungsten oxide can exist in different crystal phases, namely in monoclinic II (ϵ - WO_3), triclinic (δ - WO_3), monoclinic I (γ - WO_3), orthorhombic (β - WO_3), tetragonal (α - WO_3) and hexagonal (h- WO_3) phases.^[17] Of these crystal phases, only the monoclinic I, hexagonal and triclinic phases are known to be stable at room temperature. The other crystal phases can only exist at low temperatures (monoclinic II WO_3) or elevated temperatures (orthorhombic and tetragonal WO_3). However, the orthorhombic phase can be stable at room temperature when nanostructured WO_3 is used. Although there are very few studies on the influence of crystal structure on the photocatalytic activity, there are implications that monoclinic WO_3 is generally

better suited than hexagonal WO_3 in photocatalytic applications.^[22, 24, 35] A remarkable property of WO_3 is that it can also exist in a nonstoichiometric form, *i.e.* that oxygen vacancies are present inside the crystal lattice.^[17, 18, 20] In such a case, tungsten oxide is referred to as WO_x , where x can for instance range from 2.63 to 2.92. The introduction of oxygen vacancies can result in an increased conductivity of the WO_3 . Also, due to the introduction of new energy levels, absorption of light with smaller photon energies becomes possible. Lastly, tungsten oxide is also known to possibly exist in a hydrated form ($\text{WO}_3 \cdot x\text{H}_2\text{O}$). In such a case, water is intercalated in the crystal structure. The best known tungsten oxide hydrates are $\text{WO}_3 \cdot 2\text{H}_2\text{O}$, $\text{WO}_3 \cdot \text{H}_2\text{O}$ and $\text{WO}_3 \cdot 0.33\text{H}_2\text{O}$. Generally, calcination at a suitable temperature will result in the removal of the water, transforming the tungsten oxide hydrates into hydrate-free WO_3 .

Photocatalysis is not the only application where the family of tungsten oxides yields promise in.^[17, 18, 20] WO_x also finds applications in amongst others dye-sensitized solar cells, gas sensing, electrochromism, supercapacitors, lithium-ion batteries, non-volatile memory devices, optical recording devices, field-emission applications, high-temperature superconductor usage and even phototherapy.

In this thesis, monoclinic I WO_3 systems, with or without hydrates, are mainly studied in photocatalytic applications. ‘Monoclinic I’ WO_3 will be referred to as ‘monoclinic’ WO_3 from this point on.

1.4 Cocatalytic nanoparticles

1.4.1 Fundamentals of cocatalytic nanoparticles

Several studies have demonstrated that the activity of photocatalytic materials can be drastically enhanced when they are loaded with cocatalytic nanoparticles.^[3, 4, 14, 36-38] This is attributed to two phenomena:

- i) The cocatalyst can act as a charge carrier beacon. Either electrons or holes preferentially migrate to the cocatalytic nanoparticle. This means that the electrons and holes are more efficiently separated and consequently the extent of recombination is reduced.
- ii) The cocatalyst can lower the activation energy (or overpotential) of the desired photocatalytic (redox) reactions.

Another major advantage of cocatalysts is that they can stabilize photocatalytic materials which are normally easily degraded. This is related to the charge carrier trapping ability of the cocatalyst. Equation 1.2 demonstrated that holes in CdS can degrade the CdS. However, when a cocatalyst is able to scavenge these holes, the oxidation of CdS will be suppressed. The efficiency of a cocatalyst in a photocatalytic reaction is determined by its physicochemical properties such as size and oxidation state. A schematic demonstrating the concept of a reduction cocatalyst is provided in Figure 1.3.

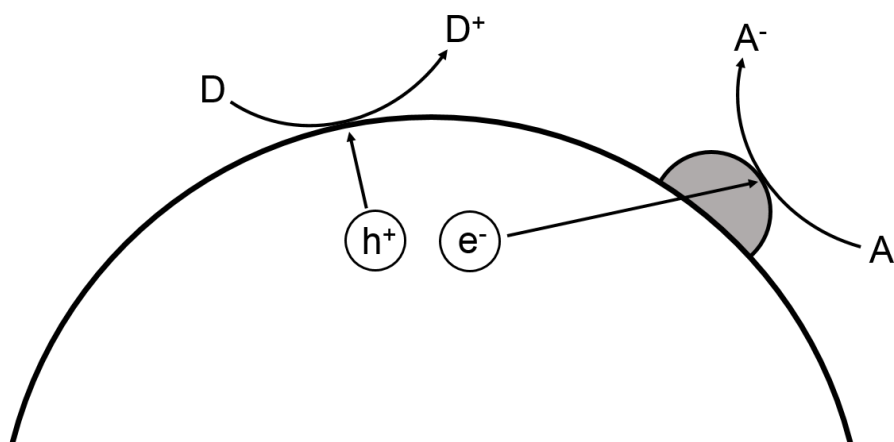


Figure 1.3. Concept of a reduction cocatalyst. Electrons migrate to the cocatalyst, where the photocatalytic reduction reaction takes place. Holes migrate to the unloaded surface, where the corresponding oxidation reaction occurs.

Initially, the photocatalytic activity will increase as a function of the amount of cocatalyst deposited. However, an optimum will be reached, and at higher loadings the photocatalytic activity will start to decrease again (Figure 1.4). This is attributed to several phenomena. Most commonly, the decrease is attributed to the following: i) too much cocatalyst will start to result in an over-coverage of the surface, effectively blocking light from reaching the photocatalyst; ii) the cocatalytic nanoparticles will start to act as charge recombination centers when the cocatalyst loading becomes too high. Apart from these two reasons, another reason for a decreased activity could relate to blocking of the active sites (one of the redox reactions does not take place over the cocatalyst). Also, when an increase in cocatalyst loading results in an increase in cocatalyst size, the specific surface area of the cocatalytic nanoparticles will become smaller. Effectively, a smaller fraction

of the total cocatalyst mass can then provide active sites for the photocatalytic reaction.

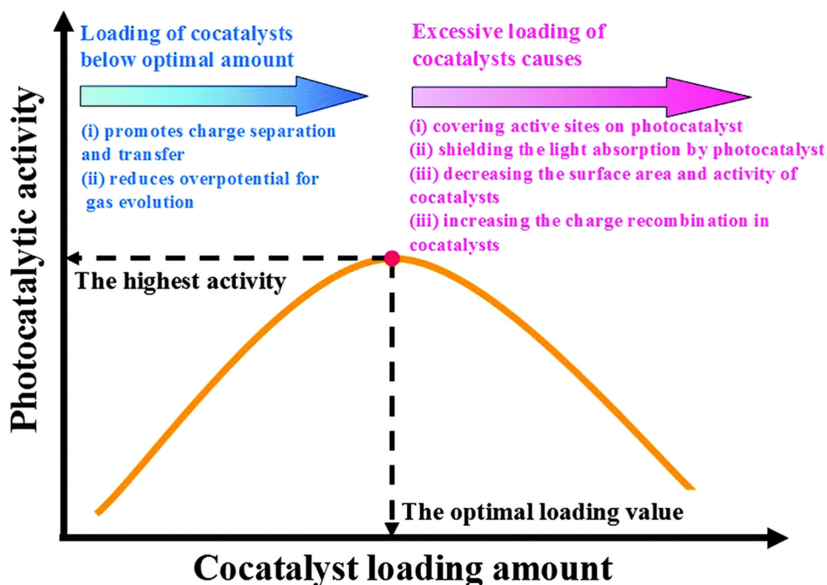


Figure 1.4. Photocatalytic activity as a function of the amount of cocatalyst present on the surface of a photocatalyst. Reproduced from Ref. [3] with permission from The Royal Society of Chemistry.

For both hydrogen reduction and oxygen activation, noble metals, such as Pt, Ag, Au or Pd, are often used as cocatalysts.^[3, 4, 14, 36, 37] In the case of water oxidation, metal oxides, such as CoO_x , IrO_2 and RuO_2 , are suited cocatalysts.^[3, 38] Several techniques exist to realize the deposition of cocatalysts on a photocatalyst. Photodeposition and impregnation are commonly used methods,^[4, 37] although other methods, such as physical mixing,^[39] are known as well. A very detailed review on photodeposition can be found in Chapter 2, as well as some references to other synthesis methods.

1.4.2 Pt-loaded WO_3

In the case of the material tungsten oxide, platinum has been considered to be a very promising cocatalyst. Normally, in oxidation reactions, electrons are used to reduce oxygen. However, the conduction band of WO_3 is at an unfavorable position for the single-electron reduction of oxygen.^[40] It is nevertheless at a favorable position for the reduction of oxygen through multi-electron reactions, creating either H_2O_2 or H_2O . By loading the WO_3 with Pt, these multi-electron reactions become more

feasible due to the carrier trapping effect and hence increased photocatalytic activities will be observed. The presence of a forbidden and allowed pathway of respectively single-electron and multi-electron reduction of O_2 can have a significant influence as well on the selectivity of the Pt/ WO_3 .^[41-43] A detailed overview of the role of Pt in a Pt/ WO_3 system will be provided in Chapter 2.

1.5 Crystal facet engineering

1.5.1 Basics of crystal facet engineering

In recent years, crystal facet engineering has started to gain attention in the photocatalysis community.^[7, 13, 18, 44] The concept relates to the synthesis of photocatalytic materials with a well-defined structure, exposing one or multiple facets dominantly. There are indications that some facets might be more reactive than others and hence it is interesting to investigate for different photocatalytic materials what facet might be the most reactive. Generally, to perform crystal facet engineering, crystal growth takes place in a solution containing surfactants, also known as capping agents. In the crystal growth process, initially nucleation of crystals will take place, followed by subsequent growth. In the absence of capping agents, the crystals will grow in a thermodynamically favorable way within the solution. When the capping agents are present however, they will adsorb on specific facets of the crystal, which results in a change in the surface energy of the facet. Subsequent growth in the direction perpendicular to that facet can suddenly be blocked and the particle will be forced to grow in another direction. By choosing the right set of capping agents and a proper solvent, a crystal can be engineered in such a way that only specific facets are exposed in a full-grown crystal. The concept of crystal facet engineering is schematically depicted in Figure 1.5. Aside from the introduction of capping agents, another method to perform crystal facet engineering is by adding both etching and capping agents to a solution containing full-grown crystals.^[44] The etching agents will normally dissolve the crystal. The capping agents however will adsorb on specific facets, protecting them from dissolving. Hence, selective dissolving of the crystals will take place.

Many crystal facet engineering studies have been performed through the usage of (microwave-assisted) hydrothermal synthesis.^[18, 44] The main advantage of this type of synthesis is that reactions in liquid conditions can be performed at temperatures higher than the boiling point of the solvent at atmospheric pressure.

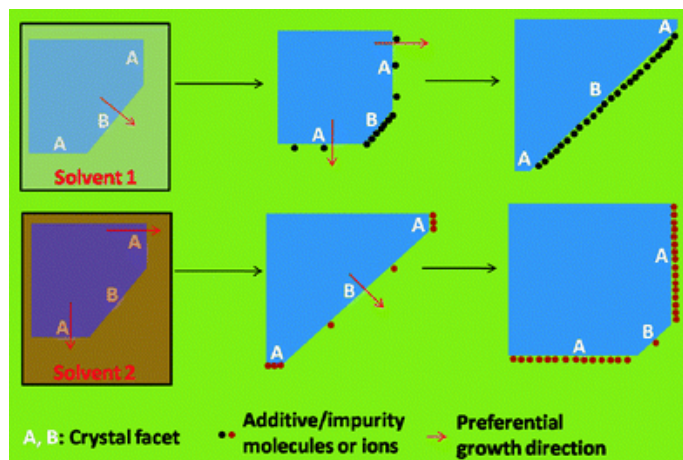


Figure 1.5. Schematic depicting the concept of crystal facet engineering. The introduction of additive/impurity molecules or ions will result in a different favorable growth orientation. Also the type of solvent can have an influence on the growth direction. Reproduced from Ref. [44] with permission from The Royal Society of Chemistry.

Crystal facet engineering has been applied on a large scale for the synthesis of well-defined TiO₂ anatase nanoparticles.^[44-48] Generally, it is accepted that a high exposure of the {001} facet compared to the normally dominant {101} facet is beneficial in photocatalytic applications of TiO₂. Therefore, many studies aim at crystal facet engineering of anatase particles with a large percentage of {001} facets. This can for instance be achieved by introducing fluorine species in the synthesis of the anatase. Nevertheless, there is some controversy in literature, as there are also studies which claim that the {001} facet does not necessarily have to be more active than the {101} facet.^[49, 50] Aside from TiO₂ anatase, crystal facet engineering has been performed on many other materials as well, for example on BiVO₄^[51] or perovskite oxides.^[52] A very good overview of work performed in crystal facet engineering (up to 2011) can be found in the review article of Liu *et al.* (Ref. [44]).

1.5.2 Crystal facet engineering of WO₃

Crystal facet engineering has also been applied on WO₃.^[17, 18, 44] WO₃ · xH₂O, h-WO₃ and m-WO₃ with well-defined morphologies have been synthesized through hydrothermal synthesis methods.^[53-56] For instance, Gu *et al.* have shown that, when sodium tungstate is used as a tungsten precursor, different hexagonal WO₃ morphologies can be grown when a combination of oxalic acid and M₂SO₄ is used (where M = Rb or K).^[53] Using this method, the authors have grown urchinlike structures (with Rb₂SO₄) and ribbonlike structures (with K₂SO₄). The addition of

other sulfates resulted in the growth of cylindrical nanowire bundles (with NaSO_4 or LiSO_4) and nanorods (with $(\text{NH}_4)_2\text{SO}_4$). In another example, Li *et al.* could control the morphology of WO_3 by hydrothermally treating a peroxy-polytungstic acid solution at different time intervals without the usage of a capping agent.^[54] At low reaction times, orthorhombic $\text{WO}_3 \cdot 0.33\text{H}_2\text{O}$ with hexagonal plate-like shapes was formed, whereas at high reaction times monoclinic cuboid WO_3 rods were obtained. WO_3 materials prepared through crystal facet engineering have been tested in photocatalytic and photoelectrochemical applications as well.^[18, 26, 27, 57-60] In particular the synthesis of monoclinic WO_3 with a large exposure of $\{002\}$ could be interesting for photocatalytic applications. Theoretical studies have demonstrated that the $\{002\}$ facet has the highest surface energy of the low-index facets.^[27, 61] This has led Zheng *et al.* to believe that the $\{002\}$ facet is the most reactive low-index facet.^[18, 61] Xie *et al.* have investigated experimentally the role of low-index facets in monoclinic WO_3 by synthesizing rectangular sheet-like WO_3 crystals with the $\{002\}$ facet dominantly being present, as well as quasi-cubic-like WO_3 crystals with a nearly equal amount of $\{002\}$, $\{020\}$ and $\{200\}$ facets.^[27] A clear difference was observed between the reaction rates of the crystals. For water oxidation (using AgNO_3 as a sacrificial agent) the quasi-cubic-like WO_3 showed better photocatalytic performance when normalized for Brunauer-Emmett-Teller (BET) surface area. However, very interestingly, the authors were able to photoreduce CO_2 to CH_4 with the rectangular sheet-like WO_3 crystals in the presence of water vapor, which was not possible with the quasi-cubic-like WO_3 . The authors related their findings to slightly different band positions of the different types of WO_3 . For the particles where $\{002\}$ was dominantly present, both the edge of the conduction and valence band were more negative compared to the band positions of the quasi-cubic-like WO_3 . This made the reduction of CO_2 possible, but oxidative power was traded in. It should be noted that $\{111\}$ facets of WO_3 could also be very interesting in photocatalytic applications, as evidenced by Zhao *et al.*^[57] The authors observed a high photocatalytic activity for monoclinic WO_3 octahedra with a thin $\text{H}_2\text{W}_{1.5}\text{O}_{5.5} \cdot \text{H}_2\text{O}$ shell in Ag^+ removal under visible light illumination.

In this thesis, crystal facet engineering is employed inspired by a method proposed by Su *et al.*^[62] These authors have grown WO_3 with well-defined morphologies using sodium tungstate dihydrate as a precursor and citric acid or L-(+)-tartaric acid as a capping agent in an aqueous solution. The pH of this solution was adjusted to 1 using a 6 M HCl aqueous solution. Using this method, the authors reported that they synthesized orthorhombic (using citric acid) and hexagonal (using L-(+)-tartaric acid) WO_3 square nanoplates. Based on the review article of Zheng *et al.*^[17] and

JCPDS cards, we think it is more likely that Su *et al.* have synthesized monoclinic WO_3 with orthorhombic $\text{WO}_3 \cdot 0.33\text{H}_2\text{O}$ groups rather than orthorhombic WO_3 , as the temperatures required for the transition of monoclinic WO_3 to orthorhombic WO_3 were never met. Nevertheless, the article of Su *et al.* has been used as a basis for the work described in this thesis.

An excellent overview of work performed in crystal facet engineering of tungsten oxide has been provided by Zheng *et al.* (Ref. [18]).

1.6 Aims and thesis outline

Heterogeneous photocatalysis could be one of the most promising techniques to deal with energy shortages or with the pollution of water and air. Therefore, it is evident that research should be performed on obtaining very efficient photocatalytic materials or systems. A key in this process will be to gain a fundamental understanding of the behavior of photocatalytic crystals, and to exploit this information for optimal usage of the photocatalyst. As discussed, the incorporation of cocatalysts and crystal facet engineering could be two techniques to obtain high photocatalytic activities. Due to the promising nature of platinum-loaded tungsten oxide, the aim of this thesis is to gain a fundamental understanding of engineering well-defined tungsten oxide particles with favored platinum positioning on these particles. To this end, the research is divided into three subgoals:

1. Performing successful crystal facet engineering of well-defined, monoclinic WO_3 nanoplates through a hydrothermal synthesis method.
2. Understanding photodeposition of Pt on commercial WO_3 on a fundamental level.
3. Applying photodeposition of Pt on the well-defined WO_3 nanoplates. The corresponding positioning of the Pt and the photocatalytic activity of the Pt/ WO_3 systems are studied.

First, literature research on the principles, mechanisms and applications of photodeposition is described in **Chapter 2**. It will be demonstrated that photodeposition is a technique that has been massively used to load cocatalytic nanoparticles on photocatalysts, but that on a fundamental level is it not explored very well. However, literature available does hint that reaction conditions in photodeposition are extremely important in achieving the desired dispersion, size and valence state of the cocatalyst. Ultimately, photodeposition can be used to probe the reductive and oxidative facets of a photocatalytic material. This can be used to

achieve very high photocatalytic activities, as amongst others demonstrated by Li and co-workers.^[63, 64]

Before further photodeposition studies are discussed, first crystal facet engineering of (dominantly) monoclinic plate-like WO_3 is touched upon. This is described in both **Chapter 3** and **Chapter 4**. In **Chapter 3**, initial studies are shown where the synthesis of plate-like WO_3 takes place based on the method by Su *et al.* earlier described in this chapter.^[62] The influence of the reaction temperature on the final crystal phase and morphology is discussed, as well as the influence of subsequent annealing treatment. The obtained crystals have been tested on their photocatalytic activity in (Fe^{3+} -assisted) Orange II sodium salt degradation. In **Chapter 4**, these studies are largely expanded with *in situ* Raman spectroscopy measurements during the growth of plate-like WO_3 with the aim of monitoring the crystal phase transitions in more detail. Also the morphology of the WO_3 nanoplates is studied as a function of reaction time. Furthermore, microwave-assisted hydrothermal synthesis experiments have been conducted to evaluate the influence of pH and temperature on the WO_3 crystal phase and morphology. A selection of WO_3 samples is evaluated in the photocatalytic oxidation of propane, with the aim to study the influence of the presence of hydrates and hydrothermal synthesis temperature on the photocatalytic activity of as-synthesized WO_3 nanoplates.

Studies on photodeposition start from **Chapter 5** and on. In **Chapter 5**, photodeposition of Pt on commercial WO_3 is studied on a fundamental level. Photodeposition kinetics are evaluated both in the presence and absence of the sacrificial agent methanol, where both the amount and oxidation state of the Pt deposited have been monitored as a function of photodeposition time. The Pt particle size has also been studied after photodeposition. For a further understanding of the material properties of as-deposited Pt, additional illumination and hydrogenation experiments have been performed as well on the platinum-loaded WO_3 .

After gaining both an understanding of plate-like WO_3 synthesis and of photodeposition of Pt on commercial WO_3 , this thesis will finally focus on the photodeposition of platinum on tungsten oxide nanoplates. In **Chapter 6**, the concept of structure-directed photodeposition of Pt on plate-like WO_3 is evaluated. Photodeposition, impregnation and atomic force microscopy studies have been conducted to evaluate whether structure-directed photodeposition of Pt on WO_3 nanoplates is the result of intrinsic charge carrier separation under illumination, or that it is driven by intrinsic differences between the WO_3 facets in surface charge.

Further photodeposition experiments of Pt on WO₃ nanoplates are described in **Chapter 7**. Here, Pt photodeposition is done on WO₃ nanoplates synthesized at different temperatures at pH = 0.5. These samples are characterized on the amount of Pt deposited, the oxidation state of the Pt and whether structure-directed photodeposition has taken place or not. Furthermore, as-obtained Pt/WO₃ nanoplates have been tested in the photocatalytic oxidation of propane. Comparisons between the photocatalytic activities and behavior between unloaded and Pt-loaded WO₃ nanoplates are made.

This thesis will conclude in **Chapter 8** with a reflection of as-obtained results, and how they could contribute to later research perspectives. Also, a brief outlook on the main challenges still open in (structure-directed) photodeposition will be given.

1.7 Bibliography

- [1] Navarro Yerga, R. M.; Consuelo Álvarez Galván, M.; del Valle, F.; Villoria de la Mano, J. A.; Fierro, J. L.; *Water splitting on semiconductor catalysts under visible-light irradiation*. ChemSusChem **2009**, 2, 471-485.
- [2] Blanco, J.; Malato, S.; Fernández-Ibañez, P.; Alarcón, D.; Gernjak, W.; Maldonado, M. I.; *Review of feasible solar energy applications to water processes*. Renewable and Sustainable Energy Reviews **2009**, 13, 1437-1445.
- [3] Ran, J.; Zhang, J.; Yu, J.; Jaroniec, M.; Qiao, S. Z.; *Earth-abundant cocatalysts for semiconductor-based photocatalytic water splitting*. Chemical Society Reviews **2014**, 43, 7787-7812.
- [4] Maeda, K.; *Photocatalytic water splitting using semiconductor particles: history and recent developments*. Journal of Photochemistry and Photobiology C: Photochemistry Reviews **2011**, 12, 237-268.
- [5] Kudo, A.; Miseki, Y.; *Heterogeneous photocatalyst materials for water splitting*. Chemical Society Reviews **2009**, 38, 253-278.
- [6] Roy, S. C.; Varghese, O. K.; Paulose, M.; Grimes, C. A.; *Toward solar fuels: photocatalytic conversion of carbon dioxide to hydrocarbons*. ACS Nano **2010**, 4, 1259-1278.
- [7] Fresno, F.; Portela, R.; Suárez, S.; Coronado, J. M.; *Photocatalytic materials: recent achievements and near future trends*. Journal of Materials Chemistry A **2014**, 2, 2863-2884.
- [8] Mo, J.; Zhang, Y.; Xu, Q.; Lamson, J. J.; Zhao, R.; *Photocatalytic purification of volatile organic compounds in indoor air: a literature review*. Atmospheric Environment **2009**, 43, 2229-2246.
- [9] Zhao, J.; Yang, X.; *Photocatalytic oxidation for indoor air purification: a literature review*. Building and Environment **2003**, 38, 645-654.

- [10] Kabra, K.; Chaudhary, R.; Sawhney, R. L.; *Treatment of hazardous organic and inorganic compounds through aqueous-phase photocatalysis: a review*. Industrial and Engineering Chemistry Research **2004**, 43, 7683-7696.
- [11] Di Paola, A.; García-López, E.; Marci, G.; Palmisano, L.; *A survey of photocatalytic materials for environmental remediation*. Journal of Hazardous Materials **2012**, 211-212, 3-29.
- [12] Palmisano, G.; García-López, E.; Marci, G.; Loddo, V.; Yurdakal, S.; Augugliaro, V.; Palmisano, L.; *Advances in selective conversions by heterogeneous photocatalysis*. Chemical Communications **2010**, 46, 7074-7089.
- [13] Tong, H.; Ouyang, S.; Bi, Y.; Umezawa, N.; Oshikiri, M.; Ye, J.; *Nanophotocatalytic materials: possibilities and challenges*. Advanced Materials **2012**, 24, 229-251.
- [14] Lee, S. K.; Mills, A.; *Platinum and palladium in semiconductor photocatalytic systems*. Platinum Metals Review **2003**, 47, 61-72.
- [15] Chong, M. N.; Jin, B.; Chow, C. W. K.; Saint, C.; *Recent developments in photocatalytic water treatment technology: a review*. Water Research **2010**, 44, 2997-3027.
- [16] Saleh, B. E. A.; Teich, M. C.; *Fundamentals of Photonics*. Second ed.; John Wiley & Sons, Inc.: Hoboken, New Jersey, **2007**; p 448.
- [17] Zheng, H.; Ou, J. Z.; Strano, M. S.; Kaner, R. B.; Mitchell, A.; Kalantar-Zadeh, K.; *Nanostructured tungsten oxide - properties, synthesis, and applications*. Advanced Functional Materials **2011**, 21, 2175-2196.
- [18] Zheng, J. Y.; Haider, Z.; Van, T. K.; Pawar, A. U.; Kang, M. J.; Kim, C. W.; Kang, Y. S.; *Tuning of the crystal engineering and photoelectrochemical properties of crystalline tungsten oxide for optoelectronic device applications*. CrystEngComm **2015**, 17, 6070-6093.
- [19] Herrmann, J. M.; *Fundamentals and misconceptions in photocatalysis*. Journal of Photochemistry and Photobiology A: Chemistry **2010**, 216, 85-93.
- [20] Huang, Z. F.; Song, J.; Pan, L.; Zhang, X.; Wang, L.; Zou, J. J.; *Tungsten oxides for photocatalysis, electrochemistry, and phototherapy*. Advanced Materials **2015**, 27, 5309-5327.
- [21] Kim, J.; Lee, C. W.; Choi, W.; *Platinized WO₃ as an environmental photocatalyst that generates OH radicals under visible light*. Environmental Science and Technology **2010**, 44, 6849-6854.
- [22] Kumar, S. G.; Rao, K. S. R. K.; *Tungsten-based nanomaterials (WO₃ & Bi₂WO₆): modifications related to charge carrier transfer mechanisms and photocatalytic applications*. Applied Surface Science **2015**, 355, 939-958.
- [23] Arai, T.; Yanagida, M.; Konishi, Y.; Ikura, A.; Iwasaki, Y.; Sugihara, H.; Sayama, K.; *The enhancement of WO₃-catalyzed photodegradation of organic substances utilizing the redox cycle of copper ions*. Applied Catalysis B: Environmental **2008**, 84, 42-47.

- [24] Hernandez-Uresti, D. B.; Sánchez-Martínez, D.; Martínez-De La Cruz, A.; Sepúlveda-Guzmán, S.; Torres-Martínez, L. M.; *Characterization and photocatalytic properties of hexagonal and monoclinic WO₃ prepared via microwave-assisted hydrothermal synthesis*. *Ceramics International* **2014**, *40*, 4767-4775.
- [25] Sayama, K.; Hayashi, H.; Arai, T.; Yanagida, M.; Gunji, T.; Sugihara, H.; *Highly active WO₃ semiconductor photocatalyst prepared from amorphous peroxy-tungstic acid for the degradation of various organic compounds*. *Applied Catalysis B: Environmental* **2010**, *94*, 150-157.
- [26] Liu, J. X.; Dong, X. L.; Liu, X. W.; Shi, F.; Yin, S.; Sato, T.; *Solvothermal synthesis and characterization of tungsten oxides with controllable morphology and crystal phase*. *Journal of Alloys and Compounds* **2011**, *509*, 1482-1488.
- [27] Xie, Y. P.; Liu, G.; Yin, L.; Cheng, H. M.; *Crystal facet-dependent photocatalytic oxidation and reduction reactivity of monoclinic WO₃ for solar energy conversion*. *Journal of Materials Chemistry* **2012**, *22*, 6746-6751.
- [28] Zhu, T.; Chong, M. N.; Chan, E. S.; *Nanostructured tungsten trioxide thin films synthesized for photoelectrocatalytic water oxidation: a review*. *ChemSusChem* **2014**, *7*, 2974-2997.
- [29] Wang, H.; Lindgren, T.; He, J.; Hagfeldt, A.; Lindquist, S. E.; *Photoelectrochemistry of nanostructured WO₃ thin film electrodes for water oxidation: mechanism of electron transport*. *Journal of Physical Chemistry B* **2000**, *104*, 5686-5696.
- [30] Amano, F.; Ishinaga, E.; Yamakata, A.; *Effect of particle size on the photocatalytic activity of WO₃ particles for water oxidation*. *Journal of Physical Chemistry C* **2013**, *117*, 22584-22590.
- [31] Liu, G.; Han, J.; Zhou, X.; Huang, L.; Zhang, F.; Wang, X.; Ding, C.; Zheng, X.; Han, H.; Li, C.; *Enhancement of visible-light-driven O₂ evolution from water oxidation on WO₃ treated with hydrogen*. *Journal of Catalysis* **2013**, *307*, 148-152.
- [32] Xin, G.; Guo, W.; Ma, T.; *Effect of annealing temperature on the photocatalytic activity of WO₃ for O₂ evolution*. *Applied Surface Science* **2009**, *256*, 165-169.
- [33] Sayama, K.; Mukasa, K.; Abe, R.; Abe, Y.; Arakawa, H.; *A new photocatalytic water splitting system under visible light irradiation mimicking a Z-scheme mechanism in photosynthesis*. *Journal of Photochemistry and Photobiology A: Chemistry* **2002**, *148*, 71-77.
- [34] Abe, R.; Higashi, M.; Domen, K.; *Overall water splitting under visible light through a two-step photoexcitation between TaON and WO₃ in the presence of an iodate-iodide shuttle redox mediator*. *ChemSusChem* **2011**, *4*, 228-237.

- [35] Szilágyi, I. M.; Fórizs, B.; Rosseler, O.; Szegedi, Á.; Németh, P.; Király, P.; Tárkányi, G.; Vajna, B.; Varga-Josepovits, K.; László, K.; Tóth, A. L.; Baranyai, P.; Leskelä, M.; *WO₃ photocatalysts: Influence of structure and composition*. Journal of Catalysis **2012**, 294, 119-127.
- [36] Zhang, L.; Mohamed, H. H.; Dillert, R.; Bahnemann, D.; *Kinetics and mechanisms of charge transfer processes in photocatalytic systems: a review*. Journal of Photochemistry and Photobiology C: Photochemistry Reviews **2012**, 13, 263-276.
- [37] Carp, O.; Huisman, C. L.; Reller, A.; *Photoinduced reactivity of titanium dioxide*. Progress in Solid State Chemistry **2004**, 32, 33-177.
- [38] Yang, J.; Wang, D.; Han, H.; Li, C.; *Roles of cocatalysts in photocatalysis and photoelectrocatalysis*. Accounts of Chemical Research **2013**, 46, 1900-1909.
- [39] Bamwenda, G. R.; Tsubota, S.; Nakamura, T.; Haruta, M.; *Photoassisted hydrogen production from a water-ethanol solution: a comparison of activities of Au-TiO₂ and Pt-TiO₂*. Journal of Photochemistry and Photobiology, A: Chemistry **1995**, 89, 177-189.
- [40] Abe, R.; Takami, H.; Murakami, N.; Ohtani, B.; *Pristine simple oxides as visible light driven photocatalysts: highly efficient decomposition of organic compounds over platinum-loaded tungsten oxide*. Journal of the American Chemical Society **2008**, 130, 7780-7781.
- [41] Tomita, O.; Abe, R.; Ohtani, B.; *Direct synthesis of phenol from benzene over platinum-loaded tungsten(VI) oxide photocatalysts with water and molecular oxygen*. Chemistry Letters **2011**, 40, 1405-1407.
- [42] Tomita, O.; Ohtani, B.; Abe, R.; *Highly selective phenol production from benzene on a platinum-loaded tungsten oxide photocatalyst with water and molecular oxygen: selective oxidation of water by holes for generating hydroxyl radical as the predominant source of the hydroxyl group*. Catalysis Science and Technology **2014**, 4, 3850-3860.
- [43] Shiraishi, Y.; Sugano, Y.; Ichikawa, S.; Hirai, T.; *Visible light-induced partial oxidation of cyclohexane on WO₃ loaded with Pt nanoparticles*. Catalysis Science and Technology **2012**, 2, 400-405.
- [44] Liu, G.; Yu, J. C.; Lu, G. Q.; Cheng, H. M.; *Crystal facet engineering of semiconductor photocatalysts: motivations, advances and unique properties*. Chemical Communications **2011**, 47, 6763-6783.
- [45] Dozzi, M. V.; Selli, E.; *Specific facets-dominated anatase TiO₂: fluorine-mediated synthesis and photoactivity*. Catalysts **2013**, 3, 455-485.
- [46] Chen, W.; Kuang, Q.; Wang, Q.; Xie, Z.; *Engineering a high energy surface of anatase TiO₂ crystals towards enhanced performance for energy conversion and environmental applications*. RSC Advances **2015**, 5, 20396-20409.

- [47] Yang, H. G.; Sun, C. H.; Qiao, S. Z.; Zou, J.; Liu, G.; Smith, S. C.; Cheng, H. M.; Lu, G. Q.; *Anatase TiO₂ single crystals with a large percentage of reactive facets*. *Nature* **2008**, 453, 638-641.
- [48] Xu, H.; Ouyang, S.; Liu, L.; Reunchan, P.; Umezawa, N.; Ye, J.; *Recent advances in TiO₂-based photocatalysis*. *Journal of Materials Chemistry A* **2014**, 2, 12642-12661.
- [49] Pan, J.; Liu, G.; Lu, G. Q.; Cheng, H. M.; *On the true photoreactivity order of {001}, {010}, and {101} facets of anatase TiO₂ crystals*. *Angewandte Chemie - International Edition* **2011**, 50, 2133-2137.
- [50] Gordon, T. R.; Cargnello, M.; Paik, T.; Mangolini, F.; Weber, R. T.; Fornasiero, P.; Murray, C. B.; *Nonaqueous synthesis of TiO₂ nanocrystals using TiF₄ to engineer morphology, oxygen vacancy concentration, and photocatalytic activity*. *Journal of the American Chemical Society* **2012**, 134, 6751-6761.
- [51] Huang, Z. F.; Pan, L.; Zou, J. J.; Zhang, X.; Wang, L.; *Nanostructured bismuth vanadate-based materials for solar-energy-driven water oxidation: a review on recent progress*. *Nanoscale* **2014**, 6, 14044-14063.
- [52] Huang, K.; Yuan, L.; Feng, S.; *Crystal facet tailoring arts in perovskite oxides*. *Inorganic Chemistry Frontiers* **2015**, 2, 965-981.
- [53] Gu, Z.; Zhai, T.; Gao, B.; Sheng, X.; Wang, Y.; Fu, H.; Ma, Y.; Yao, J.; *Controllable assembly of WO₃ nanorods/nanowires into hierarchical nanostructures*. *Journal of Physical Chemistry B* **2006**, 110, 23829-23836.
- [54] Li, J.; Huang, J.; Wu, J.; Cao, L.; Yanagisawa, K.; *Morphology-controlled synthesis of tungsten oxide hydrates crystallites via a facile, additive-free hydrothermal process*. *Ceramics International* **2012**, 38, 4495-4500.
- [55] Zhu, J.; Wang, S.; Xie, S.; Li, H.; *Hexagonal single crystal growth of WO₃ nanorods along a [110] axis with enhanced adsorption capacity*. *Chemical Communications* **2011**, 47, 4403-4405.
- [56] Sonia, A.; Djaoued, Y.; Subramanian, B.; Jacques, R.; Eric, M.; Ralf, B.; Achour, B.; *Synthesis and characterization of novel nanorod superstructures and twin octahedral morphologies of WO₃ by hydrothermal treatment*. *Materials Chemistry and Physics* **2012**, 136, 80-89.
- [57] Zhao, Z. G.; Liu, Z. F.; Miyauchi, M.; *Nature-inspired construction, characterization, and photocatalytic properties of single-crystalline tungsten oxide octahedra*. *Chemical Communications* **2010**, 46, 3321-3323.
- [58] Biswas, S. K.; Baeg, J. O.; *A facile one-step synthesis of single crystalline hierarchical WO₃ with enhanced activity for photoelectrochemical solar water oxidation*. *International Journal of Hydrogen Energy* **2013**, 38, 3177-3188.
- [59] Biswas, S. K.; Baeg, J. O.; Moon, S. J.; Kong, K. J.; So, W. W.; *Morphologically different WO₃ nanocrystals in photoelectrochemical water oxidation*. *Journal of Nanoparticle Research* **2012**, 14.

- [60] Shi, J.; Hu, G.; Cong, R.; Bu, H.; Dai, N.; *Controllable synthesis of $WO_3 \cdot nH_2O$ microcrystals with various morphologies by a facile inorganic route and their photocatalytic activities*. *New Journal of Chemistry* **2013**, 37, 1538-1544.
- [61] Zheng, J. Y.; Song, G.; Hong, J.; Van, T. K.; Pawar, A. U.; Kim, D. Y.; Kim, C. W.; Haider, Z.; Kang, Y. S.; *Facile fabrication of WO_3 nanoplates thin films with dominant crystal facet of (002) for water splitting*. *Crystal Growth and Design* **2014**, 14, 6057-6066.
- [62] Su, X.; Xiao, F.; Li, Y.; Jian, J.; Sun, Q.; Wang, J.; *Synthesis of uniform WO_3 square nanoplates via an organic acid-assisted hydrothermal process*. *Materials Letters* **2010**, 64, 1232-1234.
- [63] Li, R.; Zhang, F.; Wang, D.; Yang, J.; Li, M.; Zhu, J.; Zhou, X.; Han, H.; Li, C.; *Spatial separation of photogenerated electrons and holes among {010} and {110} crystal facets of $BiVO_4$* . *Nature Communications* **2013**, 4.
- [64] Li, R.; Han, H.; Zhang, F.; Wang, D.; Li, C.; *Highly efficient photocatalysts constructed by rational assembly of dual-cocatalysts separately on different facets of $BiVO_4$* . *Energy and Environmental Science* **2014**, 7, 1369-1376.

Chapter 2

Principles, mechanism, and applications of photodeposition in (photo)catalysis

Abstract

Photodeposition is a simple and green method to deposit cocatalytic nanoparticles on photocatalytic materials. However, a fundamental understanding of the concepts of photodeposition is required to engineer cocatalytic nanoparticles with desired size, dispersion and oxidation state. In this chapter a review of the concepts of photodeposition and research performed on this methodology is given. The basic concepts are discussed, as well as the most important fundamental research done on the photodeposition of cocatalytic particles on titania, with a strong emphasis on the photodeposition of platinum. A brief overview of studies of silver deposition on zinc oxide is provided as well. Given the scope of this thesis, the photodeposition of platinum on tungsten oxide is extensively discussed and to a lesser extent the photodeposition of other cocatalytic nanoparticles. Furthermore a very detailed overview is given on structure-directed photodeposition, which could ultimately be employed to obtain highly active photocatalytic systems. Finally, points for improvement in the synthesis of nanoparticles on semiconductors by photodeposition are discussed.

This chapter is based on Wenderich, K.; Romão, J. S. and Mul, G.; Principles, mechanism, and applications of photodeposition in (photo)catalysis: a review. Accepted for submission in Chemical Reviews.

2.1 Introduction to photodeposition

Photocatalysis is an important emerging technology which finds applications in solar fuel synthesis,^[1-3] wastewater treatment^[4, 5] and indoor air purification.^[6, 7] For enhancement of photocatalytic activities, cocatalysts can be loaded on a semiconductor, constituting effective photocatalysts.^[2, 5, 8] With an appropriate loading, these cocatalysts can improve activity considerably due to i) the cocatalyst behaving as a charge carrier beacon, repressing electron/hole recombination and ii) providing active sites for photocatalytic reactions. Another advantage of cocatalysts is that they can increase the stability of a photocatalyst. Several methods exist to deposit cocatalytic nanoparticles on photocatalytic materials, such as impregnation,^[9] chemical reduction,^[10, 11] electrodeposition,^[10, 11] atomic layer deposition (ALD),^[12] sputtering^[13] and physical mixing.^[14] From a green energy perspective, a far more suitable deposition method is the technique of photodeposition. While the other techniques might be efficient, most of them need a non-green energy feed, for example in the form of high temperatures or an applied bias. In the case of photodeposition, the green properties of the photocatalyst itself are used to load the cocatalyst. In the most basic form of photodeposition, merely illumination of an aqueous solution containing a cocatalyst precursor and the photocatalyst is sufficient. Some researchers add a sacrificial electron donor or acceptor to the slurry system, with the purpose to increase photodeposition rate. Other possibilities used in photodeposition involve de-aeration of the solution through nitrogen or argon bubbling. In some cases, the pH of the solution can be changed as well. In multiple studies, research has been performed to find an optimal loading of a cocatalyst for subsequent photocatalytic applications. It is advocated that such an optimum exists because at too high loadings the cocatalytic nanoparticles start to act as recombination centers or block incident light.^[15] Variations on classical photodeposition also exist. For instance, some authors coat their photocatalytic material with a metal salt first. Then, in non-aqueous conditions the photodeposition itself takes place.^[16-19] Others perform photodeposition in classical (aqueous) conditions, but monitor the formation of *e.g.* H₂ during the photodeposition process *in situ*.^[20-23] Over the past decade, interest in photodeposition has expanded immensely (Figure 2.1).

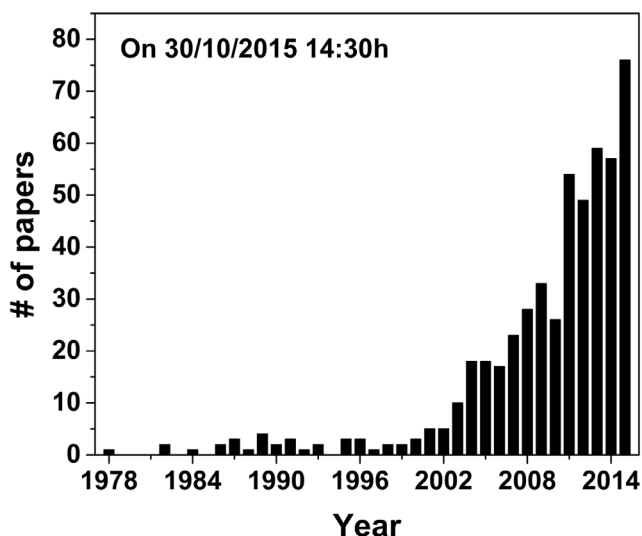
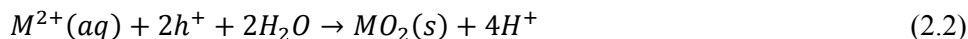


Figure 2.1. Overview of the amounts of papers published on ‘photodepo* AND photocat*’ as a function of years as searched on in Scopus on 30/10/2015, 14:30h. Note: not all research related to photodeposition is shown in this image, as photodeposition is not the only name used for this phenomenon. It is also known as e.g. ‘photoreduction’ or ‘photochemical deposition’.

We can distinguish between two types of photodeposition: reductive photodeposition and oxidative photodeposition. Reductive photodeposition occurs when photo-excited electrons are used to reduce a metal ion in solution to solid metal M particles. An example of a reductive photodeposition process could be:



Its counterpart, oxidative photodeposition, is the formation of a metal oxide through an oxidative photoreaction. An example could be:



A schematic overview of both reductive and oxidative photodeposition is depicted in Figure 2.2.

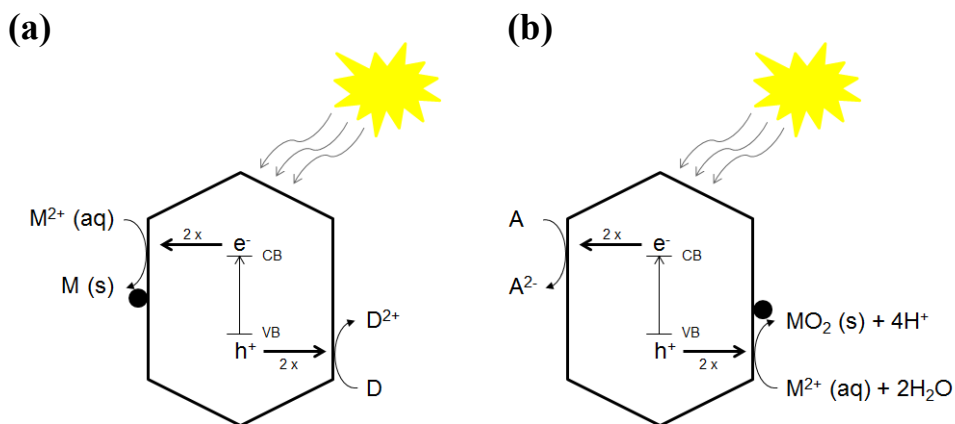


Figure 2.2. Schematic overview of (a) reductive photodeposition and (b) oxidative photodeposition.

Photodeposition was already performed in at least 1965 by Clark and Vondjidis.^[24] Using infrared studies the authors discussed that metallic silver was formed after a mixture of titanium dioxide and silver nitrate was illuminated. However, the report which really sparked interest in photodeposition was published by Kraeutler and Bard in 1978.^[25] Here, platinum was loaded on titanium dioxide (TiO_2 , anatase) by illuminating a slurry system containing anatase powder, hexachloroplatinic acid (H_2PtCl_6), hydrochloric acid (HCl), sodium carbonate and acetic acid, the latter acting as a sacrificial hole acceptor. During the reaction, a nitrogen flush was used to remove O_2 and CO_2 and the slurry system was heated to $55\text{ }^\circ\text{C}$. After this research was published, photodeposition has been used extensively by many researchers. However, the understanding of photodeposition on a fundamental level is surprisingly limited.

Comparisons have been made between metal-loaded photocatalysts, where the metal loading was achieved through (*in situ*) photodeposition or through another technique.^[14, 23, 26-31] Reports on what the most efficient method of deposition is are inconsistent. Some authors claim that photodeposition is more suited to obtain highly active photocatalytic systems than other deposition methods,^[14, 26, 30] whereas others claim the contrary.^[27-29] Likely, differences in material properties of the applied cocatalysts will play a role in the observed differences. Generally, if photodeposition is to be used as a technique for loading cocatalysts on photocatalytic materials, a full

control over size, dispersion and oxidation state is desired, and hence in depth understanding of the chemical principles of photodeposition is needed.

A brief overview of studies performed using photodeposition will be provided in this chapter. Photodeposition on TiO₂ on a fundamental level will be briefly discussed (with an emphasis on platinum), as well as photodeposition of silver on zinc oxide (ZnO). Given the scope of this thesis, a special emphasis will be given to tungsten oxide (WO₃), and on the technique of structure-directed photodeposition. This chapter will be concluded with points for improvement needed for preparation of highly dispersed nanoparticles on semiconductors by photodeposition.

2.2 Photodeposition of particles on TiO₂

Photodeposition of nanoparticles on TiO₂ has been employed by many researchers. The nanoparticles studied include noble metals such as Pt,^[15, 25, 32-43] Ag,^[24, 44, 45] Au^[31, 46, 47] and Pd,^[48, 49] metal oxides such as PbO₂^[50] and RuO₂^[51] and more complex nanoparticles such as CoPi.^[52] Even the photodeposition of another photocatalyst, CdS, on TiO₂ has been performed.^[53, 54] In some cases, photodeposition has also been employed to achieve core-shell particles,^[55-58] bimetallic cocatalysts^[59, 60] or even trimetallic cocatalysts, sometimes involving an annealing step.^[60] Despite a vast amount of research where photodeposition on TiO₂ has been employed, the availability of research performed at understanding the photodeposition itself on a fundamental level is limited. Many researchers have tried to find an optimum wt loading of a cocatalyst when photodeposition is employed for creation of effective photocatalytic materials.^[15, 31, 42-44] However studies on the influence of parameters such as the role of a sacrificial reagent,^[32-35] the influence of pH,^[35-37, 46] the influence of precursor,^[38, 39] *etc.* are not so abundant. Here, we will focus on studies performed on understanding photodeposition of Pt on TiO₂.

Already in 1984 Sungbom *et al.* demonstrated the importance of using a sacrificial agent in the photodeposition process of Pt on anatase.^[32] The authors showed that the presence or absence of a CH₃COOH-CH₃COONa buffer yielded very different results regarding the oxidation state of Pt after photodeposition on TiO₂. At no or low concentrations of CH₃COOH-CH₃COONa, the authors found that Pt^{II} and Pt^{IV} had formed rather than Pt⁰. With an increase in the concentration of CH₃COOH-CH₃COONa, the average valence state of the Pt became lower, ultimately resulting in a combination of Pt⁰ and Pt^{II}. Interestingly, when photocatalytic methanol decomposition was performed using as-obtained Pt-loaded TiO₂, oxidized platinum

was easily reduced to metallic Pt⁰. This behavior was not observed when benzene was oxidized. Nakamatsu *et al.* found a year later that the dispersion of Pt when photodeposited on TiO₂ (mostly rutile with some anatase) was largely dependent on the type of sacrificial agent used.^[33] They found that the order of gaining a high to low Pt dispersion was ethanol > methanol \approx 2-propanol > acetic acid \approx 2-methylpropan-2-ol. The authors proposed a model where the radicals of these organic compounds, which are formed when these are oxidized, also provide electrons for the reduction of Pt. They claimed that using radicals with higher reducing power should result in obtaining a finer dispersion of Pt deposits. However, using ethanol, which possesses the highest reduction potential, did not provide the photocatalytically most active Pt/TiO₂ species. Optimal results were obtained in hydrogen production (from ethanol) when photodeposition was performed with acetic acid, as shown in Figure 2.3.

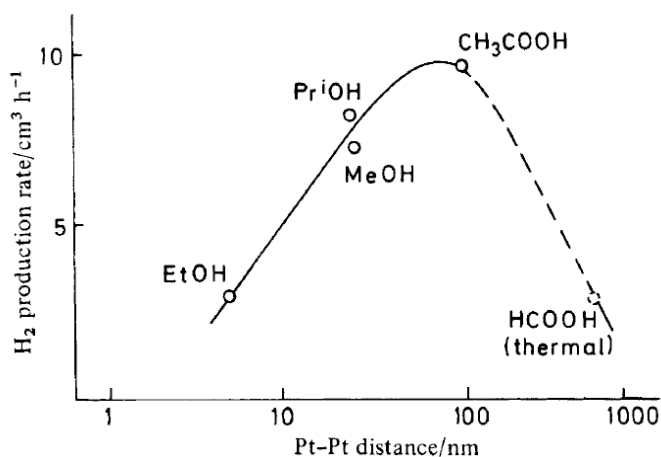
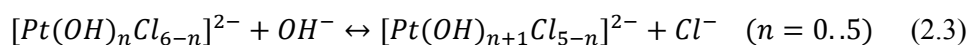


Figure 2.3. Photocatalytic hydrogen production in an aqueous ethanol solution as a function of Pt-Pt distance, the latter being related to the platinum dispersion. The circles imply the sacrificial agents used in the photodeposition procedure and serve as data points for this graph. The broken circle relates to Pt/TiO₂ synthesized through thermal reduction in formic acid rather than photodeposition. Reproduced from Ref. [33] with permission from the PCCP Owner Societies.

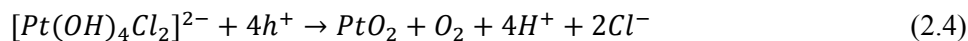
The importance of using a sacrificial agent to get fully reduced Pt was once more confirmed by Lee and Choi.^[34] In this case, methanol was employed at a high and at a low concentration. Reduction to Pt⁰ particles took place in the first case, whereas Pt^{II} remained the dominant oxidation state in the latter case. Again, this difference was ascribed due to the formation of methanol radicals which contribute to the

reduction of the Pt. Furthermore, usage of a high methanol concentration resulted in larger Pt particles than when a low concentration was employed. The authors briefly stated that when they incidentally de-aerated their solution, an even higher fraction of Pt⁰ formed. Interestingly, further reduction of (oxidized) platinum took place when Pt/TiO₂ was used in photocatalytic experiments.

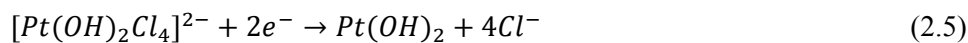
Also the pH can play a significant role in photodeposition kinetics. Xi *et al.* discussed that hydrolysis of [PtCl₆]²⁻ (provided that this anionic complex is used as a precursor) is formed in the photodeposition procedure.^[35]



This would imply that at high pH more hydroxyl groups are present in the Pt precursor, which could have an effect on the photodeposition kinetics. Indeed, in the absence of a sacrificial agent, the authors found photodeposited Pt(OH)₂ on TiO₂ at low and neutral pH, and additionally formed PtO₂ at high pH. The authors hypothesized that PtO₂ formation is possible through the following oxidation reaction:



The formation of [Pt(OH)₄Cl₂]²⁻ is favored at high pH and will not be present at lower pH values. For the formation of Pt(OH)₂, the authors speculated that less hydroxyl groups are required in the Pt complex. For instance, [Pt(OH)₂Cl₄]²⁻ could be reduced via the following reduction pathway:



When a sacrificial agent was present in the form of acetic acid, however, metallic Pt⁰ was formed at a low pH and Pt(OH)₂ at a high pH. This increased amount of reduction is in agreement with the studies by Sungbom *et al.*^[32] Likely, the oxidation of acetic acid is energetically preferred over the oxidation of [Pt(OH)₄Cl₂]²⁻, preventing PtO₂ formation. The authors also speculated that acetic acid radicals formed might contribute to the additional reduction. Interestingly, the authors measured with XPS that at lower pH values less Pt was found at the surface of the TiO₂, using identical photodeposition times. Also the addition of Cl⁻ turned out to be detrimental for the amount of Pt deposited, which would prevent the occurrence of the hydrolysis of [PtCl₆]²⁻. No PtO₂ was measured at a high pH when a large amount

of Cl^- was added ($\text{Pt}(\text{OH})_2$ was though), and no Pt formation at all was detected at a low pH. The detrimental effect of Cl^- addition in photodeposition was also confirmed for $[\text{PtCl}_n(\text{H}_2\text{O})_{4-n}]^{2-n}$ ($n = 0..4$) in acidic conditions (and no sacrificial agent) by Mahlamvana & Kriek, even resulting in no photodeposition when only $[\text{PtCl}_4]^{2-}$ was present.^[38] In contrast to the paper by Xi *et al.*, Zhang *et al.* demonstrated that a higher Pt photodeposition rate on TiO_2 is achieved at lower pH's than at higher pH's (using ethanol as hole scavenger and nitrogen to remove the oxygen).^[36] Again, the oxidation state was found to be dependent on the pH: metallic Pt^0 was formed at a pH lower than 5, and PtO_2 was formed at pH's higher than 9. In the pH range of 5-7 both Pt and PtO were found, in the pH range of 7-9 both PtO and PtO_2 . Just as Xi *et al.*, the authors attributed this phenomenon to hydrolysis of the $[\text{PtCl}_6]^{2-}$ precursor (equation 2.3). With the exception of the pH range of 5-7, a higher dispersion and a more narrow size distribution of platinum particles was observed at a high pH rather than a low pH. This was attributed to the platinum complex- TiO_2 interactions: at pH values above the isoelectric point of TiO_2 (6.25), the Pt-complex and TiO_2 repel each other, ultimately resulting in low deposition rates and narrow size distributions of the Pt. At low pH values, the Pt-complex and TiO_2 attract each other, resulting in a high photodeposition rate, but ultimately resulting in large Pt particles. Around the isoelectric point, the TiO_2 particles agglomerate, resulting in only part of the TiO_2 surface being available for photodeposition. As a result, large agglomerates of Pt particles are formed in this pH range. This study is very promising, as it demonstrates that with a combination of photodeposition at a desired pH and potentially subsequent hydrogen treatment, the size and distribution of (metallic) Pt particles on TiO_2 can be carefully controlled. Inspired by amongst others this study, Lee and Choi synthesized two platinum-loaded TiO_2 samples: one containing metallic Pt using a low pH and a high concentration of an electron donor (methanol), and one containing oxidized Pt using a high pH and no electron donor.^[34] The authors demonstrated that Pt/ TiO_2 with metallic Pt was more active in the photocatalytic degradation of several chlorinated organic compounds. Recent pH-dependent photodeposition studies by Qamar and Ganguli confirmed that the photodeposition rate of Pt is lower at higher pH's.^[37] Also, a high pH during photodeposition resulted in lower photocatalytic activities in triclopyr and methyl orange degradation. Remarkably, agglomerates of Pt were only observed in the pH range of 5 to 9, and not at a pH lower than 5 (and above 9). The authors claimed a favorable distribution of small platinum nanoparticles on the TiO_2 surface in acidic conditions, which is contradictory to the studies of Zhang *et al.*^[36]

Herrmann *et al.* studied the photodeposition of Pt on TiO₂ when different Pt precursors were used, namely H₂PtCl₆, Na₂PtCl₆, H₂Pt(OH)₆ and Pt(NO₂)₂(NH₃)₂.^[39] Only in the latter case a lower photodeposition rate was observed, whereas this was identical for the other precursors. This is somewhat remarkable, as we have just discussed that pH might have a very important influence on the photodeposition rate. The pH was presumably significantly higher when H₂Pt(OH)₆ was used. It is likely that the pH was different as well when H₂PtCl₆ rather than Na₂PtCl₆ was used. Nevertheless, the lower photodeposition rate of Pt(NO₂)₂(NH₃)₂ was ascribed to a higher stability of the complex and/or a smaller adsorption coefficient (because of its nonionic character). Aside from precursors, Herrmann *et al.* also demonstrated that the initial photodeposition rate was linearly dependent on the photon flux, linearly dependent on the precursor concentration until a plateau was reached, and that it was independent on the presence or absence of air. Furthermore, a dependency of reaction temperature (roughly in the range of 0 to 80 °C) was shown. From an Arrhenius plot the authors calculated an initial activation energy of 6 kJ. Therefore adsorption/desorption effects are not negligible in the photodeposition process. Furthermore, Herrmann *et al.* observed that initially Pt was deposited as small Pt particles, whereas large agglomerates were formed at longer illumination times. In contrast to these studies, Mahlamvana & Kriek demonstrated in their photodeposition experiments that the presence of oxygen had a very profound negative influence on the photodeposition rate.^[38] This was attributed to O₂ acting as a competing electron scavenger. Furthermore, the authors demonstrated that the type of precursor mattered a lot for the initial photodeposition rate. The order of most to least reactive precursor was K₂PtCl₆ > H₂PtCl₆ > [PtCl₃(H₂O)]⁻ > [PtCl₄]²⁻, with the latter showing no activity at all. Clearly [PtCl₆]²⁻ was preferred for an efficient photodeposition process. An overview of these findings is provided in Figure 2.4. It is very interesting to notify that it could be hypothesized that [PtCl₆]²⁻ is first reduced to [PtCl₄]²⁻, before being reduced to metallic Pt⁰. However, the lack of activity in the photodeposition of [PtCl₄]²⁻ by Mahlamvana & Kriek would imply that this is not the mechanism occurring during the photodeposition of [PtCl₆]²⁻.

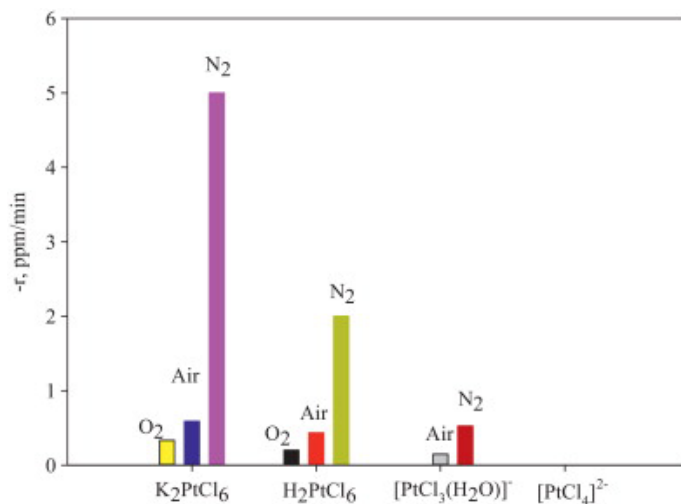


Figure 2.4. Initial photoreduction rates of different Pt precursors on TiO₂ in different atmospheres. Reprinted from Ref. [38], Copyright 2016, with permission from Elsevier.

Murcia *et al.* recognized the importance of engineering Pt particles of desired oxidation state, dispersion and size on the TiO₂ surface.^[40] Therefore they studied the photodeposition kinetics of Pt on TiO₂, including the obtained weight percentage, oxidation state and particle size of Pt on TiO₂ as a function of photodeposition time under mild light intensity (using N₂ purge and isopropanol). Remarkably, the authors did not observe full photodeposition of all precursor Pt on TiO₂. When the aim was to photodeposit 2 wt% of Pt on TiO₂, the authors even observed a decrease in the amount of Pt deposited after 60 minutes. This was attributed to re-oxidation of Pt nanoparticles and desorption effects due to hydroxyl radicals. For 0.5 wt% Pt, the authors observed that the Pt particle size increased as a function of photodeposition time (roughly 3 nm after 15 min and 6 nm after 240 min). At 2 wt%, aggregates of Pt particles were observed both at short and long photodeposition times. Both the growth of individual particles and aggregates were attributed to a cocatalytic effect of Pt. During the photodeposition of 2 wt% Pt, the percentage of metallic Pt⁰ increased until a steady state was reached around 60%. This is somewhat contradictory to the earlier mentioned study by Lee and Choi.^[34] Although these authors also observed reduction to Pt⁰ over time, the fraction of metallic Pt formed was considerably larger. Murcia *et al.* measured that the photocatalytic degradation of phenol and methyl orange was improved when the Pt⁰ fraction became higher, in agreement with the studies by Lee and Choi.

While much attention has been paid at the photodeposition of Pt on TiO₂, research on the photodeposition of other cocatalysts is available as well. For instance, pH-dependency (in the range of 3 to 9) has been studied for the photodeposition of Au (in the presence of methanol).^[46] Similar to Pt photodeposition, the particle size of Au decreased when the pH increased (from acidic to neutral pH). Different, however, was that the oxidation state of Au was always metallic, and therefore the highest photocatalytic activity in oxalic acid degradation was found at a pH of 7. Differences in photodeposition behavior between Pt and Pd have been observed as well. Mahlamvana & Kriek have shown that Cl⁻ is detrimental in the photodeposition of [PtCl_n(H₂O)_{4-n}]²⁻ⁿ (n = 0..4).^[38] However, PdCl₂(H₂O)₂ yielded a better deposition rate than both [PdCl₄]²⁻ and [Pd(H₂O)₄]²⁺.^[48] Further, Borgarello *et al.* demonstrated that oxygen has a negative influence on the reduction of Rh^{III}, but not on Pd^{II}, but that both reactions benefit from the sacrificial agent methanol.^[49] Different pH dependencies in the removal rate of an ionic metal compound were found as well for different aqueous metal ion mixtures.^[49, 61] Through a modelling study it was demonstrated that the extent of influence of a sacrificial agent (citric acid) can be different for the reduction of Cu^{II}, Ni^{II}, Zn^{II} and Pb^{II}.^[62] Borgarello *et al.* even showed that it is possible to selectively remove each metal compound from a solution containing multiple metal compounds by changing photodeposition parameters.^[49]

Finally, some researchers have tried to study photoreduction of metals on TiO₂ using *in situ* EXAFS spectroscopy, generally providing much information on the photodeposition process. This includes the deposition of Pt,^[41] Au^[47] and Rh^[63, 64]. Interestingly, one of the studies concerning Rh/TiO₂ revealed that the type of sacrificial agent used matters for the photodeposition rate, with the order in high to low rate being methanol > ethanol >> 1-propanol > 2-propanol.^[63] Again this might be related to the reduction potential of the radical formed by hole transfer to these alcohol derivatives.

2.3 Photodeposition of Ag on ZnO

Aside from TiO₂, photodeposition has also been employed for other metal oxides, such as ZnO,^[17, 65-86] BiVO₄,^[87-89] Ga₂O₃,^[20, 90, 91] and Ta₂O₅,^[92] perovskites,^[28, 90, 93] metal sulfides (in particular cadmium sulfide (CdS))^[21, 22, 94-101] and (oxy)nitrides.^[19, 20, 90, 102, 103] In particular, the photodeposition of Pt on CdS^[21, 94-99] and Ag on ZnO^[17, 65-82] have been explored relatively well in the literature. We will briefly address the latter, as it might serve as a model for photodeposition of a metal on a metal oxide.

As with TiO₂, the composition of the reducing media has a large influence on the photodeposition process of Ag on ZnO.^[17, 65, 66] Liu *et al.* have studied photodeposition of Ag on ZnO nanorods (grown on glass substrates) in an aqueous solution without sacrificial agent and in an aqueous solution with ethanol.^[17] Also, they have chosen to dip one glass substrate with ZnO nanorods in an aqueous solution with AgNO₃, after which they got it out and then started illumination. There was a major difference between the different samples in i) Ag loading, ii) dispersion, iii) morphology and iv) photocatalytic activity under visible light irradiation. An overview of the different properties of the samples can be found in Table 2.1 and Figure 2.5. Clearly, a sacrificial agent improved the photodeposition rate greatly. Also the morphology was dependent on the reducing media. It is remarkable that when no sacrificial agents were used, two different kinds of morphologies were formed: small nanoparticles (10-20 nm in size) at the sides of the nanorods and huge nanosheets at the top. When ethanol was introduced, no particles were deposited at the sides and huge nanoclusters of Ag (500-800 nm in size) were formed at the top. We speculate that this difference in selective deposition might be the result of a change in sorption properties of the ZnO when ethanol was introduced. Furthermore we believe that the formation of two kinds of morphologies without sacrificial agent could be due to additional Ag₂O or AgO formation besides metallic Ag formation (although the authors mentioned that no Ag₂O was formed). A remarkable higher photocatalytic activity in Rhodamine B (RhB) degradation under visible light was observed when no ethanol was used compared to when it was used. The authors contributed this to be likely the result of i) Ag blocking RhB reaction sites or ii) Ag inhibiting visible light access to the Ag/ZnO interface, reducing the amount of surface plasmon resonance and thus the photocatalytic activity. Although photodeposition in air was an interesting experiment, no obvious advantages were reported.

Table 2.1. Properties of samples synthesized by Liu *et al.*^[17]

Photodeposition in	At%	Morphology Ag	Dispersion	RhB photodegraded (visible light irradiation) over 4 hours
Water	7.68	Nanosheets + nanoparticles	Nanosheets at the top, nanoparticles at the sides	82%
Water + Ethanol	26.1	Irregular polygon shape	Only at the top	27.3%
Air	1.35	Nanoribbons	Only at the top, hardly observable	39.4%

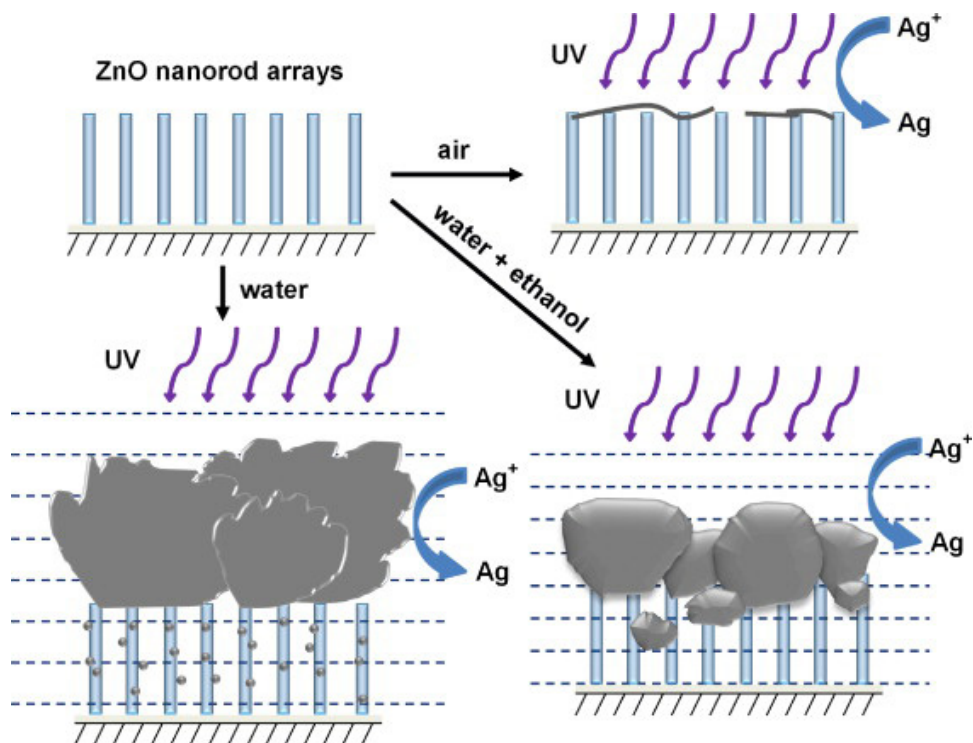


Figure 2.5. Schematic demonstrating the influence of reducing medium on the photodeposition of Ag on ZnO nanorods. Reprinted from Ref. [17], Copyright 2016, with permission from Elsevier.

Huang *et al.* also confirmed the importance of sacrificial agents during photodeposition of Ag on ZnO.^[65] These authors performed Ag photodeposition on ZnO nanoflowers using AgNO_3 solutions containing i) no sacrificial agent, ii) ethanol and iii) glycol. They found weight percentages of 27.56 wt%, 23.62 wt% and 35.03 wt% respectively. Although glycol definitely was beneficial for the deposited amount of loading, it is remarkable that ethanol was not, especially when compared to the studies by Liu *et al.*^[17] Again, differences in morphology and particle size were observed. The size of the Ag particles when photodeposited with ethanol was considerably larger (100 nm) than when no ethanol (10 nm) was used. Ag/ZnO showed superior activity in surface-enhanced Raman scattering (SARS) performance and photocatalytic dye degradation when it was prepared with glycol as a sacrificial agent. When no sacrificial agent was used in photodeposition, the results were less optimal than when a sacrificial agent was used. Finally, in a study by Wang *et al.*, photodeposition of Ag on tetrapod-like ZnO whiskers was performed using different concentrations of polyethylene glycol (PEG) in an AgNO_3 aqueous

solution.^[66] Under the same illumination conditions, an increase in PEG concentration resulted in an increase of the amount of Ag deposited and in smaller Ag mean particle sizes. Correspondingly, the amount of PEG concentration used in photodeposition had a large influence on the photocatalytic performance of Ag/ZnO in Methyl Orange (MO) degradation under UV illumination. The authors found an optimal PEG concentration of 0.08 mol/L. Noteworthy is the mechanism of photodeposition the authors mentioned: they attributed the reduction of Ag^+ to Ag not necessarily to electrons formed in ZnO. Instead, they mentioned that PEG captures $\text{OH}\cdot$ radicals formed by the ZnO, forming aldehyde or acid. These compounds then reduce Ag^+ to Ag.

Some authors have studied the influence of illumination time as well during photodeposition.^[67-72] Lin *et al.* observed that with increasing irradiation time, more Ag was deposited and the Ag particle size also increased (13.4 nm after 5 minutes up to 15.9 nm after 25 min).^[69] Li *et al.* observed similar behaviour (11 nm after 30 minutes up to 29 nm after 8 hours).^[70] This resulted in increased performance in H_2O_2 and SERS-based rhodamine 6G (R6G) sensing. Studies by Behnajady *et al.* and Peng *et al.* have shown that initially the performance of Ag/ZnO (in this case for Methyl Orange photodegradation) changes with increasing irradiation time of photodeposition, but becomes constant later on. This was logically attributed to full Ag^+ to Ag reduction.^[68, 72] Of special note are studies by Kawano *et al.* and Chen & Nickel.^[67, 71] Kawano *et al.* were mainly interested in using ZnO as a photocatalyst to remove Ag^+ from an aqueous solution. They monitored Ag deposition over time on a Zn polar surface (0001) and an O polar surface (000 $\bar{1}$). After 10 seconds of illumination, a considerably higher amount of Ag particles was found at the Zn polar surface than at the O polar surface (ratio 20:1), indicating that the Zn polar surface was far more active. Increased irradiation time showed a considerable growth in the Ag particle size deposited on the O polar surface, which was not observed for the Zn polar surface. The authors stated that the latter might have been the result of i) not sufficient Ag ions being present in the solution anymore and ii) as-deposited Ag changing the absorption efficiency of the material. Chen & Nickel studied the photodeposition kinetics of Ag on ultrafine ZnO in the presence of Zn^{2+} and OH^- excess ions in de-aerated ethanol.^[71] They found that in the presence of Zn^{2+} excess ions, mainly large metallic Ag particles were formed, whereas in the presence of an over-excess of OH^- initially Ag_2O was formed, which would transform to metallic Ag.

A major advantage of performing photodeposition of Ag on ZnO is that Ag will stabilize the ZnO.^[73, 74] Xie *et al.* performed photodegradation of crystal violet (CV) using a UV lamp over 8 cycles with both unloaded and Ag-loaded ZnO, as demonstrated in Figure 2.6.^[73] A drastic decrease in activity was observed for unloaded ZnO, whereas for ZnO loaded with 0.2 wt% Ag hardly any deactivation was observed. The authors discussed that, according to Kislov *et al.*,^[75] photocorrosion of ZnO ($\text{ZnO} + 2\text{h}^+ \rightarrow \text{Zn}^{2+} + 0.5\text{O}_2$) mainly happens at surface defect sites. Xie *et al.* demonstrated through photoluminescence studies that during photodeposition, Ag is deposited at these defect sites. Therefore, photocorrosion of ZnO is prevented at these sites and thus the photocatalyst will become far more stable.

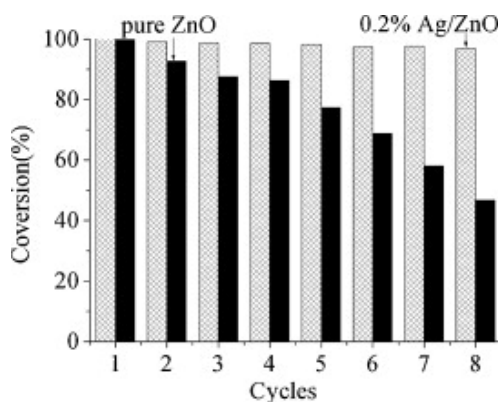


Figure 2.6. Photocatalytic conversion of crystal violet using pure ZnO and Ag/ZnO over multiple cycles. The activity of ZnO decreased, whereas the activity of Ag/ZnO did not. Reprinted from Ref. [73], Copyright 2016, with permission from Elsevier.

One aspect we would like to address are X-ray photoelectron spectroscopy (XPS) studies to confirm whether metallic Ag had been formed or not. Theoretically, according to the Handbook of X-Ray Photoelectron Spectroscopy, metallic Ag can be recognized by amongst others binding energies of 368.2 eV and 374.2 eV, corresponding to Ag 3d_{5/2} and Ag 3d_{3/2} respectively.^[104] After photodeposition, many authors reported in their XPS spectra a shift in the binding energy of Ag 3d_{5/2} and Ag 3d_{3/2}.^[65, 66, 74, 76-80] Those authors attributed this to be the result of electron transfer from Ag to ZnO at the interface due to Fermi level alignment. Binding energies of Ag 3d_{5/2} reported by the authors are in the range of 366.5 to 367.7 eV. However, these values could also be attributed to Ag₂O (367.6 eV) or AgO (367.2 eV) rather than being the result of interaction between Ag and ZnO.^[105] Some authors discussed the possible formation of Ag₂O in their photodeposition as well.^[65, 66] Through X-

ray diffraction (XRD) studies, they reported that they only observed peaks corresponding with metallic Ag and they did not detect any peaks corresponding to Ag₂O. Also, Wang *et al.* studied in their XPS results whether an O 1s peak assigned to Ag₂O was detected and reported that they did not observe this.^[66] Interestingly, all the as-mentioned authors performed their photodeposition experiments without any gas purging. Thus, photodeposition of Ag on ZnO was most likely performed in oxygen-rich conditions, which might contribute to Ag₂O or AgO formation. Zhang *et al.* reported that when the solution was purged with N₂ during the experiment, binding energy peaks were observed at 368.3 and 374.2 eV.^[81] These peaks do correspond with metallic Ag 3d_{5/2} and Ag 3d_{3/2} respectively and are clearly different from the earlier mentioned reported values. On the other hand, Chen *et al.* also performed photodeposition with N₂ purging, and they did report a shift in XPS binding energy.^[82] Although we do not exclude the possibility that the shift in binding energy is the result of interaction between Ag and ZnO, we would still like to urge researchers to perform photodeposition of Ag on ZnO in de-aerated conditions. In such way, it is less likely that Ag₂O or AgO will be formed. Preferably, a study should be performed where Ag is photodeposited on ZnO both in oxygen-rich and oxygen-free conditions. The as-synthesized samples can be analyzed by XPS and it can be confirmed whether the shift in XPS binding energy is a result of Ag₂O or AgO formation, or if it is indeed the result of electrons being transferred to the ZnO.

2.4 Photodeposition of particles on WO₃

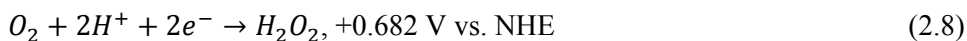
Of emerging interest in the community studying photocatalysis is the material tungsten oxide. Although its conduction band is not at a favorable position for the reduction of protons, it is non-toxic, stable under acidic conditions and has a relative narrow bandgap.^[106-109] The latter makes the material very suitable for solar-driven photocatalysis, *e.g.* in water^[110, 111] or air purification.^[112, 113] Also of interest is the implementation of WO₃ in a Z-scheme for full water splitting.^[29, 114, 115] Recent studies have demonstrated that WO₃ can be loaded through photodeposition with Pt,^[29, 30, 109, 111, 112, 116-130] Pd,^[131, 132] Ag^[18, 133] and Au.^[130, 134-136] In many cases, an increase in photocatalytic activity has been observed. Reiche *et al.* have demonstrated that Cu²⁺ removal from wastewater is possible as well by performing photodeposition of Cu on WO₃.^[137]

2.4.1 Photodeposition of Pt on WO₃

Over recent years, the photodeposition of Pt on WO₃ has gained wide-spread attention. Multiple studies have shown that loading tungsten oxide with Pt nanoparticles can enhance the photocatalytic activity significantly.^[109, 111, 112, 116, 121] For example, in a study by Abe *et al.*, photocatalytic decomposition of acetic acid, acetaldehyde and isopropyl alcohol (IPA) was studied using (Pt)/WO₃ under visible light irradiation ($400 < \lambda < 500$ nm).^[116] Unloaded WO₃ showed some activity in the decomposition of acetaldehyde, but for acetic acid and isopropyl alcohol, this was hardly present. When photodeposition of Pt on WO₃ took place, activities were enhanced drastically: a 30-fold and 100-fold increase in respectively acetic acid and IPA decomposition rate were observed. Photocatalytic decomposition studies of acetic acid are depicted in Figure 2.7. For acetaldehyde also an increase took place, but not as drastic as for the other two compounds. However, no complete acetaldehyde decomposition took place over bare WO₃, whereas this was possible for Pt/WO₃. It should be noted that different wt% loadings have been used for the different reactions, indicating that for different photochemical reactions different optimal wt% loadings were required (1 wt% of Pt for acetic acid decomposition, 0.1 wt% for acetaldehyde decomposition and 0.5 wt% for IPA decomposition). An explanation of this increase in activity has been provided by the authors as well. For the oxidation of the as-mentioned compounds, the corresponding reduction reaction has to be the reduction of oxygen:



The conduction band of WO₃ is at an unfavorable position for these reduction reactions, meaning that single-electron reduction cannot be performed with WO₃. However, theoretically, the photocatalyst should be able to perform multi-electron reactions in O₂ reduction:



Abe *et al.* discussed that Pt might act as a sink for electrons, making the as-mentioned multi-electron reactions more feasible. Indeed, the authors have shown convincingly with photoacoustic spectroscopic measurements that photoexcited electrons can

react with O_2 and that the reaction speed increases when Pt is loaded on the WO_3 surface.

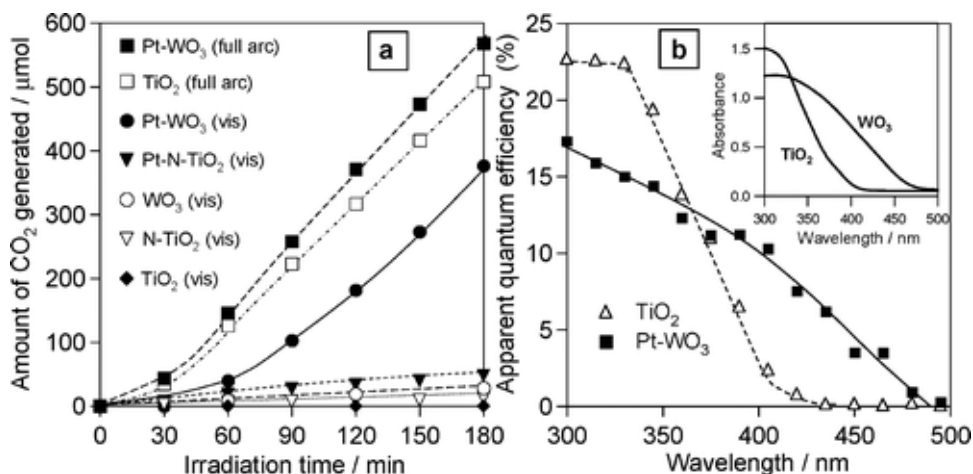


Figure 2.7. (a) Photocatalytic CO_2 production from acetic acid degradation using different photocatalysts and either full-arc ($300 < \lambda < 500$ nm) or visible light ($400 < \lambda < 500$ nm) illumination. (b) Action spectra of the photocatalytic degradation of acetic acid using TiO_2 and Pt/WO_3 . Reprinted with permission from Ref. [116]. Copyright 2016 American Chemical Society.

The formation of H_2O_2 has been confirmed by several other studies.^[109, 117-119] Kim *et al.* used photodeposition to prepare Pt/WO_3 (typically 0.5 wt% Pt), which was used to photodegrade multiple organic components under visible light illumination ($\lambda > 420$ nm).^[109] The authors demonstrated that $OH\cdot$ radicals are produced during this degradation through the photoreductive decomposition of H_2O_2 . The latter could only have formed through the earlier mentioned two-electron reduction of oxygen. For some organic compounds the authors showed that degradation took place due to $OH\cdot$ radical attacks, for others they did not observe this. In a different study by Tomita *et al.* photodegradation of phenol took place due to $OH\cdot$ radical attacks.^[117] However, these authors advocated that $OH\cdot$ is generated from water oxidation rather than H_2O_2 reduction. Some researchers have discussed as well that the lack of $O_2\cdot^-$ or $HO_2\cdot$ production can have significant consequences for the selectivity of Pt/WO_3 in photocatalysis.^[117, 119, 120]

Clearly, photodeposition of platinum can play a very important role in photocatalytic reactions concerning tungsten oxide. Detailed studies to understand this photodeposition on a fundamental level are missing however, answering questions

what the influence is of *e.g.* pH, de-aeration or the presence/absence of a sacrificial agent on for example the oxidation state of Pt or on the photodeposition speed. In most cases a sacrificial agent has been applied, mostly in the form of methanol,^[109, 112, 117, 119, 121-124] although ethanol^[124, 130] and oxalic acid^[136] have been used as well. In some cases, photodeposition took place first without a sacrificial agent, after which methanol was added later.^[111, 116, 125] To the best of our knowledge, it is not clear however why this was done. Also to the best of our knowledge, (a form of) H_2PtCl_6 has been used as a precursor in each study related to the photodeposition of Pt on WO_3 . Other parameters in literature are less consistent. For instance, some authors made use of deoxygenation,^[112, 119, 124] whereas others did not mention this.^[111, 117, 125, 126] Also, different illumination sources and illumination times were used in photodeposition. For instance, Kim *et al.* used 30 minutes of illumination using a 200 W Hg lamp,^[109] whereas Abe *et al.* used 4 hours of illumination (of which 2 hours with MeOH) using a 300 W Xe lamp in combination with a cut-off filter at 400 nm.^[116] Qamar *et al.* even demonstrated that photodeposition could be achieved with a 355 nm laser beam rather than with conventional illumination.^[124] In this study, a higher photocatalytic activity in Rhodamine 6G degradation was observed when the Pt/ WO_3 was prepared through 1 hour of laser irradiation rather than preparing this through 1 hour of conventional illumination. The morphology of the WO_3 was also different between photodeposition studies. Some people used commercial WO_3 ,^[109, 119, 121] whereas others synthesized their own WO_3 particles.^[124, 126-128] Some researchers tried to photodeposit Pt on different WO_3 samples, either by using different commercial WO_3 brands or by synthesizing the WO_3 themselves.^[111, 112, 117, 120, 123, 129] In some cases the Pt loading only served to activate the WO_3 and consequently only the Pt/ WO_3 samples were compared to each other.^[111, 117, 120] In other cases the activities between the different WO_3 samples were compared both before and after loading of platinum.^[112, 123, 129] For these studies, quite different results have been obtained. Both Xu *et al.* and Aminian *et al.* did not observe any change in the order of photocatalytic activity in acetic acid and isopropyl alcohol (IPA) degradation respectively between different self-synthesized WO_3 samples loaded with Pt.^[123, 129] However, in the latter case a comparison was also made with commercial WO_3 , which became relatively more active than the self-synthesized samples. Also, noteworthy is that the Pt/ WO_3 samples already showed some activity in the dark concerning IPA decomposition. In an interesting study by Wicaksana *et al.* not only the influence of morphology on the photodeposition process was investigated, but also the influence of the type of illumination was studied.^[112] The authors synthesized WO_3 particles with different morphologies and different crystal structures, and performed photodeposition of Pt

particles on these crystals using either 3 hours of visible light illumination or 1 hour of UV illumination. From TEM studies the authors concluded that using different WO_3 samples (hexagonal nanorod bundles, mainly monoclinic nanocubes with partially orthorhombic $\text{WO}_3 \cdot \frac{1}{3}\text{H}_2\text{O}$ and monoclinic, commercial WO_3 nanoparticles) and different illumination wavelengths will result in different kinds of Pt deposits (Figure 2.8). It should be noted that XPS studies on as-synthesized, platinumized nanocubes demonstrated that the Pt was not purely metallic (Pt^0), but slightly oxidic as well (Pt^{II}). When visible light illumination was employed, the relative Pt^{II} amount was considerably larger than when UV-illumination was used. The authors did not rule out that the total amount of photons was not sufficient to fully reduce the Pt precursor. For all samples, the authors observed a higher photocatalytic activity in ethylene conversion when UV light was employed rather than visible light. Remarkably, loading the monoclinic WO_3 samples with Pt resulted in a larger increase in photocatalytic activity than when hexagonal WO_3 nanobundles were used. Hence, the order of activity of the WO_3 samples was different before and after Pt loading.

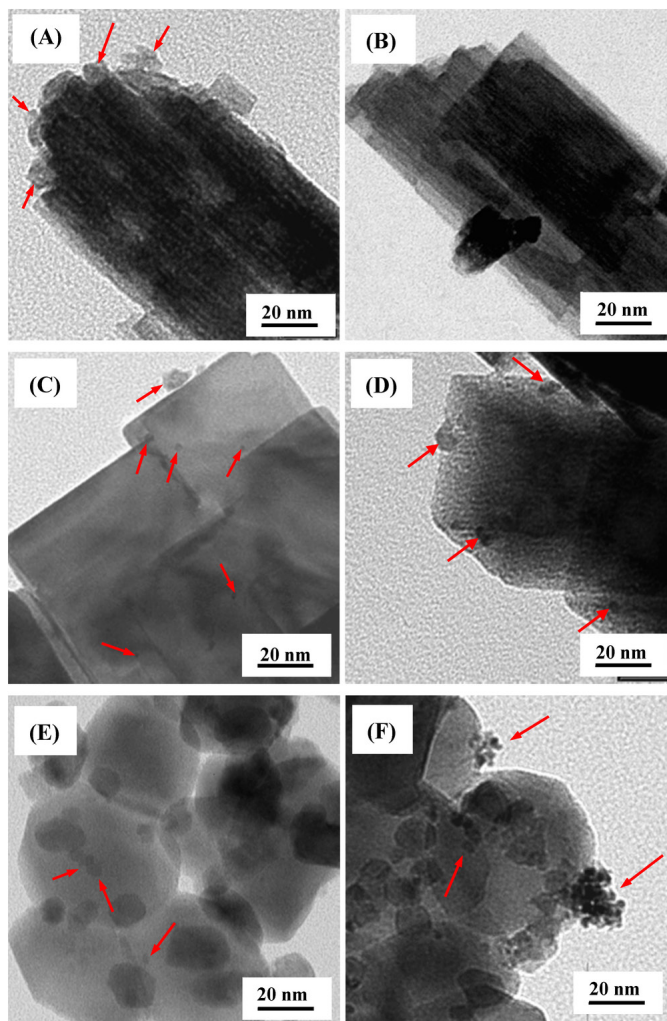


Figure 2.8. TEM images of Pt/WO₃ obtained by photodeposition of Pt on (a, b) WO₃ nanorod bundles, (c, d) WO₃ nanocubes and (e, f) commercial WO₃. Photodeposition was performed using (a, c, e) UV-A light and (b, d, f) visible light. Pt deposits are indicated with arrows. Reprinted from Ref. [112].

A parameter which has been studied relatively in detail is the percentage of wt loading on the photocatalytic activity of Pt/WO₃.^[121, 130] For instance, Sclafani *et al.* have prepared Pt/WO₃ with different loadings of Pt (ranging from 0.5 to 3 wt%).^[121] In their photodeposition procedure, methanol was used as a sacrificial agent, nitrogen flow to get rid of O₂ inside the solution and illumination times of 24 to 48 hours were used as well. The as-prepared Pt/WO₃ samples were analyzed through

several techniques, including XPS. The latter showed that Pt/WO₃ with a Pt loading of 0.5 and 1 wt% were oxidic in nature (Pt^{II}), whereas the other samples contained metallic Pt⁰. A clear explanation is not provided by the authors why this oxidized form of Pt is present. The authors have noted some other interesting features though. They advocated through their XPS studies that an increase of platinum concentration will result in larger Pt particles deposited on the WO₃ surface. Sclafani *et al.* demonstrated in phenol photo-oxidation that the samples with a higher Pt weight loading (2-3 wt% compared to 0.5-1 wt%) showed a higher photoactivity. In their discussion, they attributed this to some extent to the higher weight loading, but especially to the difference in Pt oxidation state.

Qamar *et al.* have investigated the role of the optimum loading of Pt in Pt/WO₃ for the photo-oxidation of Methyl Orange as well.^[130] They showed that 1 wt% was the optimal loading after 6 hours of illumination in their (conventional) photodeposition setup. At lower illumination times, lower activities were observed, likely the result of incomplete Pt photodeposition. Other studies have looked at the optimal wt% of Pt in the photocatalytic degradation of acetic acid (1 wt%^[116, 123] or 1.5 wt%^[122]), acetaldehyde (0.1 wt%^[116]), isopropyl alcohol (0.5 wt%^[116]) and amaranth (1 wt%^[125]). 0.2 wt% turned out to be optimal for the partial photo-oxidation of cyclohexane^[119] and 0.1 wt% for the production of phenol from benzene.^[117]

Despite the many different parameters used in photodeposition studies, the particle size of Pt photodeposited is always remarkably similar. In most cases they are on average in the range of 2 to 10 nm,^[109, 116, 117] with the exception of one study where Pt clusters of 30 nm were reported.^[122] Indeed, Shiraishi *et al.* found that the Pt particle size was more or less independent of the Pt loading (using methanol as a sacrificial reagent in the photodeposition).^[119] They found that at 0.2 wt%, the average Pt particle size was 4.7 nm and at 1.3 wt%, the average Pt particle size was 4.8 nm. Still, these results are somewhat surprising. Due to the cocatalytic effect of Pt, we would expect additional photodeposition of Pt on the Pt particles on WO₃. Thus, either the Pt particles would grow or agglomerations of Pt would be observed. Indeed, this has been shown for Pt on TiO₂^[40] or Ag on ZnO.^[69, 70] Also, we have mentioned that Sclafani *et al.* advocated an increase in Pt particle size as well at increased Pt loading on WO₃.^[121]

2.4.2 Photodeposition of other metals on WO₃

Aside from Pt, more noble metals have been photodeposited on WO₃ such as Au,^[130, 134-136] Ag^[18, 133] or Pd.^[131, 132] Qamar *et al.* demonstrated that the photodeposition of Au on WO₃ might be less interesting than Pt.^[130] The photocatalytic activity of WO₃

in Methyl Orange and 2,4-Dichlorophenoxyacetic acid decomposition was drastically enhanced when Pt was photodeposited on the sample, whereas Au turned out to be detrimental for this activity. The authors contributed this difference to the particle size of the Pt particles (2-4 nm at 1 wt% loading) and the Au particles (10-15 nm at 1 wt% loading). They claimed that shadowing of the WO_3 took place due to the relative large size of the Au particles. In contrast, Karácsonyi *et al.* and Iliev *et al.* observed higher activities in oxalic acid degradation for Au/WO_3 over respectively Pt/WO_3 and bare WO_3 .^[135, 136]

In both the photodeposition of Ag and Pd on WO_3 , enhancements in photocatalytic activity have been observed: for Ag/WO_3 in the decolorization of Acid Red 88^[133] and in acetaldehyde degradation^[18] and for Pd/WO_3 in methylene blue,^[132] oleic acid^[131] and acetaldehyde degradation.^[131, 132] It should be noted that in the studies concerning decolorization of Acid Red 88, an even further improvement in activity was observed when CuO was additionally impregnated on the Ag/WO_3 . Generally, as with Pt, the increased activity was attributed again to Ag or Pd acting as electron trapping centers, thus promoting charge separation. As shown for Pt/WO_3 by Kim *et al.*,^[109] Katsumata *et al.* demonstrated that for Ag/WO_3 $\text{OH}\cdot$ radicals are formed due to photoreduction of oxygen under visible light.^[133] The authors observed initially H_2O_2 production as well, and they attributed the $\text{OH}\cdot$ formation to H_2O_2 reduction. Strangely, the concentration of H_2O_2 decreased after 15 minutes in the experiment, likely due to reaction with additional electrons. H_2O_2 formation by Pd/WO_3 was also discussed by Sakai *et al.*^[132] However, these authors attributed the formation of H_2O_2 to superoxide formation. As the conduction band of WO_3 is not at a favorable position for this formation, we think it is more likely that the H_2O_2 was formed due to multi-electron reduction.

It should be noted that in some applications Ag photodeposition was merely performed due to AgNO_3 being used as an electron acceptor in water oxidation using WO_3 ^[138-140] or even Pt/WO_3 .^[117, 141]

In the photodeposition of Pd on WO_3 , Sakai *et al.* have demonstrated that reduction of PdCl_2 to dominantly metallic Pd can take place with black illumination in de-aerated conditions (using Ar), surprisingly without the addition of a sacrificial agent.^[132] The authors have investigated thoroughly the optimum loading of Pd on WO_3 for the degradation of aqueous methylene blue (MB) and gaseous acetaldehyde. Like Abe *et al.* for Pt/WO_3 ,^[116] they found that the optimum loading differed for different photocatalytic reactions: 0.5 wt% Pd was optimal for enhanced MB degradation, whereas 0.1 wt% Pd was optimal for acetaldehyde decomposition.

Compared to unloaded WO_3 , the activity was increased a 27-fold for MB degradation and 5.9-fold for initial acetaldehyde decomposition under optimal loading. In the studies of Abe *et al.*,^[116] a less drastic increase was observed under optimal Pt loading (0.1 wt%) for acetaldehyde decomposition. This would imply that Pd/ WO_3 would not only be cheaper to use than Pt/ WO_3 for acetaldehyde decomposition, it might also be more effective. To get a full comparison, acetaldehyde decomposition should be performed with WO_3 , Pt/ WO_3 and Pd/ WO_3 under the same reaction conditions.

Shibuya and Miyauchi studied the photodeposition of Pd on films of hexagonal WO_3 nanotrees in the presence of ethanol using different irradiation wavelengths ($\lambda = 330, 400, 500$ or 600 nm).^[131] The location of where the Pd was deposited was dependent on the wavelength. At 400 nm, more Pd particles were encountered on a lower position regarded from the top of the nanotrees than when 330 nm was used. The authors contributed this due to visible light penetrating deeper into the WO_3 nanotrees than UV light. Also, the nanotrees were more crystalline at the bottom than at the top, resulting in no deposition of Pd particles at the top of the nanotrees under visible light. Shibuya and Miyauchi also observed positioning of Pd particles at the bottom of the nanotrees at $\lambda = 500$ and 600 nm. However, hexagonal WO_3 should not be able to reduce Pd at these wavelengths due to a too large bandgap^[142, 143] (although in the case of $\lambda = 500$ nm part of the spectrum might still have been able to excite the WO_3). It is more likely that a different mechanism was responsible for reducing the PdCl_2 at the bottom of the nanotrees at these wavelengths rather than photodeposition. The authors studied the photocatalytic activity of their Pd/ WO_3 systems for the decomposition of oleic acid and acetaldehyde and found that when the Pd particles were deposited on the bottom rather than on the top, this had a beneficial influence on the photocatalytic activity. The authors contributed this amongst others to Pd particles deposited at the top shadowing the WO_3 nanotrees.

2.4.3 Photodeposition of Ag/AgX (X = Cl or Br) particles on WO_3

In recent years, loading WO_3 species with Ag/AgX (X = Cl or Br) has also attracted attention.^[144-146] These core/shell particles are plasmonic photocatalysts, where the core is made of a AgX semiconductor and the shell is made of Ag.^[144] Although the synthesis procedure of these cocatalysts is not through conventional photodeposition (where a metal ion in solution is reduced or oxidized on the surface of the photocatalyst), it is worth mentioning that an easy photochemical reduction route is used to create these particles. Typically, AgX crystals are deposited on (a form of) WO_3 particles, *e.g.* by ion exchange.^[146] Then, illumination takes place and the outer AgX is reduced to Ag, creating a Ag/AgX particle. As-synthesized Ag/AgX/ WO_3

species have been used for several photocatalytic applications: Ag/AgBr/WO₃ · H₂O for the destruction of *E. Coli* (and the degradation of Methyl Orange),^[146] Ag/AgCl/WO₃ nanoplates for the decomposition of Rhodamine B (RhB)^[145] and Ag/AgCl/W₁₈O₄₉ for the degradation of Methyl Orange.^[144]

2.4.4 Photodeposition on composite photocatalysts containing WO₃

Photodeposition does not necessarily have to be performed on a single photocatalyst. Studies are known where the concept of photodeposition was applied to prepare metal-loaded composite photocatalysts. For WO₃ this has been done for WO₃/TiO₂,^[135, 136, 147, 148] WO₃/C₃N₄,^[149] CaFe₂O₄/WO₃^[150] and CoFe₂O₄/WO₃.^[151] In such a case, either i) the photodeposition has been performed on one of the two photocatalysts first, after which the other photocatalyst was added^[136, 149, 150] or ii) the composite photocatalyst was synthesized first, after which the photodeposition took place.^[135, 147, 148, 151] For example Karácsonyi *et al.* performed photodeposition of Au and Pt on WO₃/TiO₂ composites.^[136] In this case, Au or Pt has been photodeposited on TiO₂ or WO₃ first. Afterwards the other metal oxide was added to the system. Reference samples (Pt/WO₃, Au/WO₃, Pt/TiO₂ and Au/TiO₂) were made as well. Remarkably, in this case, the bandgap of WO₃ drastically seemed to change when gold was photodeposited on WO₃, whereas this did not seem to be the case for TiO₂. The production of H₂ was studied when oxalic acid was degraded in O₂-deficient conditions under UV illumination. The oxalic acid decomposition and the H₂ production were measured. In the case of oxalic acid decomposition, the performance of the catalysts from most to least active was Pt/TiO₂ > Au/TiO₂ > Au/WO₃ > Pt/WO₃. The poor performance of Pt/WO₃ is not surprising: after all, there is no O₂ to be reduced and the CB of WO₃ is at an unfavorable position for the production of H₂. The authors found that for their hybrid systems, 3.5 to 10 wt% of WO₃ compared to TiO₂ and 1 wt% of the cocatalyst (Pt or Au) was in most cases beneficial for the oxalic acid degradation. However, differences in activities were observed when the noble metal was first photodeposited on TiO₂ than when the metal was first loaded on WO₃. For the H₂ production rate however, it turned out that the best activities were observed when no WO₃ was incorporated in the system.

2.5 Structure-directed photodeposition

In recent years, the field of structure-directed photodeposition has become popular. The concept of this kind of deposition is that in the case of reductive photodeposition, the positioning of the reduced particles reveal the reductive sites and facets of a photocatalytic material; in the case of oxidative photodeposition, the location of

oxidized particles show where the oxidative sites and facets are. Thus, the photodeposition itself is used for probing the photocatalytic active sites of a material. For instance, this concept can be used for photocatalytic systems consisting of a combination of semiconductor and metal (oxide) particles, revealing on which semiconductor/metal reduction or oxidation takes place.^[152-154] There is also evidence that favored reductive and oxidative sites exist in a single photocatalytic particle, as probed by structure-directed photodeposition. Here, we will focus on the latter.

Although the field of structure-directed deposition is relatively new, research on reductive facets has already been performed in the 90's.^[155-157] In 1998, Morris Hotsenpiller *et al.* already tried to relate the photoreduction rate of Ag^+ to the surface orientation of rutile.^[155, 156] Initially, they demonstrated that rutile films with (101), (111) and (001) orientations are more active in Ag photoreduction than films with (100) and (110) orientations.^[155] Not much later they revealed the same kind of behavior for rutile polycrystals, where they concluded that the most reactive surfaces were near the {101} plane.^[156] Although the authors did not draw real conclusions yet, they did speculate that differences between the surfaces in adsorption/desorption mechanisms, as well as differences in efficient charge separation, could be possible explanations for the differences in reduction rates. In 1999 Farneth *et al.* demonstrated structure-directed photodeposition of Ag as well on rutile.^[157] They hypothesize that this must have taken place on the {110} faces. Ohno *et al.* demonstrated in 2002 through Pt photoreduction that the favored reduction site of rutile is again the {110} face.^[50] Clearly, the results of Farneth *et al.* and Ohno *et al.* are quite different from the results of Morris Hotsenpiller *et al.* Ohno *et al.* also notified this and hypothesized that the differences observed between the different authors is due to the size of the faces: Morris Hotsenpiller *et al.* looked at films or very large crystallites, whereas Farneth *et al.* and Ohno *et al.* looked at considerably smaller particles. Therefore Ohno *et al.* thought that Morris Hotsenpiller *et al.* must have looked at isolated crystal faces, making a synergistic effect between them improbable.

Structure-directed photodeposition has sparked a lot of interest since Ohno *et al.* have demonstrated that Pt is selectively deposited on the {110} and {011} facet of respectively rutile and anatase through photoreduction.^[50] In their studies, they also showed that PbO_2 is selectively deposited on the {011} facet for rutile and the {001} facet for anatase through photo-oxidation. As-found particles are depicted in Figure 2.9. One should keep in mind however that the latter photodeposition was

done when the TiO_2 was already loaded with Pt; increased charge separation will take place on the latter due to Pt acting as an electron sink as well.^[23, 34] Nevertheless, the article has formed an important basis for subsequent studies in structure-directed photodeposition. Photocatalysts studied include TiO_2 ,^[50, 158-161] TiO_x ,^[162] SrTiO_3 ,^[163, 164] ZnO ,^[165, 166] Cu_2O ,^[167-169] BiVO_4 ,^[87, 88, 170, 171] WO_3 ,^[127] PbTiO_3 ,^[172] (La-doped) NaTaO_3 ,^[173] $\text{BaLa}_4\text{Ti}_4\text{O}_{15}$,^[28, 174] $[\text{H}_{1-x}\text{Ca}_2\text{Nb}_3\text{O}_{10}]^x$,^[175] $[\text{TBA, H}]\text{-Ca}_2\text{Nb}_3\text{O}_{10}$,^[176] CdS ,^[177] Cu_2WS_4 ,^[101] BiOCl ^[178] and AgI .^[179] A selection of important papers where both photoreduction as well as photo-oxidation have taken place to probe the reactive facets is provided in Table 2.2 (at the end of this paragraph). Typically, a noble metal such as Pt, Ag or Au is deposited in the photoreduction reactions, revealing the reductive site of a photocatalyst, whereas a metal oxide such as PbO_2 , Co_3O_4 or MnO_x is deposited in the oxidation reaction, revealing the oxidative site. However, structure-directed photodeposition does not always have to occur. Sabio *et al.* tried to perform both reductive and oxidative photodeposition using multiple cocatalysts on $[\text{TBA, H}]\text{-Ca}_2\text{Nb}_3\text{O}_{10}$ nanosheets.^[176] However, the authors observed the cocatalysts on both the edges and the nanosheet surface. Aside from the photocatalysts mentioned, structure-directed photodeposition has also been attempted to obtain metal-tipped ZnO nanorods/nanowires^[80, 180] or pyramids.^[181, 182] In these cases, structure-directed photodeposition does not occur on a specific facet, but rather on a single location.

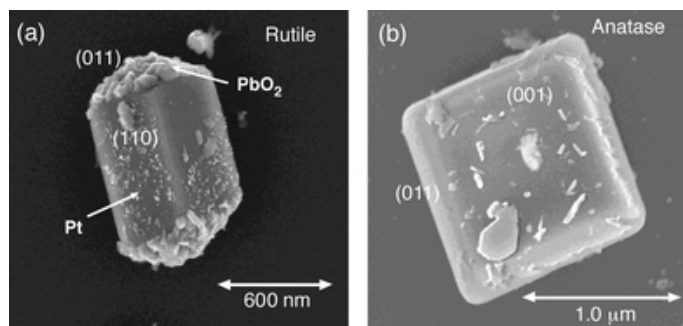


Figure 2.9. SEM images of (a) rutile and (b) anatase particles after photodeposition with first Pt, then PbO_2 . Reproduced from Ref. [50] with permission from the Centre National de la Recherche Scientifique (CNRS) and The Royal Society of Chemistry.

In general, an accepted explanation of why structure-directed photodeposition occurs is related to light-induced charge separation.^[50, 87] In such a case, the band structures of different facets will be slightly different, resulting in slight shifts of conduction bands and valence bands. Electrons and holes will migrate to the facet which is energetically the most favorable for each, resulting in favored reduction and

oxidation sites. Despite this theory, some authors (including ourselves) discussed that other phenomena may contribute to structure-directed photodeposition.^[127, 165, 177, 183] Although for several cases this may be the dominant driving force, it should not be ruled out that adsorption phenomena could play an important role as well.^[127, 177] We have demonstrated that when the latter is the dominant driving force, impregnation will result in structure-directed deposition as well.^[127] Furthermore, we have shown that additional AFM studies can be conducted to verify if different sites of a photocatalytic material yield different surface charges. Liu *et al.* have advocated that another possibility might be that other ionic compounds in the metal precursor can adsorb as well on specific facets (such as Cl⁻ in H₂PtCl₆), blocking these facets for (structure-directed) photodeposition.^[183] They based this conclusion on a study performed by Read *et al.*, where structure-directed photodeposition of Au on ZnO hexagonal rods was not observed in the absence of Cl⁻.^[165] However, when Cl⁻ was present during photodeposition, no Au was found anymore on the {0001} facet (Figure 2.10). The authors concluded that Cl⁻ must have adsorbed on this particular facet, blocking possible Au formation. These studies make clear that several verification measurements are required before it may be concluded that a photocatalytic particle exhibits favorable reduction and oxidation sites. For instance, impregnation studies could be done to rule out adsorption phenomena.

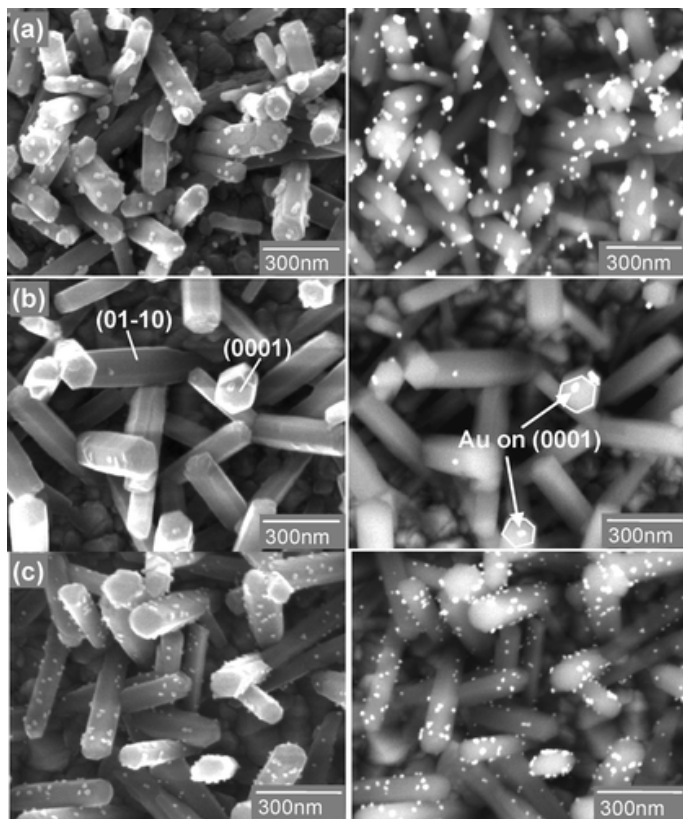


Figure 2.10. Left: Au/ZnO nanorods prepared through photodeposition using (a) 0.1 mM $\text{Au}(\text{CH}_3\text{COO})_3$, (b) 0.05 mM $\text{Au}(\text{CH}_3\text{COO})_3$ and (c) 0.05 mM AuCl_3 ethanol solution. Right: corresponding back scattered electron images. Reprinted with permission from Ref. [165]. Copyright 2016 American Chemical Society.

When structure-directed photodeposition is indeed the result of spatial charge carrier separation, possibilities for a drastic increase in the activity of a photocatalyst open up. In such a case, reduction and oxidation cocatalysts can be loaded on facets where electrons and holes accumulate respectively. A good example of a very complete study in this field has been provided by Li *et al.*, where the structure-directed photodeposition was ultimately used to obtain a BiVO_4 system with a very high photocatalytic activity.^[87] Initially, the authors demonstrated that Au, Pt and Ag were deposited on the $\{010\}$ facet of BiVO_4 through photoreduction using both anionic ($[\text{AuCl}_4]^-$, $[\text{PtCl}_6]^{2-}$) and cationic (Ag^+) precursors. In a similar way, they showed that MnO_x and PbO_2 were selectively formed on the $\{110\}$ facet through the photo-oxidation of Mn^{2+} and Pb^{2+} . These phenomena did not only happen when oxidative/reductive photodeposition was performed separately, but also when this

took place simultaneously (Figure 2.11). Also several precursors were used for MnO_x deposition (MnCl_2 , $\text{Mn}(\text{NO}_3)_2$ and MnSO_4), all resulting in similar structure-directed photodeposition. When impregnation was performed, a uniform distribution of metals/metal oxides was observed. Interestingly, the photocatalytic activity in water oxidation (with IO_3^- as electron acceptor) of BiVO_4 loaded with Pt and MnO_x through photodeposition was a lot higher than when impregnation was used. In a later study, Li *et al.* demonstrated the same phenomenon for $\text{Pt}/\text{Co}_3\text{O}_4/\text{BiVO}_4$ (in dye degradation).^[88] Comparisons between structure-directed photodeposition and impregnation have been made by other authors as well.^[28, 172] Zhen *et al.* showed that higher photocatalytic activities in hydrogen production were achieved with Pt-loaded ferroelectric PbTiO_3 when Pt was selectively photodeposited on the positively charged $\{001\}$ facet, than when the Pt was randomly distributed using impregnation.^[172] Structure-directed photodeposition does not always have to result in the highest activity of a photocatalytic material though. Jiang *et al.* showed that higher photocatalytic activities under visible light were achieved in rhodamine B degradation when an ‘*in situ* photodeposition’ method was used rather than a ‘classical photodeposition’ method to load anatase with Ag.^[159] In the case of the *in situ* photodeposition method, NaIO_3 was additionally added to a solution containing anatase and AgNO_3 . The authors hypothesized that AgIO_3 was formed during stirring in the dark, which could uniformly coat on all facets of the anatase particles. As a result, structure-directed photodeposition was only observed when classical photodeposition was used. The authors elaborated that the size of the Ag particles themselves played a large role in the photocatalytic activity, effecting the surface plasmon resonance: the *in situ* method yielded small Ag particles (1-6 nm) compared to 20 nm Ag particles when classical structure-directed photodeposition was used. Iizuka *et al.* also demonstrated that a liquid phase chemical reduction of Ag on $\text{BaLa}_4\text{Ti}_4\text{O}_{15}$ plates yielded a higher photocatalytic activity in CO_2 reduction than when either *in situ* photodeposition or impregnation was used.^[28] In this case Ag was at first randomly distributed on the $\text{BaLa}_4\text{Ti}_4\text{O}_{15}$ plates, but after 1 hour of photocatalytic reaction, the authors found that Ag particles were disappearing from the basal plane and reappearing at the edges. The authors attributed this to the photo-oxidation of Ag particles on the basal plane, which were selectively photodeposited on the edges afterwards. The size of the rephotodeposited Ag particles was smaller than the size of the classical *in situ* photodeposited Ag particles (<10 nm vs. 30-40 nm), explaining the higher activity in CO_2 reduction.

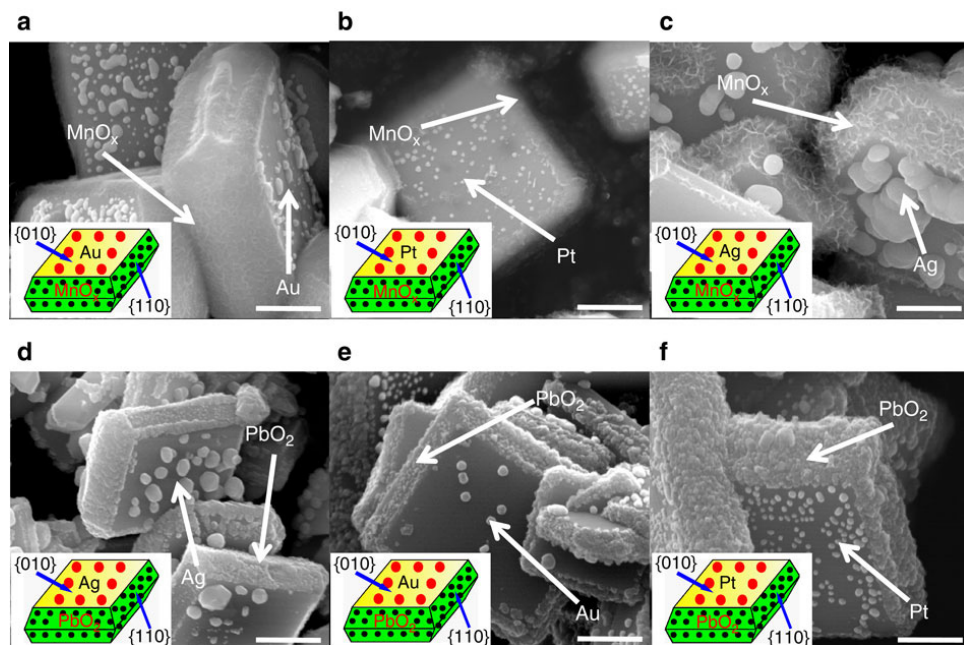


Figure 2.11. $M/MO/BiVO_4$ samples ($M = Au, Pt, Ag$; $MO = MnO_x, PbO_2$), where M and MO were simultaneously deposited through respectively photoreduction and photo-oxidation over $BiVO_4$. 5 wt% of metals/metal oxides was loaded, and the scale bar corresponds to 500 nm. Reprinted by permission from Macmillan Publishers Ltd: *Nature Communications* Ref. [87], copyright 2016.

Summarizing, structure-directed photodeposition could be a useful tool to analyze what the reductive and oxidative facets are of a photocatalyst with a well-defined morphology, provided that it is not the result of adsorption effects. Additionally, loading the reductive facet with a reduction cocatalyst and the oxidative facet with an oxidation cocatalyst can enhance the photocatalytic activity of a system drastically. Indeed, a full understanding of both the mechanism of photodeposition, as well as the concept of structure-directed photodeposition could contribute greatly to engineering a very active photocatalytic system.

Table 2.2. Selection of articles in which structure-directed photodeposition on photocatalysts has been studied distinguishing sites for reduction and oxidation. N.A. stands for not available.

<u>Photocatalyst</u>	<u>Reduction reaction</u>	<u>Oxidation reaction</u>	<u>Photo-catalytic activity after deposition</u>	<u>Additional notes</u>	<u>Ref.</u>
TiO ₂ (Rutile)	Pt {110} facet	PbO ₂ {011} facet	N.A.	Photo-oxidation performed after photoreduction	[50]
TiO ₂ (Anatase)	Pt {011} facet	PbO ₂ {001} facet	N.A.	Photo-oxidation performed after photoreduction	[50]
TiO ₂ (Decahedral anatase)	Pt {101} facet	PbO ₂ {001} facet	N.A.		[158]
TiO _x (Nanosheets)	Ag, Cu, Cu ₂ O Edges	MnO ₂ All over the surface	N.A.		[162]
SrTiO ₃ (Faceted)	Ag {100} surfaces	PbO ₂ {100} surfaces	N.A.	{100} surface is non-polar	[163]
SrTiO ₃ (Cube and tetrahedron)	Pt {001} facet	PbO ₂ {023} facet	N.A.		[164]
BaLa ₄ Ti ₄ O ₁₅ (Plate-like)	Pt: All over the surface Au: Edges Ni: Basal plane	PbO ₂ Basal plane	Ni oxidized to NiO _x . Activity lower than when NiO _x is prepared by impregnation	Two Pt precursors used. [Pt(NH ₃) ₄] ²⁺ yielded larger particles at the edge than on the basal plane. Structure-directed deposition not observed for CaLa ₄ Ti ₄ O ₁₅	[174]
BiVO ₄	Au, Pt, Ag {010} facet	PbO ₂ , MnO _x {110} facet	Increased activity in photocatalytic water oxidation and photoelectrochemical performances	Impregnation studies performed as a reference study	[87]
BiVO ₄	Pt {010} facet	Co ₃ O ₄ , MnO _x {110} facet	Increased activity in water oxidation and RhB & MO degradation	Impregnation studies performed as a reference study	[88]

Cu ₂ O (Multifaceted)	Pt Apices with high index	PbO ₂ {100} facet	N.A.		[167]
Cu ₂ O (p-type, with 26 anisotropic facets)	Au, Ag, Pt {001} facet	Co ₃ O ₄ , MnO _x {111} facet	Increased activity in MO degradation	Cu ₂ O with 8 isotropic facets did not yield structure- directed photodeposition	[168]
PbTiO ₃ (Ferroelectric nanoplates)	Pt, Au, Ag Positively charged {001} facet	MnO _x Negatively charged {001} facet	Increased activity in H ₂ generation for Pt/PbTiO ₃	Impregnation studies with Pt performed as a reference study	[172]
AgI (Microplates with polar 0001 facets)	Ag (0001) facet	MnO _x (000 $\bar{1}$) facet	Increased activity in MO degradation		[179]
Cu ₂ WS ₄	Pt, Ru {001} facet	MnS, PbS Evenly dispersed	Increased activity in H ₂ generation for Pt/Cu ₂ WS ₄	Structure-directed etching through photo-oxidation observed	[101]
BiOCl	Au {001} facet	MnO _x {110} facet in simultaneous deposition. All over the surface in single deposition	Increased activity in water splitting. Also photoelectro- chemical studies performed		[178]

2.6 Points for improvement in photodeposition studies

Although photodeposition has been used in many applications to deposit cocatalytic particles on photocatalysts, there is still room for improvement, both in fundamental understanding and in determination of optimal parameters. In this paragraph, we will describe briefly on what points improvement can be achieved.

2.6.1 Loading vs. doping

One of the most encountered misconceptions is that many researchers mistakenly describe *loading* of a cocatalyst as *doping*. To understand the difference between *loading* and *doping*, we emphasize the fundamental definition of the two concepts and the goals researchers want to achieve with this.

- *Loading* of a material on a photocatalyst is the concept of depositing the material on the surface. The goal researchers want to achieve is to enhance photocatalytic activity by the nanoparticles acting as a cocatalyst.
- *Doping* of a material is the introduction of new atoms in the crystal lattice of a photocatalyst. This is done to introduce a new energy level in between

conduction and valence band, hence allowing the photocatalyst to absorb visible light.

2.6.2 Verification of the valence state of as-deposited particles

Although some authors do pay attention through XPS to study the oxidation state of the metal they have deposited, not all authors do this. Before any conclusions can be drawn on the behaviour of cocatalytic particles, it should always be verified that the cocatalyst has the desired valence state. This has been emphasized earlier as well by Lee & Choi and Murcia *et al.*^[34, 40]

2.6.3 Verification of wt loading

After photodeposition, it is important that authors verify the wt loading of the metal (oxide) on the photocatalyst. It cannot be assumed that all the material has been deposited, unless verified by XRF or ICP. If ICP is used, measuring the metal ion content present in the precursor solution after reaction is advised over dissolving synthesized powder in a new solution, for example aqua regia. The latter has to do with the possible deposition of (unwanted) metal oxides. It cannot always be assumed that as-formed metal oxides dissolve in the newly used solution like metallic particles do. The authors will then only obtain information about the metal content, but none on the metal oxide content.

2.6.4 Measuring of the photon flux

When most photodeposition setups are described, the type of lamp and the corresponding wattage are often mentioned. However, the exact photon flux illuminating the solution containing the precursor is not. An indication of the photon flux incident on the solution during photodeposition (in mW/cm^2) might help in making better comparisons between photodeposition studies.

2.6.5 Conclusions about bandgap change

Some authors determine the bandgap of their photocatalyst, both without and with metals deposited on the material. This is done for example through UV-Vis diffuse reflectance spectroscopy. In some cases, the authors deduct a change in absorbance between the loaded and the unloaded photocatalyst, leading them to believe that there has been a change in bandgap of the photocatalyst. We consider this to be very unlikely, as only surface properties of a photocatalyst are changed, not the bulk properties. At the interface of the metal particle and the semiconductor there will be interaction, but this will be band bending: the energy gap between conduction band and valence band will remain constant. It is more likely that the as-recorded diffuse

reflectance spectrum is the sum of the diffuse reflectance spectra of both the photocatalyst and the metal nanoparticles. This will sometimes result in a (minor) shift in the absorbance deducted bandgap.

2.6.6 Conclusions on favored reductive and oxidative sites

As discussed earlier, structure-directed photodeposition is an upcoming field of study to determine the reductive and oxidative sites of a photocatalytic particle. However, we have also discussed that other phenomena might play a very important role in selective deposition of metal (oxide) particles on a photocatalyst. Therefore, researchers working in the field of structure-directed photodeposition should always verify with an additional experiment whether the positioning of metal (oxide) particles is indeed the result of site-selective deposition, and not related to (dark) sorption phenomena.

2.6.7 High temperature treatment

A final issue is that some authors perform high temperature treatment after performing photodeposition. In such a way, the authors will change properties of as-deposited particles. However, this temperature treatment should not be necessary, as careful nanoparticle engineering can be achieved solely through finding optimal photodeposition conditions. From a cost perspective, careful photodeposition studies are recommended over a post-high temperature treatment: the whole concept of photodeposition is that it is a green approach of obtaining metal (oxide) loaded photocatalysts. By calcining at high temperatures, this advantage will be forfeit.

2.7 Summary and future perspectives of photodeposition

In this chapter, we have discussed the concepts of photodeposition and the promise it might hold for efficiently loading cocatalytic nanoparticles on photocatalytic materials. We have discussed that to some extent research in photodeposition has been performed on a fundamental level for TiO_2 and for the photodeposition of Ag on ZnO. Photodeposition of Pt on WO_3 is considered very promising, but the amount of fundamental studies is limited. We have given an overview of what research has been performed in this field. To a lesser extent, we have also demonstrated what other materials than Pt nanoparticles have been photodeposited upon WO_3 . Another emerging field of research is structure-directed photodeposition: photodeposition is then used to detect favorable reductive and oxidative sites of a photocatalyst prepared through crystal facet engineering. Ultimately, loading of cocatalysts on desired sites can result in very high photocatalytic activities.

In the future, more studies on the understanding of photodeposition on a fundamental level should be performed. With the right set of conditions, it should be possible to engineer photocatalytic materials with cocatalysts of desired size, oxidation state and dispersion. Combined with crystal facet engineering, structure-directed photodeposition, either driven by light-induced charge separation or sorption, may result in highly active photocatalytic systems.

2.8 Bibliography

- [1] Kudo, A.; Miseki, Y.; *Heterogeneous photocatalyst materials for water splitting*. Chemical Society Reviews **2009**, 38, 253-278.
- [2] Maeda, K.; *Photocatalytic water splitting using semiconductor particles: history and recent developments*. Journal of Photochemistry and Photobiology C: Photochemistry Reviews **2011**, 12, 237-268.
- [3] Roy, S. C.; Varghese, O. K.; Paulose, M.; Grimes, C. A.; *Toward solar fuels: photocatalytic conversion of carbon dioxide to hydrocarbons*. ACS Nano **2010**, 4, 1259-1278.
- [4] Chong, M. N.; Jin, B.; Chow, C. W. K.; Saint, C.; *Recent developments in photocatalytic water treatment technology: a review*. Water Research **2010**, 44, 2997-3027.
- [5] Ahmed, S.; Rasul, M. G.; Martens, W. N.; Brown, R.; Hashib, M. A.; *Heterogeneous photocatalytic degradation of phenols in wastewater: a review on current status and developments*. Desalination **2010**, 261, 3-18.
- [6] Zhao, J.; Yang, X.; *Photocatalytic oxidation for indoor air purification: a literature review*. Building and Environment **2003**, 38, 645-654.
- [7] Di Paola, A.; García-López, E.; Marci, G.; Palmisano, L.; *A survey of photocatalytic materials for environmental remediation*. Journal of Hazardous Materials **2012**, 211-212, 3-29.
- [8] Ran, J.; Zhang, J.; Yu, J.; Jaroniec, M.; Qiao, S. Z.; *Earth-abundant cocatalysts for semiconductor-based photocatalytic water splitting*. Chemical Society Reviews **2014**, 43, 7787-7812.
- [9] Maeda, K.; Abe, R.; Domen, K.; *Role and function of ruthenium species as promoters with TaON-based photocatalysts for oxygen evolution in two-step water splitting under visible light*. Journal of Physical Chemistry C **2011**, 115, 3057-3064.
- [10] Kang, J. G.; Sohn, Y.; *Interfacial nature of Ag nanoparticles supported on TiO₂ photocatalysts*. Journal of Materials Science **2012**, 47, 824-832.
- [11] Ma, L. L.; Cui, Z. D.; Li, Z. Y.; Zhu, S. L.; Liang, Y. Q.; Yin, Q. W.; Yang, X. J.; *The fabrication of SnSe/Ag nanoparticles on TiO₂ nanotubes*. Materials Science and Engineering B: Solid-State Materials for Advanced Technology **2013**, 178, 77-82.
- [12] Dasgupta, N. P.; Liu, C.; Andrews, S.; Prinz, F. B.; Yang, P.; *Atomic layer deposition of platinum catalysts on nanowire surfaces for*

- photoelectrochemical water reduction*. Journal of the American Chemical Society **2013**, 135, 12932-12935.
- [13] Murata, A.; Oka, N.; Nakamura, S.; Shigesato, Y.; *Visible-light active photocatalytic WO₃ films loaded with Pt nanoparticles deposited by sputtering*. Journal of Nanoscience and Nanotechnology **2012**, 12, 5082-5086.
- [14] Bamwenda, G. R.; Tsubota, S.; Nakamura, T.; Haruta, M.; *Photoassisted hydrogen production from a water-ethanol solution: a comparison of activities of Au-TiO₂ and Pt-TiO₂*. Journal of Photochemistry and Photobiology, A: Chemistry **1995**, 89, 177-189.
- [15] Chowdhury, P.; Malekshoar, G.; Ray, M. B.; Zhu, J.; Ray, A. K.; *Sacrificial hydrogen generation from formaldehyde with Pt/TiO₂ photocatalyst in solar radiation*. Industrial and Engineering Chemistry Research **2013**, 52, 5023-5029.
- [16] Kydd, R.; Scott, J.; Teoh, W. Y.; Chiang, K.; Amal, R.; *Understanding photocatalytic metallization of preadsorbed ionic gold on titania, ceria, and zirconia*. Langmuir **2010**, 26, 2099-2106.
- [17] Liu, Y.; Wei, S.; Gao, W.; *Ag/ZnO heterostructures and their photocatalytic activity under visible light: effect of reducing medium*. Journal of Hazardous Materials **2015**, 287, 59-68.
- [18] Sun, S.; Wang, W.; Zeng, S.; Shang, M.; Zhang, L.; *Preparation of ordered mesoporous Ag/WO₃ and its highly efficient degradation of acetaldehyde under visible-light irradiation*. Journal of Hazardous Materials **2010**, 178, 427-433.
- [19] Cavalca, F.; Laursen, A. B.; Kardynal, B. E.; Dunin-Borkowski, R. E.; Dahl, S.; Wagner, J. B.; Hansen, T. W.; *In situ transmission electron microscopy of light-induced photocatalytic reactions*. Nanotechnology **2012**, 23.
- [20] Busser, G. W.; Mei, B.; Muhler, M.; *Optimizing the deposition of hydrogen evolution sites on suspended semiconductor particles using on-line photocatalytic reforming of aqueous methanol solutions*. ChemSusChem **2012**, 5, 2200-2206.
- [21] Rufus, I. B.; Viswanathan, B.; Ramakrishnan, V.; Kuriacose, J. C.; *Cadmium sulfide with iridium sulfide and platinum sulfide deposits as a photocatalyst for the decomposition of aqueous sulfide*. Journal of Photochemistry and Photobiology, A: Chemistry **1995**, 91, 63-66.
- [22] Chen, X.; Chen, W.; Gao, H.; Yang, Y.; Shangguan, W.; *In situ photodeposition of NiO_x on CdS for hydrogen production under visible light: enhanced activity by controlling solution environment*. Applied Catalysis B: Environmental **2014**, 152-153, 68-72.
- [23] Jiang, X.; Fu, X.; Zhang, L.; Meng, S.; Chen, S.; *Photocatalytic reforming of glycerol for H₂ evolution on Pt/TiO₂: fundamental understanding the effect of co-catalyst Pt and the Pt deposition route*. Journal of Materials Chemistry A **2015**, 3, 2271-2282.

- [24] Clark, W. C.; Vondjidis, A. G.; *An infrared study of the photocatalytic reaction between titanium dioxide and silver nitrate*. Journal of Catalysis **1965**, 4, 691-696.
- [25] Kraeutler, B.; Bard, A. J.; *Heterogeneous photocatalytic preparation of supported catalysts. Photodeposition of platinum on titanium dioxide powder and other substrates*. Journal of the American Chemical Society **1978**, 100, 4317-4318.
- [26] Kozlova, E. A.; Vorontsov, A. V.; *Influence of mesoporous and platinum-modified titanium dioxide preparation methods on photocatalytic activity in liquid and gas phase*. Applied Catalysis B: Environmental **2007**, 77, 35-45.
- [27] Li, J.; Xu, J.; Dai, W. L.; Fan, K.; *Dependence of Ag deposition methods on the photocatalytic activity and surface state of TiO₂ with twistlike helix structure*. Journal of Physical Chemistry C **2009**, 113, 8343-8349.
- [28] Iizuka, K.; Wato, T.; Miseki, Y.; Saito, K.; Kudo, A.; *Photocatalytic reduction of carbon dioxide over Ag cocatalyst-loaded ALA₄Ti₄O₁₅ (A = Ca, Sr, and Ba) using water as a reducing reagent*. Journal of the American Chemical Society **2011**, 133, 20863-20868.
- [29] Abe, R.; Higashi, M.; Domen, K.; *Overall water splitting under visible light through a two-step photoexcitation between TaON and WO₃ in the presence of an iodate-iodide shuttle redox mediator*. ChemSusChem **2011**, 4, 228-237.
- [30] Gunji, T.; Tsuda, T.; Jeevagan, A. J.; Hashimoto, M.; Tanabe, T.; Kaneko, S.; Miyauchi, M.; Saravanan, G.; Abe, H.; Matsumoto, F.; *Visible light induced decomposition of organic compounds on WO₃ loaded PtPb co-catalysts*. Catalysis Communications **2014**, 56, 96-100.
- [31] Oros-Ruiz, S.; Pedraza-Avella, J. A.; Guzmán, C.; Quintana, M.; Moctezuma, E.; Del Angel, G.; Gómez, R.; Pérez, E.; *Effect of gold particle size and deposition method on the photodegradation of 4-chlorophenol by Au/TiO₂*. Topics in Catalysis **2011**, 54, 519-526.
- [32] Sungbom, C.; Kawai, M.; Tanaka, K.; *XPS studies of the platinum species photodeposited on titania from aqueous chloroplatinic acid*. Bulletin of the Chemical Society of Japan **1984**, 57, 871-872.
- [33] Nakamatsu, H.; Kawai, T.; Koreeda, A.; Kawai, S.; *Electron-microscopic observation of photodeposited Pt on TiO₂ particles in relation to photocatalytic activity*. Journal of the Chemical Society, Faraday Transactions 1: Physical Chemistry in Condensed Phases **1986**, 82, 527-531.
- [34] Lee, J.; Choi, W.; *Photocatalytic reactivity of surface platinized TiO₂: substrate specificity and the effect of Pt oxidation state*. Journal of Physical Chemistry B **2005**, 109, 7399-7406.
- [35] Chanjuan, X.; Zhengshi, C.; Qinglin, L.; Zhensheng, J.; *Effects of H⁺, Cl⁻ and CH₃COOH on the photocatalytic conversion of PtCl₆²⁻ in aqueous TiO₂ dispersion*. Journal of Photochemistry and Photobiology A: Chemistry **1995**, 87, 249-255.

- [36] Zhang, F.; Chen, J.; Zhang, X.; Gao, W.; Jin, R.; Guan, N.; Li, Y.; *Synthesis of titania-supported platinum catalyst: the effect of pH on morphology control and valence state during photodeposition*. *Langmuir* **2004**, *20*, 9329-9334.
- [37] Qamar, M.; Ganguli, A. K.; *Self-assembling behaviour of Pt nanoparticles onto surface of TiO₂ and their resulting photocatalytic activity*. *Bulletin of Materials Science* **2013**, *36*, 945-951.
- [38] Mahlamvana, F.; Kriek, R. J.; *Photocatalytic reduction of platinum(II and IV) from their chloro complexes in a titanium dioxide suspension in the absence of an organic sacrificial reducing agent*. *Applied Catalysis B: Environmental* **2014**, *148-149*, 387-393.
- [39] Herrmann, J. M.; Disdier, J.; Pichat, P.; *Photoassisted platinum deposition on TiO₂ powder using various platinum complexes*. *Journal of Physical Chemistry* **1986**, *90*, 6028-6034.
- [40] Murcia, J. J.; Navío, J. A.; Hidalgo, M. C.; *Insights towards the influence of Pt features on the photocatalytic activity improvement of TiO₂ by platinisation*. *Applied Catalysis B: Environmental* **2012**, *126*, 76-85.
- [41] Yang, J. C.; Kim, Y. C.; Shul, Y. G.; Shin, C. H.; Lee, T. K.; *Characterization of photoreduced Pt/TiO₂ and decomposition of dichloroacetic acid over photoreduced Pt/TiO₂ catalysts*. *Applied Surface Science* **1997**, *121-122*, 525-529.
- [42] Li, Y.; Lu, G.; Li, S.; *Photocatalytic hydrogen generation and decomposition of oxalic acid over platinized TiO₂*. *Applied Catalysis A: General* **2001**, *214*, 179-185.
- [43] Zhao, W.; Chen, C.; Li, X.; Zhao, J.; Hidaka, H.; Serpone, N.; *Photodegradation of sulforhodamine-B dye in platinized titania dispersions under visible light irradiation: influence of platinum as a functional co-catalyst*. *Journal of Physical Chemistry B* **2002**, *106*, 5022-5028.
- [44] Sclafani, A.; Mozzanega, M. N.; Pichat, P.; *Effect of silver deposits on the photocatalytic activity of titanium dioxide samples for the dehydrogenation or oxidation of 2-propanol*. *Journal of Photochemistry and Photobiology, A: Chemistry* **1991**, *59*, 181-189.
- [45] Piwoński, I.; Kdziola, K.; Kisiełowska, A.; Soliwoda, K.; Wolszczak, M.; Lisowska, K.; Wrońska, N.; Felczak, A.; *The effect of the deposition parameters on size, distribution and antimicrobial properties of photoinduced silver nanoparticles on titania coatings*. *Applied Surface Science* **2011**, *257*, 7076-7082.
- [46] Iliev, V.; Tomova, D.; Bilyarska, L.; Tyuliev, G.; *Influence of the size of gold nanoparticles deposited on TiO₂ upon the photocatalytic destruction of oxalic acid*. *Journal of Molecular Catalysis A: Chemical* **2007**, *263*, 32-38.
- [47] Fernandez, A.; Caballero, A.; Gonzalez-Elipe, A. R.; Herrmann, J. M.; Dexpert, H.; Villain, F.; *In situ EXAFS study of the photocatalytic reduction*

- and deposition of gold on colloidal titania. *Journal of Physical Chemistry* **1995**, 99, 3303-3309.
- [48] Kriek, R. J.; Mahlamvana, F.; *Dependency on chloride concentration and 'in-sphere' oxidation of H₂O for the effective TiO₂-photocatalysed electron transfer from H₂O to [PdCl_n(H₂O)_{4-n}]²⁻ⁿ (n = 0-4) in the absence of an added sacrificial reducing agent.* *Applied Catalysis A: General* **2012**, 423-424, 28-33.
- [49] Borgarello, E.; Serpone, N.; Emo, G.; Harris, R.; Pelizzetti, E.; Minero, C.; *Light-induced reduction of rhodium(III) and palladium(II) on titanium dioxide dispersions and the selective photochemical separation and recovery of gold(III), platinum(IV), and rhodium(III) in chloride media.* *Inorganic Chemistry* **1986**, 25, 4499-4503.
- [50] Ohno, T.; Sarukawa, K.; Matsumura, M.; *Crystal faces of rutile and anatase TiO₂ particles and their roles in photocatalytic reactions.* *New Journal of Chemistry* **2002**, 26, 1167-1170.
- [51] Li, C.; Zhang, S.; Zhang, B.; Su, D.; He, S.; Zhao, Y.; Liu, J.; Wang, F.; Wei, M.; Evans, D. G.; Duan, X.; *Photohole-oxidation-assisted anchoring of ultra-small Ru clusters onto TiO₂ with excellent catalytic activity and stability.* *Journal of Materials Chemistry A* **2013**, 1, 2461-2467.
- [52] Khnayzer, R. S.; Mara, M. W.; Huang, J.; Shelby, M. L.; Chen, L. X.; Castellano, F. N.; *Structure and activity of photochemically deposited "CoPi" oxygen evolving catalyst on titania.* *ACS Catalysis* **2012**, 2, 2150-2160.
- [53] Fujii, M.; Nagasuna, K.; Fujishima, M.; Akita, T.; Tada, H.; *Photodeposition of CdS quantum dots on TiO₂: preparation, characterization, and reaction mechanism.* *Journal of Physical Chemistry C* **2009**, 113, 16711-16716.
- [54] Qin, N.; Liu, Y.; Wu, W.; Shen, L.; Chen, X.; Li, Z.; Wu, L.; *One-dimensional CdS/TiO₂ nanofiber composites as efficient visible-light-driven photocatalysts for selective organic transformation: synthesis, characterization, and performance.* *Langmuir* **2015**, 31, 1203-1209.
- [55] Zhu, H.; Yang, B.; Xu, J.; Fu, Z.; Wen, M.; Guo, T.; Fu, S.; Zuo, J.; Zhang, S.; *Construction of Z-scheme type CdS-Au-TiO₂ hollow nanorod arrays with enhanced photocatalytic activity.* *Applied Catalysis B: Environmental* **2009**, 90, 463-469.
- [56] Kim, M.; Kim, Y. K.; Lim, S. K.; Kim, S.; In, S. I.; *Efficient visible light-induced H₂ production by Au@CdS/TiO₂ nanofibers: synergistic effect of core-shell structured Au@CdS and densely packed TiO₂ nanoparticles.* *Applied Catalysis B: Environmental* **2015**, 166-167, 423-431.
- [57] Zhou, H.; Pan, J.; Ding, L.; Tang, Y.; Ding, J.; Guo, Q.; Fan, T.; Zhang, D.; *Biomass-derived hierarchical porous CdS/M/TiO₂ (M = Au, Ag, Pt, Pd) ternary heterojunctions for photocatalytic hydrogen evolution.* *International Journal of Hydrogen Energy* **2014**, 39, 16293-16301.

- [58] Tanaka, A.; Fuku, K.; Nishi, T.; Hashimoto, K.; Kominami, H.; *Functionalization of Au/TiO₂ plasmonic photocatalysts with Pd by formation of a core-shell structure for effective dechlorination of chlorobenzene under irradiation of visible light*. Journal of Physical Chemistry C **2013**, 117, 16983-16989.
- [59] Herrmann, J. M.; Disdier, J.; Pichat, P.; Fernández, A.; González-Elipe, A.; Munuera, G.; Leclercq, C.; *Titania-supported bimetallic catalyst synthesis by photocatalytic codeposition at ambient temperature: preparation and characterization of Pt-Rh, Ag-Rh, and Pt-Pd couples*. Journal of Catalysis **1991**, 132, 490-497.
- [60] Qiao, P.; Zou, S.; Xu, S.; Liu, J.; Li, Y.; Ma, G.; Xiao, L.; Lou, H.; Fan, J.; *A general synthesis strategy of multi-metallic nanoparticles within mesoporous titania via in situ photo-deposition*. Journal of Materials Chemistry A **2014**, 2, 17321-17328.
- [61] Chaudhary, R.; Singh, C.; *Removal of metal ions by means of solar oxidation processes based on pH, TiO₂ and oxidants*. Desalination and Water Treatment **2014**, 52, 1263-1271.
- [62] Kabra, K.; Chaudhary, R.; Sawhney, R. L.; *Solar photocatalytic removal of Cu(II), Ni(II), Zn(II) and Pb(II): speciation modeling of metal-citric acid complexes*. Journal of Hazardous Materials **2008**, 155, 424-432.
- [63] Teramura, K.; Okuoka, S. I.; Yamazoe, S.; Kato, K.; Shishido, T.; Tanaka, T.; *In situ time-resolved energy-dispersive XAFS study on photodeposition of Rh particles on a TiO₂ photocatalyst*. Journal of Physical Chemistry C **2008**, 112, 8495-8498.
- [64] Ohyama, J.; Teramura, K.; Okuoka, S. I.; Yamazoe, S.; Kato, K.; Shishido, T.; Tanaka, T.; *Investigation of the formation process of photodeposited Rh nanoparticles on TiO₂ by in situ time-resolved energy-dispersive XAFS analysis*. Langmuir **2010**, 26, 13907-13912.
- [65] Huang, Q.; Liu, S.; Wei, W.; Yan, Q.; Wu, C.; *Selective synthesis of different ZnO/Ag nanocomposites as surface enhanced Raman scattering substrates and highly efficient photocatalytic catalysts*. RSC Advances **2015**, 5, 27075-27081.
- [66] Wang, J.; Fan, X. M.; Tian, K.; Zhou, Z. W.; Wang, Y.; *Largely improved photocatalytic properties of Ag/tetrapod-like ZnO nanocompounds prepared with different PEG contents*. Applied Surface Science **2011**, 257, 7763-7770.
- [67] Kawano, K.; Komatsu, M.; Yajima, Y.; Haneda, H.; Maki, H.; Yamamoto, T.; *Photoreduction of Ag ion on ZnO single crystal*. Applied Surface Science **2002**, 189, 265-270.
- [68] Behnajady, M. A.; Modirshahla, N.; Shokri, M.; Zeininezhad, A.; Zamani, H. A.; *Enhancement photocatalytic activity of ZnO nanoparticles by silver doping with optimization of photodeposition method parameters*. Journal of

- Environmental Science and Health - Part A Toxic/Hazardous Substances and Environmental Engineering **2009**, 44, 666-672.
- [69] Lin, C. Y.; Lai, Y. H.; Balamurugan, A.; Vittal, R.; Lin, C. W.; Ho, K. C.; *Electrode modified with a composite film of ZnO nanorods and Ag nanoparticles as a sensor for hydrogen peroxide*. Talanta **2010**, 82, 340-347.
- [70] Li, R.; Han, C.; Chen, Q. W.; *A facile synthesis of multifunctional ZnO/Ag sea urchin-like hybrids as highly sensitive substrates for surface-enhanced Raman detection*. RSC Advances **2013**, 3, 11715-11722.
- [71] Chen, S.; Nickel, U.; *Synthesis of hybrid metal-semiconductor ultrafine particles. Photochemical deposition of silver on a ZnO colloid surface*. Journal of the Chemical Society - Faraday Transactions **1996**, 92, 1555-1562.
- [72] Peng, F.; Zhu, H.; Wang, H.; Yu, H.; *Preparation of Ag-sensitized ZnO and its photocatalytic performance under simulated solar light*. Korean Journal of Chemical Engineering **2007**, 24, 1022-1026.
- [73] Xie, W.; Li, Y.; Sun, W.; Huang, J.; Xie, H.; Zhao, X.; *Surface modification of ZnO with Ag improves its photocatalytic efficiency and photostability*. Journal of Photochemistry and Photobiology A: Chemistry **2010**, 216, 149-155.
- [74] Deng, Q.; Duan, X.; Ng, D. H. L.; Tang, H.; Yang, Y.; Kong, M.; Wu, Z.; Cai, W.; Wang, G.; *Ag nanoparticle decorated nanoporous ZnO microrods and their enhanced photocatalytic activities*. ACS Applied Materials and Interfaces **2012**, 4, 6030-6037.
- [75] Kislov, N.; Lahiri, J.; Verma, H.; Goswami, D. Y.; Stefanakos, E.; Batzill, M.; *Photocatalytic degradation of methyl orange over single crystalline ZnO: orientation dependence of photoactivity and photostability of ZnO*. Langmuir **2009**, 25, 3310-3315.
- [76] Alammar, T.; Mudring, A. V.; *Facile preparation of Ag/ZnO nanoparticles via photoreduction*. Journal of Materials Science **2009**, 44, 3218-3222.
- [77] Habibi, M. H.; Sheibani, R.; *Nanostructure silver-doped zinc oxide films coating on glass prepared by sol-gel and photochemical deposition process: application for removal of mercaptan*. Journal of Industrial and Engineering Chemistry **2013**, 19, 161-165.
- [78] Liang, Y.; Guo, N.; Li, L.; Li, R.; Ji, G.; Gan, S.; *Fabrication of porous 3D flower-like Ag/ZnO heterostructure composites with enhanced photocatalytic performance*. Applied Surface Science **2015**, 332, 32-39.
- [79] Ren, C.; Yang, B.; Wu, M.; Xu, J.; Fu, Z.; Lv, Y.; Guo, T.; Zhao, Y.; Zhu, C.; *Synthesis of Ag/ZnO nanorods array with enhanced photocatalytic performance*. Journal of Hazardous Materials **2010**, 182, 123-129.
- [80] Wang, T.; Jiao, Z.; Chen, T.; Li, Y.; Ren, W.; Lin, S.; Lu, G.; Ye, J.; Bi, Y.; *Vertically aligned ZnO nanowire arrays tip-grafted with silver nanoparticles for photoelectrochemical applications*. Nanoscale **2013**, 5, 7552-7557.

- [81] Zhang, Y.; Guo, S.; Ma, J.; Ge, H.; *Preparation, characterization, catalytic performance and antibacterial activity of Ag photodeposited on monodisperse ZnO submicron spheres*. Journal of Sol-Gel Science and Technology **2014**, 72, 171-178.
- [82] Chen, C.; Zheng, Y.; Zhan, Y.; Lin, X.; Zheng, Q.; Wei, K.; *Enhanced Raman scattering and photocatalytic activity of Ag/ZnO heterojunction nanocrystals*. Dalton Transactions **2011**, 40, 9566-9570.
- [83] Wu, J. J.; Tseng, C. H.; *Photocatalytic properties of nc-Au/ZnO nanorod composites*. Applied Catalysis B: Environmental **2006**, 66, 51-57.
- [84] Lu, L.; Hu, S.; Lee, H. I.; Wöll, C.; Fischer, R. A.; *Photoinduced growth of Cu nanoparticles on ZnO from CuCl₂ in methanol*. Journal of Nanoparticle Research **2007**, 9, 491-496.
- [85] Gomathisankar, P.; Hachisuka, K.; Katsumata, H.; Suzuki, T.; Funasaka, K.; Kaneco, S.; *Enhanced photocatalytic hydrogen production from aqueous methanol solution using ZnO with simultaneous photodeposition of Cu*. International Journal of Hydrogen Energy **2013**, 38, 11840-11846.
- [86] Stroyuk, A. L.; Shvalagin, V. V.; Kuchmii, S. Y.; *Photochemical synthesis and optical properties of binary and ternary metal-semiconductor composites based on zinc oxide nanoparticles*. Journal of Photochemistry and Photobiology A: Chemistry **2005**, 173, 185-194.
- [87] Li, R.; Zhang, F.; Wang, D.; Yang, J.; Li, M.; Zhu, J.; Zhou, X.; Han, H.; Li, C.; *Spatial separation of photogenerated electrons and holes among {010} and {110} crystal facets of BiVO₄*. Nature Communications **2013**, 4.
- [88] Li, R.; Han, H.; Zhang, F.; Wang, D.; Li, C.; *Highly efficient photocatalysts constructed by rational assembly of dual-cocatalysts separately on different facets of BiVO₄*. Energy and Environmental Science **2014**, 7, 1369-1376.
- [89] Kohtani, S.; Hiro, J.; Yamamoto, N.; Kudo, A.; Tokumura, K.; Nakagaki, R.; *Adsorptive and photocatalytic properties of Ag-loaded BiVO₄ on the degradation of 4-n-alkylphenols under visible light irradiation*. Catalysis Communications **2005**, 6, 185-189.
- [90] Maeda, K.; Lu, D.; Teramura, K.; Domen, K.; *Direct deposition of nanoparticulate rhodium-chromium mixed-oxides on a semiconductor powder by band-gap irradiation*. Journal of Materials Chemistry **2008**, 18, 3539-3542.
- [91] Busser, G. W.; Mei, B.; Pougin, A.; Strunk, J.; Gutkowski, R.; Schuhmann, W.; Willinger, M. G.; Schlögl, R.; Muhler, M.; *Photodeposition of copper and chromia on gallium oxide: the role of co-catalysts in photocatalytic water splitting*. ChemSusChem **2014**, 7, 1030-1034.
- [92] Zhou, C.; Shang, L.; Yu, H.; Bian, T.; Wu, L. Z.; Tung, C. H.; Zhang, T.; *Mesoporous plasmonic Au-loaded Ta₂O₅ nanocomposites for efficient visible light photocatalysis*. Catalysis Today **2014**, 225, 158-163.
- [93] Sasaki, Y.; Iwase, A.; Kato, H.; Kudo, A.; *The effect of co-catalyst for Z-scheme photocatalysis systems with an Fe³⁺/Fe²⁺ electron mediator on*

- overall water splitting under visible light irradiation. *Journal of Catalysis* **2008**, 259, 133-137.
- [94] Li, Q.; Chen, Z.; Zheng, X.; Jin, Z.; *Study of photoreduction of $PtCl_6^{2-}$ on CdS*. *Journal of Physical Chemistry* **1992**, 96, 5959-5962.
- [95] Jin, Z.; Chen, Z.; Li, Q.; Xi, C.; Zheng, X.; *On the conditions and mechanism of PtO_2 formation in the photoinduced conversion of H_2PtCl_6* . *Journal of Photochemistry and Photobiology, A: Chemistry* **1994**, 81, 177-182.
- [96] Wang, Y.; Wang, Y.; Xu, R.; *Photochemical deposition of Pt on CdS for H_2 evolution from water: markedly enhanced activity by controlling Pt reduction environment*. *Journal of Physical Chemistry C* **2013**, 117, 783-790.
- [97] Fox, M. A.; Pettit, T. L.; *Photoactivity of zeolite-supported cadmium sulfide: hydrogen evolution in the presence of sacrificial donors*. *Langmuir* **1989**, 5, 1056-1061.
- [98] Dukovic, G.; Merkle, M. G.; Nelson, J. H.; Hughes, S. M.; Alivisatos, A. P.; *Photodeposition of Pt on colloidal CdS and CdSe/CdS semiconductor nanostructures*. *Advanced Materials* **2008**, 20, 4306-4311.
- [99] Ma, G.; Yan, H.; Shi, J.; Zong, X.; Lei, Z.; Li, C.; *Direct splitting of H_2S into H_2 and S on CdS-based photocatalyst under visible light irradiation*. *Journal of Catalysis* **2008**, 260, 134-140.
- [100] Li, T. L.; Cai, C. D.; Yeh, T. F.; Teng, H.; *Capped $CuInS_2$ quantum dots for H_2 evolution from water under visible light illumination*. *Journal of Alloys and Compounds* **2013**, 550, 326-330.
- [101] Li, N.; Liu, M.; Zhou, Z.; Zhou, J.; Sun, Y.; Guo, L.; *Charge separation in facet-engineered chalcogenide photocatalyst: a selective photocorrosion approach*. *Nanoscale* **2014**, 6, 9695-9702.
- [102] Hara, M.; Nunoshige, J.; Takata, T.; Kondo, J. N.; Domen, K.; *Unusual enhancement of H_2 evolution by Ru on TaON photocatalyst under visible light irradiation*. *Chemical Communications* **2003**, 9, 3000-3001.
- [103] Liu, Y.; Zhou, Y.; Chen, G.; Guo, T.; Wang, L.; Huang, X.; Zeng, W.; *Loading cobalt phosphate on TaON surface as efficient noble-metal-free cocatalyst for enhanced photocatalytic water oxidation performance*. *Materials Letters* **2015**, 148, 155-158.
- [104] Moudler, J. F.; Stickle, W. F.; Sobol, P. E.; Bomben, K. D.; *Handbook of X-ray photoelectron spectroscopy: a reference book of standard spectra for identification and interpretation of XPS data*. **1992**.
- [105] La Surface. <http://www.lasurface.com> (accessed January 5th 2016).
- [106] Zheng, H.; Ou, J. Z.; Strano, M. S.; Kaner, R. B.; Mitchell, A.; Kalantar-Zadeh, K.; *Nanostructured tungsten oxide - properties, synthesis, and applications*. *Advanced Functional Materials* **2011**, 21, 2175-2196.
- [107] Kumar, S. G.; Rao, K. S. R. K.; *Tungsten-based nanomaterials (WO_3 & Bi_2WO_6): modifications related to charge carrier transfer mechanisms and photocatalytic applications*. *Applied Surface Science* **2015**, 355, 939-958.

- [108] Huang, Z. F.; Song, J.; Pan, L.; Zhang, X.; Wang, L.; Zou, J. J.; *Tungsten oxides for photocatalysis, electrochemistry, and phototherapy*. *Advanced Materials* **2015**, *27*, 5309-5327.
- [109] Kim, J.; Lee, C. W.; Choi, W.; *Platinized WO₃ as an environmental photocatalyst that generates OH radicals under visible light*. *Environmental Science and Technology* **2010**, *44*, 6849-6854.
- [110] Arai, T.; Yanagida, M.; Konishi, Y.; Ikura, A.; Iwasaki, Y.; Sugihara, H.; Sayama, K.; *The enhancement of WO₃-catalyzed photodegradation of organic substances utilizing the redox cycle of copper ions*. *Applied Catalysis B: Environmental* **2008**, *84*, 42-47.
- [111] Joshi, U. A.; Darwent, J. R.; Yiu, H. H. P.; Rosseinsky, M. J.; *The effect of platinum on the performance of WO₃ nanocrystal photocatalysts for the oxidation of Methyl Orange and iso-propanol*. *Journal of Chemical Technology and Biotechnology* **2011**, *86*, 1018-1023.
- [112] Wicaksana, Y.; Liu, S.; Scott, J.; Amal, R.; *Tungsten trioxide as a visible light photocatalyst for volatile organic carbon removal*. *Molecules* **2014**, *19*, 17747-17762.
- [113] Arai, T.; Horiguchi, M.; Yanagida, M.; Gunji, T.; Sugihara, H.; Sayama, K.; *Complete oxidation of acetaldehyde and toluene over a Pd/WO₃ photocatalyst under fluorescent- or visible-light irradiation*. *Chemical Communications* **2008**, 5565-5567.
- [114] Sayama, K.; Mukasa, K.; Abe, R.; Abe, Y.; Arakawa, H.; *Stoichiometric water splitting into H₂ and O₂ using a mixture of two different photocatalysts and an IO₃⁻/I⁻ shuttle redox mediator under visible light irradiation*. *Chemical Communications* **2001**, 2416-2417.
- [115] Sayama, K.; Mukasa, K.; Abe, R.; Abe, Y.; Arakawa, H.; *A new photocatalytic water splitting system under visible light irradiation mimicking a Z-scheme mechanism in photosynthesis*. *Journal of Photochemistry and Photobiology A: Chemistry* **2002**, *148*, 71-77.
- [116] Abe, R.; Takami, H.; Murakami, N.; Ohtani, B.; *Pristine simple oxides as visible light driven photocatalysts: highly efficient decomposition of organic compounds over platinum-loaded tungsten oxide*. *Journal of the American Chemical Society* **2008**, *130*, 7780-7781.
- [117] Tomita, O.; Ohtani, B.; Abe, R.; *Highly selective phenol production from benzene on a platinum-loaded tungsten oxide photocatalyst with water and molecular oxygen: selective oxidation of water by holes for generating hydroxyl radical as the predominant source of the hydroxyl group*. *Catalysis Science and Technology* **2014**, *4*, 3850-3860.
- [118] Gunji, T.; Jeevagan, A. J.; Hashimoto, M.; Nozawa, T.; Tanabe, T.; Kaneko, S.; Miyauchi, M.; Matsumoto, F.; *Photocatalytic decomposition of various organic compounds over WO₃-supported ordered intermetallic PtPb co-catalysts*. *Applied Catalysis B: Environmental* **2016**, *181*, 475-480.

- [119] Shiraishi, Y.; Sugano, Y.; Ichikawa, S.; Hirai, T.; *Visible light-induced partial oxidation of cyclohexane on WO₃ loaded with Pt nanoparticles*. Catalysis Science and Technology **2012**, 2, 400-405.
- [120] Tomita, O.; Abe, R.; Ohtani, B.; *Direct synthesis of phenol from benzene over platinum-loaded tungsten(VI) oxide photocatalysts with water and molecular oxygen*. Chemistry Letters **2011**, 40, 1405-1407.
- [121] Sclafani, A.; Palmisano, L.; Marci, G.; Venezia, A. M.; *Influence of platinum on catalytic activity of polycrystalline WO₃ employed for phenol photodegradation in aqueous suspension*. Solar Energy Materials and Solar Cells **1998**, 51, 203-219.
- [122] Wang, S.; Wang, T.; Liu, Y.; Gao, Y.; Ding, Y.; Xu, X.; Zhang, X.; Chen, W.; *Visible light-driven photodecomposition system: preparation and application of highly dispersed Pt-loaded WO₃ microparticles*. Micro and Nano Letters **2011**, 6, 229-232.
- [123] Xu, Z.; Tabata, I.; Hirogaki, K.; Hisada, K.; Wang, T.; Wang, S.; Hori, T.; *Preparation of platinum-loaded cubic tungsten oxide: a highly efficient visible light-driven photocatalyst*. Materials Letters **2011**, 65, 1252-1256.
- [124] Qamar, M.; Gondal, M. A.; Yamani, Z. H.; *Removal of Rhodamine 6G induced by laser and catalyzed by Pt/WO₃ nanocomposite*. Catalysis Communications **2010**, 11, 768-772.
- [125] Purwanto, A.; Widiyandari, H.; Ogi, T.; Okuyama, K.; *Role of particle size for platinum-loaded tungsten oxide nanoparticles during dye photodegradation under solar-simulated irradiation*. Catalysis Communications **2011**, 12, 525-529.
- [126] Zhang, G.; Guan, W.; Shen, H.; Zhang, X.; Fan, W.; Lu, C.; Bai, H.; Xiao, L.; Gu, W.; Shi, W.; *Organic additives-free hydrothermal synthesis and visible-light-driven photodegradation of tetracycline of WO₃ nanosheets*. Industrial and Engineering Chemistry Research **2014**, 53, 5443-5450.
- [127] Wenderich, K.; Klaassen, A.; Siretanu, I.; Mugele, F.; Mul, G.; *Sorption-determined deposition of platinum on well-defined platelike WO₃*. Angewandte Chemie - International Edition **2014**, 53, 12476-12479.
- [128] Sadakane, M.; Sasaki, K.; Kunioku, H.; Ohtani, B.; Ueda, W.; Abe, R.; *Preparation of nano-structured crystalline tungsten(VI) oxide and enhanced photocatalytic activity for decomposition of organic compounds under visible light irradiation*. Chemical Communications **2008**, 6552-6554.
- [129] Aminian, M. K.; Ye, J.; *Morphology influence on photocatalytic activity of tungsten oxide loaded by platinum nanoparticles*. Journal of Materials Research **2010**, 25, 141-148.
- [130] Qamar, M.; Yamani, Z. H.; Gondal, M. A.; Alhooshani, K.; *Synthesis and comparative photocatalytic activity of Pt/WO₃ and Au/WO₃ nanocomposites under sunlight-type excitation*. Solid State Sciences **2011**, 13, 1748-1754.

- [131] Shibuya, M.; Miyauchi, M.; *Site-selective deposition of metal nanoparticles on aligned WO₃ nanotrees for super-hydrophilic thin films*. *Advanced Materials* **2009**, 21, 1373-1376.
- [132] Sakai, Y.; Shimanaka, A.; Shioi, M.; Kato, S.; Satokawa, S.; Kojima, T.; Yamasaki, A.; *Fabrication of high-sensitivity palladium loaded tungsten trioxide photocatalyst by photodeposit method*. *Catalysis Today* **2015**, 241, 2-7.
- [133] Katsumata, H.; Oda, Y.; Kaneco, S.; Suzuki, T.; *Photocatalytic activity of Ag/CuO/WO₃ under visible-light irradiation*. *RSC Advances* **2013**, 3, 5028-5035.
- [134] Chen, X.; Li, P.; Tong, H.; Kako, T.; Ye, J.; *Nanoarchitectonics of a Au nanoprism array on WO₃ film for synergistic optoelectronic response*. *Science and Technology of Advanced Materials* **2011**, 12.
- [135] Iliev, V.; Tomova, D.; Rakovsky, S.; Eliyas, A.; Puma, G. L.; *Enhancement of photocatalytic oxidation of oxalic acid by gold modified WO₃/TiO₂ photocatalysts under UV and visible light irradiation*. *Journal of Molecular Catalysis A: Chemical* **2010**, 327, 51-57.
- [136] Karácsonyi, É.; Baia, L.; Dombi, A.; Danciu, V.; Mogyorósi, K.; Pop, L. C.; Kovács, G.; Coșoveanu, V.; Vulpoi, A.; Simon, S.; Pap, Z.; *The photocatalytic activity of TiO₂/WO₃/noble metal (Au or Pt) nanoarchitectures obtained by selective photodeposition*. *Catalysis Today* **2013**, 208, 19-27.
- [137] Reiche, H.; Dunn, W. W.; Bard, A. J.; *Heterogeneous photocatalytic and photosynthetic deposition of copper on TiO₂ and WO₃ powders*. *Journal of Physical Chemistry* **1979**, 83, 2248-2251.
- [138] Erbs, W.; Desilvestro, J.; Borgarello, E.; Grätzel, M.; *Visible-light-induced O₂ generation from aqueous dispersions of WO₃*. *Journal of Physical Chemistry* **1984**, 88, 4001-4006.
- [139] Amano, F.; Ishinaga, E.; Yamakata, A.; *Effect of particle size on the photocatalytic activity of WO₃ particles for water oxidation*. *Journal of Physical Chemistry C* **2013**, 117, 22584-22590.
- [140] Xie, Y. P.; Liu, G.; Yin, L.; Cheng, H. M.; *Crystal facet-dependent photocatalytic oxidation and reduction reactivity of monoclinic WO₃ for solar energy conversion*. *Journal of Materials Chemistry* **2012**, 22, 6746-6751.
- [141] Hong, S. J.; Jun, H.; Borse, P. H.; Lee, J. S.; *Size effects of WO₃ nanocrystals for photooxidation of water in particulate suspension and photoelectrochemical film systems*. *International Journal of Hydrogen Energy* **2009**, 34, 3234-3242.
- [142] Huang, K.; Zhang, Q.; Yang, F.; He, D.; *Ultraviolet photoconductance of a single hexagonal WO₃ nanowire*. *Nano Res.* **2010**, 3, 281-287.
- [143] Pang, H. F.; Xiang, X.; Li, Z. J.; Fu, Y. Q.; Zu, X. T.; *Hydrothermal synthesis and optical properties of hexagonal tungsten oxide nanocrystals*

- assisted by ammonium tartrate*. Physica Status Solidi (A) Applications and Materials Science **2012**, 209, 537-544.
- [144] Sun, S.; Chang, X.; Dong, L.; Zhang, Y.; Li, Z.; Qiu, Y.; *W₁₈O₄₉ nanorods decorated with Ag/AgCl nanoparticles as highly-sensitive gas-sensing material and visible-light-driven photocatalyst*. Journal of Solid State Chemistry **2011**, 184, 2190-2195.
- [145] Chen, D.; Li, T.; Chen, Q.; Gao, J.; Fan, B.; Li, J.; Li, X.; Zhang, R.; Sun, J.; Gao, L.; *Hierarchically plasmonic photocatalysts of Ag/AgCl nanocrystals coupled with single-crystalline WO₃ nanoplates*. Nanoscale **2012**, 4, 5431-5439.
- [146] Wang, P.; Huang, B.; Qin, X.; Zhang, X.; Dai, Y.; Whangbo, M. H.; *Ag/AgBr/WO₃·H₂O: visible-light photocatalyst for bacteria destruction*. Inorganic Chemistry **2009**, 48, 10697-10702.
- [147] Kovács, G.; Baia, L.; Vulpoi, A.; Radu, T.; Karácsonyi, T.; Dombi, A.; Hernádi, K.; Danciu, V.; Simon, S.; Pap, Z.; *TiO₂/WO₃/Au nanoarchitectures' photocatalytic activity, "from degradation intermediates to catalysts' structural peculiarities", Part I: Aeroxide P25 based composites*. Applied Catalysis B: Environmental **2014**, 147, 508-517.
- [148] Baia, L.; Vulpoi, A.; Radu, T.; Karácsonyi, T.; Dombi, A.; Hernádi, K.; Danciu, V.; Simon, S.; Norén, K.; Canton, S. E.; Kovács, G.; Pap, Z.; *TiO₂/WO₃/Au nanoarchitectures' photocatalytic activity "from degradation intermediates to catalysts' structural peculiarities" Part II: Aerogel based composites - fine details by spectroscopic means*. Applied Catalysis B: Environmental **2014**, 148-149, 589-600.
- [149] Ohno, T.; Murakami, N.; Koyanagi, T.; Yang, Y.; *Photocatalytic reduction of CO₂ over a hybrid photocatalyst composed of WO₃ and graphitic carbon nitride (g-C₃N₄) under visible light*. Journal of CO₂ Utilization **2014**, 6, 17-25.
- [150] Liu, Z.; Zhao, Z. G.; Miyauchi, M.; *Efficient visible light active CaFe₂O₄/WO₃ based composite photocatalysts: effect of interfacial modification*. Journal of Physical Chemistry C **2009**, 113, 17132-17137.
- [151] Yaipimai, W.; Subjaleerdee, N.; Tumcharern, G.; Intasanta, V.; *Multifunctional metal and metal oxide hybrid nanomaterials for solar light photocatalyst and antibacterial applications*. Journal of Materials Science **2015**, 50, 7681-7697.
- [152] Chen, Y. C.; Pu, Y. C.; Hsu, Y. J.; *Interfacial charge carrier dynamics of the three-component In₂O₃-TiO₂-Pt heterojunction system*. Journal of Physical Chemistry C **2012**, 116, 2967-2975.
- [153] Wei, Y.; Jiao, J.; Zhao, Z.; Zhong, W.; Li, J.; Liu, J.; Jiang, G.; Duan, A.; *3D ordered macroporous TiO₂-supported Pt@CdS core-shell nanoparticles: design, synthesis and efficient photocatalytic conversion of CO₂ with water to methane*. Journal of Materials Chemistry A **2015**, 3, 11074-11085.

- [154] Townsend, T. K.; Browning, N. D.; Osterloh, F. E.; *Overall photocatalytic water splitting with NiO_x-SrTiO₃ - a revised mechanism*. Energy and Environmental Science **2012**, 5, 9543-9550.
- [155] Morris Hotsenpiller, P. A.; Bolt, J. D.; Farneth, W. E.; Lowekamp, J. B.; Rohrer, G. S.; *Orientation dependence of photochemical reactions on TiO₂ surfaces*. Journal of Physical Chemistry B **1998**, 102, 3216-3226.
- [156] Lowekamp, J. B.; Rohrer, G. S.; Morris Hotsenpiller, P. A.; Bolt, J. D.; Farneth, W. E.; *Anisotropic photochemical reactivity of bulk TiO₂ crystals*. Journal of Physical Chemistry B **1998**, 102, 7323-7327.
- [157] Farneth, W. E.; Scott McLean, R.; Bolt, J. D.; Dokou, E.; Barteau, M. A.; *Tapping mode atomic force microscopy studies of the photoreduction of Ag⁺ on individual submicrometer TiO₂ particles*. Langmuir **1999**, 15, 8569-8573.
- [158] Murakami, N.; Kurihara, Y.; Tsubota, T.; Ohno, T.; *Shape-controlled anatase titanium(IV) oxide particles prepared by hydrothermal treatment of peroxy titanate acid in the presence of polyvinyl alcohol*. Journal of Physical Chemistry C **2009**, 113, 3062-3069.
- [159] Jiang, Z.; Ouyang, Q.; Peng, B.; Zhang, Y.; Zan, L.; *Ag size-dependent visible-light-responsive photoactivity of Ag-TiO₂ nanostructure based on surface plasmon resonance*. Journal of Materials Chemistry A **2014**, 2, 19861-19866.
- [160] Sofianou, M. V.; Boukos, N.; Vaimakis, T.; Trapalis, C.; *Decoration of TiO₂ anatase nanoplates with silver nanoparticles on the {101} crystal facets and their photocatalytic behaviour*. Applied Catalysis B: Environmental **2014**, 158-159, 91-95.
- [161] Bian, Z.; Tachikawa, T.; Kim, W.; Choi, W.; Majima, T.; *Superior electron transport and photocatalytic abilities of metal-nanoparticle-loaded TiO₂ superstructures*. Journal of Physical Chemistry C **2012**, 116, 25444-25453.
- [162] Matsumoto, Y.; Ida, S.; Inoue, T.; *Photodeposition of metal and metal oxide at the TiO_x nanosheet to observe the photocatalytic active site*. Journal of Physical Chemistry C **2008**, 112, 11614-11616.
- [163] Giocondi, J. L.; Salvador, P. A.; Rohrer, G. S.; *The origin of photochemical anisotropy in SrTiO₃*. Topics in Catalysis **2007**, 44, 529-533.
- [164] Wang, B.; Shen, S.; Guo, L.; *SrTiO₃ single crystals enclosed with high-indexed {023} facets and {001} facets for photocatalytic hydrogen and oxygen evolution*. Applied Catalysis B: Environmental **2015**, 166-167, 320-326.
- [165] Read, C. G.; Steinmiller, E. M. P.; Choi, K. S.; *Atomic plane-selective deposition of gold nanoparticles on metal oxide crystals exploiting preferential adsorption of additives*. Journal of the American Chemical Society **2009**, 131, 12040-12041.
- [166] Yu, Z. B.; Xie, Y. P.; Liu, G.; Lu, G. Q.; Ma, X. L.; Cheng, H. M.; *Self-assembled CdS/Au/ZnO heterostructure induced by surface polar charges*

- for efficient photocatalytic hydrogen evolution. *Journal of Materials Chemistry A* **2013**, 1, 2773-2776.
- [167] Zhang, L.; Shi, J.; Liu, M.; Jing, D.; Guo, L.; *Photocatalytic reforming of glucose under visible light over morphology controlled Cu₂O: efficient charge separation by crystal facet engineering*. *Chemical Communications* **2014**, 50, 192-194.
- [168] Li, R.; Tao, X.; Chen, R.; Fan, F.; Li, C.; *Synergetic effect of dual cocatalysts on the activity of p-type Cu₂O crystals with anisotropic facets*. *Chemistry - A European Journal* **2015**, 21, 14337-14341.
- [169] Wang, L.; Ge, J.; Wang, A.; Deng, M.; Wang, X.; Bai, S.; Li, R.; Jiang, J.; Zhang, Q.; Luo, Y.; Xiong, Y.; *Designing p-type semiconductor-metal hybrid structures for improved photocatalysis*. *Angewandte Chemie - International Edition* **2014**, 53, 5107-5111.
- [170] Li, H.; Sun, Y.; Cai, B.; Gan, S.; Han, D.; Niu, L.; Wu, T.; *Hierarchically Z-scheme photocatalyst of Ag@AgCl decorated on BiVO₄ (040) with enhancing photoelectrochemical and photocatalytic performance*. *Applied Catalysis B: Environmental* **2015**, 170-171, 206-214.
- [171] Booshehri, A. Y.; Chun-Kiat Goh, S.; Hong, J.; Jiang, R.; Xu, R.; *Effect of depositing silver nanoparticles on BiVO₄ in enhancing visible light photocatalytic inactivation of bacteria in water*. *Journal of Materials Chemistry A* **2014**, 2, 6209-6217.
- [172] Zhen, C.; Yu, J. C.; Liu, G.; Cheng, H. M.; *Selective deposition of redox cocatalyst(s) to improve the photocatalytic activity of single-domain ferroelectric PbTiO₃ nanoplates*. *Chemical Communications* **2014**, 50, 10416-10419.
- [173] Kato, H.; Asakura, K.; Kudo, A.; *Highly efficient water splitting into H₂ and O₂ over lanthanum-doped NaTaO₃ photocatalysts with high crystallinity and surface nanostructure*. *Journal of the American Chemical Society* **2003**, 125, 3082-3089.
- [174] Miseki, Y.; Kato, H.; Kudo, A.; *Water splitting into H₂ and O₂ over niobate and titanate photocatalysts with (111) plane-type layered perovskite structure*. *Energy and Environmental Science* **2009**, 2, 306-314.
- [175] Compton, O. C.; Carroll, E. C.; Kim, J. Y.; Larsen, D. S.; Osterloh, F. E.; *Calcium niobate semiconductor nanosheets as catalysts for photochemical hydrogen evolution from water*. *Journal of Physical Chemistry C* **2007**, 111, 14589-14592.
- [176] Sabio, E. M.; Chi, M.; Browning, N. D.; Osterloh, F. E.; *Charge separation in a niobate nanosheet photocatalyst studied with photochemical labeling*. *Langmuir* **2010**, 26, 7254-7261.
- [177] Li, Y.; Hu, Y.; Peng, S.; Lu, G.; Li, S.; *Synthesis of CdS nanorods by an ethylenediamine assisted hydrothermal method for photocatalytic hydrogen evolution*. *Journal of Physical Chemistry C* **2009**, 113, 9352-9358.

- [178] Zhang, L.; Wang, W.; Sun, S.; Jiang, D.; Gao, E.; *Selective transport of electron and hole among {001} and {110} facets of BiOCl for pure water splitting*. Applied Catalysis B: Environmental **2015**, 162, 470-474.
- [179] Kuang, Q.; Zheng, X.; Yang, S.; *AgI microplate monocrystals with polar {0001} facets: spontaneous photocarrier separation and enhanced photocatalytic activity*. Chemistry - A European Journal **2014**, 20, 2637-2645.
- [180] Pacholski, C.; Kornowski, A.; Weller, H.; *Site-specific photodeposition of silver on ZnO nanorods*. Angewandte Chemie - International Edition **2004**, 43, 4774-4777.
- [181] Yao, K. X.; Liu, X.; Zhao, L.; Zeng, H. C.; Han, Y.; *Site-specific growth of Au particles on ZnO nanopyramids under ultraviolet illumination*. Nanoscale **2011**, 3, 4195-4200.
- [182] Chanaewa, A.; Schmitt, J.; Meyns, M.; Volkmann, M.; Klinke, C.; Von Hauff, E.; *Charge Redistribution and Extraction in Photocatalytically Synthesized Au-ZnO Nanohybrids*. Journal of Physical Chemistry C **2015**, 119, 21704-21710.
- [183] Liu, G.; Yu, J. C.; Lu, G. Q.; Cheng, H. M.; *Crystal facet engineering of semiconductor photocatalysts: motivations, advances and unique properties*. Chemical Communications **2011**, 47, 6763-6783.

Chapter 3

Towards temperature-dependent crystal facet engineering of hydrate-free WO_3 with plate-like morphology

Abstract

The effect of temperature on the morphology and crystal structure of WO_3 is studied when synthesized by hydrothermal treatment of sodium tungstate in an aqueous solution of citric acid and hydrochloric acid ($\text{pH} \approx 1$). At a synthesis temperature of $120\text{ }^\circ\text{C}$ an orthorhombic tungstate hydrate phase ($WO_3 \cdot H_2O$) is formed additionally to monoclinic WO_3 , as determined by X-ray diffraction analysis. Formation of this hydrate phase is prevented by performing the hydrothermal synthesis at $170\text{ }^\circ\text{C}$, in agreement with a thermogravimetric analysis of the hydrate phase showing water elimination initiating at around $150\text{ }^\circ\text{C}$. The latter synthesis also yields particles with a well-defined morphology, albeit with somewhat lower overall surface area as compared to the synthesis conducted at $120\text{ }^\circ\text{C}$. The relevance of this study is demonstrated by determining the performance of the samples in Fe^{3+} -assisted photocatalytic dye degradation, in which the sample containing the tungstate hydrate phase is significantly less active than the monoclinic phase of WO_3 .

3.1 Introduction

Over the past decades, photocatalysis has become a promising field in the area of hydrogen production,^[1-3] water purification^[4, 5] and air purification.^[5, 6] More recently, researchers have tried to synthesize photocatalytic materials with well-defined facets through crystal facet engineering.^[7, 8] This can result in the exposure of facets which could contribute greatly to the reactivity and the selectivity of a photocatalytic material. Most research in the field of crystal facet engineering has been conducted on TiO₂. Several studies have demonstrated that extensive exposure of the {001} facet of anatase compared to the {101} facet is beneficial for the photocatalytic activity.^[9-11] However, there are reports claiming that this does not always have to be the case.^[12, 13] For instance Pan *et al.* have synthesized different (Pt-loaded) anatase crystals with either a predominant {001}, a predominant {101} or a predominant {010} facet.^[12] They found that anatase with a predominant {001} facet yielded lower photocatalytic activities in hydrogen and hydroxyl radical production than anatase with a predominant {101} facet. The highest activities were found when the {010} facet was predominantly exposed. Crystal facet engineering has also been applied for other semiconductor materials, such as zinc oxide (ZnO),^[14, 15] iron oxide (Fe₂O₃),^[16, 17] cuprous oxide (Cu₂O)^[18, 19] and bismuth vanadate (BiVO₄).^[20, 21]

One of the metal oxide photocatalysts which is very interesting for crystal facet engineering studies is tungsten oxide (WO₃). Its non-toxicity, stability in acidic conditions and narrow bandgap (around 2.62 eV for monoclinic WO₃) make it an excellent material for visible light photocatalytic applications in purification of water and air and in water oxidation.^[22-25] Many methods have been employed to synthesize WO₃, such as solvothermal synthesis,^[26, 27] sol-gel methods,^[28] chemical vapor deposition,^[29] spray pyrolysis,^[30] template directed synthesis^[31] and electrochemical etching.^[32] An easy method which opens up numerous possibilities for crystal facet engineering of WO₃ is hydrothermal synthesis. Indeed, this has already been used for the synthesis of nanoplates/nanosheets,^[33-35] nanocubes,^[34] nanowires,^[36, 37] nanorods,^[38-40] octahedra,^[41] nano-urchins^[36, 42] and flower-like morphologies.^[41, 43, 44] The importance of employing crystal facet engineering in photocatalysis using WO₃ is for instance demonstrated very well by Xie *et al.*^[34] The authors synthesized both WO₃ with a rectangular sheet-like morphology exposing dominantly the {002} facet and WO₃ with a quasi-cubic-like morphology exposing {002}, {200} and {020} facets in a nearly equal amount. When corrected for surface area the quasi-cubic-like WO₃ showed a considerably higher photocatalytic activity in oxygen production from water (sacrificial agent: AgNO₃) than the sheet-like WO₃.

On the other hand, CH₄ production from photocatalytic CO₂ reduction (in the presence of water vapor) turned out to be only possible when the sheet-like WO₃ was used. The authors contributed these phenomena to different crystal facet orientations yielding different electronic band structures.

In this chapter, we discuss crystal facet engineering of plate-like WO₃, inspired by a hydrothermal synthesis method published by Su *et al.*^[33] We emphasize the influence of synthesis temperature on the crystal phase and the obtained morphology of the WO₃ particles. The photocatalytic activity of the as-synthesized samples is evaluated in photodegradation of Orange II sodium salt, using either O₂ or Fe³⁺ as an electron scavenger. A comparison of the activity is made with commercially available WO₃. The results are discussed on the basis of crystal morphology and surface area.

3.2 Materials and methods

All chemicals of analytical grades were purchased from Sigma-Aldrich. In a typical hydrothermal synthesis, 1 g of sodium tungstate dihydrate (Na₂WO₄ · 2H₂O) and 0.6 g of citric acid were suspended in 60 mL of distilled water. Stirring was maintained until all ingredients were dissolved. Then, concentrated HCl (4.5 to 6 M) was used to adjust the pH of the solution to approximately 1. Stirring continued until a yellow precipitate was formed. Afterwards, the solution was transferred to a 125 mL Teflon-lined autoclave (4748 acid digestion vessel, Parr Instruments, in combination with a Teflon vessel insert), which was sealed off. The solution was inserted in an oven at 120 °C or 170 °C and treated for 24 hours. The samples are labeled as W120 and W170 respectively (Table 3.1).

After treatment, the autoclave was allowed to cool down. The resulting solid and solution were separated by centrifugation at 8500 rpm for 30 min. After pouring off the filtrate, the sample was washed with water and with ethanol consecutively. The remaining gel was collected and dried at a maximum temperature of 100 °C. A fraction of the samples was subsequently calcined at 250 °C for 16 hours in air applying a heating rate of 10 K min⁻¹. The calcined products are named W120-250 and W170-250 respectively (Table 3.1).

Table 3.1. Names of synthesized WO₃ samples with corresponding hydrothermal synthesis temperatures and, if applied, post-calcination temperatures.

Sample name	Hydrothermal synthesis T (°C)	Calcination T (°C)
W120	120	None
W120-250	120	250
W170	170	None
W170-250	170	250

As synthesized WO₃ samples were characterized by X-ray diffraction (XRD) (Bruker D2 Powder), thermogravimetric analysis (TGA) (Netzsch STA449 F3), high resolution-scanning electron microscopy (HR-SEM) (Zeiss MERLIN HR-SEM) and Brunauer–Emmett–Teller (BET) surface area measurements (Micromeritics Tristar 3000 measuring apparatus). XRD analysis was performed using the copper K α line under an accelerating voltage of 30 kV. TGA analysis was performed using a heating rate of 10 K min⁻¹ in a N₂ atmosphere. The measurements took place with 5.84 mg of W120 and 8.93 mg of W170. Roughly 44.5 hours prior to BET surface area measurements samples were outgassed at 300 °C. The amounts of samples used were 179 mg, 122 mg and 244 mg for W120-250, W170-250 and commercial WO₃ respectively. Measurements of the Kubelka-Munk plot and the corresponding Tauc plot were performed using diffuse reflectance spectroscopy. In the latter case, a DRS-cell (Harrick, Praying Mantis) was combined with a UV-Vis spectrophotometer (Thermo Scientific, Evolution 600). As described by Montini *et al.* the intersection of the slope of the Tauc plot with the baseline was used to determine the bandgap of the materials.^[45]

The photocatalytic performance of commercial WO₃, W120-250 and W170-250 was tested and compared in (Fe³⁺-assisted) photodegradation of Orange II sodium salt. To this end, 25 mg of photocatalyst was added to 50 mL of a 0.15 mM Orange II sodium salt aqueous solution, which was adjusted to pH \approx 3 (using HCl). The slurry solution was first stirred for an hour in the dark to get an even distribution of the photocatalytic particles and to achieve adsorption/desorption equilibrium of the dye. Then, illumination took place inside a black box reactor as described by Romão *et al.* under continuous stirring.^[46] All Philips TL-D 18W BLB lamps ($\lambda = 375$ nm, $I = 3.21$ mW cm⁻²) were used. In the initial experiments, only O₂ acted as reducing agent (electron scavenger). At each measurement, a small amount of slurry solution was pipetted out, the powder was filtered out (using Whatman Spartan 30/02 RC filters) and the absorption spectrum of the remaining filtrate was measured with a UV-Vis spectrophotometer (Thermo Scientific, Evolution 600). According to

Lambert-Beer's law, the absorbance of the filtrate correlates linearly to the concentration of the dye. The largest absorption maximum of the absorption spectrum of Orange II sodium salt is centered at 485 nm. By monitoring this absorption maximum of the solution over time, a photodegradation profile was determined. Before the measurements took place, the lamps were allowed to reach full intensity for 1 to 2 minutes. Inspired by Kato *et al.*,^[47] the Orange II sodium salt photodegradation measurements were also performed using Fe³⁺ rather than O₂ as an electron scavenger. To this end, 2.0 mM FeCl₃ was added to the Orange II sodium salt solution and the pH subsequently lowered to 1.6 (using HCl).

3.3 Results and discussion

3.3.1 Characterization of as-synthesized WO₃ samples

Figure 3.1 shows typical X-ray diffraction (XRD) patterns of the synthesized WO₃ samples. For W120, diffraction lines of both orthorhombic WO₃ · H₂O and monoclinic WO₃ are observed (JCPDS No. 84-0886 and JCPDS No. 83-0950, respectively). Calcination of these powders at 250 °C results in the transition of orthorhombic WO₃ · H₂O to monoclinic WO₃. For W170, the XRD pattern corresponds dominantly to the monoclinic structure with minor WO₃ · 0.33H₂O groups being present (JCPDS No. 87-1203). No formation of orthorhombic WO₃ · H₂O is detected. In this case, calcination at 250 °C does not yield any phase transformations.

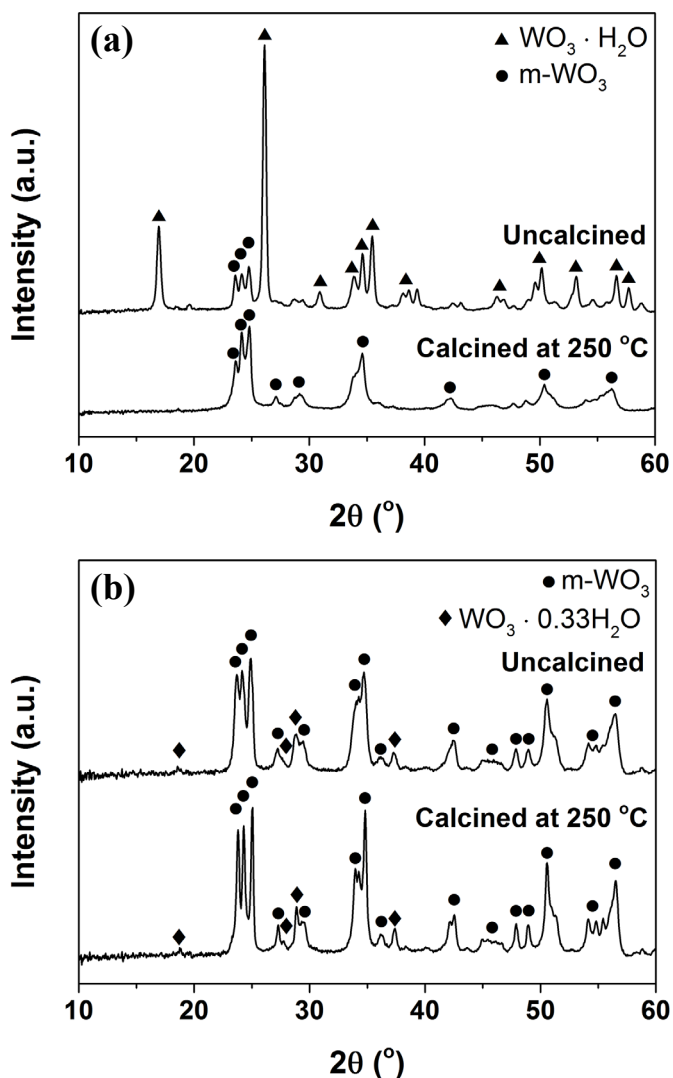


Figure 3.1. XRD patterns of WO_3 samples hydrothermally synthesized at (a) 120 °C and (b) 170 °C, before and after calcination at 250 °C.

TGA measurements (Figure 3.2) confirm that the hydrate phase is thermally not very stable. The hydrate decomposes in the temperature range of 150–250 °C. Earlier studies by Sánchez-Martínez *et al.* confirm that orthorhombic $\text{WO}_3 \cdot \text{H}_2\text{O}$ is decomposed in monoclinic WO_3 in the temperature range of at least 120 °C to 450 °C.^[48]

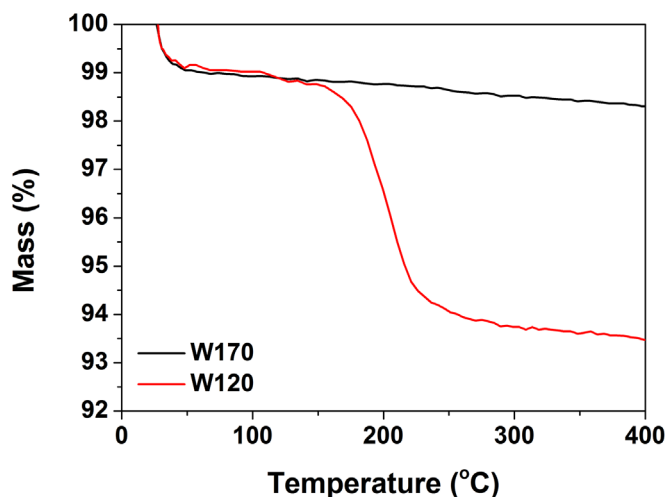


Figure 3.2. TGA profiles of W120 and W170. Evaporation of physisorbed water contributes to the initial mass loss below 100 °C.

Contrary to the observed formation of the monoclinic phase, Su *et al.* stated that using citric acid as a capping agent will result in the formation of orthorhombic WO_3 square nanoplates. However, according to a paper by Zheng *et al.*, the orthorhombic crystal phase of WO_3 particles is much less likely to be formed than the monoclinic phase, based on differences in thermodynamic stability.^[22] When we compare the XRD pattern of Su *et al.* with the XRD patterns of Jiayin *et al.*,^[49] we hypothesize that Su *et al.* have also obtained the monoclinic WO_3 crystal structure, with traces of orthorhombic $\text{WO}_3 \cdot 0.33\text{H}_2\text{O}$.

Typical HR-SEM images of W120-250 and W170-250 are depicted in Figure 3.3. For comparison a HR-SEM image of commercial WO_3 (Aldrich, nanopowder, <100 nm particle size (TEM)) is also included. The as-synthesized samples show plate-like morphology. For W120-250 the morphology is not really well-defined. The edges are somewhat irregular and some irregularities are also present on the main facets of the particles. The morphology is more defined for W170-250. These particles exhibit sharp edges and clear planes. Commercial WO_3 clearly has a totally different morphology: the particles are sphere-like shaped, where the surface of the spheres exposes multiple facets.

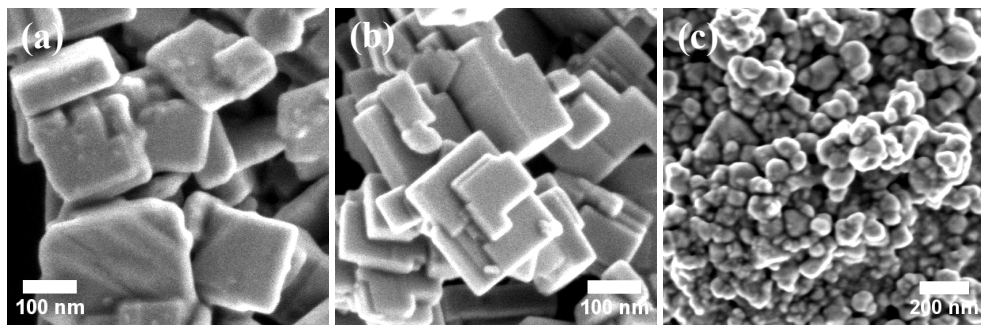


Figure 3.3. HR-SEM images of (a) W120-250, (b) W170-250 and (c) commercial WO_3 .

The BET surface area of the as-synthesized WO_3 samples was determined using N_2 adsorption/desorption isotherms (typical results are depicted in Table 3.2 and in the appendix, Figure A3.1). For comparison, the BET surface area of commercial WO_3 (<100 nm particle size) is reported in Table 3.2 as well.

Table 3.2. BET surface areas of different WO_3 particles.

Sample name	BET surface area ($\text{m}^2 \text{g}^{-1}$)
W120-250	12.8
W170-250	8.4
Commercial WO_3	7.3

The BET surface areas of the as-synthesized samples are in agreement with the HR-SEM results depicted in Figure 3.3: a larger BET surface area is expected for W120-250 than for W170-250, as W120-250 exhibits more irregularities on the surface. The commercial WO_3 has an apparently smaller surface area as compared to the as-synthesized samples.

The Kubelka-Munk and Tauc plots constructed from the diffuse reflectance spectra of the as-synthesized materials and commercial WO_3 are depicted in Figure 3.4. Clearly, the bandgaps of the synthesized materials and commercial WO_3 are similar (around 2.63 eV) and in correspondence with the values mentioned in the literature.

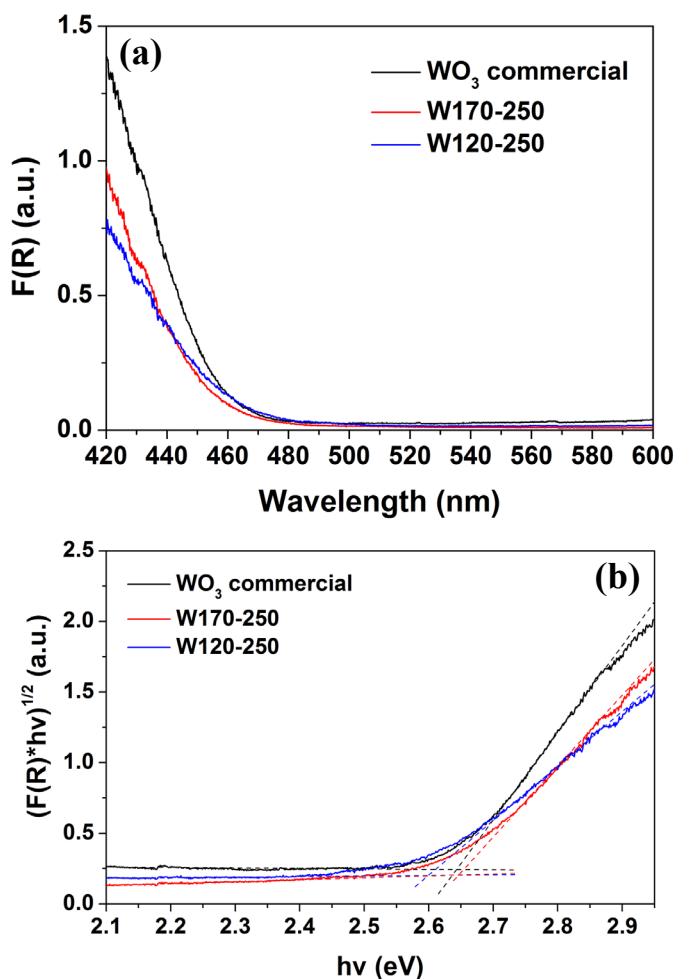


Figure 3.4. (a) Kubelka-Munk plot and (b) Tauc plot of the synthesized samples and commercial WO_3 .

3.3.2 Photocatalytic performance of synthesized WO_3 samples

Figure 3.5 shows an example of a photodegradation profile of Orange II sodium salt using commercial WO_3 as a photocatalyst and O_2 as an electron scavenger. The dye is degraded into a less colorful product over time. A plot of the absorption maxima in Figure 3.5 can be linearized by assuming first order behaviour in Orange II sodium salt decomposition (Figure 3.6a). Using Equation 3.1 the rate constant (k) per surface area is calculated:

$$\frac{dC_A}{dt} = -k \cdot A_{cat} \cdot C_A \quad (3.1)$$

C_A is the concentration of the dye, t is the illumination time (where $t = 0$ corresponds to the start of illumination inside the reactor) and A_{cat} is the available surface area (Table 3.2) of the catalyst present in the reactor. The calculated rate constants per surface area of the different samples are compared in Figure 3.6b.

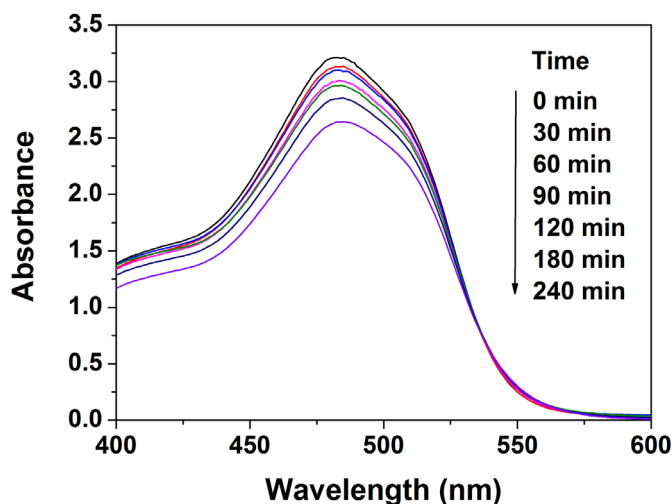


Figure 3.5. Absorbance spectrum of 50 mL of 0.15 mM Orange II sodium salt solution, illuminated in a slurry solution containing 25 mg of commercial WO_3 .

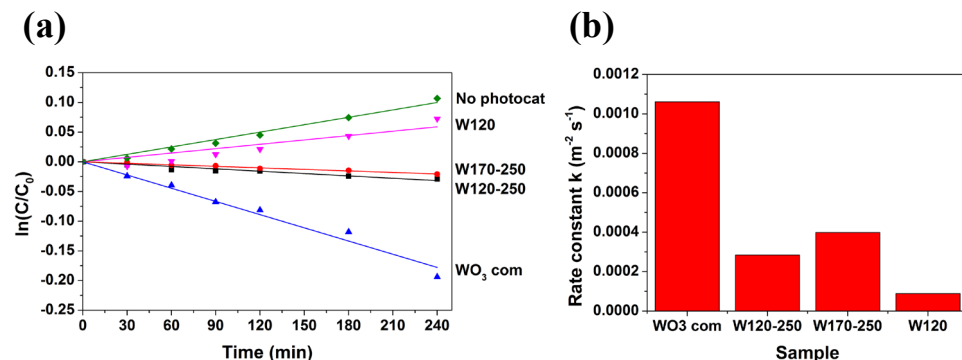


Figure 3.6. (a) Photocatalytic degradation of 0.15 mM Orange II sodium salt and (b) corresponding rate constants ($m^2 s^{-1}$) using different WO_3 samples and O_2 as an electron scavenger. The calculated rate constants are corrected for evaporation of the solution during the experiment, which causes the rising slope for the blank experiment in (a). For the calculation of the rate constant of W120, the surface area of W120-250 ($12.8 m^2 g^{-1}$) is used.

Commercial WO₃ shows low photocatalytic activity, whereas W120-250 and W170-250 are even less active; W120 has the lowest activity due to the presence of the orthorhombic hydrate phase, which presumably provides recombination centers for electrons and holes. In general, the lack of activity of WO₃ is likely due to the low catalytic activity of WO₃ for oxygen reduction. The differences in rate constants of the samples can be explained by the exposed facets of the materials. For W170-250, only three kinds of facets are intensively exposed: the {002} facet, the {200} facet and the {020} facet. This is to a lesser extent also true for W120-250. In the case of commercial WO₃, presumably many facets are exposed to reactants. Apparently, the facets exposed in W170-250 and W120-250 are particularly unreactive for sorption and reduction of O₂, whereas one or more of the facets exposed in commercial WO₃ presumably contribute to oxygen sorption and reduction efficiency.

When Fe³⁺ is used as an electron scavenger, in addition to O₂, clearly a higher dye degradation activity is observed for W120-250, W170-250 and commercial WO₃ (Figure 3.7). Again, W120 doesn't show any enhancement in degradation rate when compared to the reference experiment, presumably related to the negative effect of the presence of the hydrate phase on the physical properties of the photocatalyst. Remarkable is that the rate constants of commercial WO₃ and W120-250 are now similar, whereas the rate constant of W170-250 is significantly smaller. Again, it can be concluded that the types of facets exposed for the various materials play an important role in determining photocatalytic activity. This time, some of the facets exposed in both commercial WO₃ and W120-250 contribute to a higher activity in Fe³⁺ reduction than the {002}, {200}, and {020} facets exposed in W170-250. Now, preferred adsorption of Fe³⁺ on different or additional facets as compared to oxygen is likely.

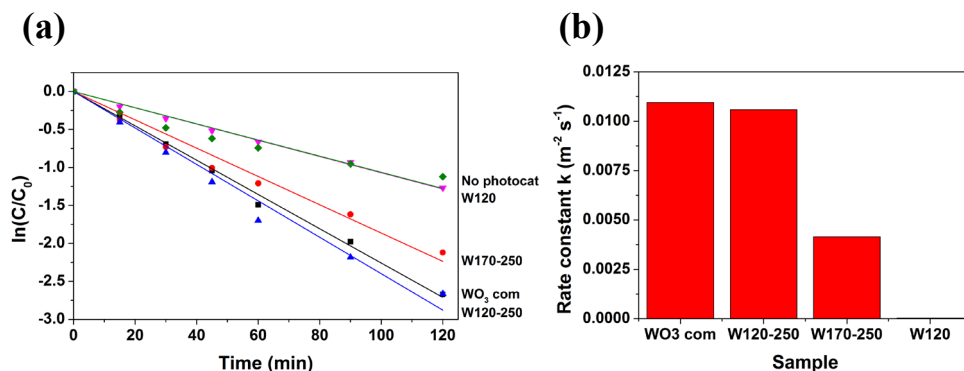


Figure 3.7. (a) Photocatalytic degradation of 0.15 mM Orange II sodium salt and (b) corresponding rate constants ($m^2 s^{-1}$) using different WO_3 samples and Fe^{3+} as an electron scavenger. The calculated rate constants are corrected for degradation of the dye during the experiment without a photocatalyst. For the calculation of the rate constant of W120, the surface area of W120-250 ($12.8 m^2 g^{-1}$) is used.

Studies on the influence of morphology of tungsten oxide (hydrates) on the photocatalytic activity have been reported previously,^[27, 41-43, 50, 51] including monoclinic WO_3 .^[34, 44, 52, 53] Sánchez Martínez *et al.* synthesized monoclinic WO_3 particles through calcination of a precursor at 500 °C, 600 °C and 700 °C and ambient pressures.^[48] They detected plate-like and ovoid-like WO_3 particles, where most particles at 500 °C were plate-like and had a high surface area, and most particles at 700 °C were ovoid-like and had a low surface area. The particles synthesized at 700 °C gave the highest activity, which led the authors to conclude that the surface area is not the dominant factor in determining photocatalytic activity, but rather the degree of crystallinity. However, they did not take into account that the morphology itself of the samples might have an influence as well. One could also hypothesize that when their photocatalytic degradation rates are actually corrected for BET surface areas, the plate-like particles are even *significantly* less active than the ovoid-like particles. This would actually be in agreement with our results. As described in the introduction, a paper which does describe the influence of WO_3 facets on photocatalytic activity in detail has been published by Xie *et al.*^[34] These studies confirm how important the exposure of specific facets can be in photocatalysis, and that controlled synthesis aimed at maximizing the presence of the most active facets is desired.^[7]

Despite the low activity in dye photodegradation of W170-250, this sample is very relevant for this thesis, which aims at understanding photodeposition of platinum on well-defined plate-like tungsten oxide.

3.4 Conclusions

Concluding, we have synthesized monoclinic WO₃ with a poorly defined, as well as a well-defined plate-like morphology. The hydrothermal synthesis temperature was found to largely affect the morphology and the amount of hydrate in the synthesized materials. A higher temperature results in the absence of WO₃ · H₂O and a better defined morphology. The presence of the hydrate phase was found detrimental to catalytic activity. When Fe³⁺ is used as an electron scavenger, the WO₃ sample with a well-defined morphology yields a relatively low photocatalytic activity, presumably due to exposure of facets unfavorable for Fe³⁺ adsorption.

3.5 Bibliography

- [1] Chen, X.; Li, C.; Grätzel, M.; Kostecki, R.; Mao, S. S.; *Nanomaterials for renewable energy production and storage*. Chemical Society Reviews **2012**, 41, 7909-7937.
- [2] Maeda, K.; *Photocatalytic water splitting using semiconductor particles: history and recent developments*. Journal of Photochemistry and Photobiology C: Photochemistry Reviews **2011**, 12, 237-268.
- [3] Osterloh, F. E.; *Inorganic nanostructures for photoelectrochemical and photocatalytic water splitting*. Chemical Society Reviews **2013**, 42, 2294-2320.
- [4] Ahmed, S.; Rasul, M. G.; Brown, R.; Hashib, M. A.; *Influence of parameters on the heterogeneous photocatalytic degradation of pesticides and phenolic contaminants in wastewater: a short review*. Journal of Environmental Management **2011**, 92, 311-330.
- [5] Di Paola, A.; García-López, E.; Marci, G.; Palmisano, L.; *A survey of photocatalytic materials for environmental remediation*. Journal of Hazardous Materials **2012**, 211-212, 3-29.
- [6] Mo, J.; Zhang, Y.; Xu, Q.; Lamson, J. J.; Zhao, R.; *Photocatalytic purification of volatile organic compounds in indoor air: a literature review*. Atmospheric Environment **2009**, 43, 2229-2246.
- [7] Liu, G.; Yu, J. C.; Lu, G. Q.; Cheng, H. M.; *Crystal facet engineering of semiconductor photocatalysts: motivations, advances and unique properties*. Chemical Communications **2011**, 47, 6763-6783.
- [8] Zheng, J. Y.; Haider, Z.; Van, T. K.; Pawar, A. U.; Kang, M. J.; Kim, C. W.; Kang, Y. S.; *Tuning of the crystal engineering and photoelectrochemical properties of crystalline tungsten oxide for optoelectronic device applications*. CrystEngComm **2015**, 17, 6070-6093.
- [9] Yang, H. G.; Liu, G.; Qiao, S. Z.; Sun, C. H.; Jin, Y. G.; Smith, S. C.; Zou, J.; Cheng, H. M.; Lu, G. Q.; *Solvothermal synthesis and photoreactivity of anatase TiO₂ nanosheets with dominant {001} facets*. Journal of the American Chemical Society **2009**, 131, 4078-4083.

- [10] Zhu, J.; Wang, S.; Bian, Z.; Xie, S.; Cai, C.; Wang, J.; Yang, H.; Li, H.; *Solvothermally controllable synthesis of anatase TiO₂ nanocrystals with dominant {001} facets and enhanced photocatalytic activity*. CrystEngComm **2010**, 12, 2219-2224.
- [11] Wu, Q.; Liu, M.; Wu, Z.; Li, Y.; Piao, L.; *Is photooxidation activity of {001} facets truly lower than that of {101} facets for anatase TiO₂ crystals?* Journal of Physical Chemistry C **2012**, 116, 26800-26804.
- [12] Pan, J.; Liu, G.; Lu, G. Q.; Cheng, H. M.; *On the true photoreactivity order of {001}, {010}, and {101} facets of anatase TiO₂ crystals*. Angewandte Chemie - International Edition **2011**, 50, 2133-2137.
- [13] Gordon, T. R.; Cargnello, M.; Paik, T.; Mangolini, F.; Weber, R. T.; Fornasiero, P.; Murray, C. B.; *Nonaqueous synthesis of TiO₂ nanocrystals using TiF₄ to engineer morphology, oxygen vacancy concentration, and photocatalytic activity*. Journal of the American Chemical Society **2012**, 134, 6751-6761.
- [14] Boppella, R.; Anjaneyulu, K.; Basak, P.; Manorama, S. V.; *Facile synthesis of face oriented ZnO crystals: tunable polar facets and shape induced enhanced photocatalytic performance*. Journal of Physical Chemistry C **2013**, 117, 4597-4605.
- [15] Zeng, J. H.; Jin, B. B.; Wang, Y. F.; *Facet enhanced photocatalytic effect with uniform single-crystalline zinc oxide nanodisks*. Chemical Physics Letters **2009**, 472, 90-95.
- [16] Wu, W.; Hao, R.; Liu, F.; Su, X.; Hou, Y.; *Single-crystalline α -Fe₂O₃ nanostructures: controlled synthesis and high-index plane-enhanced photodegradation by visible light*. Journal of Materials Chemistry A **2013**, 1, 6888-6894.
- [17] Chen, J. S.; Zhu, T.; Yang, X. H.; Yang, H. G.; Lou, X. W.; *Top-down fabrication of α -Fe₂O₃ single-crystal nanodiscs and microparticles with tunable porosity for largely improved lithium storage properties*. Journal of the American Chemical Society **2010**, 132, 13162-13164.
- [18] Jiang, D.; Xing, C.; Liang, X.; Shao, L.; Chen, M.; *Synthesis of cuprous oxide with morphological evolution from truncated octahedral to spherical structures and their size and shape-dependent photocatalytic activities*. Journal of Colloid and Interface Science **2016**, 461, 25-31.
- [19] Zhang, Y.; Deng, B.; Zhang, T.; Gao, D.; Xu, A. W.; *Shape effects of Cu₂O polyhedral microcrystals on photocatalytic activity*. Journal of Physical Chemistry C **2010**, 114, 5073-5079.
- [20] Li, R.; Zhang, F.; Wang, D.; Yang, J.; Li, M.; Zhu, J.; Zhou, X.; Han, H.; Li, C.; *Spatial separation of photogenerated electrons and holes among {010} and {110} crystal facets of BiVO₄*. Nature Communications **2013**, 4.
- [21] Li, C.; Zhang, P.; Lv, R.; Lu, J.; Wang, T.; Wang, S.; Wang, H.; Gong, J.; *Selective deposition of Ag₃PO₄ on monoclinic BiVO₄(040) for highly efficient photocatalysis*. Small **2013**, 9, 3951-3956.

- [22] Zheng, H.; Ou, J. Z.; Strano, M. S.; Kaner, R. B.; Mitchell, A.; Kalantar-Zadeh, K.; *Nanostructured tungsten oxide - properties, synthesis, and applications*. *Advanced Functional Materials* **2011**, 21, 2175-2196.
- [23] Kim, J.; Lee, C. W.; Choi, W.; *Platinized WO_3 as an environmental photocatalyst that generates OH radicals under visible light*. *Environmental Science and Technology* **2010**, 44, 6849-6854.
- [24] Huang, Z. F.; Song, J.; Pan, L.; Zhang, X.; Wang, L.; Zou, J. J.; *Tungsten oxides for photocatalysis, electrochemistry, and phototherapy*. *Advanced Materials* **2015**, 27, 5309-5327.
- [25] Sun, S.; Wang, W.; Zeng, S.; Shang, M.; Zhang, L.; *Preparation of ordered mesoporous Ag/WO_3 and its highly efficient degradation of acetaldehyde under visible-light irradiation*. *Journal of Hazardous Materials* **2010**, 178, 427-433.
- [26] Choi, H. G.; Jung, Y. H.; Kim, D. K.; *Solvothermal synthesis of tungsten oxide nanorod/nanowire/nanosheet*. *Journal of the American Ceramic Society* **2005**, 88, 1684-1686.
- [27] Zhao, Z. G.; Miyauchi, M.; *Shape modulation of tungstic acid and tungsten oxide hollow structures*. *Journal of Physical Chemistry C* **2009**, 113, 6539-6546.
- [28] Deepa, M.; Joshi, A. G.; Srivastava, A. K.; Shivaprasad, S. M.; Agnihotry, S. A.; *Electrochromic nanostructured tungsten oxide films by sol-gel: structure and intercalation properties*. *Journal of the Electrochemical Society* **2006**, 153, C365-C376.
- [29] Shankar, N.; Yu, M. F.; Vanka, S. P.; Glumac, N. G.; *Synthesis of tungsten oxide (WO_3) nanorods using carbon nanotubes as templates by hot filament chemical vapor deposition*. *Materials Letters* **2006**, 60, 771-774.
- [30] Regragui, M.; Addou, M.; Outzourhit, A.; Bernéde, J. C.; El Idrissi, E.; Benseddik, E.; Kachouane, A.; *Preparation and characterization of pyrolytic spray deposited electrochromic tungsten trioxide films*. *Thin Solid Films* **2000**, 358, 40-45.
- [31] Satishkumar, B. C.; Govindaraj, A.; Nath, M.; Rao, C. N. R.; *Synthesis of metal oxide nanorods using carbon nanotubes as templates*. *Journal of Materials Chemistry* **2000**, 10, 2115-2119.
- [32] Gu, G.; Zheng, B.; Han, W. Q.; Roth, S.; Liu, J.; *Tungsten oxide nanowires on tungsten substrates*. *Nano Letters* **2002**, 2, 849-851.
- [33] Su, X.; Xiao, F.; Li, Y.; Jian, J.; Sun, Q.; Wang, J.; *Synthesis of uniform WO_3 square nanoplates via an organic acid-assisted hydrothermal process*. *Materials Letters* **2010**, 64, 1232-1234.
- [34] Xie, Y. P.; Liu, G.; Yin, L.; Cheng, H. M.; *Crystal facet-dependent photocatalytic oxidation and reduction reactivity of monoclinic WO_3 for solar energy conversion*. *Journal of Materials Chemistry* **2012**, 22, 6746-6751.

- [35] Wang, J.; Lee, P. S.; Ma, J.; *Synthesis, growth mechanism and room-temperature blue luminescence emission of uniform WO₃ nanosheets with W as starting material*. Journal of Crystal Growth **2009**, 311, 316-319.
- [36] Gu, Z.; Zhai, T.; Gao, B.; Sheng, X.; Wang, Y.; Fu, H.; Ma, Y.; Yao, J.; *Controllable assembly of WO₃ nanorods/nanowires into hierarchical nanostructures*. Journal of Physical Chemistry B **2006**, 110, 23829-23836.
- [37] Gu, Z.; Li, H.; Zhai, T.; Yang, W.; Xia, Y.; Ma, Y.; Yao, J.; *Large-scale synthesis of single-crystal hexagonal tungsten trioxide nanowires and electrochemical lithium intercalation into the nanocrystals*. Journal of Solid State Chemistry **2007**, 180, 98-105.
- [38] Mo, R. F.; Jin, G. Q.; Guo, X. Y.; *Morphology evolution of tungsten trioxide nanorods prepared by an additive-free hydrothermal route*. Materials Letters **2007**, 61, 3787-3790.
- [39] Wang, J.; Khoo, E.; Lee, P. S.; Ma, J.; *Synthesis, assembly, and electrochromic properties of uniform crystalline WO₃ nanorods*. Journal of Physical Chemistry C **2008**, 112, 14306-14312.
- [40] Zhu, J.; Wang, S.; Xie, S.; Li, H.; *Hexagonal single crystal growth of WO₃ nanorods along a [110] axis with enhanced adsorption capacity*. Chemical Communications **2011**, 47, 4403-4405.
- [41] Zhao, Z. G.; Liu, Z. F.; Miyauchi, M.; *Nature-inspired construction, characterization, and photocatalytic properties of single-crystalline tungsten oxide octahedra*. Chemical Communications **2010**, 46, 3321-3323.
- [42] Jeon, S.; Yong, K.; *Morphology-controlled synthesis of highly adsorptive tungsten oxide nanostructures and their application to water treatment*. Journal of Materials Chemistry **2010**, 20, 10146-10151.
- [43] Yu, J.; Qi, L.; *Template-free fabrication of hierarchically flower-like tungsten trioxide assemblies with enhanced visible-light-driven photocatalytic activity*. Journal of Hazardous Materials **2009**, 169, 221-227.
- [44] Biswas, S. K.; Baeg, J. O.; *A facile one-step synthesis of single crystalline hierarchical WO₃ with enhanced activity for photoelectrochemical solar water oxidation*. International Journal of Hydrogen Energy **2013**, 38, 3177-3188.
- [45] Montini, T.; Gombac, V.; Hameed, A.; Felisari, L.; Adami, G.; Fornasiero, P.; *Synthesis, characterization and photocatalytic performance of transition metal tungstates*. Chemical Physics Letters **2010**, 498, 113-119.
- [46] Romão, J. S.; Hamdy, M. S.; Mul, G.; Baltrusaitis, J.; *Photocatalytic decomposition of cortisone acetate in aqueous solution*. Journal of Hazardous Materials **2015**, 282, 208-215.
- [47] Kato, H.; Hori, M.; Kōta, R.; Shimodaira, Y.; Kudo, A.; *Construction of Z-scheme type heterogeneous photocatalysis systems for water splitting into H₂ and O₂ under visible light irradiation*. Chemistry Letters **2004**, 33, 1348-1349.

- [48] Sánchez-Martínez, D.; Martínez-De La Cruz, A.; López-Cuéllar, E.; *Synthesis of WO_3 nanoparticles by citric acid-assisted precipitation and evaluation of their photocatalytic properties*. Materials Research Bulletin **2013**, 48, 691-697.
- [49] Jiayin, L.; Jianfeng, H.; Jianpeng, W.; Liyun, C.; Yanagisawa, K.; *Morphology-controlled synthesis of tungsten oxide hydrates crystallites via a facile, additive-free hydrothermal process*. Ceramics International **2012**, 38, 4495-4500.
- [50] He, X.; Hu, C.; Yi, Q.; Wang, X.; Hua, H.; Li, X.; *Preparation and improved photocatalytic activity of $WO_3 \cdot 0.33H_2O$ nanonetworks*. Catalysis Letters **2012**, 142, 637-645.
- [51] Yu, J.; Yu, H.; Guo, H.; Li, M.; Mann, S.; *Spontaneous formation of a tungsten trioxide sphere-in-shell superstructure by chemically induced self-transformation*. Small **2008**, 4, 87-91.
- [52] Chen, D.; Ye, J.; *Hierarchical WO_3 hollow shells: dendrite, sphere, dumbbell, and their photocatalytic properties*. Advanced Functional Materials **2008**, 18, 1922-1928.
- [53] Zhang, L.; Tang, X.; Lu, Z.; Wang, Z.; Li, L.; Xiao, Y.; *Facile synthesis and photocatalytic activity of hierarchical WO_3 core-shell microspheres*. Applied Surface Science **2011**, 258, 1719-1724.

3.6 Appendix

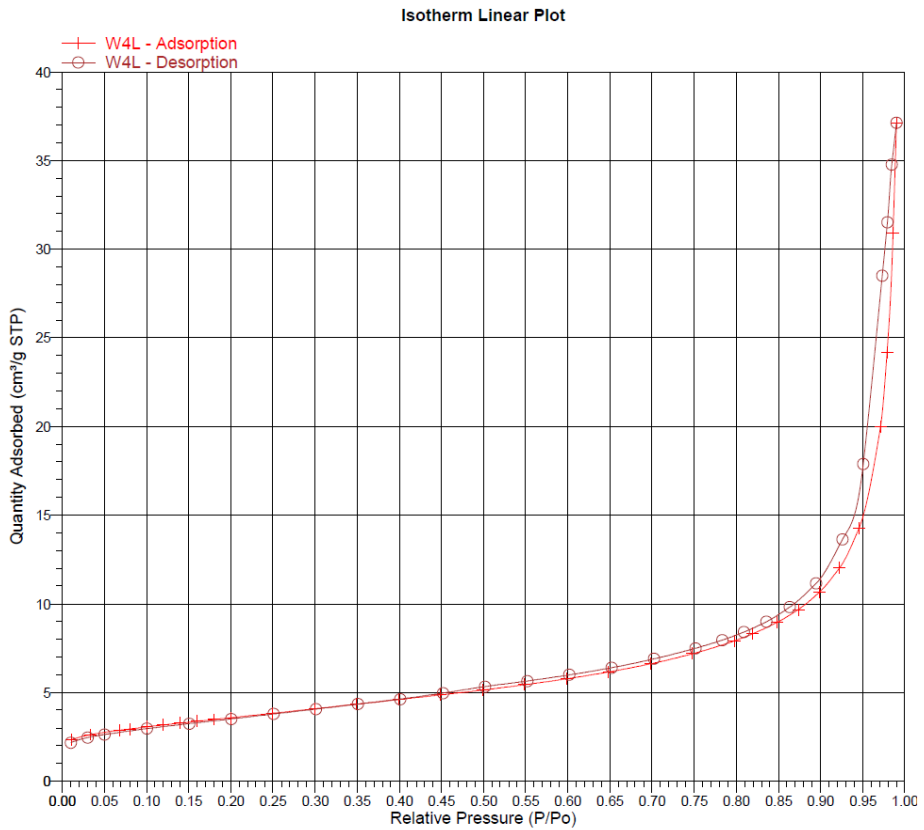


Figure A3.1. (a) N₂ adsorption/desorption isotherms of W120-250.

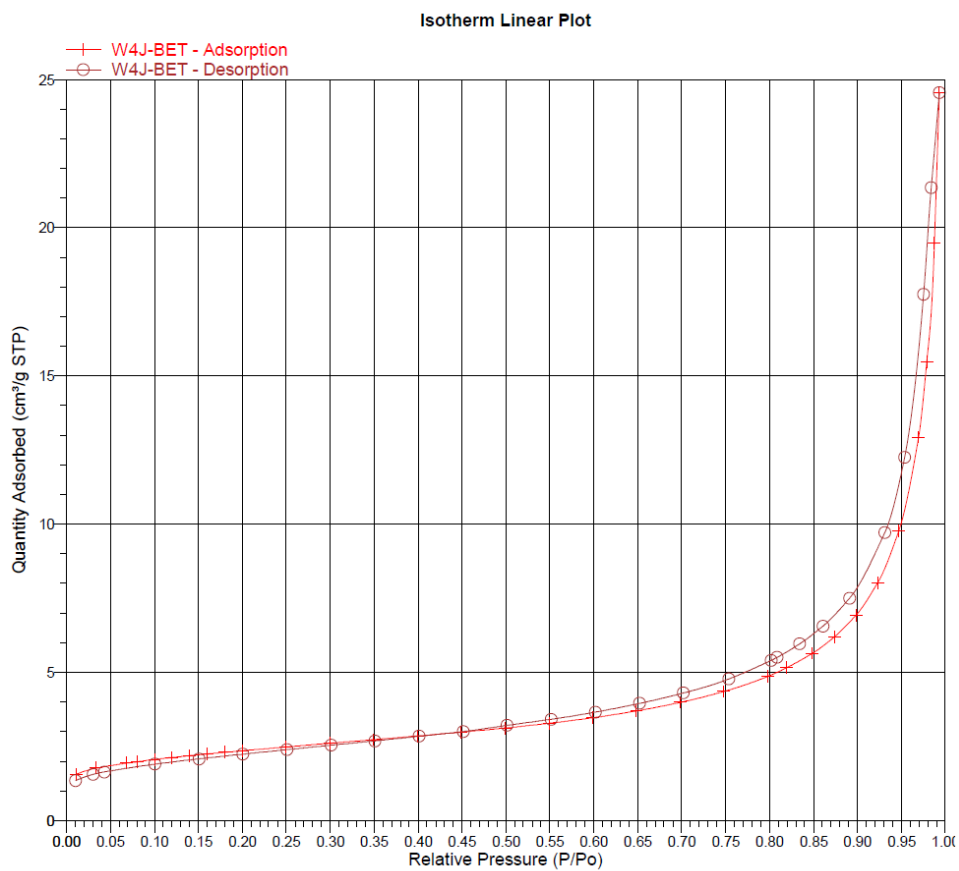


Figure A3.1. (b) N_2 adsorption/desorption isotherms of W170-250.

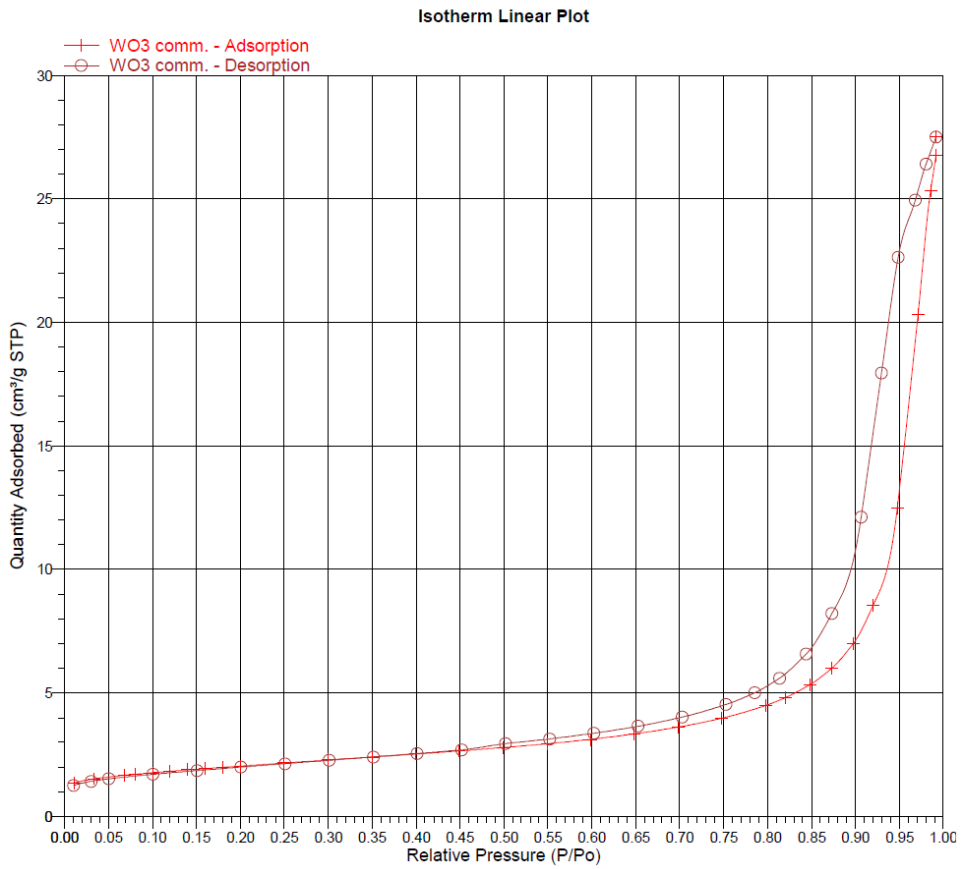


Figure A3.1. (c) N_2 adsorption/desorption isotherms of commercial WO_3 .

Chapter 4

Phase transformations in citric acid-assisted hydrothermal growth of WO₃ and implications for photocatalytic performance

Abstract

The crystallization of tungsten trioxide (WO₃) nanoparticles with well-defined plate-like morphology under hydrothermal conditions from sodium tungstate in the presence of citric acid was studied by *in situ* Raman spectroscopy. Additionally, samples were withdrawn from the reaction vessel, to follow crystal phase transformation through X-ray diffraction and to investigate morphological changes of the sample through scanning electron microscopy. The results suggest that mainly WO₃ · 2H₂O is precipitated from the tungstate solution on acidification to pH ≤ 1 at room temperature. This is first transformed to WO₃ · H₂O starting from T = 70 °C. At temperatures starting from 150 °C, the crystallization of monoclinic WO₃ was observed by Raman spectroscopy, while traces of WO₃ · 0.33H₂O were found by XRD analysis. Microwave-assisted hydrothermal synthesis experiments were performed to fully understand the role of pH and temperature during citric acid-assisted growth of plate-like WO₃. The reaction temperature has a strong influence on the phase transformation and crystal growth. The defect concentration was determined for samples prepared at different temperatures. A correlation between the crystal phase of as-synthesized WO₃ and the activity in photocatalytic oxidation of propane using visible light is demonstrated.

This chapter is based on Wenderich, K.; Noack, J.; Kärger, A.; Trunschke, A. and Mul, G.; Phase transformations in citric acid-assisted hydrothermal growth of WO₃ and implications for photocatalytic performance. Submitted to Inorganic Chemistry.

4.1 Introduction

One of the most promising semiconductor materials in photocatalysis is tungsten trioxide (WO_3). Although the conduction band minimum is below the reduction potential of protons, positive features are that WO_3 is chemically stable, nontoxic and has a relative small bandgap (ranging from 2.4 to 2.8 eV).^[1-3] Due to the latter property, WO_3 is able to absorb visible light in the blue range of the visible spectrum. Significant activity of WO_3 in photocatalytic wastewater treatment has been reported, as well as water splitting activity in a Z-scheme configuration using visible light.^[4, 5] Methods to synthesize WO_3 include sol-gel methods,^[6] solvothermal synthesis,^[7, 8] electrochemical etching,^[9] spray pyrolysis,^[10] chemical vapor deposition^[11] and template directed synthesis.^[12] The hydrothermal synthesis route gives access to WO_3 particles with a well-defined morphology, such as nanorods,^[13-15] nanowires,^[16, 17] nanoplates/nanosheets,^[18-20] nanocubes,^[20] octahedra,^[21] nanourchins^[17, 22] and flower-like morphologies.^[23-25] Often capping agents are used to control the morphology and crystal phase of the samples. These capping agents can adsorb on the surface of a crystal during hydrothermal growth, and thus influence the final morphology.^[26]

In this chapter, we discuss the influence of temperature on the hydrothermal synthesis of plate-like WO_3 based on a method proposed by Su *et al.*^[18] The crystal phase transitions of tungstates during the hydrothermal synthesis experiments at temperatures up to 170 °C and pH values as low as 0.5 were investigated by *in situ* Raman spectroscopy. These measurements have been performed in an analytical autoclave setup made from corrosion resistant Hastelloy C-22.^[27] Here, we put emphasis on the analysis of the crystal phase and the obtained morphology of the plate-like WO_3 . Although first experiments performed to understand the citric acid-assisted growth mechanism of plate-like WO_3 in microwave hydrothermal synthesis have been reported by Sungpanich *et al.*,^[28] we largely expand these studies to elucidate the role of pH and temperature in the hydrothermal synthesis. Different WO_3 samples were tested for their photocatalytic activity through the oxidation of propane, from which the results can be translated to the feasibility for conversion of harmful organic compounds in contaminated air using visible light.^[29, 30]

4.2 Materials and methods

All chemicals of analytical grades were purchased from Sigma-Aldrich, Merck and Alfa Aesar. In a typical hydrothermal experiment, 4.33g of sodium tungstate dihydrate ($\text{Na}_2\text{WO}_4 \cdot 2\text{H}_2\text{O}$) and 2.60g of citric acid (CA) were dissolved, each in 30 g of Millipore water. The solutions were further diluted in an additional 200 mL

of Millipore water and filled into an MED1075 autoclave giving a total W-concentration of 0.05 M and a molar ratio of approximately W/CA = 1:1. The pH was adjusted to 0.5-1.0 using concentrated HCl (32%). The solution was heated to the reaction temperature of 150-170 °C with a rate of approximately 1.5 K min⁻¹ and kept isothermal for 17 hours. During the entire experiment, the solution was stirred at 300 rpm. *In situ* Raman measurements were performed using a Kaiser Optics Raman Spectrometer RXN1 equipped with a fiber-optic probehead (laser wavelength at 785 nm, 125 mW). Samples were withdrawn from the vessel at different temperatures and reaction times for X-ray diffraction (XRD) and scanning electron microscopy (SEM) investigations of the precipitates, after washing with water and drying. Temperature/pressure profiles of the experiments can be found in the appendix (Figure A4.1). The as-prepared products were washed with water, then either with ethanol or a 1:2 water/ethanol mixture and were dried overnight at a maximum temperature of 100 °C.

Microwave hydrothermal synthesis studies have been performed with a Multiwave PRO from Anton Paar using 80 ml quartz vessels. In a typical synthesis, 2.64g of $Na_2WO_4 \cdot 2H_2O$ and 1.68g of citric acid were each dissolved in 80 mL H_2O . Afterwards, the solutions were mixed together and the pH was adjusted in a range of 0.5 to 2 using diluted HCl. After dilution with H_2O to a total volume of 160 mL, the solution was equally distributed over four cuvettes, which were placed in the microwave hydrothermal synthesis oven. The reaction was conducted at temperatures in the range of 150 °C to 250 °C for 2 hours using a heating rate of 10 K min⁻¹. It should be noted that both the heating rate and the material of the autoclaves was different compared to the experiments with the MED1075 autoclave. The samples synthesized by microwave hydrothermal synthesis were characterized for their crystal phase composition and morphology using XRD, SEM and Brunauer–Emmett–Teller (BET) surface area measurements. For the WO_3 samples synthesized at a pH of 0.5, the amount of defects was estimated using thermogravimetric analysis (TGA) (Mettler-Toledo TGA/SDTA Module). As described by Lin *et al.*, defect-rich tungsten oxide (WO_{3-x}) will increase in mass from 455 °C and on, provided that TGA is performed in oxygen-rich conditions.^[31] We calculate the amount of defects from the oxidation of WO_{3-x} to WO_3 at elevated temperatures using TGA in oxygen-rich conditions. An increase in mass will take place, which corresponds with the initial amount of defects x . Using the studies by Lin *et al.*, we define the point where mass increase starts at 455 °C. The maximum amount of mass percentage observed for each sample in the TGA curves was considered the point where all defects were removed from the WO_3 samples. From these values, the amount of defects x in WO_{3-x} was calculated. TGA was performed

in a (natural) air environment using a heating step of $4 \text{ K} \cdot \text{min}^{-1}$. The amount of mass of the WO_3 samples was in the range of 22 to 26 mg.

Photocatalytic activity measurements were performed with as-synthesized plate-like WO_3 through photocatalytic oxidation of propane (C_3H_8), of which the products were analyzed by gas chromatography. To this end a 2 mL batch reactor in combination with an Agilent 7820 GC system (containing a Varian CP7584 column and a Methanizer-FID combination) as described by Fraters *et al.* was used.^[29] Before the samples were loaded into the reaction cell, coatings of these samples on glass substrates (25.3 mm x 25.8 mm) were made through dropcasting, using a stock slurry solution of 3 mL Millipore H_2O (pH = 2, pH adjusted with concentrated HCl) with 150 mg of as-synthesized WO_3 . The glass substrates were cleaned through sonication in acetone first, then in ethanol, followed by treatment for 30 minutes in a mixture of H_2O , H_2O_2 ($\geq 35\%$) and NH_4OH (28-30% NH_3 content) with a ratio of 5:1:1. After treatment, the substrates were put on a heating plate preheated at $100 \text{ }^\circ\text{C}$. 750 μL of the slurry solution was dropcasted on each glass plate. After evaporation of the water a uniform coating was obtained. To ensure tightness of the reactor cell, coating was removed so that an inner circle with a diameter of 1.25 cm remained (corresponding with a sample area of 0.61 cm^2). The mass of the sample present on the coating was calculated to be approximately 7.05 mg.

As-made coatings were loaded into the reaction cell for photocatalytic testing. Prior to the measurements, the batch reactor was purged with a gas mixture containing 80 vol% N_2 , 19.5 vol% O_2 and 5000 vol ppm propane (C_3H_8) for a minimum of 21 minutes. Afterwards, the valves of the batch reactor were closed, followed by illumination for 10 minutes with a 420 nm LED (intensity 6.2 mW/cm^2 at the coating surface). Afterwards, the reactor was purged with He and the gas mixture was analysed by gas chromatography. For each coating, the following sequence of runs was performed: i) two runs in the dark, followed by six runs under illumination, ii) a sequence of runs under different illumination times, iii) a sequence of runs under different reaction times in the dark and iv) again, two runs in the dark, followed by six runs under illumination.

We will focus on the formation of CO_2 , as selectivity towards this compound was by far the highest. The reaction rate r of CO_2 formation ($\text{mol g}^{-1} \text{ h}^{-1}$) was calculated as follows, inspired by Fraters *et al.*:^[29]

$$r = \frac{P \cdot X_{\text{CO}_2} \cdot V}{R \cdot T} \cdot \frac{1}{m \cdot S_{\text{BET}}} \cdot \frac{3600}{t} \quad (4.1)$$

In equation 4.1, P is the pressure inside the batch reactor (Pa), V the gas volume inside the reactor (m³), R the gas constant (m³ Pa mol⁻¹ K⁻¹), T the temperature inside the reactor (K), m the mass of the catalyst (g), S_{BET} the BET surface area of the sample (m² g⁻¹), t the illumination time (s) and X_{CO_2} the gas fraction of CO₂ present inside the reactor. Our experience is that the WO₃ samples need to stabilize over multiple runs to obtain a constant propane oxidation rate. Therefore, we will focus in this chapter mainly on the last three runs of the 4th sequence. From these runs we calculated the average reaction rate of CO₂ formation. By repeating this measurement using either additional measurements on the same coating and/or other coatings, a final average reaction rate including error bars was calculated.

4.3 Results and discussion

4.3.1 In situ Raman spectroscopy of crystal phases during hydrothermal synthesis of WO₃

Figure 4.1 shows the Raman spectra in the typical range of $\nu(W=O)$, $\nu(O-W-O)$ and $\delta(O-W-O)$ vibrations measured during the heating phase of the hydrothermal reaction of sodium tungstate at a pH of 0.5 in the presence of citric acid, and up to a temperature of 170 °C. At room temperature, the acidification of the tungstate solution leads to the precipitation of tungstic acid. This formation can be observed by the Raman bands in the spectra.^[32-35] In its monohydrate form (WO₃ · H₂O), tungstic acid is composed of layers of octahedrally coordinated WO₅(H₂O) units connected by 4 vertices in the plane. The dihydrate form (WO₃ · 2H₂O) is structurally quite similar with additional water molecules intercalated between the layers. Both phases can be identified in the Raman spectra by their characteristic $\nu(W=O)$ bands at 945 and 958 cm⁻¹, respectively. Additionally, bands from 632 to 650 cm⁻¹ and at 884 cm⁻¹ are found, which correspond to $\nu(O-W-O)$ vibrations. While at low temperatures up to approximately 70 °C the dihydrate is the major phase, during heating of the solution, its bands gradually decrease in intensity for the benefit of the monohydrate. Starting from 150 °C, WO₃ · H₂O is consumed and bands at 806, 714, 323 and 269 cm⁻¹ appear, indicating the formation of monoclinic WO₃. From those measurements, WO₃ · 0.33H₂O phase exhibiting intense bands at 945, 805, 680 cm⁻¹ as a possible intermediate in the transformation to monoclinic WO₃ is not clearly identified.^[34] Also, Raman bands from the citric acid acting as structure directing agent added in the synthesis are not observed. The XRD pattern of the precipitate after washing and drying (appendix, Figure A4.2) exclusively shows peaks corresponding to monoclinic WO₃.

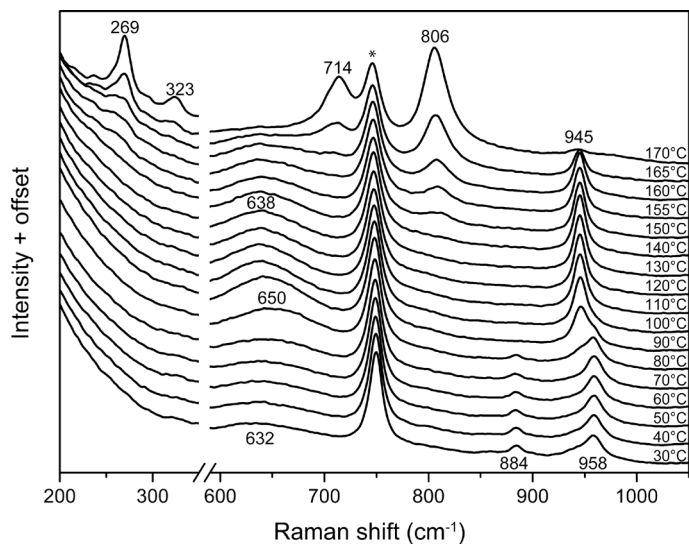


Figure 4.1. Raman spectra measured *in situ* during hydrothermal synthesis during the heating of an aqueous sodium tungstate solution (0.05 M) at pH = 0.5 in the presence of citric acid. The band at 746 cm^{-1} marked with * corresponds with the sapphire window of the Raman probe. The reaction temperature profile is given in Figure A4.1.

To further investigate the formation of monoclinic WO_3 , experiments were conducted at 150 $^\circ\text{C}$, which is the initial transformation temperature from the monohydrate to monoclinic WO_3 . Also the pH was slightly increased, to demonstrate that this also affects the phase transformation. A similar behavior is observed in this experiment compared to the previous one as seen from the *in situ* Raman spectra (Figure A4.3). Reaching 150 $^\circ\text{C}$, the band at 806 cm^{-1} is increasing in intensity while the characteristic bands of the monohydrate phase at 945 and 639 cm^{-1} vanish. From 1 to 15 hours of reaction time, the absolute and relative intensities of the bands barely change, indicating complete phase transformation already occurs one hour after the isothermal point is reached. Again, the XRD pattern of the precipitate after washing and drying shows exclusively peaks corresponding to monoclinic WO_3 (Figure A4.4). Comparison of the Raman spectra shows the pH to have slight impact on the speciation at low temperatures. While Figure 4.1 exhibits no sign of $\text{WO}_3 \cdot \text{H}_2\text{O}$ at pH = 0.5 at low temperatures, its existence is observed in Figure A4.3 in addition to the dihydrate, by the band at 945 cm^{-1} . The SEM images of the two as-discussed experiments with 170 and 150 $^\circ\text{C}$ reaction temperatures (Figures A4.2 and A4.4) show plate-like particles exhibiting sharp edges, reflecting the monoclinic crystal structure of WO_3 . This overall anisotropy in the particle dimensions is also

observed in the XRD patterns by an under-estimation of the reflections involving the crystallographic a-axis and has thus been considered in the Rietveld fit-model.

Besides analysis of the final products, the transients observed in the *in situ* Raman experiments are complemented by XRD and SEM investigations of samples drawn from the hydrothermal vessel at different points during the hydrothermal reaction at 150 °C. The XRD patterns in Figure 4.2a show the formation of the monohydrate phase precipitating from the acidified solution of Na₂WO₄ at temperatures above 100 °C and its decomposition to monoclinic WO₃ starting at 150 °C. This phase transformation is best seen by decreasing intensity of the reflections at $2\theta = 16.5, 25.6$ and 52.7° and appearance of a trifold of reflections at $2\theta = 23.1, 23.6$ and 24.4° . As seen *e.g.* by the reflections at $2\theta = 14.1^\circ$ and 18.0° , little amounts of WO₃ · 0.33H₂O are formed as a side phase, which slowly decompose during the reaction at 150 °C. In the Raman spectra, these traces are not observed due to a strong overlap of the individual bands. The SEM images (Figure 4.2b) of the samples drawn during heating at 130 °C and after 1, 7 and 17 h of isothermal reaction at 150 °C reflect the transformation of the irregularly shaped hydrate phase into the nicely defined rectangular shape of the final monoclinic WO₃. Defects in the crystal morphology are reduced and the mean particle size gets more uniform as a result of Ostwald ripening with increasing reaction time at 150 °C.

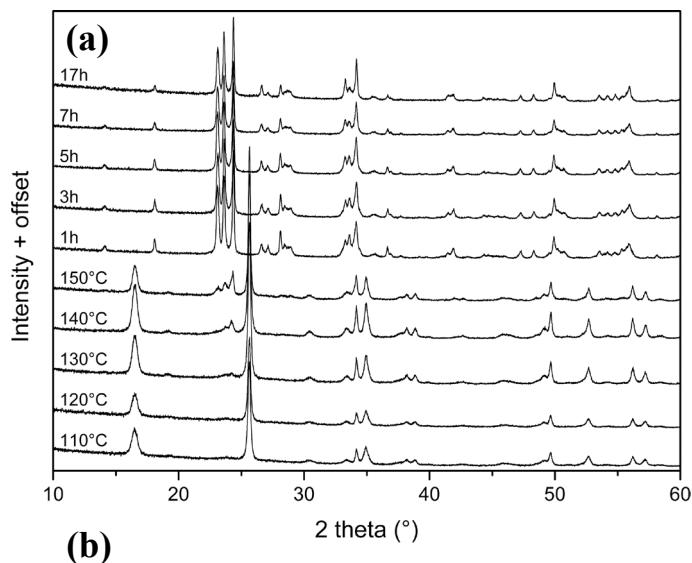


Figure 4.2. (a) XRD patterns of samples drawn from the reactor at different times during the synthesis of WO_3 at 150°C and (b) SEM images of samples after reaching 130°C and hydrothermal reaction at 150°C for 1, 7 and 17 h.

4.3.2 Microwave-assisted hydrothermal synthesis experiments

The *in situ* Raman spectroscopy measurements demonstrate the role of temperature in crystal phase transitions during hydrothermal synthesis. Ideally, these studies need to be expanded with experiments elucidating the reaction network of WO_3 formation as a function of temperature and pH. Due to the complicated nature of the analytical autoclave setup, such reactions were performed in a microwave-assisted

hydrothermal reactor, up to 250 °C. Here, only 2 hours of hydrothermal synthesis was sufficient to obtain useful information. The crystal phase composition of as-prepared products was determined through X-ray diffraction. As seen from Table 4.1, the pH value as well as the reaction temperature play a crucial role on the final crystal phase of WO₃. Generally, monoclinic WO₃ phase formation benefits from higher temperatures and lower pH values during the synthesis. At a pH of 1.5 hexagonal WO₃ and WO₃ · 0.33H₂O are predominantly formed. Monoclinic WO₃ is only observed in small quantities at high temperatures of 230 °C and above. At a pH of 2, only a significant amount of precipitate is formed at T = 150 °C and T = 170 °C, which corresponds to the hexagonal crystal phase. Above these temperatures, not sufficient precipitate is formed to analyze. Looking at the results obtained at a pH of 1, we observe that pure monoclinic WO₃ is formed at T ≥ 200 °C. When T = 150 °C, a significant amount of WO₃ · H₂O is present, as well as a small amount of WO₃ · 0.33H₂O. At T = 170 °C, no WO₃ · H₂O is formed anymore, but traces of WO₃ · 0.33H₂O are still left. At a pH of 0.5 formation of WO₃ · 0.33H₂O is not observed anymore, but when T is too low (T = 150 °C), WO₃ · H₂O is still observed. Figure 4.2a demonstrates that sufficient time at the isothermal stage at 150 °C will result in full transition of WO₃ · H₂O to monoclinic WO₃. However, the duration of the isothermal stage was only 2 hours in the microwave hydrothermal synthesis experiments. Then, no full crystal phase transition has taken place yet. The structure of the individual phases is also reflected in the overall particle morphology (see Figure A4.5).

Table 4.1. Formed crystal phases during microwave-assisted hydrothermal synthesis at different pH and different T, as measured through X-ray diffraction. m-WO₃ is an abbreviation for monoclinic WO₃, h-WO₃ for hexagonal WO₃. N.A. means not available, meaning the amount of formed precipitate was so low that this could not be analyzed.

T pH	150 °C	170 °C	200 °C	230 °C	250 °C
0.5	60% m-WO ₃ 40% WO ₃ · H ₂ O	m-WO ₃	m-WO ₃	m-WO ₃	m-WO ₃
1	62% m-WO ₃ 32% WO ₃ · H ₂ O 6% WO ₃ · 0.33H ₂ O	94% m-WO ₃ 6% WO ₃ · 0.33H ₂ O	m-WO ₃	m-WO ₃	m-WO ₃
1.5	h-WO ₃ WO ₃ · 0.33H ₂ O	h-WO ₃ WO ₃ · 0.33H ₂ O	h-WO ₃ WO ₃ · 0.33H ₂ O	h-WO ₃ WO ₃ · 0.33H ₂ O m-WO ₃	h-WO ₃ WO ₃ · 0.33H ₂ O m-WO ₃
2	h-WO ₃	h-WO ₃	N.A.	N.A.	N.A.

In order to compare a set of pure WO_3 samples with similar reaction conditions except for the reaction temperature, the samples synthesized at a pH of 0.5 are further compared. Table 4.2 shows the BET surface areas in $\text{m}^2 \text{g}^{-1}$ as a function of synthesis temperature. An increase in reaction temperature results in a slight decrease in BET surface area of the monoclinic WO_3 samples, which is possibly the result of the nanoplates becoming smoother and larger in size. The sample prepared at 150°C consists of a mixture with hydrate phase, which causes a slightly higher surface area.

Table 4.2. BET surface area as a function of temperature of samples synthesized through microwave hydrothermal synthesis at $\text{pH} = 0.5$.

T ($^\circ\text{C}$)	BET ($\text{m}^2 \text{g}^{-1}$)
150	17.61
170	14.76
200	13.84
230	13.44
250	13.41

As-calculated values for the amount of defects x as expressed in WO_{3-x} are depicted in Figure 4.3. The corresponding original and corrected TGA profiles can be found in the appendix (Figure A4.6 and A4.7 respectively).

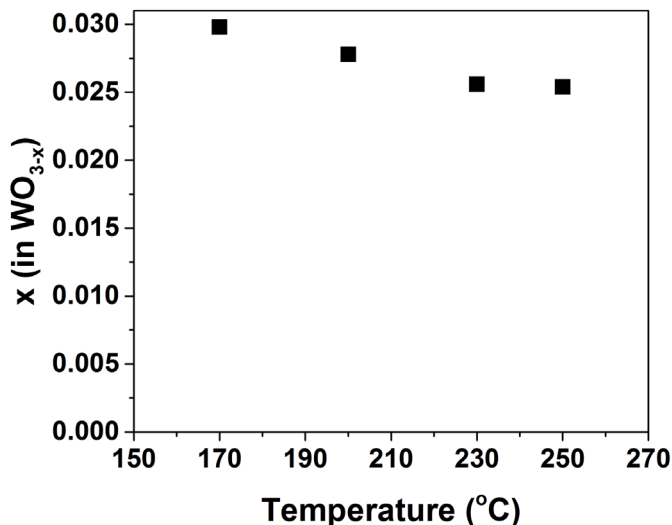


Figure 4.3. Calculated amount of x in WO_{3-x} .

An increase in reaction time results in a decrease of defects. Higher synthesis temperatures result obviously in higher crystallinity, although surface defects are still observed at 250 °C. For the sample prepared at 150 °C an initial loss of mass in the early stages of the TGA experiment is observed (Figure A4.6), which can be ascribed to the loss of hydrates in the WO₃ · H₂O-containing crystal. Indeed, Sánchez-Martínez *et al.* have demonstrated that at least in the temperature range of 120 to 450 °C, WO₃ · H₂O is decomposed to monoclinic WO₃.^[36] We hypothesize that due to this water loss, recrystallization of the WO₃ crystal takes place, making comparison with the other crystals meaningless.

4.3.3 Photocatalytic activity tests

To demonstrate the relevance of this work for photocatalysis, the samples synthesized by the microwave hydrothermal method at a pH of 0.5 are analyzed for photocatalytic activity in the oxidation of propane. As CO₂ was very dominantly formed, a 100% selectivity of propane to CO₂ is assumed. This implies that the WO₃ acts as an (almost) full oxidation photocatalyst and could thus be useful in the degradation of harmful organic compounds. A typical measurement is included in Figure 4.4. Figure 4.4a demonstrates the rate of CO₂ formation after a constant reaction time of 10 minutes, whereas Figure 4.4b demonstrates the yield of CO₂ as a function of reaction time. In the dark-measurements hardly any CO₂ is formed, whereas considerably large amounts of CO₂ are formed under illumination at 420 nm. Figure 4.4a demonstrates that over time the amounts of CO₂ formed per run stabilize (cycle 1) until reaching reproducible conversion rates after 8 runs. The initially higher activity in propane conversion might be correlated to the defects of the catalyst surface being poisoned by adsorption of propane or oxidation products. A repetition of this particular experiment (cycle 2 in Figure 4.4a) at a later time shows that the coating recovers almost to its initial activity. Stabilization in the CO₂ formation rate takes place to approximately the same value as in the first cycle. Figure 4.4b shows that initially the relationship between the amount of CO₂ formed and the reaction time is linear.

Figure 4.5 depicts the average rate of CO₂ formation during the last three runs during a typical sequence of propane photo-oxidation runs over a WO₃ photocatalyst, corrected for BET surface area. When the synthesis temperature was 170, 200, 230 or 250 °C, the rate is approximately similar (around 6.3 to 7 μmol CO₂ m⁻² h⁻¹ formed). Apparently the difference in the amount of defects in the crystal does not contribute significantly to the photocatalytic activity of the samples. On the other hand, the sample synthesized at 150 °C is considerably less active in its photocatalytic activity than the other samples (around 2.9 μmol CO₂ m⁻² h⁻¹ formed).

Obviously, the main difference between this sample and the others is that in the case of 150 °C, both monoclinic and $\text{WO}_3 \cdot \text{H}_2\text{O}$ were formed, whereas in the other samples only monoclinic WO_3 is present. This underlines that the presence of the $\text{WO}_3 \cdot \text{H}_2\text{O}$ seems detrimental for the photocatalytic activity.

The hexagonal WO_3 sample synthesized at 170 °C and a pH of 2 has been tested on its photocatalytic activity as well. However, the activity under visible light is inferior to its monoclinic counterpart (not shown in this chapter).

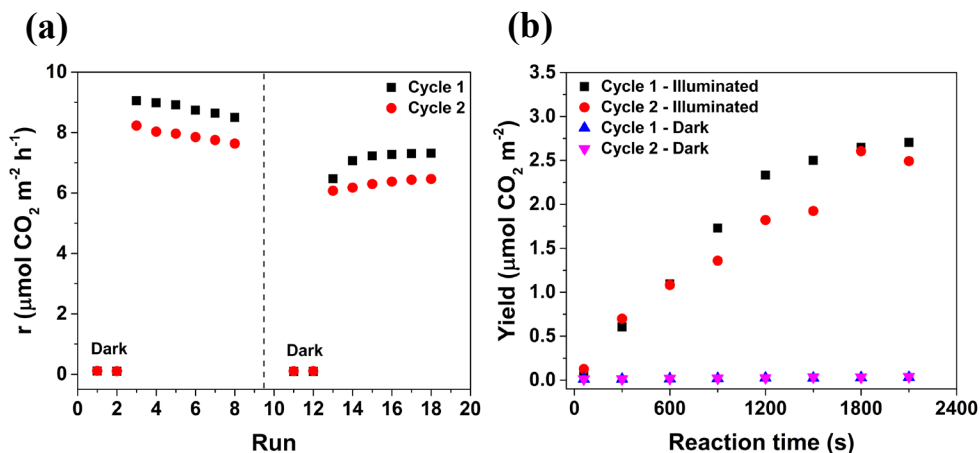


Figure 4.4. CO_2 amounts formed during photocatalytic oxidation of propane in visible light (420 nm) at (a) constant ($t = 10$ min) and (b) fluctuating reaction times over a coating of WO_3 nanoplates, synthesized at $\text{pH} = 0.5$ and $T = 200$ °C in a microwave. The same set of experiments was done twice (cycles 1 & 2). The dashed line in (a) represents the moment that the measurements of (b) took place.

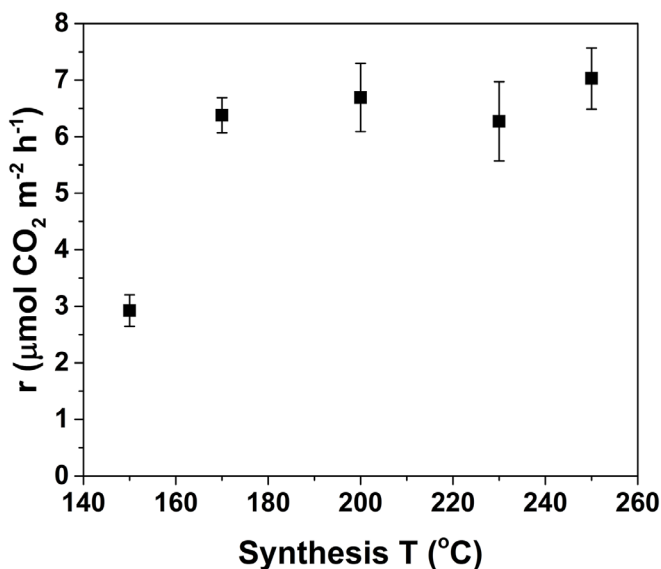


Figure 4.5. Average CO_2 production rates during photocatalytic oxidation of propane using coatings of WO_3 nanoplates, corrected for BET surface area.

4.4 Conclusions

In this chapter, we have studied hydrothermal plate-like WO_3 crystal growth in a custom built autoclave using *in situ* Raman spectroscopy and withdrawing samples during synthesis. Initially, when the pH of the aqueous sodium tungstate solution containing citric acid is 1 or lower, mainly tungsten oxide dihydrate ($WO_3 \cdot 2H_2O$) is formed. During heating, starting from 70 °C, the tungsten oxide dihydrate is first transformed to tungsten oxide monohydrate ($WO_3 \cdot H_2O$). At temperatures from 150 °C, $WO_3 \cdot H_2O$ is transformed mainly into monoclinic WO_3 . To a minor extent, $WO_3 \cdot 0.33H_2O$ is also formed, but this crystal phase is slowly decomposed into monoclinic WO_3 as well in the isothermal stage.

Microwave-assisted hydrothermal synthesis experiments indicate that there is a tipping point in pH in the synthesis: underneath this pH, the dominant crystal phase becomes monoclinic WO_3 , provided T is high enough to prevent formation of hydrated WO_3 . Furthermore, BET and TGA measurements have demonstrated that an increase in reaction temperature results in more uniform samples with less defects present in the crystal lattice.

The photocatalytic activity of the samples synthesized through microwave hydrothermal synthesis at a pH of 0.5 has been tested through the photo-oxidation of propane under visible light (420 nm). We observe that the synthesis temperature

does matter for the amounts of CO₂ formed: when the synthesis temperature is too low, photocatalytically inactive hydrates (WO₃ · H₂O) will be present inside the WO₃ crystal, resulting in a decrease of photocatalytic activity. When T is high enough, only monoclinic WO₃ will be formed and the photocatalytic activity will be considerably higher. Despite a different amount of defects, the monoclinic WO₃ samples did not show a significant difference in photocatalytic activity.

The studies as performed in this chapter can contribute greatly to understanding crystal growth of WO₃ using citric acid and to use this in optimizing crystal facet engineering of WO₃. For example, we have recently published studies on structure-directed deposition of Pt on WO₃ particles synthesized in a Teflon-lined 4748 acid digestion vessel.^[37]

4.5 Bibliography

- [1] Zheng, H.; Ou, J. Z.; Strano, M. S.; Kaner, R. B.; Mitchell, A.; Kalantar-Zadeh, K.; *Nanostructured tungsten oxide - properties, synthesis, and applications*. *Advanced Functional Materials* **2011**, 21, 2175-2196.
- [2] Kim, J.; Lee, C. W.; Choi, W.; *Platinized WO₃ as an environmental photocatalyst that generates OH radicals under visible light*. *Environmental Science and Technology* **2010**, 44, 6849-6854.
- [3] Kudo, A.; Miseki, Y.; *Heterogeneous photocatalyst materials for water splitting*. *Chemical Society Reviews* **2009**, 38, 253-278.
- [4] Chan, S. H. S.; Yeong Wu, T.; Juan, J. C.; Teh, C. Y.; *Recent developments of metal oxide semiconductors as photocatalysts in advanced oxidation processes (AOPs) for treatment of dye waste-water*. *Journal of Chemical Technology and Biotechnology* **2011**, 86, 1130-1158.
- [5] Abe, R.; Higashi, M.; Domen, K.; *Overall water splitting under visible light through a two-step photoexcitation between TaON and WO₃ in the presence of an iodate-iodide shuttle redox mediator*. *ChemSusChem* **2011**, 4, 228-237.
- [6] Deepa, M.; Joshi, A. G.; Srivastava, A. K.; Shivaprasad, S. M.; Agnihotry, S. A.; *Electrochromic nanostructured tungsten oxide films by sol-gel: structure and intercalation properties*. *Journal of the Electrochemical Society* **2006**, 153, C365-C376.
- [7] Choi, H. G.; Jung, Y. H.; Kim, D. K.; *Solvothermal synthesis of tungsten oxide nanorod/nanowire/nanosheet*. *Journal of the American Ceramic Society* **2005**, 88, 1684-1686.
- [8] Zhao, Z. G.; Miyauchi, M.; *Shape modulation of tungstic acid and tungsten oxide hollow structures*. *Journal of Physical Chemistry C* **2009**, 113, 6539-6546.
- [9] Gu, G.; Zheng, B.; Han, W. Q.; Roth, S.; Liu, J.; *Tungsten oxide nanowires on tungsten substrates*. *Nano Letters* **2002**, 2, 849-851.

- [10] Regragui, M.; Addou, M.; Outzourhit, A.; Bernéde, J. C.; El Idrissi, E.; Benseddik, E.; Kachouane, A.; *Preparation and characterization of pyrolytic spray deposited electrochromic tungsten trioxide films*. *Thin Solid Films* **2000**, 358, 40-45.
- [11] Shankar, N.; Yu, M. F.; Vanka, S. P.; Glumac, N. G.; *Synthesis of tungsten oxide (WO_3) nanorods using carbon nanotubes as templates by hot filament chemical vapor deposition*. *Materials Letters* **2006**, 60, 771-774.
- [12] Satishkumar, B. C.; Govindaraj, A.; Nath, M.; Rao, C. N. R.; *Synthesis of metal oxide nanorods using carbon nanotubes as templates*. *Journal of Materials Chemistry* **2000**, 10, 2115-2119.
- [13] Zhu, J.; Wang, S.; Xie, S.; Li, H.; *Hexagonal single crystal growth of WO_3 nanorods along a $[110]$ axis with enhanced adsorption capacity*. *Chemical Communications* **2011**, 47, 4403-4405.
- [14] Wang, J.; Khoo, E.; Lee, P. S.; Ma, J.; *Synthesis, assembly, and electrochromic properties of uniform crystalline WO_3 nanorods*. *Journal of Physical Chemistry C* **2008**, 112, 14306-14312.
- [15] Mo, R. F.; Jin, G. Q.; Guo, X. Y.; *Morphology evolution of tungsten trioxide nanorods prepared by an additive-free hydrothermal route*. *Materials Letters* **2007**, 61, 3787-3790.
- [16] Gu, Z.; Li, H.; Zhai, T.; Yang, W.; Xia, Y.; Ma, Y.; Yao, J.; *Large-scale synthesis of single-crystal hexagonal tungsten trioxide nanowires and electrochemical lithium intercalation into the nanocrystals*. *Journal of Solid State Chemistry* **2007**, 180, 98-105.
- [17] Gu, Z.; Zhai, T.; Gao, B.; Sheng, X.; Wang, Y.; Fu, H.; Ma, Y.; Yao, J.; *Controllable assembly of WO_3 nanorods/nanowires into hierarchical nanostructures*. *Journal of Physical Chemistry B* **2006**, 110, 23829-23836.
- [18] Su, X.; Xiao, F.; Li, Y.; Jian, J.; Sun, Q.; Wang, J.; *Synthesis of uniform WO_3 square nanoplates via an organic acid-assisted hydrothermal process*. *Materials Letters* **2010**, 64, 1232-1234.
- [19] Wang, J.; Lee, P. S.; Ma, J.; *Synthesis, growth mechanism and room-temperature blue luminescence emission of uniform WO_3 nanosheets with W as starting material*. *Journal of Crystal Growth* **2009**, 311, 316-319.
- [20] Xie, Y. P.; Liu, G.; Yin, L.; Cheng, H. M.; *Crystal facet-dependent photocatalytic oxidation and reduction reactivity of monoclinic WO_3 for solar energy conversion*. *Journal of Materials Chemistry* **2012**, 22, 6746-6751.
- [21] Zhao, Z. G.; Liu, Z. F.; Miyauchi, M.; *Nature-inspired construction, characterization, and photocatalytic properties of single-crystalline tungsten oxide octahedra*. *Chemical Communications* **2010**, 46, 3321-3323.
- [22] Jeon, S.; Yong, K.; *Morphology-controlled synthesis of highly adsorptive tungsten oxide nanostructures and their application to water treatment*. *Journal of Materials Chemistry* **2010**, 20, 10146-10151.

- [23] Zhao, Y.; Chen, H.; Wang, X.; He, J.; Yu, Y.; He, H.; *Flower-like tungsten oxide particles: synthesis, characterization and dimethyl methylphosphonate sensing properties*. *Analytica Chimica Acta* **2010**, 675, 36-41.
- [24] Yu, J.; Qi, L.; *Template-free fabrication of hierarchically flower-like tungsten trioxide assemblies with enhanced visible-light-driven photocatalytic activity*. *Journal of Hazardous Materials* **2009**, 169, 221-227.
- [25] Biswas, S. K.; Baeg, J. O.; *A facile one-step synthesis of single crystalline hierarchical WO₃ with enhanced activity for photoelectrochemical solar water oxidation*. *International Journal of Hydrogen Energy* **2013**, 38, 3177-3188.
- [26] Liu, G.; Yu, J. C.; Lu, G. Q.; Cheng, H. M.; *Crystal facet engineering of semiconductor photocatalysts: motivations, advances and unique properties*. *Chemical Communications* **2011**, 47, 6763-6783.
- [27] Noack, J.; Rosowski, F.; Schlögl, R.; Trunschke, A.; *Speciation of molybdates under hydrothermal conditions*. *Zeitschrift für Anorganische und Allgemeine Chemie* **2014**, 640, 2730-2736.
- [28] Sungpanich, J.; Thongtem, T.; Thongtem, S.; *Large-scale synthesis of WO₃ nanoplates by a microwave-hydrothermal method*. *Ceramics International* **2012**, 38, 1051-1055.
- [29] Fraters, B. D.; Amrollahi, R.; Mul, G.; *How Pt nanoparticles affect TiO₂-induced gas-phase photocatalytic oxidation reactions*. *Journal of Catalysis* **2015**, 324, 119-126.
- [30] Khajeh Aminian, M.; Hakimi, M.; *Surface modification by loading alkaline hydroxides to enhance the photoactivity of WO₃*. *Catalysis Science and Technology* **2014**, 4, 657-664.
- [31] Lin, H. C.; Su, C. Y.; Lin, C. K.; *High-yield fabrication of W₁₈O₄₉@TiO₂ core-shell nanoparticles: microstructures and optical-thermal properties*. *Journal of Nanoparticle Research* **2011**, 13, 4549-4555.
- [32] Souza-Filho, A. G.; Freire, V. N.; Sasaki, J. M.; Mendes Filho, J.; Julião, J. F.; Gomes, U. U.; *Coexistence of triclinic and monoclinic phases in WO₃ ceramics*. *Journal of Raman Spectroscopy* **2000**, 31, 451-454.
- [33] Baserga, A.; Russo, V.; Di Fonzo, F.; Bailini, A.; Cattaneo, D.; Casari, C. S.; Li Bassi, A.; Bottani, C. E.; *Nanostructured tungsten oxide with controlled properties: synthesis and Raman characterization*. *Thin Solid Films* **2007**, 515, 6465-6469.
- [34] Gotić, M.; Ivanda, M.; Popović, S.; Musić, S.; *Synthesis of tungsten trioxide hydrates and their structural properties*. *Materials Science and Engineering B: Solid-State Materials for Advanced Technology* **2000**, 77, 193-201.
- [35] Daniel, M. F.; Desbat, B.; Lassegues, J. C.; Gerand, B.; Figlarz, M.; *Infrared and Raman study of WO₃ tungsten trioxides and WO₃ · xH₂O tungsten trioxide hydrates*. *Journal of Solid State Chemistry* **1987**, 67, 235-247.

- [36] Sánchez-Martínez, D.; Martínez-De La Cruz, A.; López-Cuéllar, E.; *Synthesis of WO₃ nanoparticles by citric acid-assisted precipitation and evaluation of their photocatalytic properties*. *Materials Research Bulletin* **2013**, 48, 691-697.
- [37] Wenderich, K.; Klaassen, A.; Siretanu, I.; Mugele, F.; Mul, G.; *Sorption-determined deposition of platinum on well-defined platelike WO₃*. *Angewandte Chemie - International Edition* **2014**, 53, 12476-12479.

4.6 Appendix

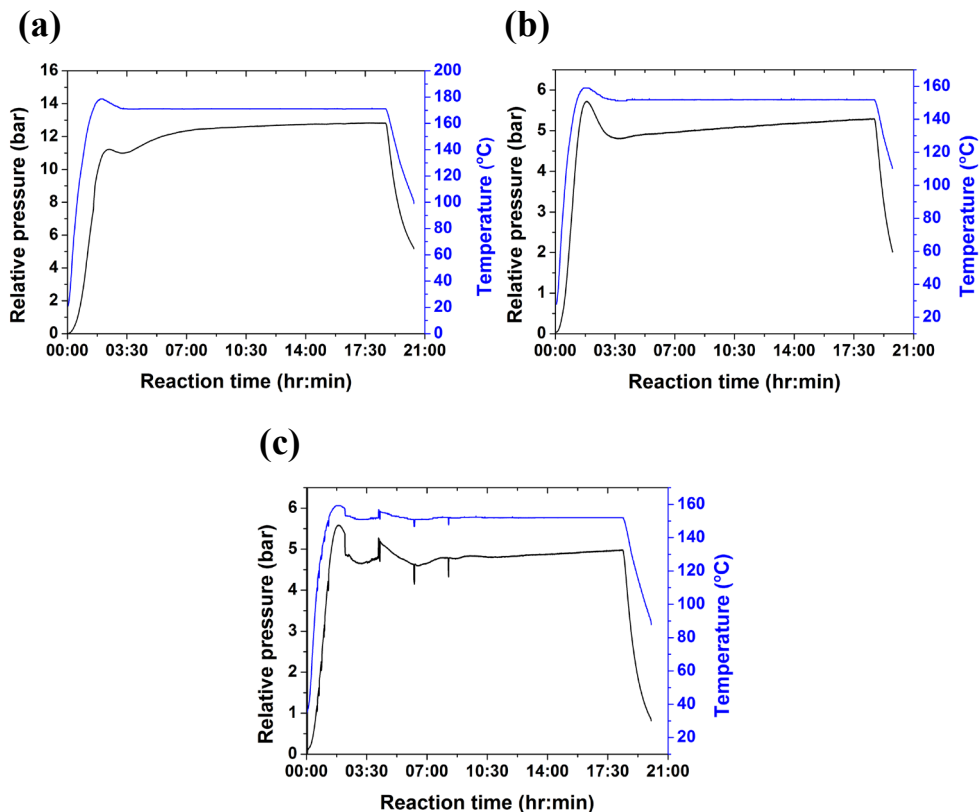


Figure A4.1. Relative pressure (black) and temperature profile (blue) within the autoclave during hydrothermal synthesis in combination with in situ Raman spectroscopy at (a) pH = 0.5 and set point $T = 170$ °C, (b) pH = 1.0 and set point $T = 150$ °C and (c) repetition of (b), but with withdrawal of samples during the hydrothermal synthesis. The relative pressure is defined as the difference between the pressure inside the autoclave minus atmospheric pressure. A slight overshoot in temperature and pressure can be observed when the isothermal set point is reached. When the temperature becomes stable, an increase in pressure is still visible over time in the hydrothermal synthesis experiments. This is likely due to citric acid decomposition into gas phase CO_2 . In the case of (c), a small drop in pressure and temperature can be observed between 02:13 and 04:11. This is caused by a temporarily lower stirring speed inside the vessel during this period. Furthermore, the reversed 'spikes' in the graph indicate points where a sample was withdrawn from the vessel to be analyzed with XRD and SEM.

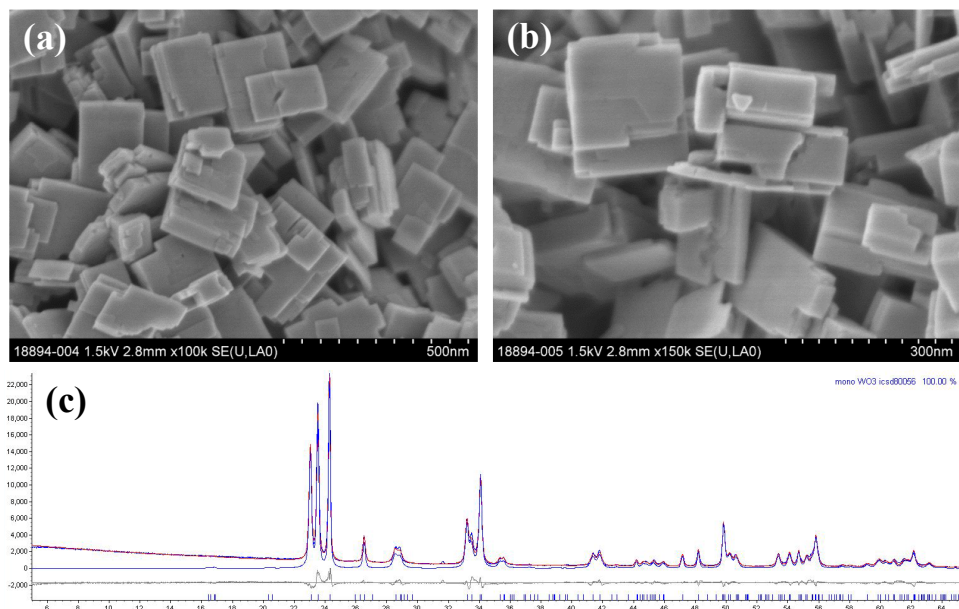


Figure A4.2. (a, b) SEM images and (c) XRD pattern of monoclinic, plate-like WO_3 , hydrothermally synthesized in the MED1075 autoclave at $T = 170^\circ C$ and $pH = 0.5$.

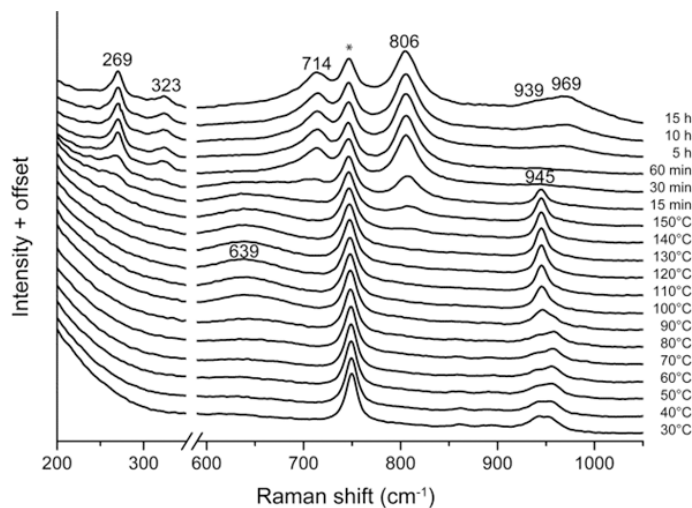


Figure A4.3. Raman spectra measured in situ during hydrothermal synthesis at $T = 150^\circ C$ and a pH of 1.0. Measurements took place during the heating procedure and after reaching the isothermal point. Similar behavior as in Figure 4.1 is observed. Although at $t = 0$ h the dominant crystal phase present is still $WO_3 \cdot H_2O$, at $t = 1$ h full transformation to monoclinic WO_3 has occurred.

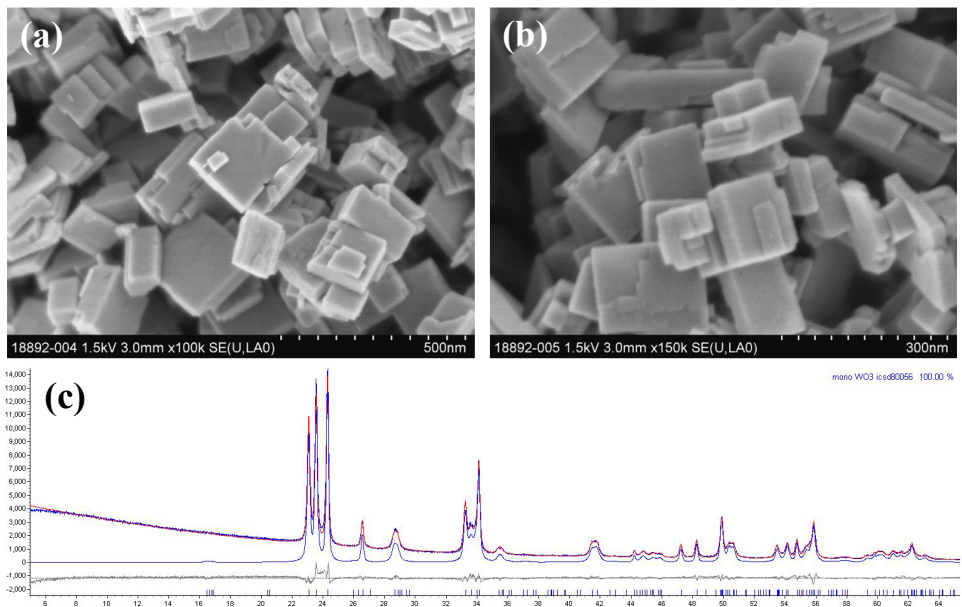


Figure A4.4. (a, b) SEM images and (c) XRD pattern of monoclinic, plate-like WO_3 hydrothermally synthesized in the MED1075 autoclave at $T = 150\text{ }^\circ\text{C}$ and $pH = 1.0$.

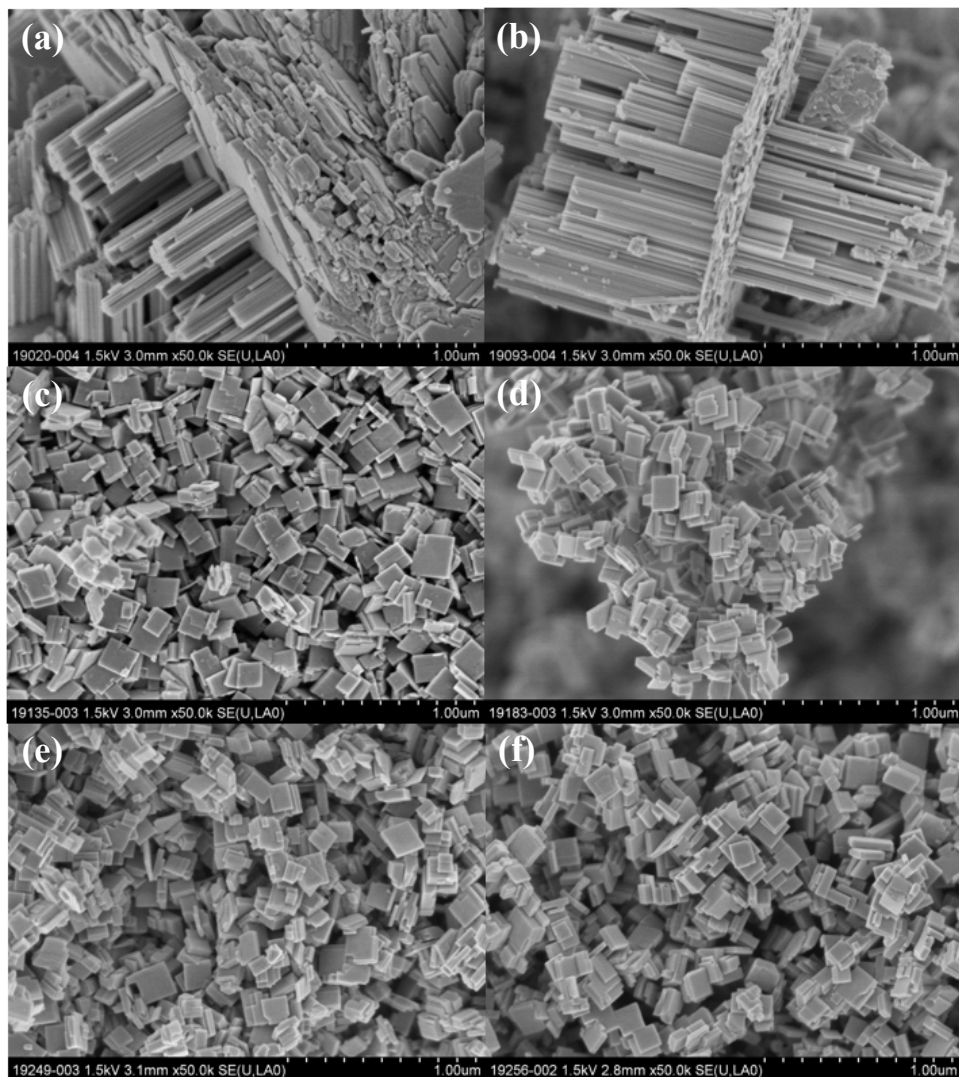


Figure A4.5. SEM images of samples synthesized through microwave-assisted hydrothermal synthesis at (a) $pH = 1.5$, $T = 200$ °C, (b) $pH = 1.5$, $T = 250$ °C, (c) $pH = 1.0$, $T = 200$ °C, (d) $pH = 1.0$, $T = 250$ °C, (e) $pH = 0.5$, $T = 170$ °C and (f) $pH = 0.5$, $T = 250$ °C.

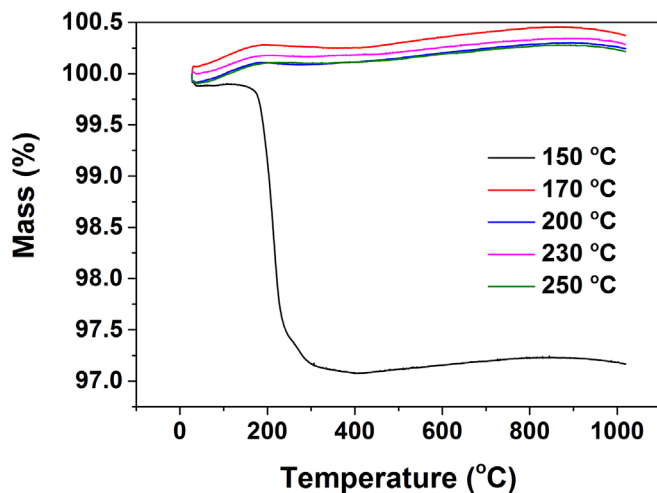


Figure A4.6. Uncorrected TGA curves of samples obtained through microwave hydrothermal synthesis at different temperatures at a pH of 0.5. $m = 100\%$ is defined at the initial temperature of the TGA experiment. An initial decrease in mass is observed, which can be attributed to desorption of H_2O . Then, for the sample synthesized at 150 °C, a large decrease in mass is observed around 200 °C. At this temperature, $WO_3 \cdot H_2O$ loses its hydrate groups and recrystallizes in monoclinic WO_3 . Initially, for the samples synthesized at 170 °C to 250 °C, an increase in mass is observed after the initial H_2O desorption. Similar behavior is observed when TGA profiles of empty cups are measured. Hence up to 455 °C, we don't attribute the increase in mass to the WO_3 samples, but only to the TGA measurement system.

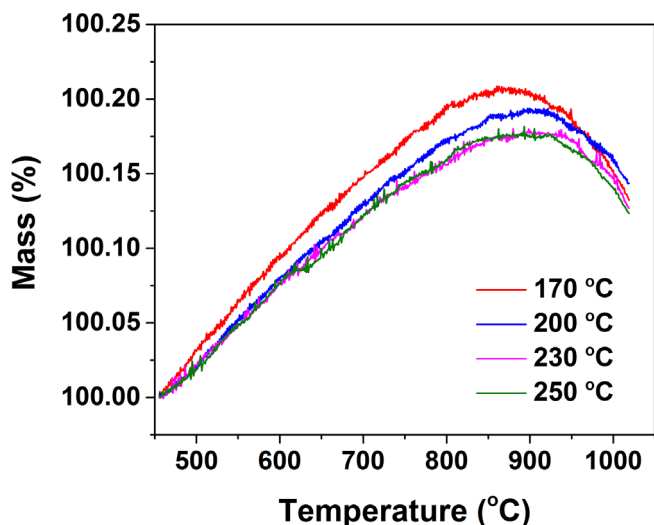


Figure A4.7. Corrected TGA curves of samples microwave hydrothermal synthesized at different temperatures at a pH of 0.5. $m = 100\%$ is defined at 455 °C.

Chapter 5

Photodeposition mechanism of platinum on tungsten oxide and its corresponding stability upon aqueous phase illumination

Abstract

We provide a detailed study on the mechanism of photodeposition of platinum from acidic $[\text{PtCl}_6]^{2-}$ solutions on commercially available tungsten oxide. It is demonstrated that the absence or presence of methanol plays a critical role in the kinetics of the photodeposition process, determining the amount of platinum deposited and the dispersion and oxidation state of the platinum particles. The first step in the deposition process is the adsorption of a platinum (IV) precursor ion on the WO_3 surface. In the absence of methanol, subsequent illumination predominantly results in the formation of highly dispersed platinum (II) hydroxide particles, the maximum achievable amount corresponding to approximately 35% of Pt present in the precursor solution. The presence of methanol not only promotes adsorption of the Pt (IV) precursor, but upon illumination results in a deposited quantity close to 100% of the aim. Such particles are often clustered, and predominantly in the metallic state. Variations in experimental conditions to which platinum or platinum (II) oxide/hydroxide particles are exposed, demonstrate that the presence of methanol is essential to prevent re-oxidation and dissolution of platinum (II) oxide/hydroxide nanoparticles in photodeposition conditions. This study greatly contributes to understanding of the photodeposition mechanism on a fundamental level, and shows that on WO_3 metallic platinum particles of high dispersion can best be prepared by photodeposition in the absence of methanol and subsequent hydrogen treatment at elevated temperatures.

This chapter is based on Wenderich, K.; Han, K. and Mul, G.; Photodeposition mechanism of platinum on tungsten oxide and its corresponding stability upon aqueous phase illumination. In preparation.

5.1 Introduction

Photocatalysis has become an increasingly studied technology for water splitting,^[1-3] air purification^[4] and water purification.^[5, 6] To enhance the activity of photocatalytic materials, cocatalytic nanoparticles can be loaded on these materials.^[3, 7-9] Techniques to realize this include impregnation,^[10-12] chemical reduction,^[13] deposition-precipitation,^[12] physical mixing,^[12] sputtering^[14] and electrodeposition.^[15] In 1978, Kraeutler and Bard demonstrated that cocatalytic nanoparticles can be deposited on photocatalytic materials using a photodeposition method.^[16] Since then, photodeposition has become a very popular technique to obtain photocatalytic materials loaded with cocatalysts.^[12, 17-21] Photo-excited states (electrons and holes) of a material are used to either reduce or oxidize metal ions to respectively metallic or metal oxide particles.^[22, 23] For deposition of metal nanoparticles a sacrificial agent such as methanol,^[7, 8, 10, 12] ethanol,^[24] isopropanol^[25] or acetate^[16, 26] can be used as hole scavenger. Some authors only add the sacrificial agent after photodeposition has already been performed for some time in pure aqueous conditions.^[8, 27-29] To the best of our knowledge, it is not clear why this is done.

Despite the large amount of research describing applications, the amount of research performed to fundamentally understand photodeposition is limited. Researchers have tried to study the influence of photodeposition parameters on *e.g.* dispersion and oxidation state. Most of this research is focused on the photodeposition of platinum (Pt) on titanium dioxide (TiO₂). Several studies include the effect of sacrificial agents on the oxidation state and particle size distribution of as-deposited platinum.^[19, 26, 30] These studies demonstrate that the valence state of Pt is lower when these sacrificial agents are used than when they are not, often favoring the formation of metallic Pt. Other studies have looked at the influence of pH on the photodeposition process.^[24, 30] A low pH results in a low platinum valence state, whereas a high pH results in a higher valence state. This phenomenon is attributed to the hydrolysis of [PtCl₆]²⁻ at higher pH-values. A higher dispersion of Pt particles was observed by Zhang *et al.* when a high pH is used.^[24] Curran *et al.* have studied photodeposition kinetics (without sacrificial agent) as a function of light intensity, [PtCl₆]²⁻ concentration, pH, temperature, ionic strength, the presence of oxygen and

the concentration of TiO_2 .^[31] Mahlamvena and Kriek studied the usage of different platinum precursors (with different Pt oxidation states) during photodeposition.^[32] Furthermore a decent amount of research has been performed in understanding the photodeposition of Pt on CdS.^[33-35]

A non-toxic, stable photocatalyst which has drawn interest over the last years is tungsten oxide (WO_3).^[7, 36] Although WO_3 is not suitable for overall water splitting, it has a relative small bandgap of 2.6 eV, making it suitable for absorption of part of the solar spectrum. It can be used for *e.g.* water oxidation^[37, 38] or water purification.^[27, 39] WO_3 can be loaded with cocatalytic materials, such as Ag^[28] or Pd,^[40, 41] to enhance the photocatalytic activity. In particular the cocatalyst Pt has been used frequently.^[14, 37, 42] Often photodeposition is used to load Pt on WO_3 .^[7, 8, 27, 29, 43] Abe *et al.* have demonstrated that the addition of Pt on WO_3 can result in a dramatic increase in photocatalytic activity.^[8] These authors advocate that in oxidation reactions, tungsten oxide is not able to reduce oxygen through single-electron reduction. However, this can be possible through multi-electron reductions. As platinum will act as an electron trap, the allowance of a multi-electron reduction reaction on the photocatalyst increases significantly.

In contrast to studies with TiO_2 and CdS, to the best of our knowledge, hardly any studies have been reported on the kinetics of photodeposition of platinum on WO_3 . This is remarkable indeed, as efficient loading of Pt on WO_3 could contribute greatly in obtaining high photocatalytic activities. One of the most important questions unanswered in photodeposition of Pt on WO_3 is what the role is of the sacrificial agent on *e.g.* the speed of the photocatalytic reaction, the dispersion and morphology of the as-deposited Pt particles, as well as on the oxidation state of the Pt deposited on WO_3 . In this chapter, we aim to understand the role of the sacrificial agent methanol on photodeposition of Pt on WO_3 . We assess the question what the effect is of methanol on the photodeposition kinetics, as well as the question what the oxidation state and the degree of dispersion is of the Pt deposited. Furthermore, we focus on the question if further reduction and/or oxidation reactions are possible on the as-obtained platinum-loaded tungsten oxide by studies involving hydrogenation, additional illumination (in aqueous phase) and additional photodeposition (in the presence of the H_2PtCl_6 precursor).

5.2 Materials and methods

5.2.1 Photodeposition

In a typical photodeposition experiment, when methanol (MeOH) was used as a sacrificial agent, a 50 mL aqueous solution containing 168 mg/L H_2PtCl_6 , an additional 12 mL of MeOH and 200 mg of WO_3 was prepared inside a quartz beakerglass, corresponding to approximately 2 wt% Pt (compared to WO_3). This beakerglass was covered by a quartz plate to prevent evaporation of the solution. Then, it was placed inside a black box reactor as described by Romão *et al.*^[44] Aluminum foil was used to cover the sides of the beakerglass to make sure that the solution was only top-illuminated. First, an hour of stirring at 450 rpm took place to obtain adsorption/desorption equilibrium. Afterwards, all lamps were switched on inside the box and reaction took place for t minutes, where $t = 2, 5, 10, 11.5, 13, 15, 30$ or 60 minutes. Solid and solution were subsequently separated by centrifugation for 30 minutes at 8500 rpm. The residue was washed 2 times with Millipore water and afterwards dried overnight at 80 °C. The residue was stored. In some cases, additional separation of the residue and remaining powder was performed before storage of the solution. To verify whether Pt adsorbs very strongly on the WO_3 surface, we repeated these experiments in the dark using different stirring times. These are labelled as $t = -59, -50, -30$ and -1 minutes, which corresponds to 1, 10, 30 and 59 minutes of stirring in the dark respectively.

When methanol was not used as a sacrificial agent, a 50 mL aqueous solution containing 168 mg/L H_2PtCl_6 and 200 mg WO_3 was prepared. Photodeposition took place as described above, but with different time intervals: $t = -50, -30, -1, 5, 15, 30, 45, 60, 180$ or 300 minutes (the negative values corresponding with $t + 60$ min stirring time in the dark). Again, centrifugation as described above took place, both to separate residue and filtrate and to wash the residue. Furthermore, we started additional photodeposition experiments without methanol and added 12 mL of methanol later. First, photodeposition took place for 1 hour without methanol. Then the methanol was added and $t = 5$ or 10 minutes of additional illumination took place, after which residue and filtrate were separated once more.

In a variation of the photodeposition experiment without MeOH described above, illumination took place for 300 minutes with a 50 mL aqueous solution containing 840 mg/L H_2PtCl_6 and 200 mg WO_3 , corresponding to approximately 10 wt% Pt (compared to WO_3). A part of this sample was hydrogenated to study whether further reduction of the as-deposited Pt could take place. To do so, the Pt/WO_3 powder was loaded inside a tube-furnace oven and treated overnight at 500 °C under a gas flow

of nitrogen containing 4.76 vol% H₂ (heating rate of 10 K/min). To verify whether full reduction had taken place, additional illumination of both the untreated and the H₂ treated Pt/WO₃ took place in a reactor as described by Zoontjes.^[45] 25 mL of aqueous solution containing 25 mg of (potentially H₂ treated) Pt/WO₃ and 0.01M H₂SO₄ (corresponding to a pH of 2) was illuminated for a minimum of 5 hours. Prior to light exposure, purging of the reactor took place with helium to remove most of the oxygen and nitrogen inside the solution. We hypothesized that if platinum was present in an oxidized state on the surface, further reduction to metallic Pt could take place by photo-excited electrons. The holes could then be used to oxidize water, producing oxygen. Therefore we monitored the amounts of oxygen formed during illumination.

The as-obtained hydrogenated powder was exposed to additional photodeposition in two different experiments. In the first case, a 50 mL aqueous solution containing 8.4 mg/L H₂PtCl₆, an additional 0.6 mL methanol and 10 mg of H₂ treated Pt/WO₃ was prepared inside a quartz beakerglass covered by a quartz plate. Additional photodeposition took place for 1 hour in the box reactor as described above. In a variation of this experiment where no methanol was used, a 50 mL aqueous solution containing 21 mg/L H₂PtCl₆ and 25 mg of H₂ treated Pt/WO₃ was prepared inside a quartz beakerglass covered by a quartz plate. Again photodeposition took place for 5 hours in the box reactor as described above.

5.2.2 Characterization

To determine how much Pt had been deposited on the various samples, the stored residues were analyzed on their Pt-content using inductively coupled plasma atomic emission spectroscopy (ICP-AES) (Varian Liberty II, Sequential ICP-AES). In the case of the samples where methanol was used, the residue was diluted a factor 6 before it was measured with ICP-AES. Further characterization of some of the solids took place using X-ray photoelectron spectroscopy (XPS) (Quantera SXM from Physical Electronics) to determine the oxidation state of Pt, and high resolution-transmission electron microscopy (HR-TEM) (FEI Instruments) to study the dispersion and morphology of as-deposited Pt.

5.3 Results and discussion

5.3.1 Kinetics of photodeposition

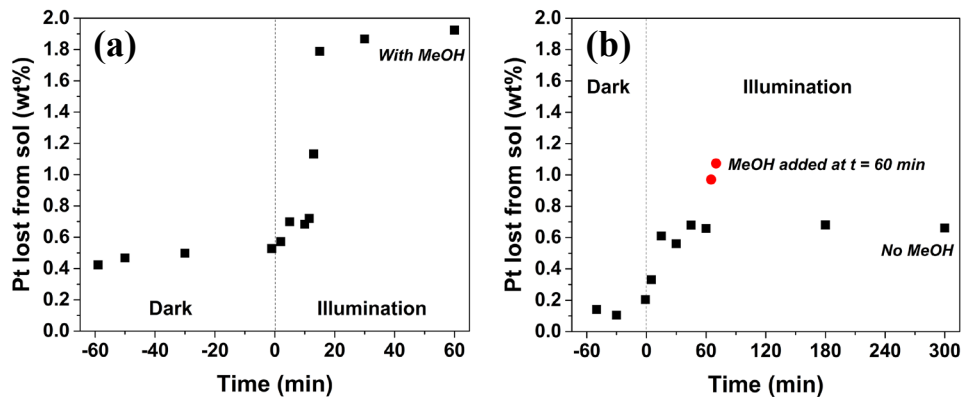


Figure 5.1. Amounts of Pt lost from the H_2PtCl_6 solution in wt% after (a) photodeposition with methanol and (b) photodeposition without methanol (or MeOH added after 1 hour of illumination).

Figure 5.1a depicts the amount of Pt lost from the H_2PtCl_6 solution during photodeposition on WO_3 when methanol was used. Before the lamps were switched on, 0.53 wt% of Pt was already present on the WO_3 . As no photodeposition could have taken place up to that point, the loss of Pt from the solution must have been due to adsorption of an anionic platinum complex on the WO_3 surface. This is in agreement with earlier studies in our group showing the importance of adsorption of platinum species on the WO_3 surface in forming Pt particles.^[46] Remarkably even washing did not result in the removal of the Pt, implying that the adsorption is very strong. When illumination was started, after a quick, but small rise, very little change is observed in the amount removed from the solution, up to about 11 minutes. Then, a quick increase in the amount of Pt deposited on the surface is evident. Within 15 minutes, almost all the Pt had been deposited on the surface of the WO_3 (1.79 wt%). Afterwards, most of the remaining Pt was deposited on the WO_3 as well with a much slower reaction speed. The kinetics of the photodeposition process can thus be divided in three intervals, as summarized in Table 5.1:

Table 5.1. Definition of intervals during photodeposition using MeOH.

Interval	Start (min)	wt%	Stop (min)	wt%	Δ wt%	Δ wt%/min
1	-1	0.53	11.5	0.72	0.19	0.017 ^a
2	11.5	0.72	15	1.79	1.07	0.31
3	15	1.79	60	1.92	0.13	0.0029

a) Over 11.5 min. It is assumed that at 0 min the same amount of wt% was present as at -1 min.

To explain the rapid increase after 11.5 min, metallic Pt is likely formed during the photodeposition process. This acts as a catalyst, increasing the photodeposition rate until all Pt has been deposited.

When no methanol is used, photodeposition kinetics occur as in Figure 5.1b. Again, adsorption of the Pt complex is observed after one hour of stirring in the dark. However, the amount of Pt lost from the solution is lower than when MeOH is used (0.20 wt% vs. 0.53 wt%). Apparently, MeOH has quite a large influence on the adsorption kinetics of a Pt complex on WO₃. It is likely that methanol itself adsorbs on the WO₃ surface. As a result, surface properties such as the surface charge are altered, likely stimulating sorption of Pt complexes. After the lights are switched on, the amount of Pt deposited on WO₃ rapidly jumps to 0.61 wt%. However, no significant increase in the amount of Pt deposited is observed afterwards (0.66 wt% after 300 minutes). This is surprising, as not all Pt from the solution has been deposited yet on the WO₃ surface. When photodeposition takes place with a larger concentration of H₂PtCl₆ (aiming to photodeposit 10 wt% of Pt on the WO₃ surface), only 1.4 wt% of Pt is deposited after 5 hours. This implies that even a lower photodeposition efficiency (14%) is obtained than when the aim is to deposit 2 wt% Pt (33%). The results seem to suggest that there is an equilibrium present between the amount of Pt photodeposited on the WO₃ surface and the amount of Pt present in the solution when no MeOH is used. Figure 5.1b also demonstrates that when methanol is introduced in the photodeposition system after 60 minutes of illumination, the amount of Pt deposited increases rapidly within 10 minutes. This implies that the reaction equilibrium is affected when MeOH is introduced during photodeposition.

5.3.2 Oxidation state of Pt after photodeposition

Figure 5.2 provides an overview of XPS spectra measured of Pt/WO₃ obtained at different time intervals of photodeposition, both with and without methanol, focusing on the Pt4f region.

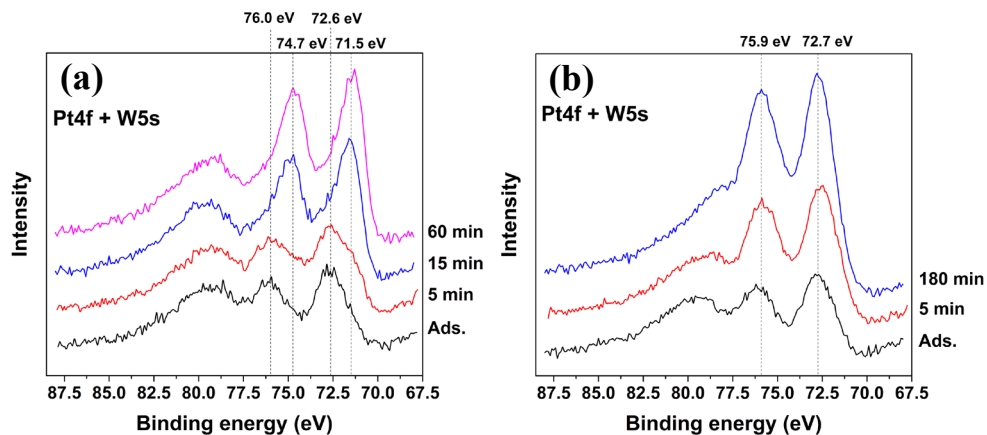


Figure 5.2. XPS spectra recorded of various samples obtained at different photodeposition times (a) with usage of methanol and (b) without usage of methanol. Spectra were recorded in the Pt4f + W5s region. Measurements labelled as ‘Ads.’, which is an abbreviation for adsorption, are measurements on samples recovered 1 minute prior to photodeposition. The peaks around 79 eV correspond to the W5s singlet.

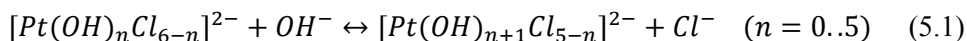
When methanol is used (Figure 5.2a), dominant XPS peaks prior and just after the start of illumination are observed at 72.6 eV and 76.0 eV, corresponding to the Pt4f doublet. These peaks quickly disappear in favor of peaks at 71.5 eV and 74.7 eV. The initial peaks correspond to an oxidized form of Pt, namely Pt^{II}, whereas the latter peaks correspond to metallic Pt⁰.^[30, 34] Figure 5.2b demonstrates that when no methanol is used, XPS peaks are found at 72.7 eV and 75.9 eV. These values correspond as well to Pt^{II}, suggesting that Pt is present in either an oxidized state PtO or an hydroxide state Pt(OH)₂. Remarkably, the oxidation state of the Pt does not change at all during photodeposition without MeOH. This is likely explained by the following: photoreduction to Pt does take place, but the oxidation state of the Pt immediately changes back to Pt^{II} due to photo-oxidation.

Comparing Figure 5.2a and 5.2b reveals that methanol clearly plays a critical role in determining the oxidation state of Pt during photodeposition and is necessary to obtain metallic Pt⁰. Remarkably, in both cases, prior to photodeposition, platinum seems already present in the Pt^{II} state. However, Pt in the precursor (H₂PtCl₆) is present as Pt^{IV}. We assume the ligands to induce a positive shift in binding energy, and still assign the initial spectra to Pt^{IV}. Further investigation is needed to verify XPS positions of various ionic Pt species present on WO₃ surfaces. Table 5.2 summarizes the amounts of Pt of Cl detected at the surface.

Table 5.2. XPS studies of different as-obtained Pt/WO₃ samples, demonstrating the at% of Pt and Cl present on the surface.

MeOH/No MeOH	Reaction time (min)	At% Pt	At% Cl
MeOH	Ads.	0.80	0.14
	5	1.09	0.23
	15	1.30	0.00
	60	1.57	0.10
No MeOH	Ads.	0.94	0.16
	5	1.41	0.36
	180	2.26	0.61

Surprisingly, the measured at% of Cl present on the surface before illumination starts is small, indicating that the adsorbed Pt complex must already have lost most of its Cl⁻ ligands. An explanation might be that hydrolysis could have taken place, replacing the Cl⁻ ligands with OH⁻ ligands.^[24, 30, 34]



However, this is surprising, as photodeposition was performed in acidic conditions, favoring the presence of Cl⁻ ligands over OH⁻ ligands in the Pt complex. It could be that Pt with OH⁻ species are much more favored for adsorption on the WO₃ surface rather than Pt with Cl⁻ species. Lastly, it is odd that the observed amounts of at% Pt detected at the surface are considerably lower when MeOH is used than when this is not the case. This is in contrast with the results observed in the ICP-AES measurements in Figure 5.1. However, one should keep in mind that XPS is a surface analysis technique. We will demonstrate in the next section that when MeOH is used, Pt is deposited as large clusters on the surface of WO₃, whereas the dispersion obtained when methanol is absent is much larger. This is in agreement with the large Pt intensities observed in Figure 5.2b.

5.3.3 Additional illumination experiments

For the Pt/WO₃ sample which was obtained through photodeposition of Pt without MeOH on WO₃ (solution amount equivalent to 10 wt%), XPS studies reveal that Pt is present as well in an oxidized Pt^{II} state. When we performed additional illumination in H₂SO₄ and *in situ* monitored the amount of oxygen formed, we observed the trend depicted in Figure 5.3. Clearly, when illumination starts, oxygen is formed. This implies that either from the PtO/Pt(OH)₂ or from oxidation of water O₂ must have formed. One would expect that this oxidation reaction is only possible

when reduction of Pt^{II} to Pt^0 takes place. However, remarkably, when XPS spectra are measured both before and after additional illumination (Figure 5.4), no shift of the binding energy to lower values is observed for Pt4f. This would imply that no reduction of the Pt^{II} could have taken place. Instead, it even seems that there is a slight shift to higher binding energies, likely being caused due to the PtO/Pt(OH)_2 interacting with altered ligands (such as the presence of SO_4^{2-} groups) compared to when photodeposition took place. Another striking feature from the as-measured XPS spectra is the amount of Pt measured. Before the additional illumination procedure, 2.76 at% of Pt is measured; after the additional illumination procedure, only 1.36 at% appears left. This implies that roughly half of the Pt must have disappeared from the WO_3 surface. It could be that PtO/Pt(OH)_2 oxidizes back in the solution, releasing oxygen in the process. The only reduction reaction possible would still be the reduction of Pt^{II} to Pt^0 however. We will go into more detail on the mechanisms involved in the additional illumination experiments in the discussion.

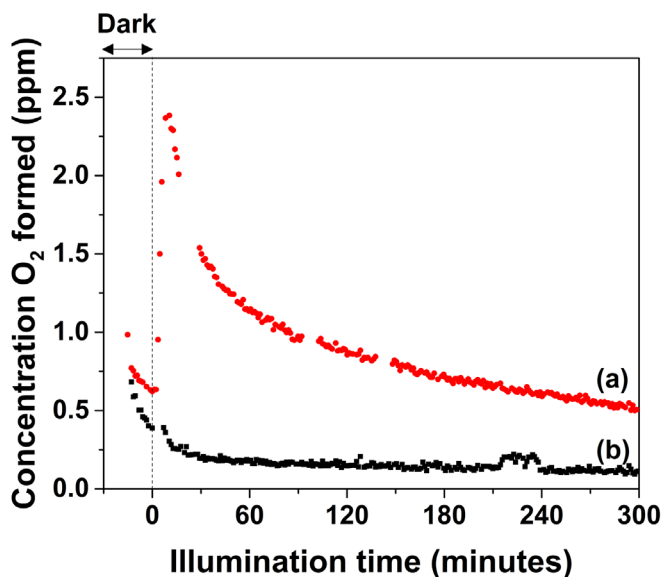


Figure 5.3. O_2 evolution during additional illumination of Pt/WO_3 (obtained without 5 hours illumination, no MeOH and an aim of 10 wt% Pt) in H_2SO_4 ; (a) without hydrogenation and (b) with hydrogenation at 500 °C. Hydrogen was not evolved in the process.

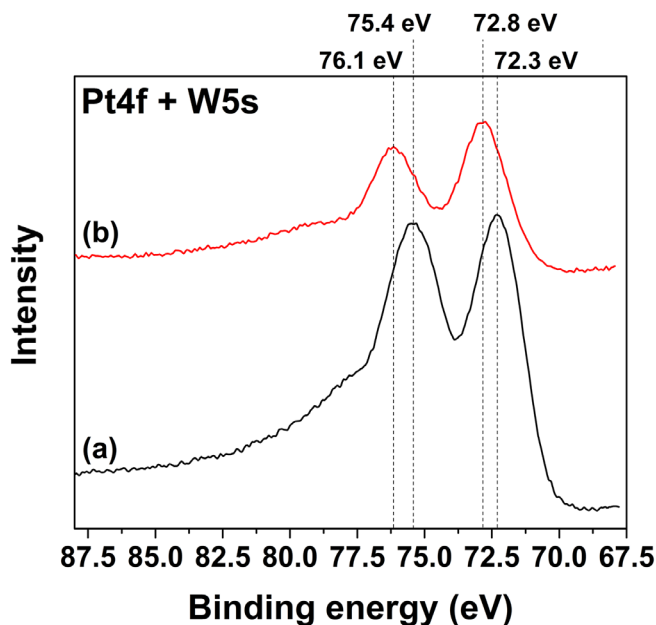


Figure 5.4. XPS spectra of Pt/WO₃ obtained through 5 hours of photodeposition without MeOH and a solution amount equivalent to 10 wt% Pt; (a) before and (b) after additional illumination in H₂SO₄.

When the hydrogen treated Pt/WO₃ sample was exposed to additional illumination in H₂SO₄, no formation of oxygen was observed (Figure 5.3). This confirms the metallic nature of Pt. XPS spectra of the hydrogenated Pt/WO₃ before and after exposure to illumination in the presence of H₂SO₄ are depicted in Figure 5.5.

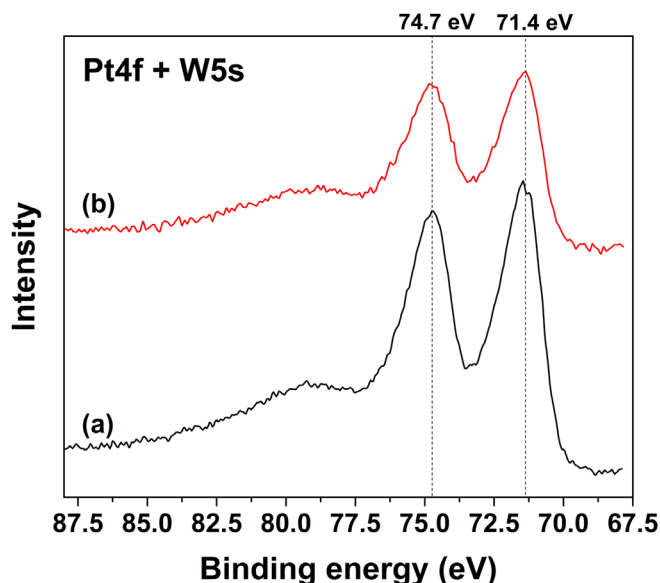


Figure 5.5. XPS spectra of hydrogenated Pt/WO_3 obtained through 5 hours of photodeposition without MeOH and an aim of 10 wt% Pt; (a) before and (b) after additional illumination in H_2SO_4 . Hydrogenation took place at 500 °C.

Again, a lower amount of Pt on the surface is measured after additional illumination than before (1.34 at% vs. 1.75 at%). However, this loss is not as extreme as when the unhydrogenated sample was used in the same experiment.

Comparison of the XPS spectra of the untreated and H_2 treated Pt/WO_3 reveal that the Pt has reduced to metallic Pt, whereas the W retains its oxidized state (appendix, Figure A5.1). According to Liu *et al.*, when significant reduction of WO_3 takes place, a broadening of the doublets corresponding to W4f should be visible in the XPS spectra, as well as a small shift to higher binding energies.^[47] Also, when the reduction is too significant, photocatalytic activity of the sample in water oxidation will disappear. In our studies however, we do neither see a broadening of the peaks, nor an upward shift in binding energy (we even observe a small shift to lower binding energies). We therefore conclude that the WO_3 is reduced only at the outermost layer, if at all.

5.3.4 Additional photodeposition experiments

When we perform additional photodeposition of Pt on the hydrogenated Pt/WO_3 sample both in the presence and absence of methanol, we observe XPS spectra and the corresponding at% of Pt and Cl on the surface as shown in Figure 5.6 and Table 5.3 respectively. When additional photodeposition is performed with MeOH,

more Pt is deposited on the surface of the WO_3 . The XPS peaks at 71.4 eV and 74.7 eV, corresponding with the Pt4f doublet, confirm that the dominant oxidation state is Pt^0 . However, when no MeOH is used, the amount of additional Pt measured on the surface is low. XPS peaks at 75.7 and 72.5 eV reveal that Pt^{II} is now just as dominantly present as Pt^0 . This large fraction of Pt^{II} could not only be attributed to the additional amount of Pt on the sample. Instead, it is far more likely that a photocatalytic oxidation of the already present Pt^0 to Pt^{II} has taken place. The corresponding photocatalytic reduction reaction in this case must have then been the reduction of Pt^{IV} to Pt^{II} . When methanol is introduced, the photocatalytic oxidation of metallic Pt^0 is prevented as the oxidation of MeOH is more favored.

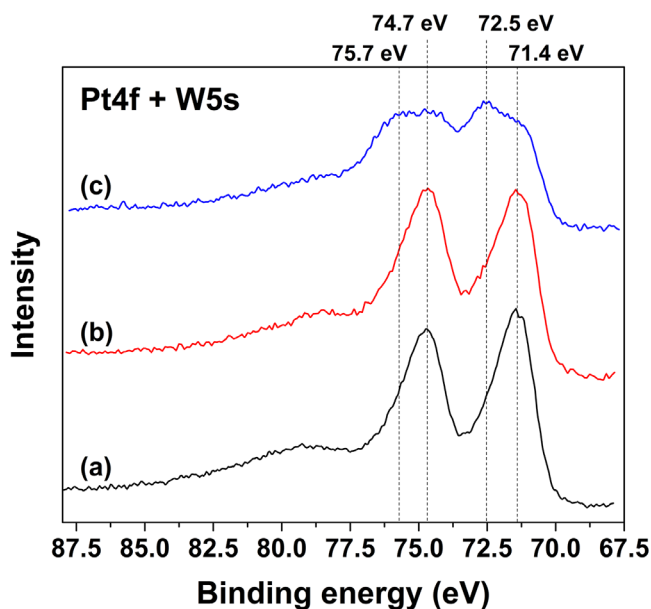


Figure 5.6. XPS spectra of hydrogenated Pt/WO_3 (a) before, (b) after an additional photodeposition experiment in the presence of methanol and (c) after an additional photodeposition experiment in the absence of methanol.

Table 5.3. XPS studies of hydrogenated Pt/WO_3 samples, demonstrating the at% of Pt and Cl present on the surface.

Sample	At% Pt	At% Cl
Before additional photodeposition	1.75	N.A. ^a
After additional photodeposition with MeOH	2.29	0.14
After additional photodeposition without MeOH	1.86	0.12

a) N.A. = Not Available

5.3.5 HR-TEM studies

Figure 5.7 displays HR-TEM images of (a) Pt/WO₃ obtained through 1 hour of photodeposition (aim: 2 wt% Pt) using methanol as a hole scavenger, (b) Pt/WO₃ obtained through 5 hours of photodeposition without MeOH (aim: 2 wt% Pt) and (c) Pt/WO₃ obtained through 5 hours of photodeposition without MeOH (aim: 10 wt% Pt). EDX studies confirm that in all cases platinum is present on the surface (appendix, Figure A5.2). When methanol is used, large clusters of metallic Pt nanoparticles (particles of 2-4 nm ranging up to clusters of even 55 nm) are deposited on the WO₃ particles. No usage of MeOH on the other hand results in very disperse, small platinum oxide particles over the WO₃ surface (in the order of roughly 1-3 nm). A different concentration of platinum in solution during photodeposition without MeOH does not result in an obvious change (except for a difference in the amount of loading as demonstrated by ICP). As the XPS studies have demonstrated, metallic Pt is formed when MeOH is used. The Pt⁰ particles will act as cocatalysts, stimulating further platinum growth at these sites, resulting in large Pt aggregates after 60 minutes. The high dispersion of the platinum oxide particles in Figures 5.7b and 5.7c hints strongly at the absence of this cocatalytic effect when no MeOH is used.

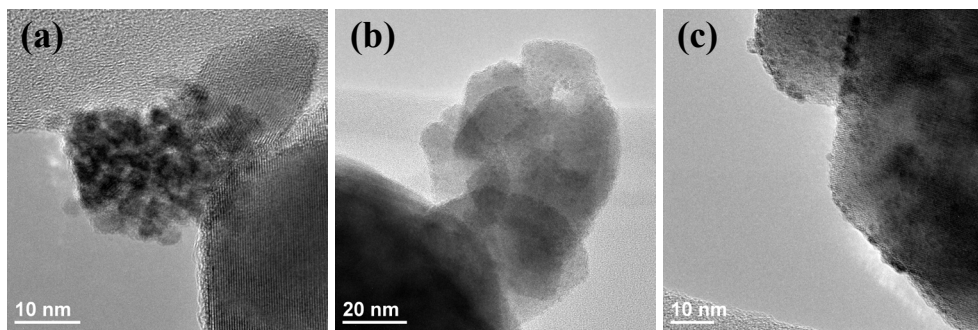


Figure 5.7. HR-TEM images of Pt/WO₃ obtained through (a) 1 hour of photodeposition using MeOH (aim: 2 wt% Pt), (b) 5 hours of photodeposition using no MeOH (aim: 2 wt% Pt) and (c) 5 hours of photodeposition using no MeOH (aim: 10 wt% Pt).

When hydrogen treatment is performed at 500 °C on the Pt/WO₃ obtained through 5 hours of photodeposition using no MeOH (aim: 10 wt% Pt), HR-TEM images reveal that the Pt particles have increased in size, ranging from roughly 3 to 11 nm (Figure 5.8a). It should be noted that it seems that a very thin layer of small particles is deposited on the surface of the WO₃. However, investigation with EDX confirms that this is not Pt. It might be more likely that the surface layer of the WO₃ is reduced due to the H₂ treatment, leading to a change in the morphology of the surface.

Interestingly, we observe that when additional photodeposition on this sample is performed in the absence of methanol, it seems that *less* Pt is observed at the surface of the WO_3 (Figure 5.8b). Although the larger Pt particles are still present on the WO_3 , the amount of these particles detected is significantly lower. Furthermore, it seems that platinum is also present on the surface of the WO_3 as small particles (1-4 nm), although these particles are hard to detect. These results are in contrast with the XPS results in Table 5.3, which suggest that a slightly larger fraction of Pt is deposited on the surface. Again, the higher XPS intensities likely confirm a higher dispersion of the Pt particles, rather than the deposition of additional Pt. After additional photodeposition without MeOH, a larger percentage of the Pt present on the surface can be detected, explaining the higher at% Pt measured. When methanol is present during the additional photodeposition, *more* Pt particles are observed at the surface of the WO_3 (Figure 5.8c). This is in agreement with the XPS results in Table 5.3.

These results seem to imply that by additional photodeposition, Pt particles are oxidized in the absence of methanol, ultimately resulting in dissolution of Pt. When methanol is present, methanol will be oxidized rather than Pt, inducing photodeposition of more Pt particles. Surprisingly, the additional Pt particles seem to have been deposited as independent Pt particles, rather than being deposited where Pt particles were already present.

When the hydrogenated Pt/ WO_3 is exposed to illumination in the presence of H_2SO_4 , no significant change is observed when compared to the hydrogenated Pt/ WO_3 before illumination (Figure 5.8d). This confirms the XPS findings.

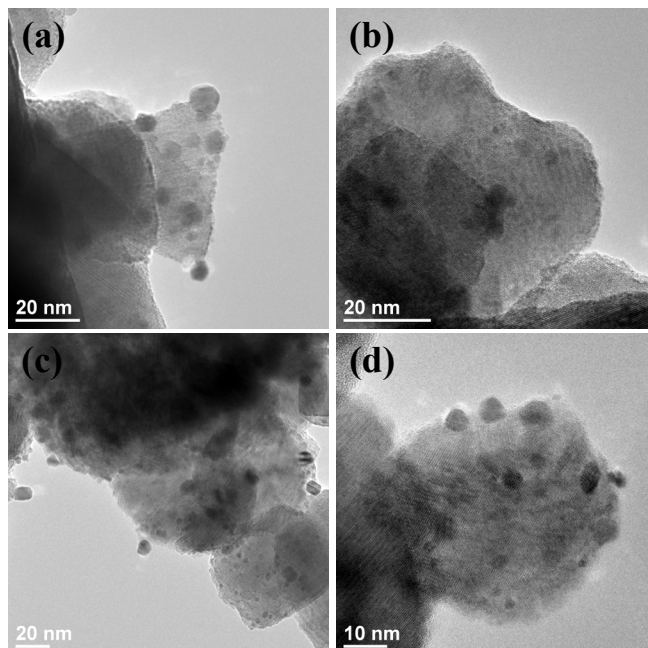
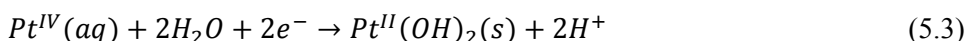


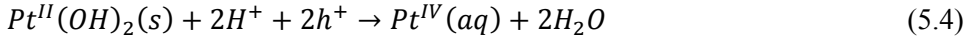
Figure 5.8. HR-TEM images of (a) hydrogen treated Pt/WO₃. The Pt/WO₃ was obtained using 5 hours of photodeposition using no MeOH (aim: 10 wt% Pt). (b) Sample A after 5 hours of additional photodeposition using no MeOH (aim: 2 wt% additional Pt). (c) Sample A after 1 hour of additional photodeposition using MeOH (aim: 2 wt% additional Pt). (d) Sample A after being exposed to illumination in the presence of H₂SO₄.

5.3.6 Discussion on photodeposition mechanism

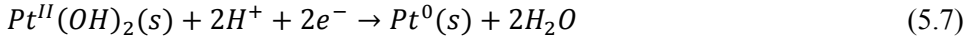
In this chapter, we have seen that the usage of methanol plays a crucial role in photodeposition of Pt on WO₃ in i) the amount of Pt deposited, ii) the oxidation state and iii) the dispersion of the Pt particles. To understand what role methanol plays in the photodeposition reaction, we explore which reduction reactions and oxidation reactions can occur, both in the presence and absence of MeOH. We hypothesize that in both cases initially photoreduction of Pt^{IV} takes place, where Pt^{IV} is present in the form of [PtCl_{6-n}(OH)_n]²⁻ (n = 0..6):



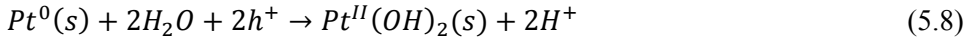
For a corresponding oxidation reaction several possibilities arise, which involve the back-oxidation of the $Pt^{II}(OH)_2$ complex, water oxidation and, if present, methanol oxidation:



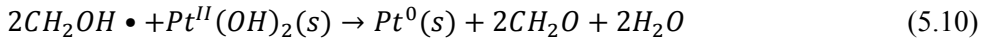
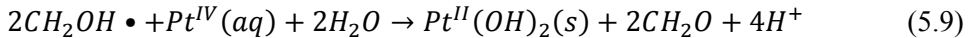
When $Pt^{II}(OH)_2$ is formed, this can be further reduced to metallic Pt^0 . In such case, the following reduction reaction takes place:



Back-oxidation of as-formed Pt^0 could also take place:



It should be kept in mind that methanol radicals can act as strong reductants in Pt reduction as well, as advocated by Lee and Choi.^[19] Therefore, these radicals can contribute to the reduction of both Pt^{IV} and $Pt^{II}(OH)_2$ as follows:



When methanol is present during the photodeposition reaction, metallic Pt^0 is formed, as evidenced in Figure 5.2a. This implies that during the reduction of Pt, methanol oxidation (equation 5.6) is the energetically favored oxidation reaction, *i.e.* the methanol oxidation potential is more negative than the other oxidation potentials (Figure 5.9). The Pt^0 particles themselves will start to act as cocatalytic nanoparticles, which will result in an increased photodeposition rate (Figure 5.1a) and cluster formation (Figure 5.7a). In the absence of methanol, $Pt^{II}(OH)_2$ seems to be the dominant oxidation state, and not all Pt could be deposited. If water oxidation (equation 5.5) is the favored oxidation reaction, such behavior would not be observed. The only conclusion which can be drawn is that the favored oxidation

reaction is actually the back-oxidation of Pt. This applies on two levels: first, $\text{Pt}^{\text{II}}(\text{OH})_2$ formed on the surface of the WO_3 can be re-oxidized to Pt^{IV} (equation 5.4), which will disperse in the solution. Second, Pt^0 formed out of $\text{Pt}^{\text{II}}(\text{OH})_2$ will be oxidized back as well. These two ‘short circuits’ present will result in the absence of Pt^0 and a lack of full Pt photodeposition. The constant deposition/dissolution kinetics in the $\text{Pt}^{\text{IV}}/\text{Pt}^{\text{II}}(\text{OH})_2$ short circuit also explain the high dispersion of the $\text{Pt}^{\text{II}}(\text{OH})_2$ particles.

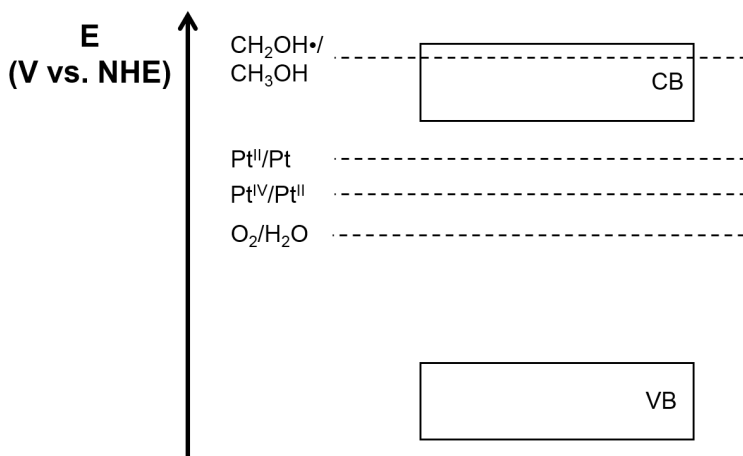
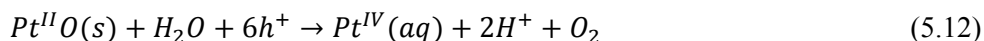
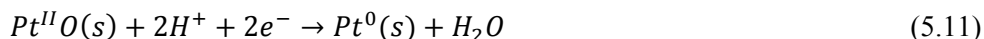
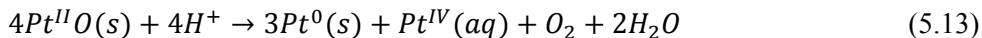


Figure 5.9. Hypothetical positions of redox potentials relevant in this study on a E (V vs. NHE) scale, compared to the band positions of WO_3 . Note that the positions are not to scale!

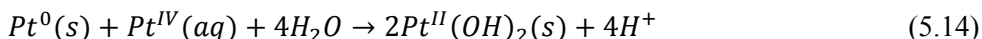
Oxygen formation is observed when additional illumination of $\text{Pt}^{\text{II}}/\text{WO}_3$ particles takes place in an aqueous H_2SO_4 solution (Figure 5.3). At first glance, one might speculate that this oxygen is formed due to water oxidation, parallel to the reduction of Pt^{II} . However, we have discussed that the oxidation of Pt^{II} is favored over the oxidation of water. Due to drying of the $\text{Pt}^{\text{II}}/\text{WO}_3$ after photodeposition, we hypothesize that the Pt^{II} particles are in a PtO state rather than a $\text{Pt}(\text{OH})_2$ state prior to the additional illumination experiments. When $\text{Pt}^{\text{II}}/\text{WO}_3$ is inserted in the H_2SO_4 solution, the following reduction and oxidation reactions become possible, making the production of oxygen feasible:



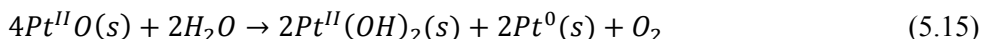
Combining equations 5.11 and 5.12 yields:



In Figure 5.3 the oxygen formation rate decreases over time. This would imply that equation 5.13 is finite. Therefore, we hypothesize that equations 5.11 and 5.12 are only initial redox reactions. When Pt^{IV} is formed, it will be reduced to $Pt^{II}(OH)_2$ (equation 5.3), while as-formed Pt^0 will be oxidized to $Pt^{II}(OH)_2$ as well (equation 5.8). Combined, these reactions can be written as follows:



Or, combining equations 5.13 and 5.14:



The whole short circuit of equations 5.3, 5.4, 5.7 and 5.8 starts over again, ultimately preventing the existence of equations 5.11 to 5.13. This also explains why considerably less Pt is detected with XPS when additional illumination takes place. Still, for each mole of $Pt^{II}(OH)_2$ formed via equation 5.15, one mole of Pt^0 is formed, implying that the metallic Pt^0 -state should have been visible in XPS studies (Figure 5.4). As none is observed however, only a small fraction of the $Pt^{II}O$ must have been exposed to redox reactions 5.11 and 5.12. From equation 5.15 we learn that when oxygen production stops, Pt^0 production stops as well. Hence, we should be able to calculate the amount of metallic Pt^0 formed by area integration of the oxygen peak in Figure 5.3. Remarkably, we find that 37% of the Pt present on the Pt/ WO_3 sample after illumination must have been in a Pt^0 state. This would imply that either the formed metallic Pt^0 must have oxidized, or that another mechanism is contributing to O_2 formation as well. Further research is required to find the origin of these contradicting data. When hydrogenated Pt/ WO_3 is used, no oxygen formation is observed, implying that equations 5.11, 5.12, 5.13 and 5.15 do not take place.

Finally, we touch upon the additional photodeposition experiments on as-obtained hydrogenated Pt/ WO_3 . In the presence of methanol, we have demonstrated that additional Pt is deposited on the surface of the hydrogenated WO_3 . Reduction of Pt^{IV} species to Pt^0 takes place (equations 5.3 and 5.7), while the oxidation of methanol is favored (equation 5.6). It should be kept in mind that this methanol can contribute

as well to the reduction of the Pt species (equations 5.9 and 5.10). When no methanol is used however, a redistribution of the platinum on the WO_3 occurs, as demonstrated in Figure 5.8b. Both Pt^0 and Pt^{II} species are observed with XPS (Figure 5.6c). When no methanol is present, reduction of Pt^{IV} will take place initially. The most favored oxidation reaction will be the oxidation of the metallic Pt^0 (equation 5.8), forming $\text{Pt}^{\text{II}}(\text{OH})_2$. In this system, the short circuits of equations 5.3, 5.4, 5.7 and 5.8 will become dominant again, meaning that $\text{Pt}^{\text{II}}(\text{OH})_2$ is oxidized to aqueous Pt^{IV} , and that redistribution of the Pt particles is evident.

5.4 Conclusions

In this chapter, we have provided a detailed study on the photodeposition kinetics of Pt on WO_3 . In particular, we demonstrate the extremely important influence of methanol during photodeposition. When MeOH is used, all Pt is deposited on the surface of WO_3 in a dominantly metallic form. This is possible due to a favored oxidation of methanol over the back-oxidation of the Pt particles. Large clusters of Pt particles are observed, hinting at a cocatalytic effect of the Pt particles on the WO_3 surface. When no MeOH is used, Pt is present in a highly dispersed, oxidized form on the surface of WO_3 . Photoreduction to metallic platinum is not possible due to a favored back-oxidation to $\text{Pt}(\text{OH})_2$. Not all Pt could be deposited on the surface of the WO_3 due to the photo-oxidation of $\text{Pt}(\text{OH})_2$ to Pt^{IV} , which will dissolve in the solution. Additional illumination experiments in H_2SO_4 confirm the instability of $\text{PtO}/\text{Pt}(\text{OH})_2$. When as-obtained PtO/WO_3 is hydrogenated and exposed once more to a photodeposition experiment without MeOH, the back-oxidation of metallic platinum is observed, ultimately resulting in a redistribution of Pt particles on the surface. Once more this redistribution could be prevented with the introduction of methanol in the photodeposition system, resulting in more Pt particles being present on the surface of the WO_3 . These studies provide two important conclusions: first of all, an important basis to engineer Pt particles of desired oxidation state and dispersion on WO_3 is provided. Second, the stability of Pt/WO_3 in photocatalytic reduction is not guaranteed as long as the oxidation of Pt is the most favored photo-oxidation reaction.

5.5 Bibliography

- [1] Abe, R.; *Recent progress on photocatalytic and photoelectrochemical water splitting under visible light irradiation*. Journal of Photochemistry and Photobiology C: Photochemistry Reviews **2010**, 11, 179-209.
- [2] Kudo, A.; Miseki, Y.; *Heterogeneous photocatalyst materials for water splitting*. Chemical Society Reviews **2009**, 38, 253-278.

- [3] Maeda, K.; *Photocatalytic water splitting using semiconductor particles: history and recent developments*. Journal of Photochemistry and Photobiology C: Photochemistry Reviews **2011**, 12, 237-268.
- [4] Mo, J.; Zhang, Y.; Xu, Q.; Lamson, J. J.; Zhao, R.; *Photocatalytic purification of volatile organic compounds in indoor air: a literature review*. Atmospheric Environment **2009**, 43, 2229-2246.
- [5] Dong, S.; Feng, J.; Fan, M.; Pi, Y.; Hu, L.; Han, X.; Liu, M.; Sun, J.; Sun, J.; *Recent developments in heterogeneous photocatalytic water treatment using visible light-responsive photocatalysts: a review*. RSC Advances **2015**, 5, 14610-14630.
- [6] Chong, M. N.; Jin, B.; Chow, C. W. K.; Saint, C.; *Recent developments in photocatalytic water treatment technology: a review*. Water Research **2010**, 44, 2997-3027.
- [7] Kim, J.; Lee, C. W.; Choi, W.; *Platinized WO₃ as an environmental photocatalyst that generates OH radicals under visible light*. Environmental Science and Technology **2010**, 44, 6849-6854.
- [8] Abe, R.; Takami, H.; Murakami, N.; Ohtani, B.; *Pristine simple oxides as visible light driven photocatalysts: highly efficient decomposition of organic compounds over platinum-loaded tungsten oxide*. Journal of the American Chemical Society **2008**, 130, 7780-7781.
- [9] Fraters, B. D.; Amrollahi, R.; Mul, G.; *How Pt nanoparticles affect TiO₂-induced gas-phase photocatalytic oxidation reactions*. Journal of Catalysis **2015**, 324, 119-126.
- [10] Abe, R.; Higashi, M.; Domen, K.; *Overall water splitting under visible light through a two-step photoexcitation between TaON and WO₃ in the presence of an iodate-iodide shuttle redox mediator*. ChemSusChem **2011**, 4, 228-237.
- [11] Arai, T.; Yanagida, M.; Konishi, Y.; Iwasaki, Y.; Sugihara, H.; Sayama, K.; *Promotion effect of CuO co-catalyst on WO₃-catalyzed photodegradation of organic substances*. Catalysis Communications **2008**, 9, 1254-1258.
- [12] Bamwenda, G. R.; Tsubota, S.; Nakamura, T.; Haruta, M.; *Photoassisted hydrogen production from a water-ethanol solution: a comparison of activities of Au-TiO₂ and Pt-TiO₂*. Journal of Photochemistry and Photobiology, A: Chemistry **1995**, 89, 177-189.
- [13] Gunji, T.; Tsuda, T.; Jeevagan, A. J.; Hashimoto, M.; Tanabe, T.; Kaneko, S.; Miyauchi, M.; Saravanan, G.; Abe, H.; Matsumoto, F.; *Visible light induced decomposition of organic compounds on WO₃ loaded PtPb co-catalysts*. Catalysis Communications **2014**, 56, 96-100.
- [14] Murata, A.; Oka, N.; Nakamura, S.; Shigesato, Y.; *Visible-light active photocatalytic WO₃ films loaded with Pt nanoparticles deposited by sputtering*. Journal of Nanoscience and Nanotechnology **2012**, 12, 5082-5086.

- [15] Xie, K.; Sun, L.; Wang, C.; Lai, Y.; Wang, M.; Chen, H.; Lin, C.; *Photoelectrocatalytic properties of Ag nanoparticles loaded TiO₂ nanotube arrays prepared by pulse current deposition*. *Electrochimica Acta* **2010**, *55*, 7211-7218.
- [16] Kraeutler, B.; Bard, A. J.; *Heterogeneous photocatalytic preparation of supported catalysts. Photodeposition of platinum on TiO₂ powder and other substrates*. *Journal of the American Chemical Society* **1978**, *100*, 4317-4318.
- [17] Maeda, K.; Teramura, K.; Lu, D.; Saito, N.; Inoue, Y.; Domen, K.; *Noble-metal/Cr₂O₃ core/shell nanoparticles as a cocatalyst for photocatalytic overall water splitting*. *Angewandte Chemie - International Edition* **2006**, *45*, 7806-7809.
- [18] Steinmiller, E. M. P.; Choi, K. S.; *Photochemical deposition of cobalt-based oxygen evolving catalyst on a semiconductor photoanode for solar oxygen production*. *Proceedings of the National Academy of Sciences of the United States of America* **2009**, *106*, 20633-20636.
- [19] Lee, J.; Choi, W.; *Photocatalytic reactivity of surface platinized TiO₂: substrate specificity and the effect of Pt oxidation state*. *Journal of Physical Chemistry B* **2005**, *109*, 7399-7406.
- [20] Dukovic, G.; Merkle, M. G.; Nelson, J. H.; Hughes, S. M.; Alivisatos, A. P.; *Photodeposition of Pt on colloidal CdS and CdSe/CdS semiconductor nanostructures*. *Advanced Materials* **2008**, *20*, 4306-4311.
- [21] Pacholski, C.; Kornowski, A.; Weller, H.; *Site-specific photodeposition of silver on ZnO nanorods*. *Angewandte Chemie - International Edition* **2004**, *43*, 4774-4777.
- [22] Ohno, T.; Sarukawa, K.; Matsumura, M.; *Crystal faces of rutile and anatase TiO₂ particles and their roles in photocatalytic reactions*. *New Journal of Chemistry* **2002**, *26*, 1167-1170.
- [23] Li, R.; Zhang, F.; Wang, D.; Yang, J.; Li, M.; Zhu, J.; Zhou, X.; Han, H.; Li, C.; *Spatial separation of photogenerated electrons and holes among {010} and {110} crystal facets of BiVO₄*. *Nature Communications* **2013**, *4*.
- [24] Zhang, F.; Chen, J.; Zhang, X.; Gao, W.; Jin, R.; Guan, N.; Li, Y.; *Synthesis of titania-supported platinum catalyst: the effect of pH on morphology control and valence state during photodeposition*. *Langmuir* **2004**, *20*, 9329-9334.
- [25] Hidalgo, M. C.; Maicu, M.; Navío, J. A.; Colón, G.; *Photocatalytic properties of surface modified platinised TiO₂: effects of particle size and structural composition*. *Catalysis Today* **2007**, *129*, 43-49.
- [26] Sungbom, C.; Kawai, M.; Tanaka, K.; *XPS studies of the platinum species photodeposited on titania from aqueous chloroplatinic acid*. *Bulletin of the Chemical Society of Japan* **1984**, *57*, 871-872.
- [27] Joshi, U. A.; Darwent, J. R.; Yiu, H. H. P.; Rosseinsky, M. J.; *The effect of platinum on the performance of WO₃ nanocrystal photocatalysts for the*

- oxidation of Methyl Orange and iso-propanol*. Journal of Chemical Technology and Biotechnology **2011**, 86, 1018-1023.
- [28] Katsumata, H.; Oda, Y.; Kaneco, S.; Suzuki, T.; *Photocatalytic activity of Ag/CuO/WO₃ under visible-light irradiation*. RSC Advances **2013**, 3, 5028-5035.
- [29] Purwanto, A.; Widiyandari, H.; Ogi, T.; Okuyama, K.; *Role of particle size for platinum-loaded tungsten oxide nanoparticles during dye photodegradation under solar-simulated irradiation*. Catalysis Communications **2011**, 12, 525-529.
- [30] Chanjuan, X.; Zhengshi, C.; Qinglin, L.; Zhensheng, J.; *Effects of H⁺, Cl⁻ and CH₃COOH on the photocatalytic conversion of PtCl₆²⁻ in aqueous TiO₂ dispersion*. Journal of Photochemistry and Photobiology A: Chemistry **1995**, 87, 249-255.
- [31] Curran, J. S.; Domenech, J.; Jaffrezic-Renault, N.; Philippe, R.; *Kinetics and mechanism of platinum deposition by photoelectrolysis in illuminated suspensions of semiconducting titanium dioxide*. Journal of Physical Chemistry **1985**, 89, 957-963.
- [32] Mahlamvana, F.; Kriek, R. J.; *Photocatalytic reduction of platinum(II and IV) from their chloro complexes in a titanium dioxide suspension in the absence of an organic sacrificial reducing agent*. Applied Catalysis B: Environmental **2014**, 148-149, 387-393.
- [33] Li, Q.; Chen, Z.; Zheng, X.; Jin, Z.; *Study of photoreduction of PtCl₆²⁻ on CdS*. Journal of Physical Chemistry **1992**, 96, 5959-5962.
- [34] Jin, Z.; Chen, Z.; Li, Q.; Xi, C.; Zheng, X.; *On the conditions and mechanism of PtO₂ formation in the photoinduced conversion of H₂PtCl₆*. Journal of Photochemistry and Photobiology, A: Chemistry **1994**, 81, 177-182.
- [35] Wang, Y.; Wang, Y.; Xu, R.; *Photochemical deposition of Pt on CdS for H₂ evolution from water: markedly enhanced activity by controlling Pt reduction environment*. Journal of Physical Chemistry C **2013**, 117, 783-790.
- [36] Zheng, H.; Ou, J. Z.; Strano, M. S.; Kaner, R. B.; Mitchell, A.; Kalantar-Zadeh, K.; *Nanostructured tungsten oxide - properties, synthesis, and applications*. Advanced Functional Materials **2011**, 21, 2175-2196.
- [37] Ma, S. S. K.; Maeda, K.; Abe, R.; Domen, K.; *Visible-light-driven nonsacrificial water oxidation over tungsten trioxide powder modified with two different cocatalysts*. Energy and Environmental Science **2012**, 5, 8390-8397.
- [38] Zhu, T.; Chong, M. N.; Chan, E. S.; *Nanostructured tungsten trioxide thin films synthesized for photoelectrocatalytic water oxidation: a review*. ChemSusChem **2014**, 7, 2974-2997.
- [39] Waldner, G.; Brüger, A.; Gaikwad, N. S.; Neumann-Spallart, M.; *WO₃ thin films for photoelectrochemical purification of water*. Chemosphere **2007**, 67, 779-784.

- [40] Arai, T.; Horiguchi, M.; Yanagida, M.; Gunji, T.; Sugihara, H.; Sayama, K.; *Complete oxidation of acetaldehyde and toluene over a Pd/WO₃ photocatalyst under fluorescent- or visible-light irradiation*. Chemical Communications **2008**, 5565-5567.
- [41] Sakai, Y.; Shimanaka, A.; Shioi, M.; Kato, S.; Satokawa, S.; Kojima, T.; Yamasaki, A.; *Fabrication of high-sensitivity palladium loaded tungsten trioxide photocatalyst by photodeposit method*. Catalysis Today **2015**, 241, 2-7.
- [42] Widiyandari, H.; Purwanto, A.; Balgis, R.; Ogi, T.; Okuyama, K.; *CuO/WO₃ and Pt/WO₃ nanocatalysts for efficient pollutant degradation using visible light irradiation*. Chemical Engineering Journal **2012**, 180, 323-329.
- [43] Qamar, M.; Yamani, Z. H.; Gondal, M. A.; Alhooshani, K.; *Synthesis and comparative photocatalytic activity of Pt/WO₃ and Au/WO₃ nanocomposites under sunlight-type excitation*. Solid State Sciences **2011**, 13, 1748-1754.
- [44] Romão, J. S.; Hamdy, M. S.; Mul, G.; Baltrusaitis, J.; *Photocatalytic decomposition of cortisone acetate in aqueous solution*. Journal of Hazardous Materials **2015**, 282, 208-215.
- [45] Zoontjes, M. G. C.; *Visible-light-induced water splitting on a chip*. Enschede, **2015**.
- [46] Wenderich, K.; Klaassen, A.; Siretanu, I.; Mugele, F.; Mul, G.; *Sorption-determined deposition of platinum on well-defined platelike WO₃*. Angewandte Chemie - International Edition **2014**, 53, 12476-12479.
- [47] Liu, G.; Han, J.; Zhou, X.; Huang, L.; Zhang, F.; Wang, X.; Ding, C.; Zheng, X.; Han, H.; Li, C.; *Enhancement of visible-light-driven O₂ evolution from water oxidation on WO₃ treated with hydrogen*. Journal of Catalysis **2013**, 307, 148-152.

5.6 Appendix

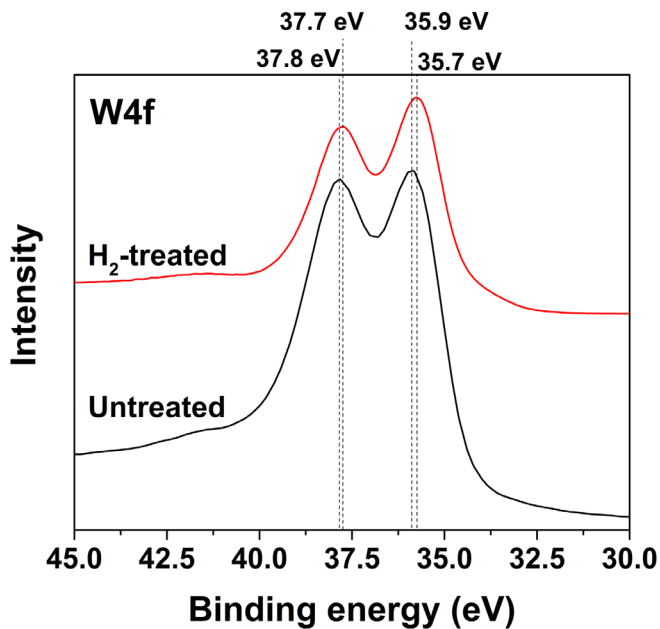


Figure A5.1. XPS spectra of the W4f region of Pt/WO₃ before and after hydrogenation. The Pt/WO₃ was obtained through 5 hours of photodeposition without MeOH and an aim of 10 wt% Pt.

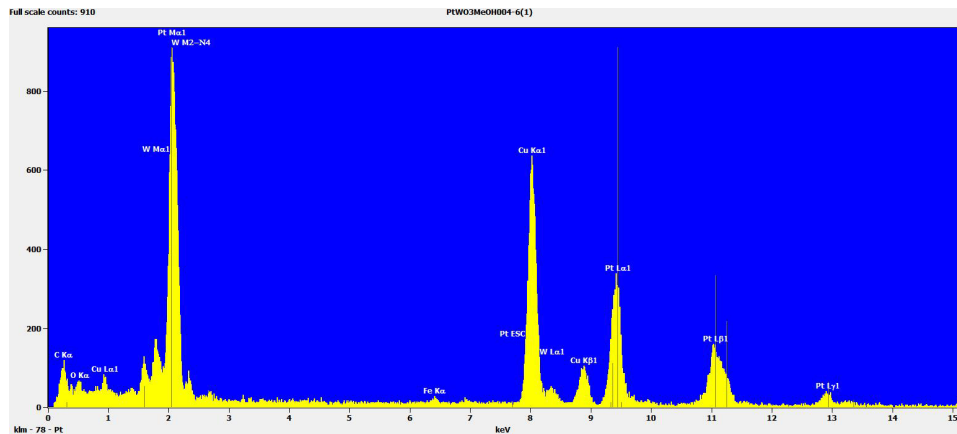


Figure A5.2a. EDX spectrum of Pt photodeposited on WO_3 using methanol, 1 hour of illumination and an aim of 2 wt% of Pt (Figure 5.7a).

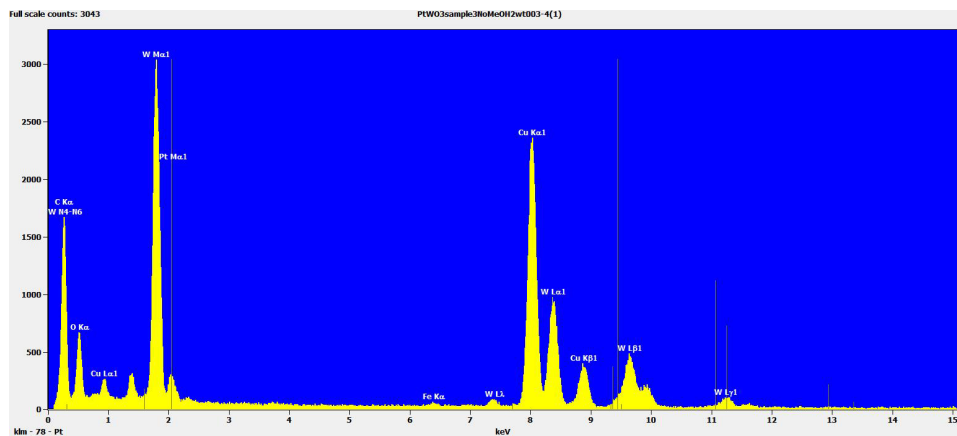


Figure A5.2b. EDX spectrum of Pt photodeposition on WO_3 using no methanol, 5 hours of illumination and an aim of 2 wt% of Pt (Figure 5.7b).

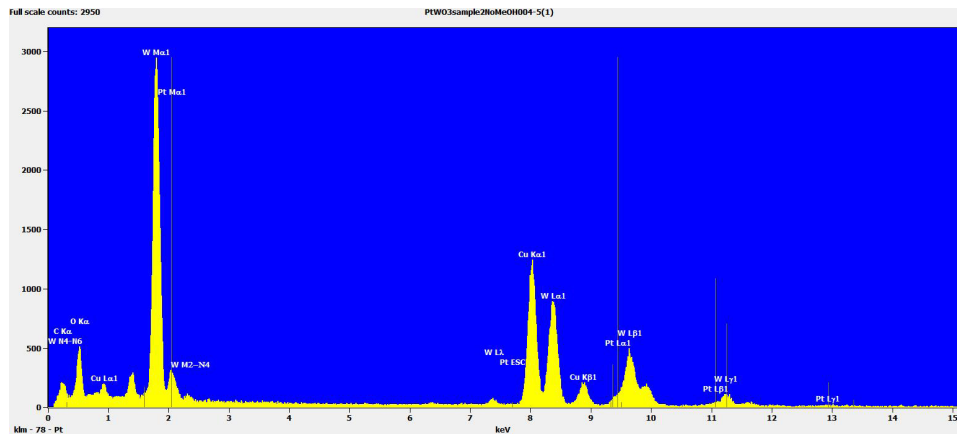


Figure A5.2c. EDX spectrum of Pt photodeposition on WO_3 using no methanol, 5 hours of illumination and an aim of 10 wt% of Pt (Figure 5.7c).

Chapter 6

Sorption-determined deposition of platinum on well-defined plate-like WO₃

Abstract

Photodeposition of Pt nanoparticles from [PtCl₆]²⁻ on plate-like WO₃ crystals preferentially occurs on the small, subordinate facets. Rather than the often used explanation of preferred light-induced charge migration, we propose that this phenomenon is due to differences in intrinsic surface charges of WO₃ facets exposed to water, inducing preferred dark sorption of [PtCl₆]²⁻ on positively charged facets/edges. This conclusion is based on i) (dark) impregnation studies which show Pt deposition also to be facet specific, and ii) aqueous phase atomic force microscopy studies which suggest intrinsic surface charges to be in agreement with sorption based Pt distributions.

*This chapter is based on Wenderich, K.; Klaassen, A.; Siretanu, I.; Mugele, F. and Mul, G.; Sorption-determined deposition of platinum on well-defined platelike WO₃. *Angewandte Chemie - International Edition* **2014**, *53*, 12476-12479*

6.1 Introduction

In recent years, photodeposition of nanoparticulate metals and metal oxides on various semiconductor crystals has been used frequently to optimize photocatalytic performance. Interestingly, various reports demonstrate a specific spatial distribution of these nanoparticles on photocatalytically active crystals. For instance Ohno *et al.* observed metal deposition preferably on the $\{110\}$ facet and the $\{011\}$ facet of respectively rutile and anatase phases, whereas (Pb) oxide deposition appeared preferred on the $\{011\}$ facet and the $\{001\}$ facet.^[1] Miseki *et al.* showed Au or Ni accumulating on very different facets of $\text{BaLa}_4\text{Ti}_4\text{O}_{15}$ as compared to PbO_2 .^[2] In addition, Iizuka *et al.* observed preferred positioning of Ag on the same $\text{BaLa}_4\text{Ti}_4\text{O}_{15}$ photocatalyst.^[3] Finally, Li *et al.* convincingly demonstrated spatial nanoparticle distributions to be present after photodeposition of Pt on BiVO_4 .^[4] Generally, two reasons for preferred photodeposition have been proposed. Ohno *et al.*, Iizuka *et al.* and Li *et al.* advocate a theory in which illumination results in preferred migration of holes and electrons to specific crystal facets, resulting in locations where reduction reactions (and metal deposition) preferably occur, and other locations where oxidation reactions are dominant (resulting in oxide deposition).^[1] Alternatively, Miseki *et al.* ascribe structure-directed deposition of Au, Ni and PbO_2 on $\text{BaLa}_4\text{Ti}_4\text{O}_{15}$ to preferred sorption phenomena, implying differences in intrinsic surface charge of facets should be present in conditions of photodeposition.^[2]

Tungsten trioxide (WO_3) is one of the most studied semiconductor materials in photocatalysis.^[5] WO_3 is chemically stable in acidic conditions, non-toxic and has a relatively narrow bandgap (ranging from 2.4 to 2.8 eV), making absorption of visible light in the blue range possible; a significant part of the solar spectrum.^[5-7] WO_3 has been used successfully in Z-scheme configurations for overall water splitting.^[8, 9] Additionally, WO_3 loaded with Pt nanoparticles shows significant photocatalytic activity in wastewater treatment.^[6, 10-13] Often photodeposition is used to prepare Pt-loaded WO_3 .^[12-15] Although the photocatalytic behavior of Pt-modified WO_3 has been reported frequently, to the best of our knowledge no detailed reports have been published on the presence of an aforementioned preferred location of deposited Pt on WO_3 crystals, and if any, which mechanism leading to such distribution prevails. Here, we will demonstrate preferred deposition of Pt on WO_3 occurs, and we will provide experimental data to explain the mechanism which induces this phenomenon.

To synthesize WO_3 -particles with well-structured facets, crystal facet engineering methods are very suitable.^[16] Using hydrothermal synthesis, researchers have been

able to obtain WO₃ with well-defined morphologies, such as nanorods,^[17-19] nanowires,^[20, 21] nanoplates/nanosheets,^[22, 23] nano-urchins,^[21, 24] and flower-like morphologies.^[25, 26] We have synthesized well-defined plate-like WO₃ based on a method described by Su *et al.*^[22] Pt photodeposition was achieved using a similar method as described by Purwanto *et al.* on the basis of H₂PtCl₆ · 6H₂O as precursor, at pH 3 and 6.^[12] We also applied impregnation of Pt on our samples, using a method proposed by Yoshimura *et al.*^[27] Finally, we performed aqueous phase AFM studies to validate whether different crystal facets of WO₃ possess (pH dependent) opposite intrinsic surface charges.

6.2 Materials and methods

All chemicals of analytical grades were purchased at Sigma-Aldrich. For the synthesis of plate-like WO₃ particles, we refer to Chapter 3 of this thesis. Initially, to perform photodeposition of Pt on plate-like WO₃, 100 mg of WO₃ was added to 50 mL of an aqueous solution containing 222 μM H₂PtCl₆ · 6H₂O. The photodeposition reactor used is schematically shown in the appendix (Figure A6.1). First, stirring of the solution took place in the dark for at least an hour to achieve an even distribution of the WO₃ particles and to reach adsorption/desorption equilibrium of the precursor ion. Then, the solution was illuminated for 2 hours using a 50 W HBO mercury lamp (Zeiss, 46 80 32 – 9902). Afterwards, 6 mL methanol was added to the solution and illumination continued overnight. Water cooling and minor air supply was provided to the solution during the process. When photodeposition was completed, solid and solution were separated by centrifuging and decantation, followed by washing with water, and ethanol, respectively. The remaining gel was collected and dried at temperatures of approximately 100 °C in static air. This sample is shown in Figure 6.2. To scale up the process of synthesis, Pt/WO₃ samples were prepared by increasing the amounts of materials involved: 200 mg of WO₃, 410 μM H₂PtCl₆ · 6H₂O and 12 mL of methanol. Such sample was used in Figure 6.1, for XPS studies, and additional particle counting (see appendix). To perform photodeposition at a pH of 6 rather than an initial pH of approximately 3, the pH of the solution was adjusted using NaOH and HCl. In attempts to photodeposit Pt on WO₃ using Pt(NH₃)₄(NO₃)₂, the same procedure was followed with 418 μM of Pt(NH₃)₄(NO₃)₂.

To perform impregnation of 2 wt% Pt on WO₃, 50 mL of an aqueous solution containing 410 ± 10 μM H₂PtCl₆ · 6H₂O was prepared, followed by addition of 200 mg of WO₃. Stirring of the suspension took place at a heating plate, which was used to evaporate the solution at temperatures of 100 °C. The remaining gel was collected

and treated at 500 °C (heating rate 10 K/min) for 3 hours in the dark. Afterwards, the sample was allowed to cool down. For impregnation of Pt on plate-like WO₃ using 418 μM Pt(NH₃)₄(NO₃)₂ the same procedure was used.

Pt-loaded WO₃ was characterized using high resolution-scanning electron microscopy (HR-SEM), high resolution-transmission electron microscopy (HR-TEM) (FEI Instruments), X-ray photoelectron spectroscopy (XPS) (Quantera SXM from Physical Electronics) and inductively coupled plasma atomic emission spectroscopy (ICP-AES) (Varian Liberty II, Sequential ICP-AES). HR-SEM measurements were performed under an accelerating voltage ranging of 2.00 kV to 10.00 kV. HR-TEM measurements were performed under an accelerating voltage of 300 kV. XPS was performed using a monochromatic aluminum source (Al Kα operating at 1486.6 eV). For ICP-AES measurements, a calibration curve was made using aqueous solutions of 1, 10 and 100 mg/L H₂PtCl₆ · 6H₂O. A solution of 5 mg/L H₂PtCl₆ · 6H₂O was used to verify the correctness of the calibration curve. To measure the loading of Pt of Pt/WO₃ samples using ICP-AES, 1.9 to 4.0 mg of sample was exposed to 2.5 mL of aqua regia, allowing the Pt to dissolve. The solution was then diluted with an additional 17.5 mL demineralized water and analyzed in the ICP spectrometer.

Atomic force microscopy (AFM) (Bruker Icon) studies with 2D force field imaging were performed on unloaded plate-like WO₃ to verify whether there is a difference in intrinsic surface charge of the different facets. A negatively charged AFM-tip made from Si was used to scan over a WO₃ plate, which was coated on a silica substrate. Experiments were performed in dynamic frequency modulation mode with constant excitation (QFM-module, nanoAnalytics GmbH). The force response of the tip was probed at 100 locations along a straight line crossing the particle. A negative force represents an attraction of the tip, indicating a positive surface charge of the sample. A positive force indicates a repulsion of the tip, suggesting a negative surface charge of the sample. Using this method, the electrostatic interactions can be analyzed very precisely and reliably, allowing for variations to be probed and mapped at 10 nm lateral resolution, which is not possible with standard macroscopic characterization tools such as macroscopic titrations, electrokinetic measurements, or most optical spectroscopies.

For atomic resolution measurements a Multimode8 AFM (Bruker Nano) equipped with Nanoscope V controller and an A-scanner was operated in standard ‘tapping mode’. For these measurements Bruker FASTSCAN-B cantilevers were used. Before imaging, tips were cleaned by rinsing with a mixture of ethanol and isopropanol (≈ 1:1) and additional ambient air plasma treatment (Harrick Plasma)

for 15–30 min. A standard tapping mode liquid probe holder without O-ring (Bruker Nano) was used for imaging. To minimize the drift, the system was allowed to thermally equilibrate at room temperature for 20–60 min before acquiring any data. The AFM was operated in amplitude-modulation mode with a free amplitude A_0 typically smaller than 2 nm, high scan rates ≈ 10 Hz and imaging amplitudes set point as high as possible (typically $A/A_0 \geq 0.8$). All images were flattened using Bruker's standard Nanoscope Analysis 1.4 package, in some cases including slight low pass filtering to improve clarity.

6.3 Results and discussion

Using the method of Su *et al.*,^[22] we obtained plate-like WO_3 particles of the monoclinic phase with well-defined facets and a specific BET surface area of approximately $8.4 \text{ m}^2/\text{g}$. After photodeposition of Pt on such WO_3 , HR-TEM, XPS and ICP-AES analyses were conducted to identify the Pt particle size and loading. As an example, Figure 6.1 depicts a HR-TEM image of the Pt particles. Energy-dispersive X-ray spectroscopy (EDX) confirms that the particles consist of Pt. Based on the electron microscopy data, we derive the Pt particles on average to be of sizes in the range of 5–10 nm in diameter. Additionally, XPS data reveal an atomic surface Pt percentage of Pt/ WO_3 obtained through photodeposition of 1.5 at%, whereas the atomic surface Pt percentage in Pt/ WO_3 obtained through impregnation is 2.9 at% (see appendix Figure A6.2, Table A6.1). ICP-AES measurements show that the Pt loading obtained through photodeposition is 0.8 wt%. When impregnation is used, the Pt loading is 1.8 wt%. Further, XPS analysis shows that chlorine or carbon contaminations possibly resulting from the WO_3 synthesis, are absent.

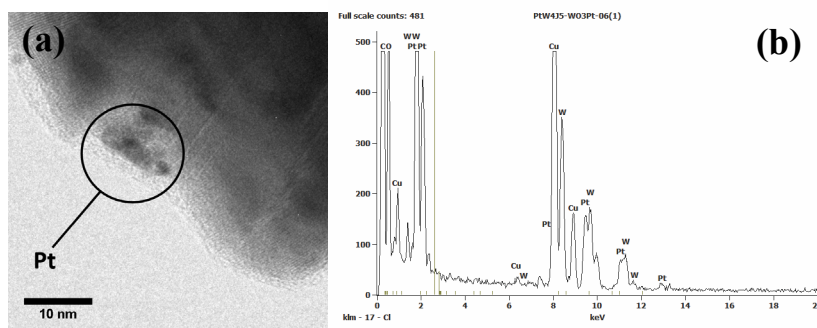


Figure 6.1. (a) HR-TEM image of Pt-loaded plate-like WO_3 obtained through photodeposition using $\text{H}_2\text{PtCl}_6 \cdot 6\text{H}_2\text{O}$ as a precursor. (b) EDX spectrum of Pt particles on plate-like WO_3 . A Pt peak is observed just above 9 keV, which indicates that Pt is present on the surface of plate-like WO_3 .

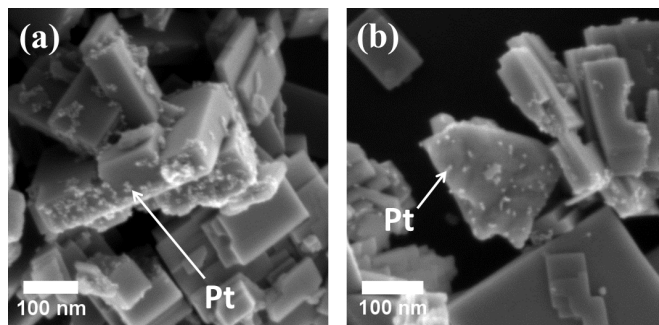


Figure 6.2. HR-SEM images of as-synthesized plate-like WO_3 loaded with Pt particles through photodeposition using $\text{H}_2\text{PtCl}_6 \cdot 6\text{H}_2\text{O}$ as a precursor. (a) Positioning of the Pt particles seems to take place at the edges/smaller facets. (b) Some WO_3 particles lose their well-defined morphology by photodeposition.

Figure 6.2 shows HR-SEM images of Pt-loaded plate-like WO_3 prepared by photodeposition in a procedure using $\text{H}_2\text{PtCl}_6 \cdot 6\text{H}_2\text{O}$. We observe two phenomena. First, a preferred positioning of Pt particles occurs for well-defined crystals of WO_3 at the smaller facets. Often, the dominant facet of the plate-like morphology is void of any Pt particles. Statistically, we have determined the ratio of Pt particles on the edges/small facets over the dominant facets to be 5:1 (see appendix, Table A6.2 and A6.3). Of these crystals we have determined the dominant facet to be the $\{002\}$ facet, and the edged facet to be $\{020\}$, as confirmed by HR-TEM and AFM studies (Figure 6.3). Second, we observe in the HR-SEM images that some crystals have lost their well-defined morphology after the photodeposition procedure. A clear preference of Pt for specific facets is not so evident in these domains of the sample. We hypothesize that during the photodeposition of Pt on WO_3 a (local) pH increase occurs, possibly induced by Pt related photocatalytic hydrogen formation, resulting in instability of the WO_3 crystals in solution. (Photo)corrosion of WO_3 is known to be significant at $\text{pH} > 4$. Indeed, when the photodeposition reaction is performed at $\text{pH} = 6$, a significantly more dramatic restructuring of WO_3 is apparent (Figure 6.4), and the phenomenon of preferred deposition no longer present. HR-SEM and AFM topography images shown in Figure 6.4 and Figure 6.5 clearly illustrate that WO_3 particles after photodeposition lost their well-defined initial plate-like structure (Figure 6.4c) and have a more rough roundish structure. It is difficult to distinguish the difference between the dominant facet and edges.

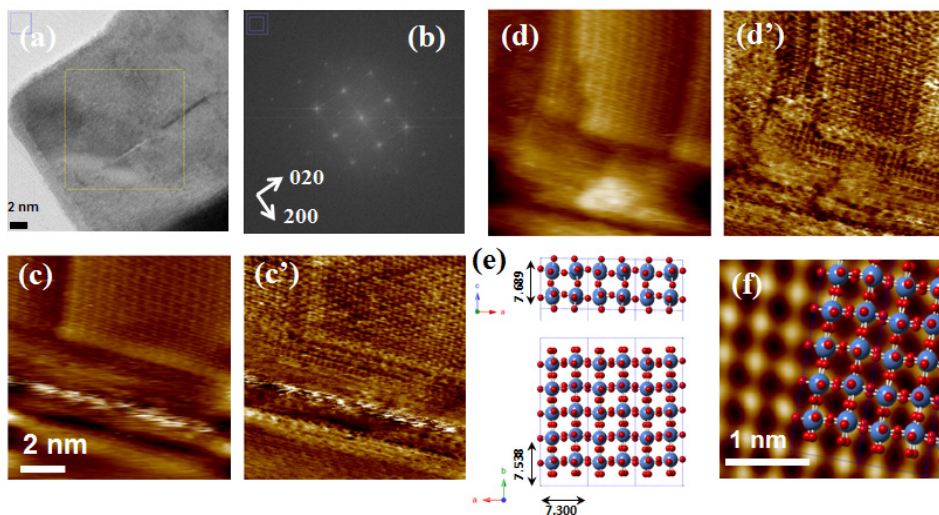


Figure 6.3. (a) Typical HR-TEM image of as-synthesized plate-like WO_3 loaded with 2 wt% of Pt particles through impregnation using $\text{Pt}(\text{NH}_3)_4(\text{NO}_3)_2$ as a precursor. (b) Fast Fourier transform of the selected area. Out of this measurement, the dominant facet of the as-synthesized plates is judged to be the $\{002\}$ facet.

Atomic-resolution non-contact AM-AFM topographic images (c, d) and phase (c', d') of WO_3 surface taken in 10 mM NaCl solution. The basal plane of the particle reveals the monoclinic symmetry caused by the arrangement of the protrusions in a quasi-square structure with spacing of ~ 0.38 nm in a and b directions, while topographic and phase images of the edges of the particle show atomic steps, a distorted lattice and the presence of various structural defects. (e) X-ray crystal structure of WO_3 in ac $\{020\}$ (top) and ab $\{002\}$ (bottom) planes. Color codes: blue-tungsten, red-oxygen atoms. (f) Zoom-in of atomic scale image of WO_3 on basal planes ($\{002\}$ facet) after processing with Fourier transformation, superimposed with the X-ray structure in the ab plane.

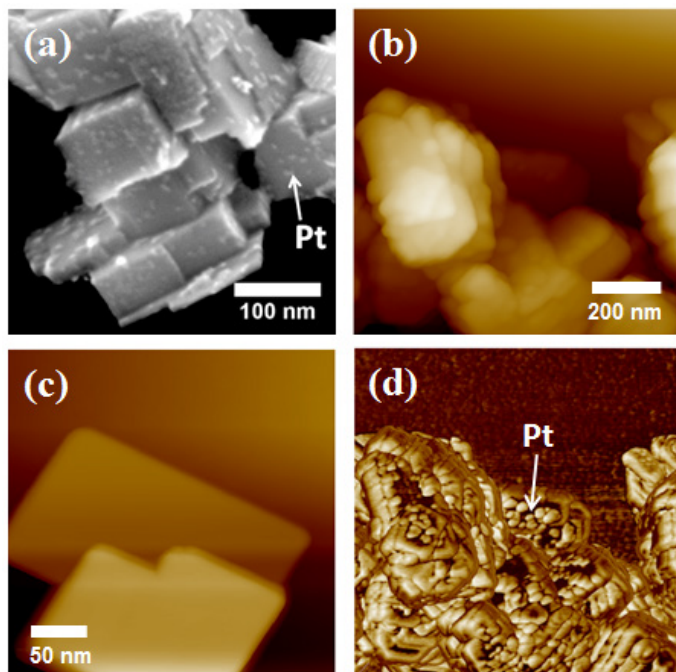


Figure 6.4. (a) HR-SEM image of as-synthesized plate-like WO_3 loaded with Pt particles through photodeposition using $\text{H}_2\text{PtCl}_6 \cdot 6\text{H}_2\text{O}$ as a precursor at $\text{pH} = 6$. AFM height (b) and phase (d) images of WO_3 loaded with Pt particles through photodeposition using $\text{H}_2\text{PtCl}_6 \cdot 6\text{H}_2\text{O}$ as a precursor at $\text{pH} = 6$ obtained in tapping mode. (c) AFM height image of as-synthesized plate-like WO_3 particles deposited on a silicon substrate obtained in tapping mode. Positioning of Pt particles is not visible anymore.

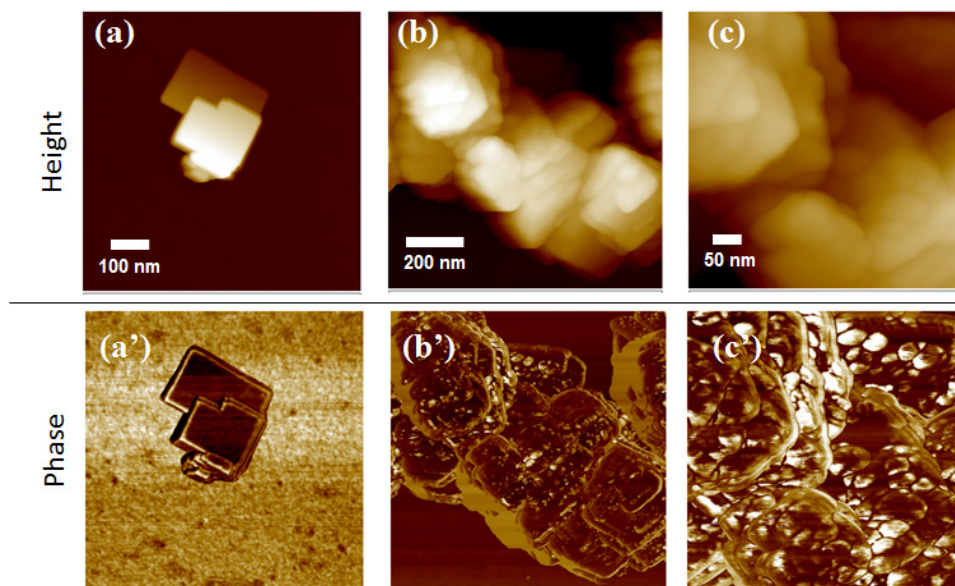


Figure 6.5. (a) AFM height image and phase (a') of an as-synthesized plate-like WO_3 particle. AFM height (b,c) and phase (b', c') images of WO_3 loaded with Pt particles through photodeposition using $\text{H}_2\text{PtCl}_6 \cdot 6\text{H}_2\text{O}$ as a precursor at $\text{pH} = 6$ obtained in tapping mode. The WO_3 particles after the photodeposition procedure lost their well-defined initial plate-like structure and have a more rough, roundish structure. It is difficult to distinguish the difference between the dominant facet and edges.

Interestingly, HR-SEM images of Pt-loaded plate-like WO_3 obtained through impregnation with the same precursor ($\text{H}_2\text{PtCl}_6 \cdot 6\text{H}_2\text{O}$) show similar phenomena (Figure 6.6). Preferred Pt deposition on the subordinate facets is observed, again with a statistic ratio of Pt particles on the edges/small facets over the dominant facets of 5:1 (see appendix, Table A6.4). This also suggests the size and distribution of the Pt particles appear not to have significantly changed as a consequence of the somewhat higher loading of the impregnated sample. Still, at significantly higher loading the geometrical particle distribution might be different. Although to less extent, some corrosion of WO_3 has also occurred in the impregnation procedure, leading to domains where Pt deposition is more arbitrary. We hypothesize that this is again caused by pH increase, in this procedure induced by decreasing HCl concentration during the water evaporation step at $100\text{ }^\circ\text{C}$.

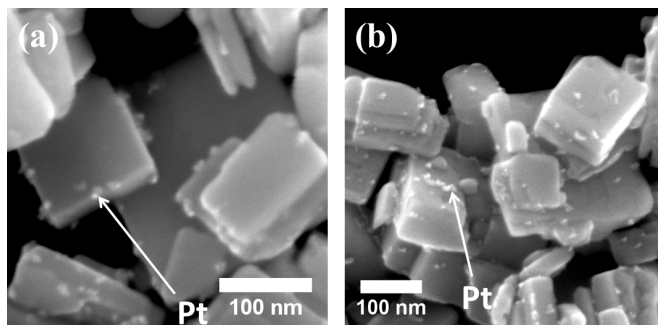


Figure 6.6. HR-SEM images of as-synthesized plate-like WO_3 loaded with Pt particles through impregnation using $\text{H}_2\text{PtCl}_6 \cdot 6\text{H}_2\text{O}$ as a precursor. (a) Again, positioning of the Pt particles seems to take place at the edges. (b) Some WO_3 particles have defects after impregnation. Structure-directed deposition is not obvious anymore in these domains.

Attempts to use the cation $[\text{Pt}(\text{NH}_3)_4]^{2+}$ rather than the anion $[\text{PtCl}_6]^{2-}$ to create Pt nanoparticles on WO_3 crystals by photodeposition were unsuccessful, since no Pt particles could be observed in SEM images, in agreement with the literature.^[28] Interestingly, impregnation using this precursor appears to yield a significant fraction of Pt particles on the dominant facets of the plate-like WO_3 (Figure 6.7). Noteworthy is that the Pt particles are also considerably larger than in the case of using $\text{H}_2\text{PtCl}_6 \cdot 6\text{H}_2\text{O}$, ranging from 10 to 25 nm in diameter. This difference in particle size is in agreement with earlier studies by Ma *et al.*^[29]

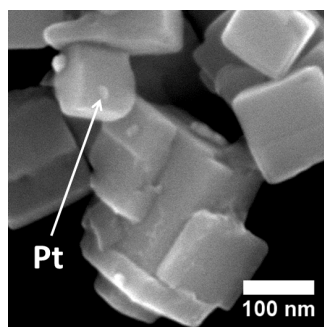


Figure 6.7. HR-SEM image of as-synthesized plate-like WO_3 loaded with Pt particles through impregnation using $\text{Pt}(\text{NH}_3)_4(\text{NO}_3)_2$ as a precursor. No obvious preferred positioning of the Pt particles is observed, with several Pt particles present on the dominant facets. The Pt particles also appear larger than when $\text{H}_2\text{PtCl}_6 \cdot 6\text{H}_2\text{O}$ is used as a precursor.

The results strongly suggest that the structure-directed (photo)deposition of Pt on monoclinic WO_3 is adsorption-induced. To validate if an intrinsic surface charge is

present for WO₃ crystals, AFM studies were conducted in water (pH \approx 3 or pH \approx 6, 10 mM NaCl) using a sharp negatively charged oxidized Si tip. A typical result is shown in Figure 6.8. At pH \approx 6 the weakly repulsive force recorded on the basal planes indicates a weak negative surface charge. The absolute value amounts to 10-20% of the much more repulsive adjacent silica substrate. The charge density of the latter amounts to $\sim -0.5 \text{ C/m}^2$ for the conditions of the present experiments.^[30] The negative charge is in agreement with the macroscopic observation by Kim *et al.*, showing negative surface charge of WO₃ by zeta potential measurements.^[6] However, the results suggest a different, in the present case slightly positive surface charge along the edges of the WO₃ crystals.

Similar behavior is observed at pH \approx 3, where the interaction force between tip and basal planes of a WO₃ particle are more repulsive compared to silica. As pH \approx 3 is very close to the isoelectric point (IEP) of silica (IEP_{SiO₂} \approx 3) compared to WO₃ (IEP_{WO₃} \approx 2), the surface is still negatively charged.^[6] This is in agreement with the observed location of the Pt nanoparticles prepared using [PtCl₆]²⁻ solutions: since the edges appear positively charged, sorption of the negatively charged [PtCl₆]²⁻ is likely preferred at these locations.

In order to understand what causes the clear preference of Pt for sorption on specific facets, we proceeded to image the WO₃ particle surface at atomic resolution. Figure 6.8c shows the amplitude modulated, height image of a WO₃ particle equilibrated in 10 mM NaCl solution at atomic resolution, obtained with a super sharp tip at room temperature. This image was recorded along the WO₃ particle, so that the basal plane and edges can be observed at the same time. The top right corner which corresponds to the basal plane of the particle, reveals the monoclinic symmetry caused by the arrangement of the protrusions in a quasi-square structure with spacing of $\sim 0.38 \text{ nm}$ in the *a* and *b* directions, consistent with the crystallographic data (as emphasized in the left bottom inset). Similar to observed earlier for gibbsite platelets,^[31] moving closer to the edge reveals a higher density of atomic steps (black line in Figure 6.8c and 6.8d), a distorted lattice, and the presence of various structural defects. These features could explain preponderant heterogeneous electrostatic interactions and charge properties, likely contributing to the observed (positive) charges and preferred [PtCl₆]²⁻ adsorption at these locations. More details can be found in Figure 6.3.

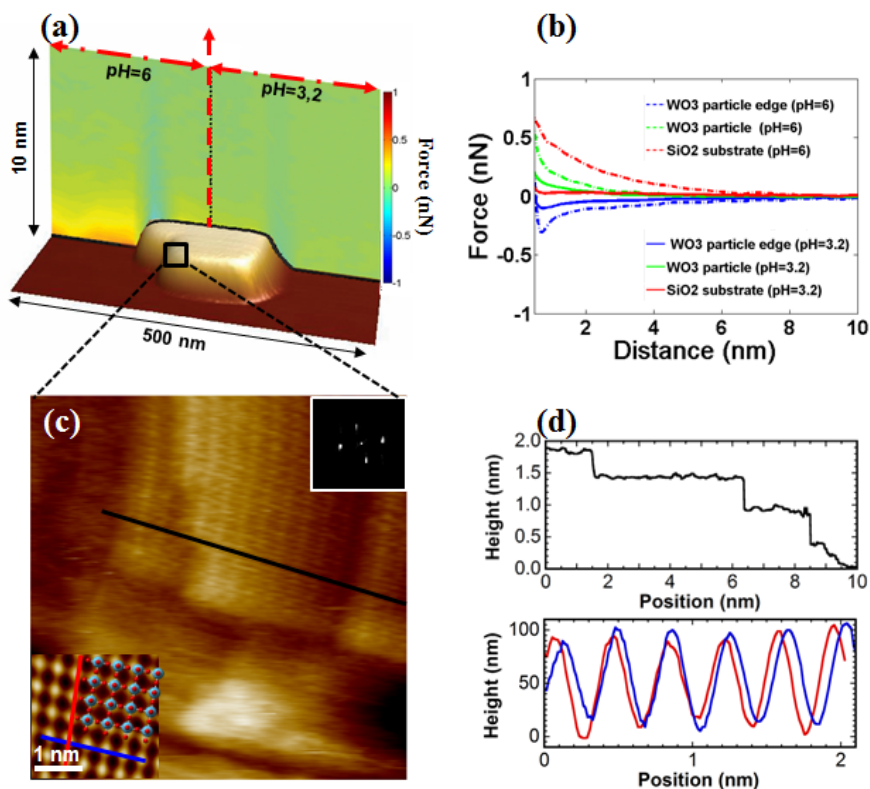


Figure 6.8. (a) Combined 2D force field obtained by measuring 55 single force vs. distance curves along a line in x -direction over a silicon oxide/ WO_3 sample in 10 mM NaCl solution at pH = 3.2 and pH = 6. (b) Averaged force curves from measurement in (a) plotted vs. tip-sample distance. At pH = 6 a mild repulsive force represents a mild negative surface charge of facets of the WO_3 particle (green), whereas an attractive force represents a positive surface charge (blue). The WO_3 particle was deposited on silica as a support, which was significantly negatively charged (red). At pH = 3.2 the interaction force between tip and basal planes of the WO_3 particle is more repulsive. (c) High-resolution non-contact AM-AFM topographic images of WO_3 surface taken in 10 mM NaCl solution. The top inset shows a two-dimensional fast Fourier transformation (2D-FFT) pattern of height images. The bottom inset represents the zoom of an atomic scale image on basal planes ($\{002\}$ facet) after processing with a Fourier transformation superimposed with an X-ray structure in the ab plane. Protrusions arranged in quasi-square structure agree well with the theoretical X-ray structure and arrangement of tungsten atoms. (d) Top height profile taken along the black line in (c) shows the atomic steps. Bottom height profiles in red and blue directions shown in bottom inset of (c). Height profiles in red and blue directions display periodicities of ~ 0.38 nm.

Speculating, similar, positively charged structural defects might be formed upon (photo)corrosion of the dominant facet of WO₃ in mildly basic conditions. [PtCl₆]²⁻ ions adsorb on these newly formed sites, explaining the presence of some particles on the dominant facets. When more drastic (photo)corrosion takes place (Figure 6.4), the vast restructuring of the crystal leads to an arbitrary deposition of Pt, which likely has a more complicated origin than simple electrostatic interactions. More detailed and extensive AFM studies at different stages of corrosion are required to investigate how structural defects are formed, and to clarify the mechanism of Pt particle formation on such severely corroded crystals.

6.4 Conclusions

In summary, facet preferred (photo)deposition of Pt on WO₃ is observed, predominantly determined by differences in intrinsic surface charge. Prior to photoreduction and/or thermal decomposition, [PtCl₆]²⁻ ions adsorb preferentially on positively charged surfaces, leading to the observed specific geometrical distribution. The AFM results are in agreement with sorption induced geometrical particle distributions,^[2] while we propose light-induced preferential migration of electron and holes to specific crystal facets to be a less valid hypothesis to explain the observed particle distributions.^[1,3,4]

Future research is underway to verify if facet preferred deposition of metals or metal oxides is consistently driven by intrinsic differences in surface charges. Second, we aim to verify if having Pt in specific, but different geometrical distribution, is of relevance for photocatalytic activity. To allow this for WO₃, pH increase should be prevented at all times, to prevent loss of integrity of the well-defined crystals of WO₃ or other semiconductor oxides, and thus loss of preferred spatial distribution of Pt deposition.

6.5 Bibliography

- [1] Ohno, T.; Sarukawa, K.; Matsumura, M.; *Crystal faces of rutile and anatase TiO₂ particles and their roles in photocatalytic reactions*. New Journal of Chemistry **2002**, 26, 1167-1170.
- [2] Miseki, Y.; Kato, H.; Kudo, A.; *Water splitting into H₂ and O₂ over niobate and titanate photocatalysts with (111) plane-type layered perovskite structure*. Energy and Environmental Science **2009**, 2, 306-314.
- [3] Iizuka, K.; Wato, T.; Miseki, Y.; Saito, K.; Kudo, A.; *Photocatalytic reduction of carbon dioxide over Ag cocatalyst-loaded ALa₄Ti₄O₁₅ (A = Ca, Sr, and Ba) using water as a reducing reagent*. Journal of the American Chemical Society **2011**, 133, 20863-20868.

- [4] Li, R.; Zhang, F.; Wang, D.; Yang, J.; Li, M.; Zhu, J.; Zhou, X.; Han, H.; Li, C.; *Spatial separation of photogenerated electrons and holes among {010} and {110} crystal facets of BiVO₄*. *Nature Communications* **2013**, 4.
- [5] Zheng, H.; Ou, J. Z.; Strano, M. S.; Kaner, R. B.; Mitchell, A.; Kalantar-Zadeh, K.; *Nanostructured tungsten oxide - properties, synthesis, and applications*. *Advanced Functional Materials* **2011**, 21, 2175-2196.
- [6] Kim, J.; Lee, C. W.; Choi, W.; *Platinized WO₃ as an environmental photocatalyst that generates OH radicals under visible light*. *Environmental Science and Technology* **2010**, 44, 6849-6854.
- [7] Kudo, A.; Miseki, Y.; *Heterogeneous photocatalyst materials for water splitting*. *Chemical Society Reviews* **2009**, 38, 253-278.
- [8] Chan, S. H. S.; Yeong Wu, T.; Juan, J. C.; Teh, C. Y.; *Recent developments of metal oxide semiconductors as photocatalysts in advanced oxidation processes (AOPs) for treatment of dye waste-water*. *Journal of Chemical Technology and Biotechnology* **2011**, 86, 1130-1158.
- [9] Abe, R.; Higashi, M.; Domen, K.; *Overall water splitting under visible light through a two-step photoexcitation between TaON and WO₃ in the presence of an iodate-iodide shuttle redox mediator*. *ChemSusChem* **2011**, 4, 228-237.
- [10] Abe, R.; Takami, H.; Murakami, N.; Ohtani, B.; *Pristine simple oxides as visible light driven photocatalysts: highly efficient decomposition of organic compounds over platinum-loaded tungsten oxide*. *Journal of the American Chemical Society* **2008**, 130, 7780-7781.
- [11] Joshi, U. A.; Darwent, J. R.; Yiu, H. H. P.; Rosseinsky, M. J.; *The effect of platinum on the performance of WO₃ nanocrystal photocatalysts for the oxidation of Methyl Orange and iso-propanol*. *Journal of Chemical Technology and Biotechnology* **2011**, 86, 1018-1023.
- [12] Purwanto, A.; Widiyandari, H.; Ogi, T.; Okuyama, K.; *Role of particle size for platinum-loaded tungsten oxide nanoparticles during dye photodegradation under solar-simulated irradiation*. *Catalysis Communications* **2011**, 12, 525-529.
- [13] Aminian, M. K.; Ye, J.; *Morphology influence on photocatalytic activity of tungsten oxide loaded by platinum nanoparticles*. *Journal of Materials Research* **2010**, 25, 141-148.
- [14] Qamar, M.; Yamani, Z. H.; Gondal, M. A.; Alhooshani, K.; *Synthesis and comparative photocatalytic activity of Pt/WO₃ and Au/WO₃ nanocomposites under sunlight-type excitation*. *Solid State Sciences* **2011**, 13, 1748-1754.
- [15] Xu, Z.; Tabata, I.; Hirogaki, K.; Hisada, K.; Wang, T.; Wang, S.; Hori, T.; *Preparation of platinum-loaded cubic tungsten oxide: a highly efficient visible light-driven photocatalyst*. *Materials Letters* **2011**, 65, 1252-1256.
- [16] Liu, G.; Yu, J. C.; Lu, G. Q.; Cheng, H. M.; *Crystal facet engineering of semiconductor photocatalysts: motivations, advances and unique properties*. *Chemical Communications* **2011**, 47, 6763-6783.

- [17] Zhu, J.; Wang, S.; Xie, S.; Li, H.; *Hexagonal single crystal growth of WO₃ nanorods along a [110] axis with enhanced adsorption capacity*. Chemical Communications **2011**, 47, 4403-4405.
- [18] Wang, J.; Khoo, E.; Lee, P. S.; Ma, J.; *Synthesis, assembly, and electrochromic properties of uniform crystalline WO₃ nanorods*. Journal of Physical Chemistry C **2008**, 112, 14306-14312.
- [19] Mo, R. F.; Jin, G. Q.; Guo, X. Y.; *Morphology evolution of tungsten trioxide nanorods prepared by an additive-free hydrothermal route*. Materials Letters **2007**, 61, 3787-3790.
- [20] Gu, Z.; Li, H.; Zhai, T.; Yang, W.; Xia, Y.; Ma, Y.; Yao, J.; *Large-scale synthesis of single-crystal hexagonal tungsten trioxide nanowires and electrochemical lithium intercalation into the nanocrystals*. Journal of Solid State Chemistry **2007**, 180, 98-105.
- [21] Gu, Z.; Zhai, T.; Gao, B.; Sheng, X.; Wang, Y.; Fu, H.; Ma, Y.; Yao, J.; *Controllable assembly of WO₃ nanorods/nanowires into hierarchical nanostructures*. Journal of Physical Chemistry B **2006**, 110, 23829-23836.
- [22] Su, X.; Xiao, F.; Li, Y.; Jian, J.; Sun, Q.; Wang, J.; *Synthesis of uniform WO₃ square nanoplates via an organic acid-assisted hydrothermal process*. Materials Letters **2010**, 64, 1232-1234.
- [23] Wang, J.; Lee, P. S.; Ma, J.; *Synthesis, growth mechanism and room-temperature blue luminescence emission of uniform WO₃ nanosheets with W as starting material*. Journal of Crystal Growth **2009**, 311, 316-319.
- [24] Jeon, S.; Yong, K.; *Morphology-controlled synthesis of highly adsorptive tungsten oxide nanostructures and their application to water treatment*. Journal of Materials Chemistry **2010**, 20, 10146-10151.
- [25] Zhao, Y.; Chen, H.; Wang, X.; He, J.; Yu, Y.; He, H.; *Flower-like tungsten oxide particles: synthesis, characterization and dimethyl methylphosphonate sensing properties*. Analytica Chimica Acta **2010**, 675, 36-41.
- [26] Yu, J.; Qi, L.; *Template-free fabrication of hierarchically flower-like tungsten trioxide assemblies with enhanced visible-light-driven photocatalytic activity*. Journal of Hazardous Materials **2009**, 169, 221-227.
- [27] Yoshimura, K.; Hakoda, T.; Yamamoto, S.; Yoshikawa, M.; *Optical detection of organic hydrides with platinum-loaded tungsten trioxide*. Journal of Physics and Chemistry of Solids **2012**, 73, 696-698.
- [28] Rao, C. R. K.; Trivedi, D. C.; *Chemical and electrochemical depositions of platinum group metals and their applications*. Coordination Chemistry Reviews **2005**, 249, 613-631.
- [29] Ma, S. S. K.; Maeda, K.; Abe, R.; Domen, K.; *Visible-light-driven nonsacrificial water oxidation over tungsten trioxide powder modified with two different cocatalysts*. Energy and Environmental Science **2012**, 5, 8390-8397.

- [30] Ebeling, D.; Van Den Ende, D.; Mugele, F.; *Electrostatic interaction forces in aqueous salt solutions of variable concentration and valency*. *Nanotechnology* **2011**, 22.
- [31] Siretanu, I.; Ebeling, D.; Andersson, M. P.; Stipp, S. L. S.; Philipse, A.; Stuart, M. C.; Van Den Ende, D.; Mugele, F.; *Direct observation of ionic structure at solid-liquid interfaces: a deep look into the Stern Layer*. *Scientific Reports* **2014**, 4.

6.6 Appendix

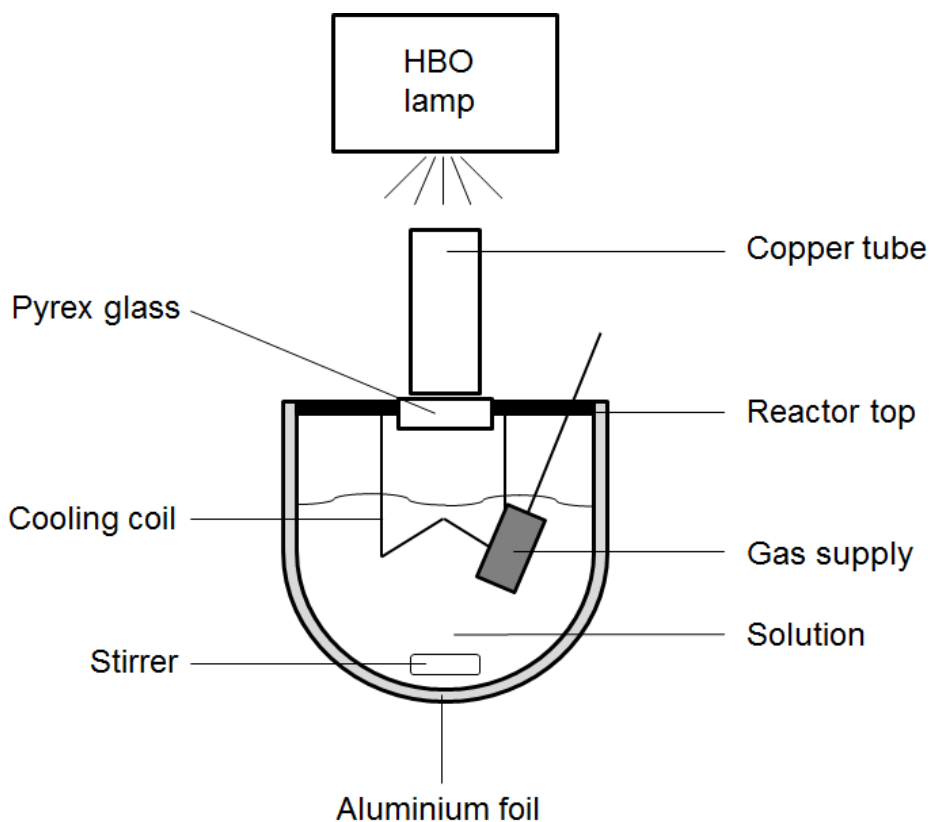


Figure A6.1. Schematic of the photodeposition reactor. The photon flux through the Pyrex glass was roughly estimated to be $2.77 \cdot 10^{-8}$ Einstein $\text{cm}^{-2} \text{s}^{-1}$. Aluminum foil was used to prevent outscattering of light as much as possible.

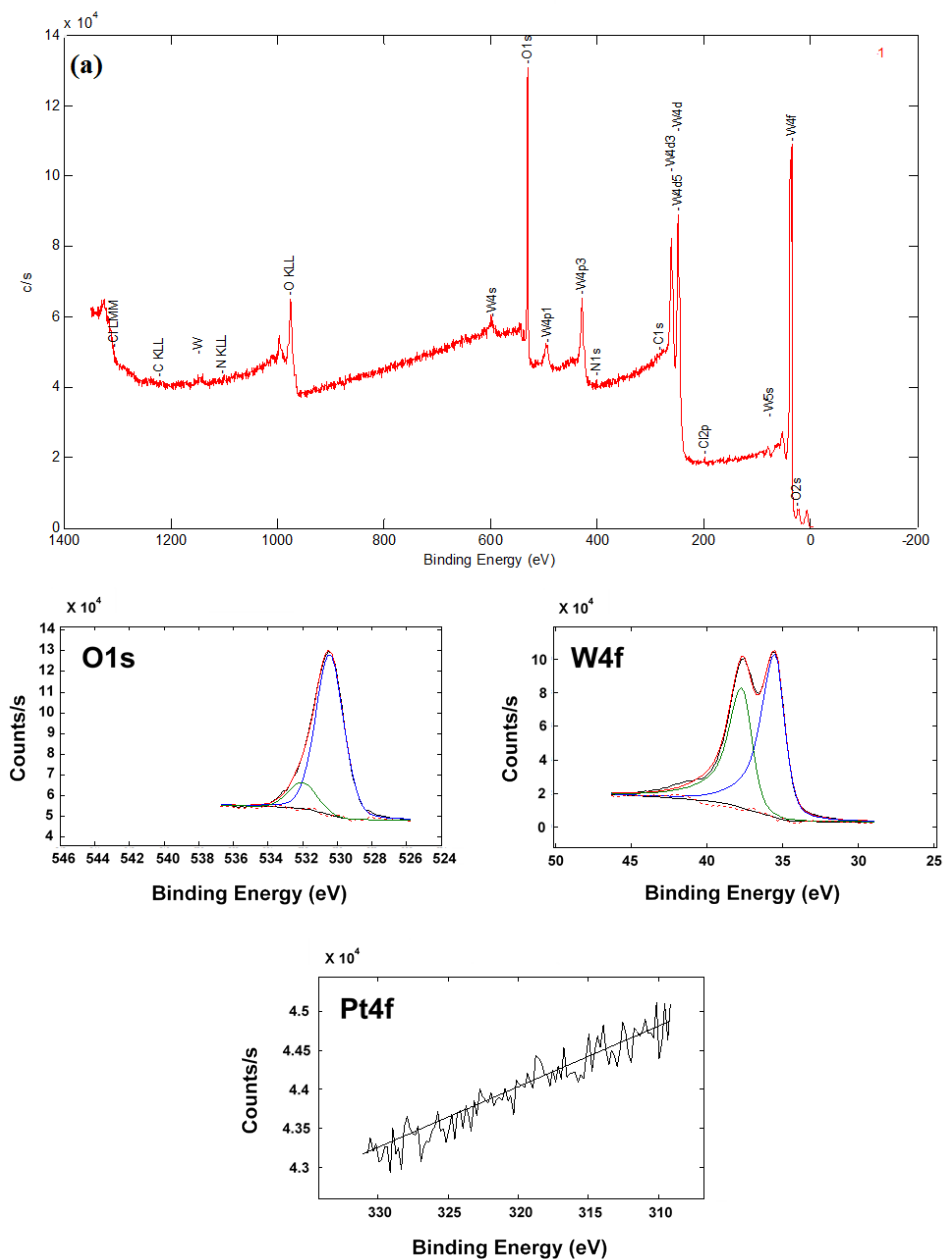


Figure A6.2. (a) XPS spectrum of plate-like WO_3 .

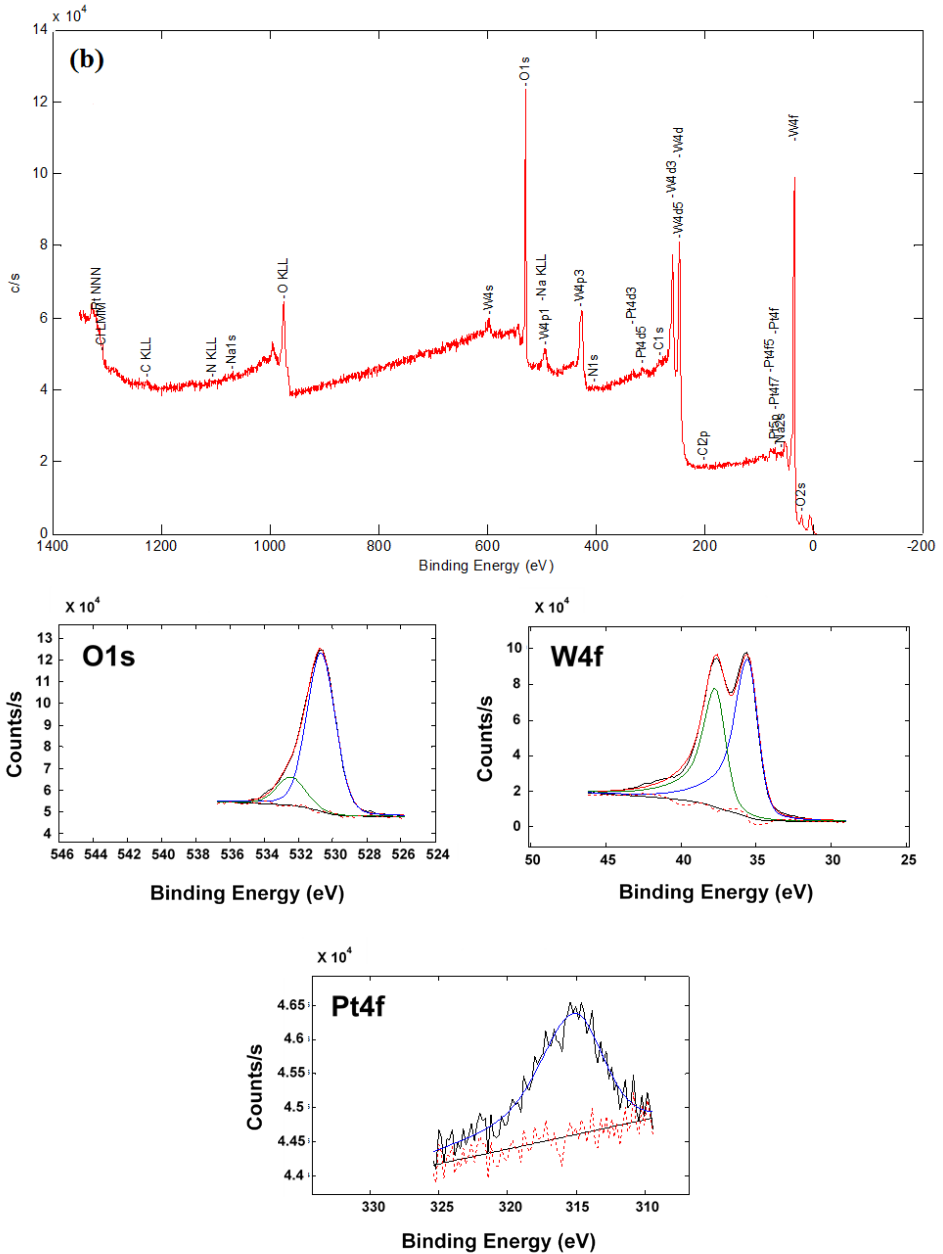


Figure A6.2. (b) XPS spectrum of Pt-loaded plate-like WO_3 obtained through photo-deposition using $H_2PtCl_6 \cdot 6H_2O$ as a precursor.

Table A6.1. Calculated atomic ratios out of XPS data.

Element Sample	C [At %]	O [At %]	Na [At %]	Cl [At %]	W [At %]	Pt [At %]	Pb [At %]
WO ₃	2.56	71.14	0.35	0.10	25.66	0.17	0.01
Pt/WO ₃ (photo- deposition)	1.70	69.65	0.76	0.05	26.35	1.48	0.00
Pt/WO ₃ (impreg- nation)	4.03	67.54	0.74	0.19	24.56	2.87	0.07
In red: unreliable calculated concentrations, standard deviation as big or bigger as averaged value							

6.7 Appendix – particle counting

In this section a statistical analysis of Pt particle counting is performed. The amount of Pt particles on the side facet or the edge of a WO₃ particle is compared to the amount of Pt particles on the dominant facet. This is first done for the Pt/WO₃ samples obtained through photodeposition. The first sample is the same sample as depicted in Figure 6.2. The second sample is Pt/WO₃ obtained through photodeposition after scaling up the amounts of materials used as described in paragraph 6.2, ‘Materials and methods’. The third sample analyzed is Pt/WO₃ obtained through impregnation. In all cases, H₂PtCl₆ · 6H₂O was used as a precursor. For each sample, six WO₃ nanoplates are analyzed where structure-directed deposition is observed. For comparison, two WO₃ nanoplates where no obvious structure-directed deposition is observed, are also studied. For each sample, a summary of Pt particle counting is shown in Tables A6.2 to A6.4 and an average ratio of the amount of Pt particles on the side facet/edge compared to the amount of Pt particles on the dominant facet is calculated. Note that rough estimations are given here. At the end of this section, HR-SEM images corresponding to these tables are shown, where a red box marks on what WO₃ particle Pt particle counting has taken place.

Table A6.2. Overview of counted Pt particles in photodeposition sample 1 and corresponding ratios.

Particles on the side facets/edges (not the dominant facet)	Particles on the dominant facet	Normalized particles ratios
112-212	10	11.2-21.2:1
33-36	0	INF:1
58	0	INF:1
28	12	2.33:1
36	8	4.5:1
10	1	10:1
6	10	0.6:1

Average normalized particles ratios (only taking the first 6 samples which confirm our theory. For the calculation, the INF:1 samples are rounded to a ratio of 33-36:1 and 58:1. Furthermore, averages are taken when it was difficult to count particles on the side facet):

20.9:1

The second and third counting are considered to be extreme cases. When they are not taken into account, the ratio becomes:

8.2:1

Table A6.3. Overview of counted Pt particles in photodeposition sample 2 and corresponding ratios.

Particles on the side facets/edges (not the dominant facet)	Particles on the dominant facet	Normalized particles ratios
19	3	6.33:1
7	3	2.33:1
14	3	4.67:1
6	4	1.5:1
5-6	1	5-6:1
9	0	INF:0
8	13	0.62:1
5	6	0.83:1

Average normalized particles ratios (only taking the first 6 samples which confirm our hypothesis. The INF:0 sample is rounded up to a ratio of 9:1):

4.88:1

Table A6.4. Overview of counted Pt particles in the impregnation sample and corresponding ratios.

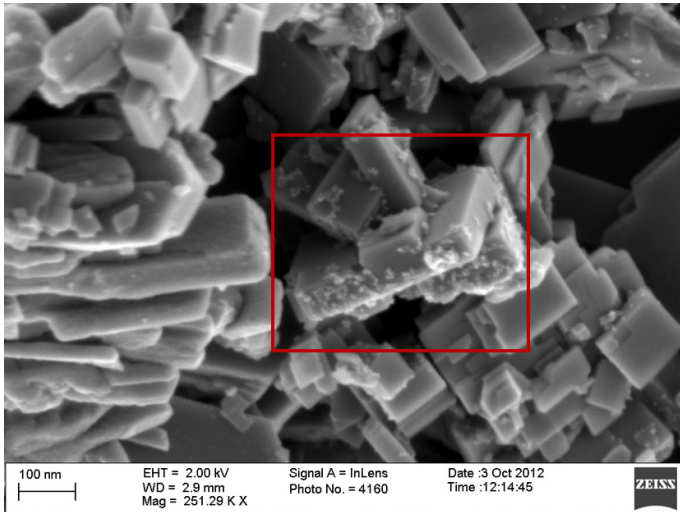
Particles on the side facets/edges (not the dominant facet)	Particles on the dominant facet	Normalized particles ratios
22	3	7.33:1
7	2	3.5:1
20	10	2:1
10	3	3.33:1
18	5	3.6:1
16	3	5.33:1
24*	10	2.4:1
1	10	0.1:1

*When the left facet is considered to be a side facet

Average normalized particles ratios (only taking the first 6 samples which confirm our hypothesis):

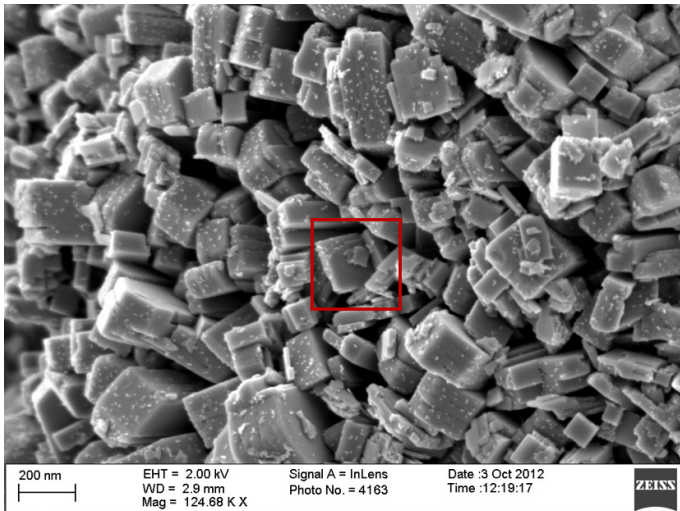
4.18:1

Photodeposition sample 1

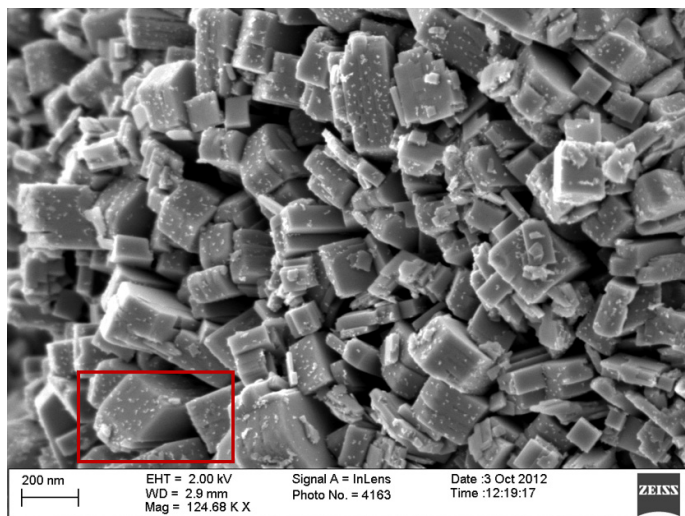


*Particles on front facet : particles on the side facet : particles on the dominant facet
100-200:12:10*

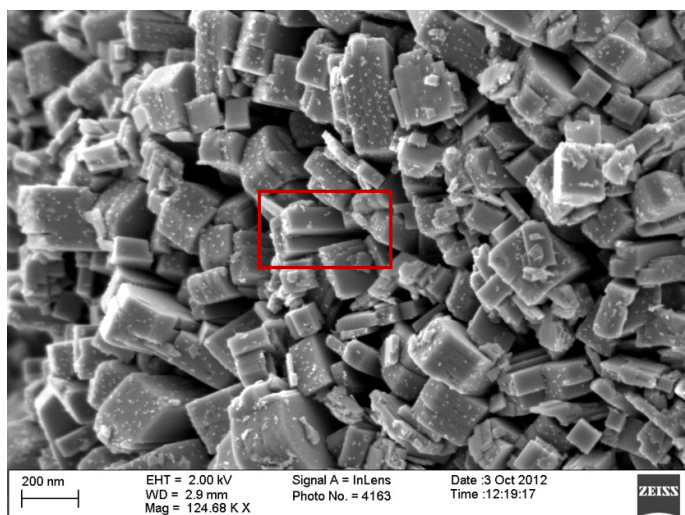
The particles on the edge in the back are not taken into account.



*Particles on the side facets/edges : particles on the dominant facet
33-36:0*

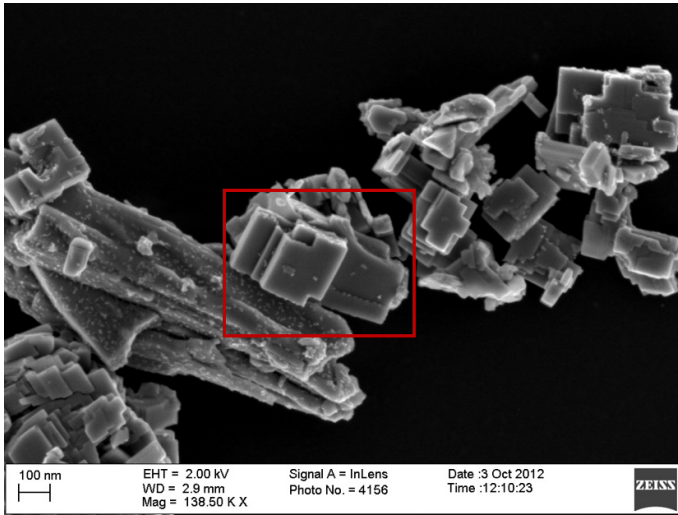


*Particles on the front (subordinate) facet : particles on the facet disappearing to the back
58 (50 to 60):0*

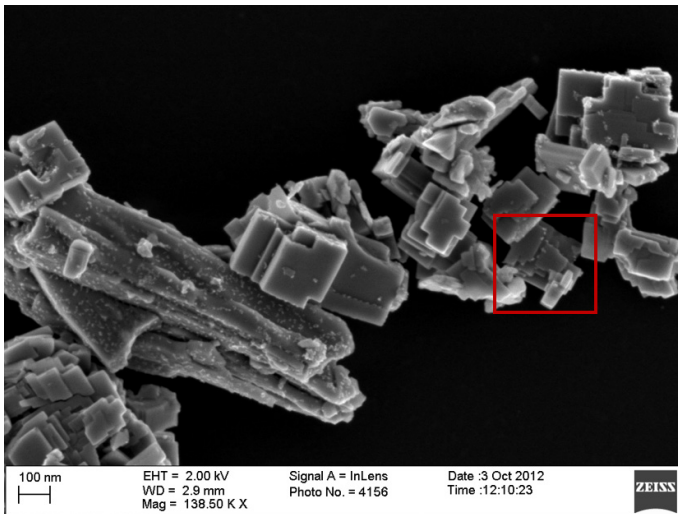


*Particles on the side facets/edges : particles on the dominant facet
28 (25 to 30):12 (10 to 15)*

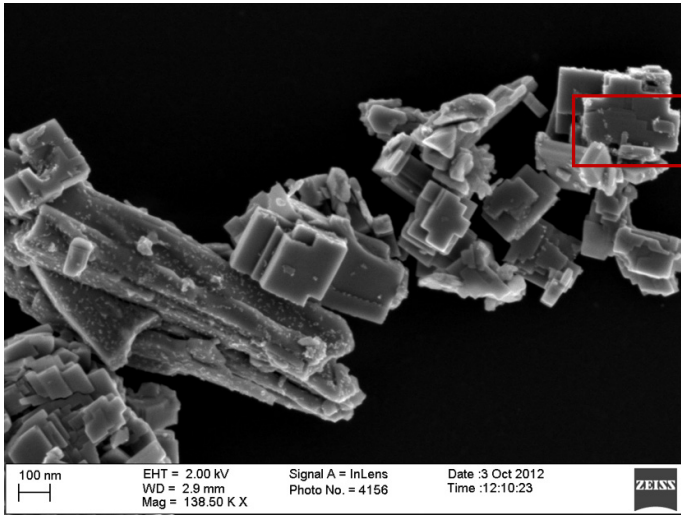
The big Pt-cluster on the side is estimated to be 15 particles. At the bottom of the subordinate facet there seems to be a 'rough' surface. The particles on this surface are not taken into account in the counting. The particles in the groove are considered to be photodeposited there due to the presence of the side facet.



*Particles on the side facets/edges : particles on the dominant facet
36 (30 to 40):8 (5 to 10)
Right and top subordinate facets are taken into account.*



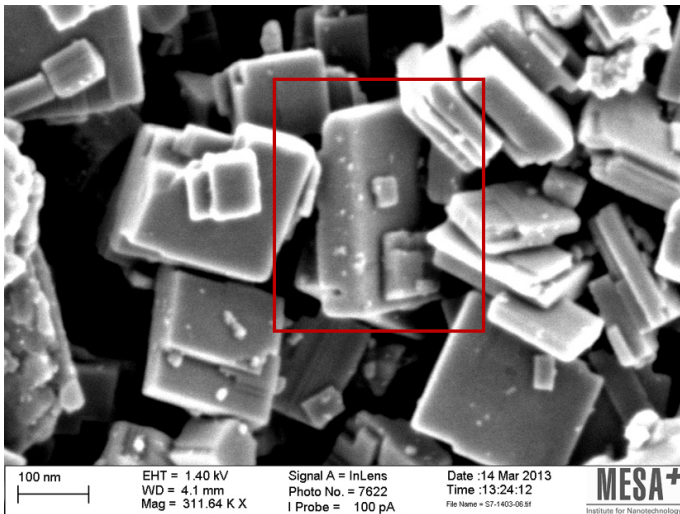
*Particles on the side facets/edges : particles on the dominant facet
10:1
Only the two top plates are considered.*



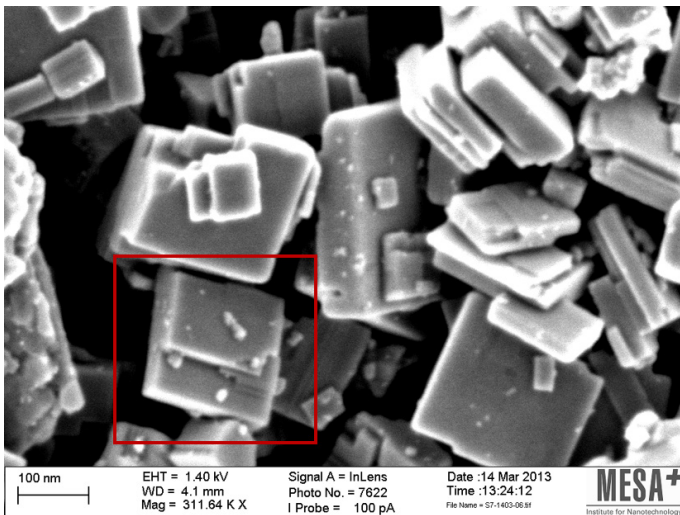
*Particles on the side facets/edges : particles on the dominant facet
6:10*

Only the plate is considered where the Pt particles are on the top of the WO₃ particle.

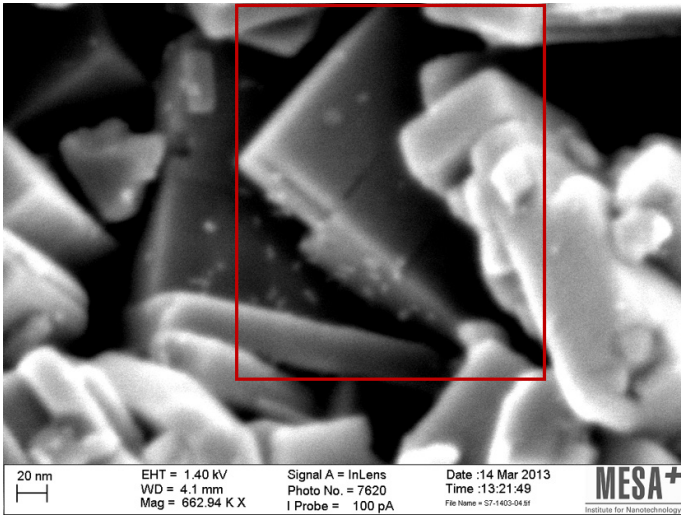
Photodeposition sample 2



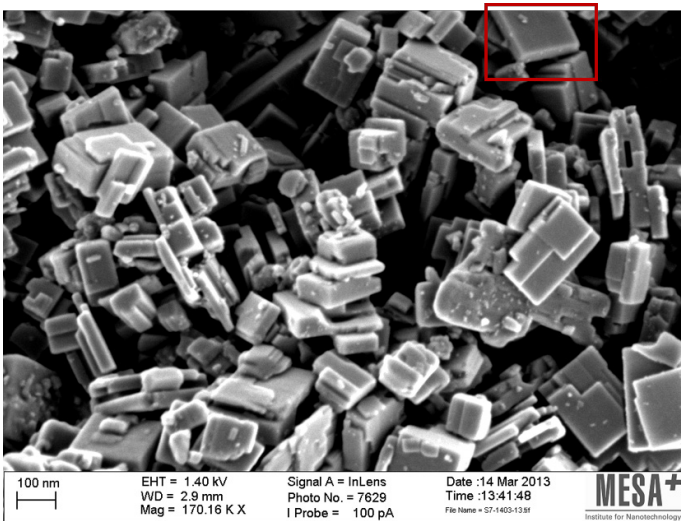
*Particles on the side facets/edges : particles on the dominant facet
19:3
Only the big plate is taken into account.*



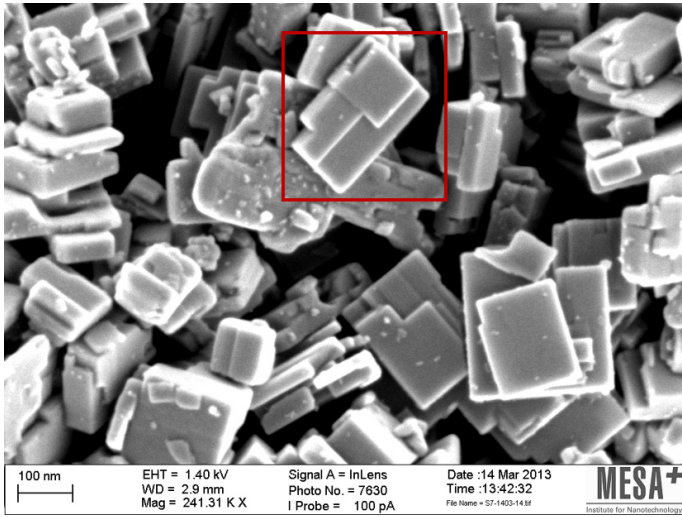
*Particles on the side facets/edges : particles on the dominant facet
7:3
The big white clusters are not considered to be Pt-clusters, but rather some kind of dirt. They are not taken into account with counting.*



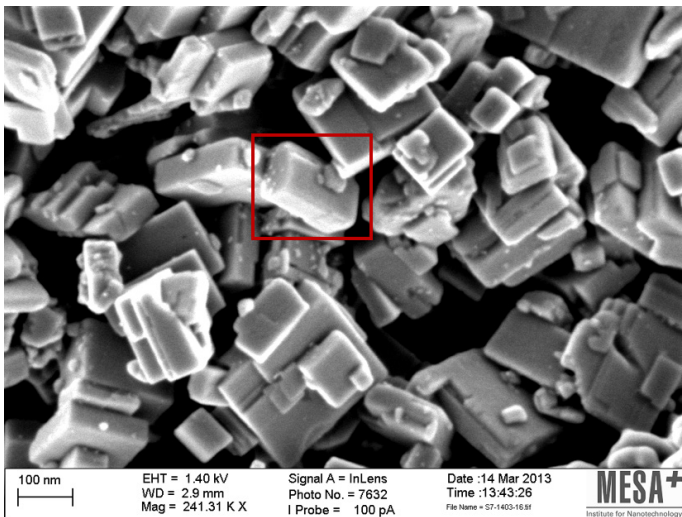
Particles on the side facets/edges : particles on the dominant facet
14:3
Upper plate taken into account.



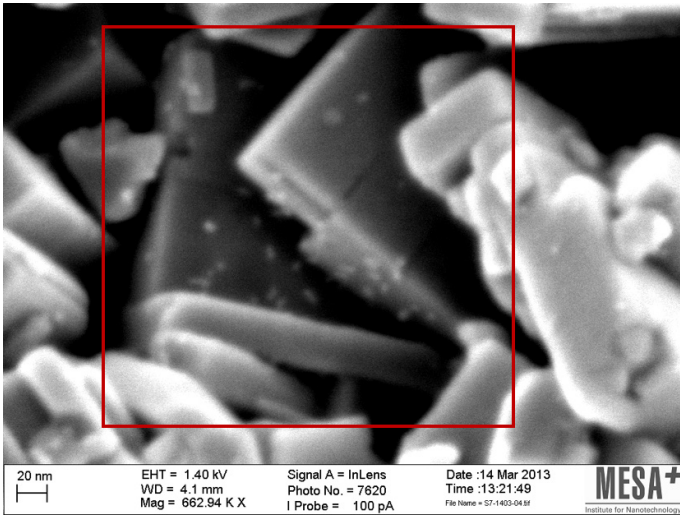
Particles on the side facets/edges : particles on the dominant facet
6:4



*Particles on the side facets/edges : particles on the dominant facet
5-6:1*

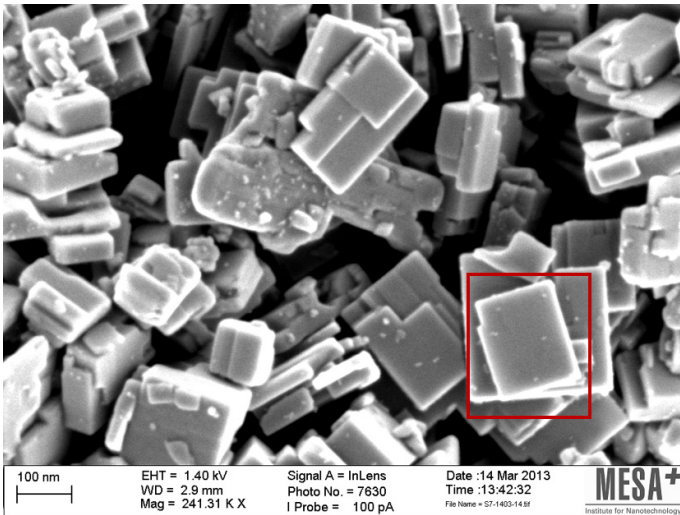


*Particles on the side facets/edges : particles on the dominant facet
9:0*



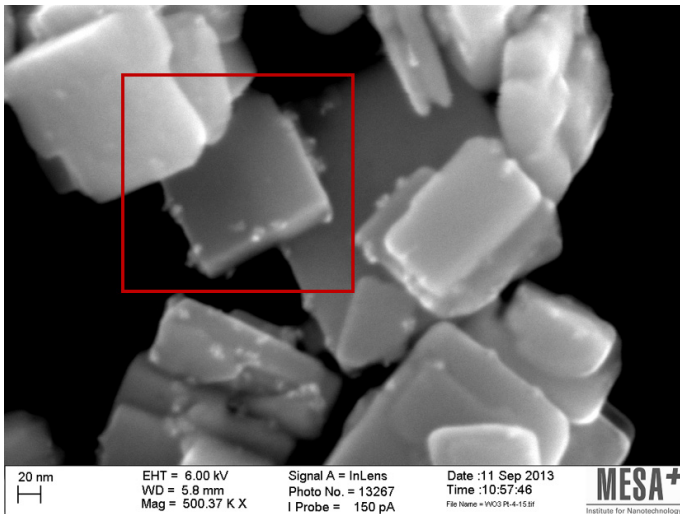
Particles on the side facets/edges : particles on the dominant facet
8:13

Lower, big plate taken into account. If carefully looked upon, it seems there is some sort of mini-hill on the surface. The particles seem deposited at this hill edge. It might be that the Pt-particles are deposited here on a sort of 'edge' as well.

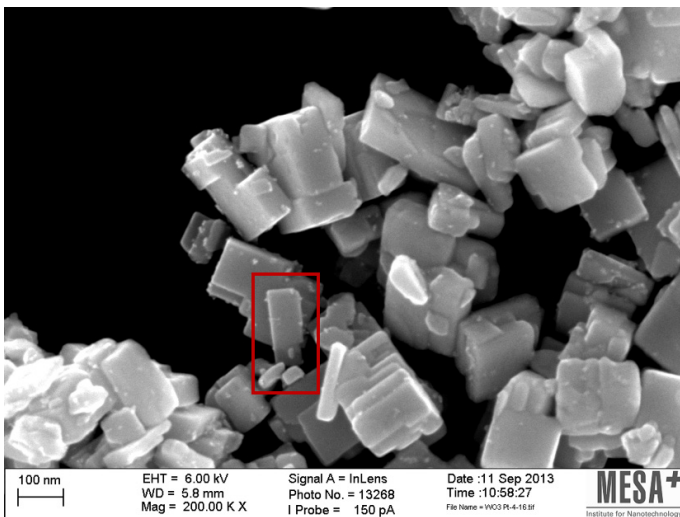


Particles on the side facets/edges : particles on the dominant facet
5:6

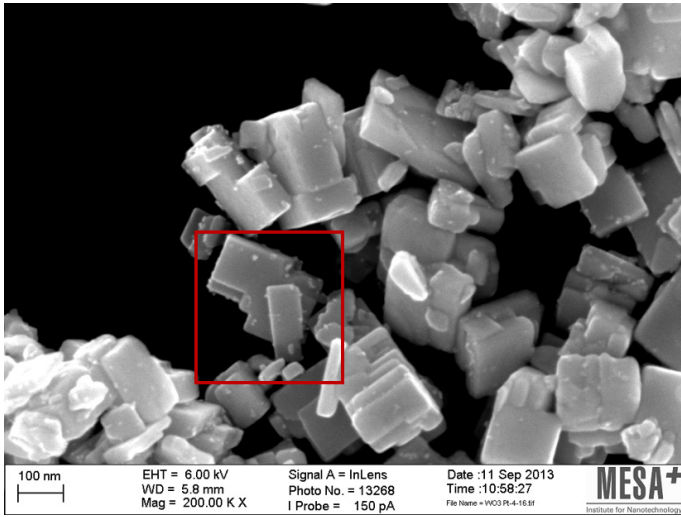
Impregnation sample



Particles on the side facets/edges : particles on the dominant facet
22:3

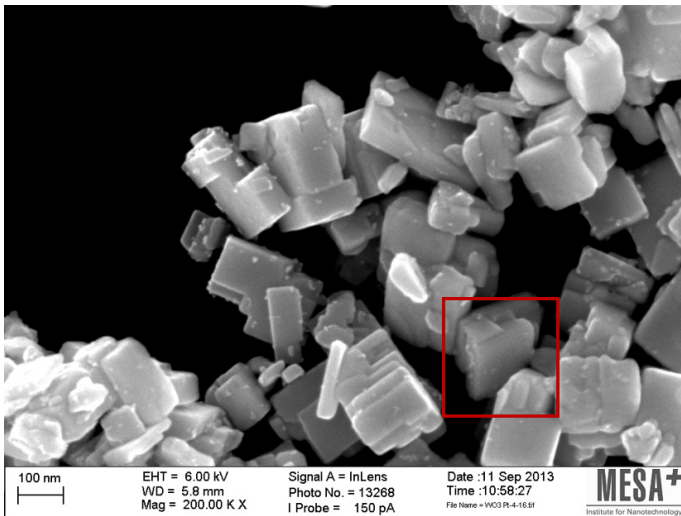


Particles on the side facets/edges : particles on the dominant facet
7:2

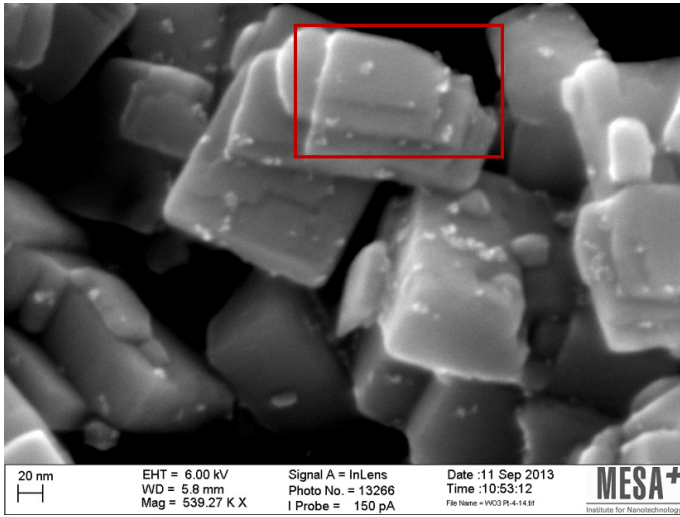


Particles on the side facets/edges : particles on the dominant facet
20:10

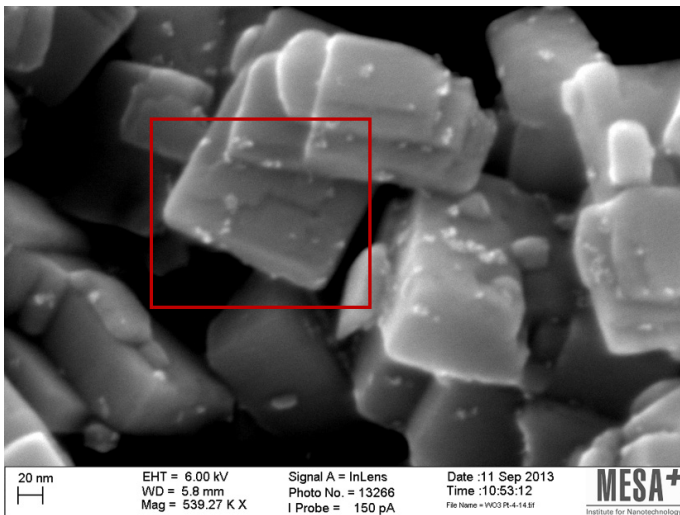
It should be noted that the Pt particles on the dominant facet are near the edges.



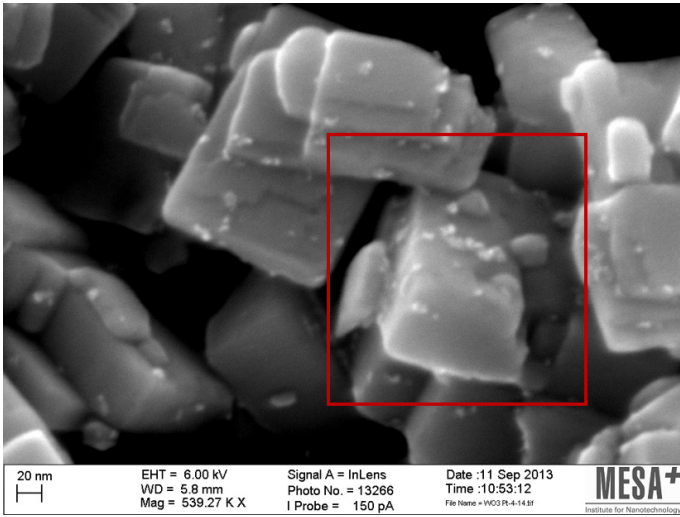
Particles on the side facets/edges : particles on the dominant facet
10:3



Particles on the side facets/edges : particles on the dominant facet
18:5

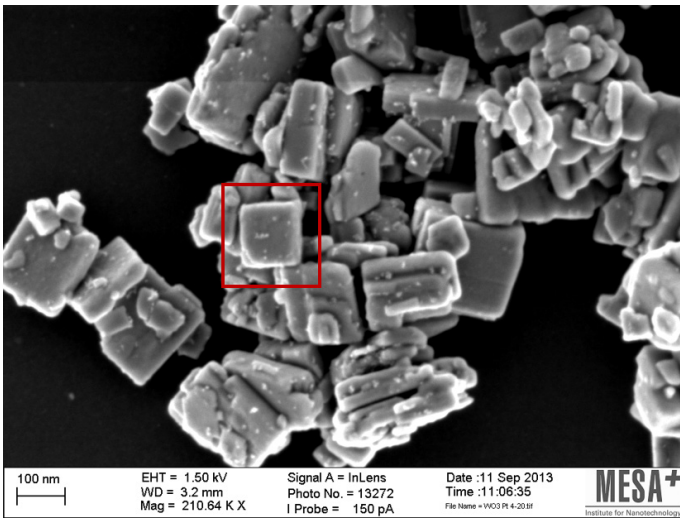


Particles on the side facets/edges : particles on the dominant facet
16:3
Only two bottom plates considered.



Particles on the edges : particles on the left facet : particles on the upper facet
9:13:10

If the left facet is considered as a subordinate facet, then:
Particles on the side facets/edges : particles on the dominant facet
24:10



Particles on the side facets/edges : particles on the dominant facet
1:10

Chapter 7

Photocatalytic propane oxidation over platinum-loaded tungsten oxide nanoplates

Abstract

The photocatalytic properties of platinum-loaded tungsten oxide nanoplates are studied in the photo-oxidation of propane, where the platinum was deposited through photodeposition in the presence of methanol. The tungsten oxide nanoplates were prepared through microwave-assisted hydrothermal synthesis at temperatures of 150 °C, 200 °C and 250 °C, where the sample synthesized at 150 °C still has some hydrates left in its crystal lattice. When the nanoplates are synthesized at 150 °C or 250 °C, platinum is mainly present in a Pt^{II} oxidation state, whereas Pt⁰ is the dominant state when the tungsten oxide is synthesized at 200 °C. The presence of platinum turns out to have a negative effect on the photocatalytic activity of the tungsten oxide nanoplates, especially when it is present in a Pt^{II} state. When Pt⁰ is mainly present, activation of the Pt/WO₃ is observed over multiple photocatalytic runs. This activation occurs much faster when pre-illumination of the Pt/WO₃ takes place. Pt⁰/WO₃ will ‘reset’ itself to its initial photocatalytic activity value when left idle in the dark. We discuss in detail that we attribute the photocatalytic behavior of Pt⁰/WO₃ to the adsorption of water on sites suited for the oxidation of propane.

This chapter is based on Wenderich, K. et al.; Photocatalytic propane oxidation over platinum-loaded tungsten oxide nanoplates. In preparation.

7.1 Introduction

Over recent years, photocatalysis has been an upcoming field for applications in the removal of volatile organic compounds (VOCs).^[1-3] By far most of the work has been performed using titanium dioxide as a photocatalytic material. A major disadvantage of titania though is that its bandgap is relatively wide, limiting absorption of wavelengths up to 380 nm (for anatase) or 410 nm (for rutile).^[3] Therefore, it is rewarding to investigate if other photocatalytic materials with smaller bandgaps could be candidates for the oxidation of harmful organic compounds as well. A possible material which comes to mind is tungsten trioxide (WO₃). Tungsten oxide is considered to be an excellent photocatalyst for visible light harvesting, despite the edge of the conduction band being at an unfavorable position for both the reduction of protons and the single-electron reduction of oxygen.^[4-6] The stability of the semiconductor under acidic conditions and its non-toxicity contribute greatly to the possibility of employing this material in commercial applications. Tungsten oxide has been extensively used in water oxidation^[7-10] as well as in water purification.^[11-14] For both cases, it has been demonstrated that loading platinum (Pt) on WO₃ results in considerable improvements in photocatalytic activities.^[15-18] Although for water oxidation the addition of an electron scavenger will remain required, Abe *et al.* demonstrated that oxygen will be reduced during the oxidation of organic contaminants.^[17] This is related to the edge of the conduction band of WO₃ being more negative than the multi-electron reduction potential of O₂ and the fact that Pt will act as an electron sink. Due to the latter, electron accumulation will take place in the cocatalytic Pt particles and thus multi-electron reduction of O₂ will become more feasible. This will result in the production of *e.g.* H₂O₂ rather than O₂^{-•} or HO₂[•]. It has been demonstrated that the prevention of single-electron reduction of O₂, but the allowance of multi-electron reduction can have consequences for the selectivity of Pt/WO₃.^[19-21]

To some extent the photocatalytic properties of tungsten oxide in gas phase oxidation have been studied.^[22-25] For instance, Chen & Ye have demonstrated that WO₃ hollow shells exhibit excellent photocatalytic activity in the degradation of gaseous 2-propanol under visible light compared to commercial WO₃.^[22] In another example, Sayama *et al.* demonstrated that WO₃ can be used in the photocatalytic oxidation of hexane.^[24] The authors also used CuO/WO₃ for the photocatalytic degradation of acetaldehyde and propane. A limited amount of research has been performed on the applications of Pt/WO₃ in gas purification. Most of this research is performed in the photodegradation of acetaldehyde.^[17, 26-28] Another application where Pt/WO₃ has

been used in is ethylene photodegradation.^[29] Both for the photodegradation of acetaldehyde and ethylene the presence of platinum contributes to higher photocatalytic activities.

We have demonstrated in Chapter 4 that tungsten oxide nanoplates can act as an excellent photocatalyst in the removal of gaseous propane in air under visible light, thus demonstrating its promising features in gas purification. In this chapter, we used such samples to verify if photodeposition of Pt on these nanoplates also has a beneficial effect on the photocatalytic activity in propane oxidation. First, we performed photodeposition of Pt on WO₃ nanoplates obtained by different hydrothermal synthesis temperatures. To do so, we used the photodeposition method as described in Chapter 5. As-obtained samples were characterized on the relative amount of Pt deposited. Also, it was verified if structure-directed photodeposition occurs once more, as described in Chapter 6. Then, the as-obtained Pt/WO₃ samples were tested in photocatalytic propane oxidation.

7.2 Materials and methods

All chemicals of analytical grades were acquired from Sigma-Aldrich, Merck and Alfa Aesar. In this research, WO₃ nanoplates were used as described in Chapter 4. Briefly, the WO₃ nanoplates have been synthesized through microwave hydrothermal synthesis using a Multiwave PRO from Anton Paar with 80 mL quartz vessels. For each sample, an aqueous solution of 160 mL containing 2.64 g of Na₂WO₄ · 2H₂O and 1.68 g of citric acid was prepared. The pH was adjusted to 0.5 using diluted HCl. The solution was equally distributed over four cuvettes, which were put in the microwave hydrothermal synthesis oven. Heating took place at 150 °C, 200 °C or 250 °C for 2 hours with a heating rate of 10 K min⁻¹.

Photodeposition of Pt (aim: 2 wt%) on as-synthesized WO₃ nanoplates took place using the photodeposition method described in Chapter 5. 50 mL aqueous solution containing 168 mg/L H₂PtCl₆, 200 mg of WO₃ and 12 mL of methanol was prepared in a quartz beakerglass, which was covered by a quartz plate to prevent evaporation of the solution. The beakerglass was then placed inside a black box reactor, described by Romão *et al.*^[30] To ensure top-illumination only, the beakerglass was covered on the sides with aluminum foil. After one hour of stirring at 450 rpm in the dark to obtain adsorption/desorption equilibrium, illumination took place for 60 minutes using all lamps inside the box reactor under continued stirring. Then, solid and solution were separated using centrifugation at 8500 rpm for 30 minutes. Washing of the filtrate took place 2 times with Millipore water, after which it was dried at 80 °C. The Pt-loaded samples were labeled as Pt/WO₃-150, Pt/WO₃-200 and

Pt/WO₃-250, corresponding to parent WO₃ samples synthesized at respectively 150 °C, 200 °C and 250 °C. Unloaded samples are referred to as WO₃-150, WO₃-200 and WO₃-250.

As-obtained Pt/WO₃ samples were characterized through X-ray photoelectron spectroscopy (XPS) (Quantera SXM from Physical Electronics) and high resolution-scanning electron microscopy (HR-SEM) (Zeiss MERLIN HR-SEM). XPS was used to compare the relative amounts and oxidation state of Pt photodeposited on the surface of the different WO₃ samples. HR-SEM was used to study whether preferred photodeposition of Pt took place. For photocatalytic activity measurements in propane (C₃H₈) oxidation by gas chromatography, each Pt/WO₃ sample was coated on glass substrates (25.3 mm x 25.8 mm) using a dropcasting method described in Chapter 4. Cleaning of the glass substrates took place by exposing them to sonication in first acetone, then ethanol. Afterwards, the glass substrates were treated for 30 minutes in a mixture of H₂O₂ (≥35%) solution, NH₄OH (28-30% NH₃ content) solution and H₂O, the ratio between the solutions being 1:1:5. Then, the glass plates were put on a heating plate preheated at 100 °C. Before dropcasting took place, 100 mg of a Pt/WO₃ sample was prepared in a slurry solution of 2 mL Millipore water with pH = 2 (prepared with concentrated HCl). 750 μL of the solution was dropcasted on each glass plate. A uniform coating was observed after evaporation took place. Then, the outer parts of the coating were removed until an inner circle remained with a diameter of 1.25 cm, which corresponded to a sample area of 0.61 cm². We calculated that approximately 7.05 mg of Pt/WO₃ was present on each glass substrate.

As-made coatings were loaded in a batch reaction cell described by Fraters *et al.*,^[31] which was connected to a gas chromatograph (GC) system (Agilent 7820 GC system containing a Varian CP7584-column and a Methanizer-FID combination). Prior to each photocatalytic propane oxidation measurement (referred to as ‘a run’), the reactor was first flushed with a gas mixture of 80 vol% N₂, 19.5 vol% O₂ and 5000 vol ppm of C₃H₈ for a minimum of 21 minutes, unless noted otherwise. Then, the valves connected to the reactor were closed and illumination of the coating took place using a 420 nm LED (6.2 mW/cm² at the coating surface) for 10 minutes. When illumination finished, helium was flushed through the reactor to transport the gas mixture towards the GC, where the mixture was analyzed on its organic content. The following sets of runs were performed for each coating: i) two runs in the dark, followed by six runs under illumination, ii) multiple runs under different illumination times, iii) multiple runs in the absence of illumination with different reaction times and iv) once more two runs in the dark, followed by six runs under illumination.

Additionally, one of the Pt/WO₃-200 coatings was exposed to additional sets of runs as well, where the change in photocatalytic activity was monitored over a large number of runs. Between some of the runs, flushing took place with either N₂ and N₂/O₂ (ratio 4:1), possibly followed by 3 hours of pre-illumination before the next run started.

As in Chapter 4, the formation of CO₂ has been monitored, as this was the product mainly formed. The reaction rate r in mol m⁻² h⁻¹ was calculated based on a method by Fraters *et al.*:^[31]

$$r = \frac{P \cdot X_{CO_2} \cdot V}{R \cdot T} \cdot \frac{1}{m \cdot S_{BET}} \cdot \frac{3600}{t} \quad (7.1)$$

P is the pressure inside the reactor (Pa), X_{CO_2} the fraction of CO₂ formed, V the gas volume inside the reaction cell (m³), R the gas constant (m³ Pa mol⁻¹ K⁻¹), T the temperature inside the reactor (K), m the mass of the catalyst (g), S_{BET} the BET surface area of the sample (m² g⁻¹) and t the reaction time (s). It was assumed that the BET surface areas of the Pt-loaded WO₃ samples are similar to the unloaded WO₃ samples. This was done for the sake of comparison between unloaded and loaded WO₃ samples. In Chapter 4 we determined that the BET surface areas of WO₃-150, WO₃-200 and WO₃-250 were 17.61 m² g⁻¹, 13.84 m² g⁻¹ and 13.41 m² g⁻¹ respectively.

7.3 Results and discussion

7.3.1 Characterization of as-synthesized Pt/WO₃

Table 7.1 depicts the amounts of elements present on the surface for each sample in at%, as determined by XPS. Clearly, less Pt is detected on Pt/WO₃-150 than on Pt/WO₃-200 and Pt/WO₃-250. This can be attributed to the lower photocatalytic activity of the tungsten oxide nanoplates when they are synthesized at 150 °C instead of 200 °C or 250 °C due to the presence of hydrates (as discussed in Chapter 4). For Pt/WO₃-150 at least, 1 hour of illumination is apparently not sufficient for full Pt photodeposition.

Table 7.1. At% of elements present on the surface of Pt/WO₃-150, Pt/WO₃-200 and Pt/WO₃-250, as determined by XPS.

Sample name	At% Pt	At% W	At% O	At% Cl
Pt/WO ₃ -150	0.24	23.83	75.69	0.23
Pt/WO ₃ -200	0.71	25.86	73.30	0.13
Pt/WO ₃ -250	0.80	24.85	74.03	0.32

In Chapter 5 we demonstrated that employment of methanol in the photodeposition procedure of Pt on commercial WO₃ should yield the formation of metallic Pt⁰ in only 15 minutes. Here, under the same reaction conditions but considerably longer illumination times (1 hour), XPS studies on the Pt4f doublet (Figure 7.1) reveal differences in the oxidation state of as-deposited Pt on WO₃-150, WO₃-200 and WO₃-250. For Pt/WO₃-150 and Pt/WO₃-250, peaks are found around 72.6 eV and 75.9 eV, corresponding to respectively Pt4f_{7/2} and Pt4f_{5/2}. These peaks imply that the Pt is in the Pt^{II} state.^[32, 33] On the contrary, the main peaks of Pt/WO₃-200 appear at 71.8 eV and 75.0 eV, demonstrating that the Pt here is mainly metallic. The shoulder at 72.6 eV indicates that to some extent Pt^{II} is still present as well. With the low reaction rate of WO₃-150, it is not surprising that no full photoreduction of the platinum precursor has taken place. However, the difference in the Pt oxidation state of the Pt/WO₃-200 and Pt/WO₃-250 is very remarkable. In Chapter 4 it was demonstrated that WO₃-200 and WO₃-250 have approximately the same photocatalytic activity. This is also evidenced by the amount of Pt which has been detected on the surface of these WO₃ nanoplates, as observed in Table 7.1. It even seems that there is slightly more Pt present on the surface of the Pt/WO₃-250 sample than on the Pt/WO₃-200 sample. Due to the similar photocatalytic activities of both WO₃-200 and WO₃-250, similar photodeposition behavior was expected as well. We speculate that a reason for the differences in photodeposition behavior might be related to the amount of surface defects. In Chapter 4, we demonstrated that WO₃-200 has more surface defects than WO₃-250. It is likely that these surface defects somehow contribute to obtain full Pt photoreduction. Further research is needed to verify why there is such a big difference in the Pt oxidation state between these samples.

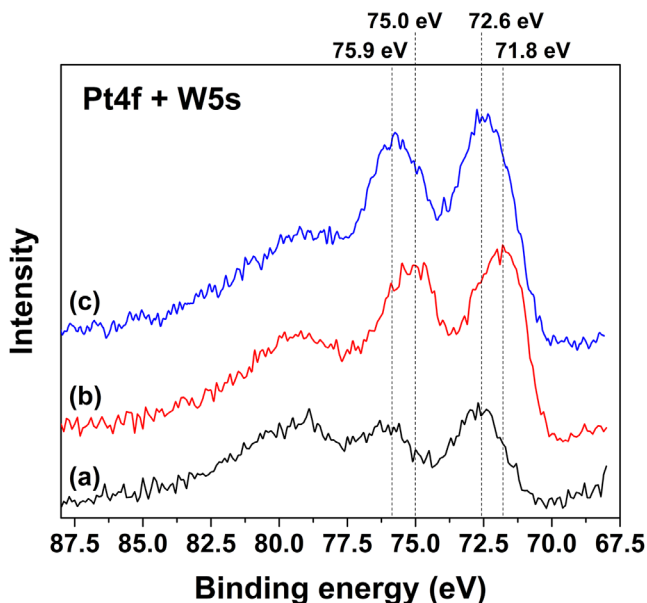


Figure 7.1. XPS spectra recorded in the Pt4f + W5s region of (a) Pt/WO₃-150, (b) Pt/WO₃-200 and (c) Pt/WO₃-250. The peaks around 79 eV correspond to the W5s singlet.

HR-SEM images of the different Pt-loaded WO₃ nanoplates are demonstrated in Figure 7.2. The low amounts of Pt loading in Pt/WO₃-150 can be observed once more (Figure 7.2a). Although careful observation shows that some Pt particles are present on the WO₃ surface, it overall seems remarkably void of these particles. It should be noted that distinguishing between Pt and WO₃ is complicated, due to the WO₃ nanoplates not having a clearly defined morphology yet. Therefore, some smaller particles observed on the surface of the WO₃ might simply be WO₃ as well rather than Pt. For Pt/WO₃-200, definitely more Pt particles are present on the WO₃ nanoplates (Figure 7.2b & c). As in Chapter 6, we observe mainly positioning of the Pt particles on the edges/side facets of the nanoplates.^[34] Remarkably, we do not observe photocorrosion of the WO₃ particles, which we did observe in Chapter 6. A possible explanation could be that shorter illumination times have been used for the samples in this chapter. Here, only 1 hour of illumination has been employed. In Chapter 6, illumination took place overnight in a different photodeposition reactor. For Pt/WO₃-250 similar behavior is observed as for Pt/WO₃-200: positioning of the Pt particles seems to occur once more at the side facets/edges (Figure 7.2d).

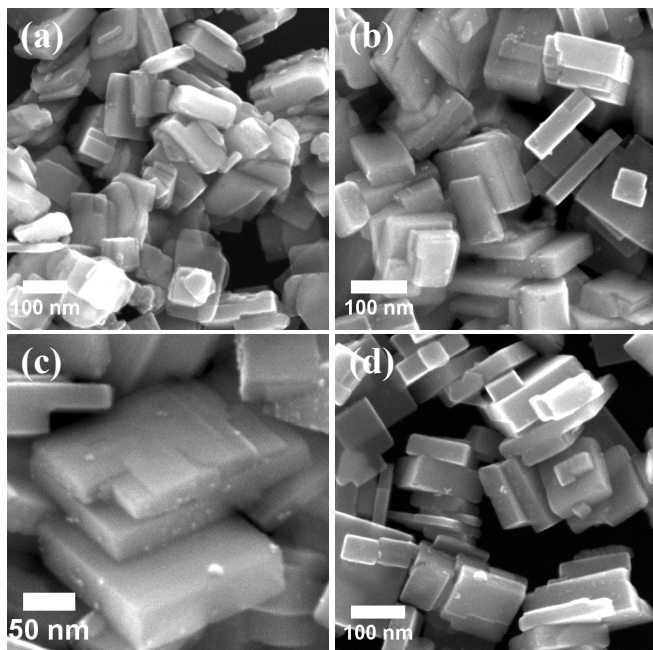


Figure 7.2. HR-SEM images of (a) Pt/WO₃-150, (b, c) Pt/WO₃-200 and (d) Pt/WO₃-250.

7.3.2 Photocatalytic propane oxidation measurements

Photocatalytic activity measurements in propane oxidation using different Pt/WO₃ samples are depicted in Figure 7.3a. Here, only the sets of runs are depicted where a fixed illumination time of 10 minutes has been used (sets i) and iv) described in paragraph 7.2, ‘Materials and methods’). An example of a set of runs where the reaction times were varied both under illumination and in the dark (sets ii) and iii)) can be found in the appendix in Figure A7.1. Comparisons of the activities between unloaded and Pt-loaded WO₃ nanoplates are demonstrated in Table 7.2, where for unloaded WO₃ the activities as measured in Chapter 4 are shown. For Pt/WO₃ the depicted activities are the averages of the last three runs as evidenced in Figure 7.3a. Photodeposition of Pt on the WO₃ nanoplates turns out to be detrimental for the photocatalytic activity, both when it is dominantly present in the Pt^{II} and, surprisingly, the Pt⁰ state. When the Pt is mainly present in its oxidized form (in the case of Pt/WO₃-150 and Pt/WO₃-250), hardly any photocatalytic activity can be observed for the Pt/WO₃ nanoplates. Even a small amount of PtO (or Pt(OH)₂) is sufficient to destroy the photocatalytic properties of the plate-like WO₃, as evidenced by Pt/WO₃-150. Initially, Pt/WO₃-200 also seems to have a minor photocatalytic activity. However, over multiple runs the sample becomes more active, ultimately reaching a reaction rate value of 2.916 μmol CO₂ m⁻² h⁻¹ averaged over the last three

runs. This activation is not permanent however. When a repetition of the experiment at a later time was performed with exactly the same coating, this behavior is observed once more (although the final photocatalytic activity is lower than in the first experiment). This is demonstrated in Figure 7.3b. A reproduction experiment of the Pt/WO₃-200 sample with a different coating yields the same kind of behavior, all be it with a higher photocatalytic activity. For this particular sample, multiple additional photocatalytic runs were performed, where flushing with N₂ and N₂/O₂ (ratio 4:1) took place for 24 hours between the sets of experiments. The most important results are depicted in Figure 7.4, where two measurement cycles are demonstrated. Again, we observe that the sample has been ‘reset’ to lower photocatalytic activity rate values before measurements have taken place. The sample is activated again over multiple runs, only to become deactivated after flushing with either N₂ or N₂/O₂. In some cases, the 24 hours of flushing was followed by 3 hours of illumination before a new set of measurements was started. In such a case, deactivation is observed as well. However, the Pt/WO₃-200 sample reaches its steady state value in photocatalytic activity much faster now than when no pre-illumination is used. The presence or absence of oxygen during the flushing does not seem to matter for as-observed behavior.

It should be noted that overall the activities of the Pt/WO₃-200 sample are somewhat lower in Figure 7.4 than in Figure 7.3b after activation. This might be related to the fact that additional experiments were performed between the measurements depicted in those figures. Here, investigation took place whether photocatalytic activity was observed in the absence of propane (to verify if the observed activation behavior was not the result of organic contaminants on the surface, which did not seem to be the case). This was followed by additional measurements to verify the influence of flushing time with N₂ or N₂/O₂ for 6 or 24 hours, where the reset was more drastic when 24 hours of flushing was used. In all cases however, activities have been observed in the same order of magnitude as the activities in Figure 7.4. Why higher activities are initially observed remains unanswered, although the conversion of residual methanol, used in the photodeposition procedure, cannot be excluded.

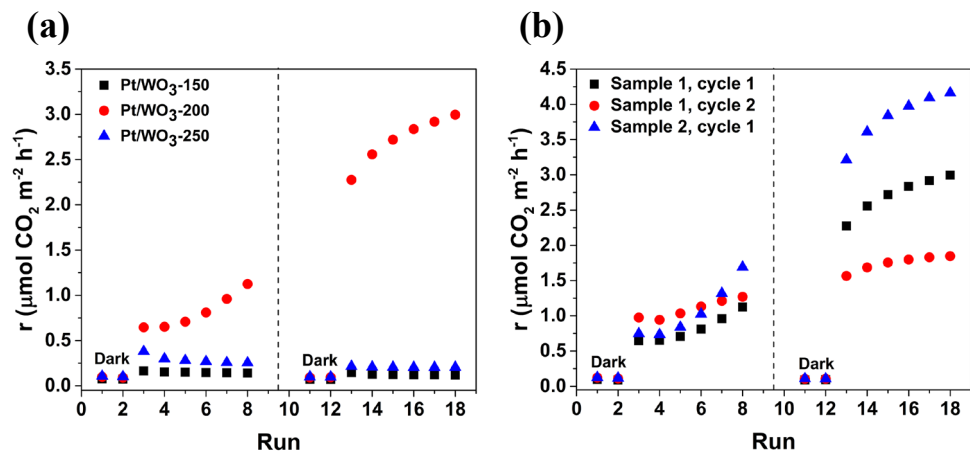


Figure 7.3. Photocatalytic CO₂ production rates from propane oxidation over (a) different Pt/WO₃ samples and (b) two Pt/WO₃-200 samples. At the place of the dashed line measurements took place to study the photocatalytic activity of the Pt/WO₃ samples as a function of time, both in the presence and absence of illumination. An example of such a measurement is depicted in the appendix (Figure A7.1).

Table 7.2. Photocatalytic CO₂ production rates measured for unloaded and Pt-loaded WO₃ nanoplates over the last three runs in a ‘standard’ measurement.

Hydrothermal synthesis T (°C)	r ($\mu\text{mol CO}_2 \text{ m}^{-2} \text{ h}^{-1}$)		Ratio Pt-loaded/unloaded
	Unloaded	Pt-loaded	
150	2.924	0.120	0.0412
200	6.692	2.916	0.4358
250	7.029	0.204	0.0291

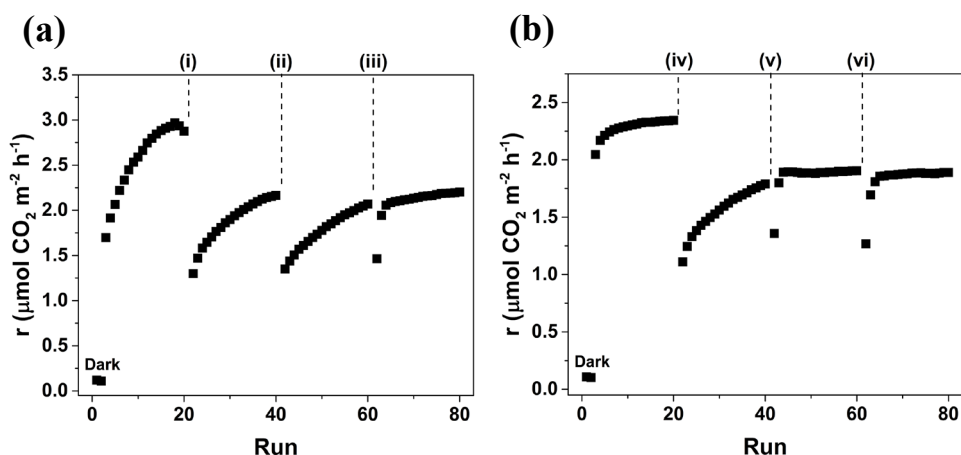


Figure 7.4. Photocatalytic CO₂ production rates from propane oxidation over one of the Pt/WO₃-200 samples (Sample 2). In between, gas flushing took place with N₂ and N₂/O₂ (ratio 4:1) and possible pre-illumination. The Roman numbers correspond in (a) to (i) 24 hours N₂ flushing, (ii) 24 hours N₂/O₂ flushing and (iii) 24 hours N₂ flushing + 3 hours pre-illumination. The Roman numbers in (b) correspond to (iv) 24 hours N₂ flushing, (v) 24 hours N₂ flushing + 3 hours pre-illumination and (vi) 24 hours N₂/O₂ flushing + 3 hours pre-illumination.

7.3.3 Discussion

The photocatalytic activity data are at a first glance very surprising, considering the fact that i) Pt/WO₃ is often considered to be much more photocatalytically active than bare WO₃^[15-18] and ii) structure-directed photodeposition could lead to enhanced photocatalytic performances.^[35, 36] However, there might be a logical explanation why the photocatalytic activity is considerably less. To understand this, we need to look at the mechanism involved in photocatalytic propane oxidation. Fraters *et al.* described the total reaction for photocatalytic propane oxidation as follows:^[31]

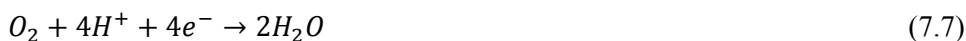


The authors ascribed this due to the following reduction reaction and one of the two following oxidation reactions occurring:



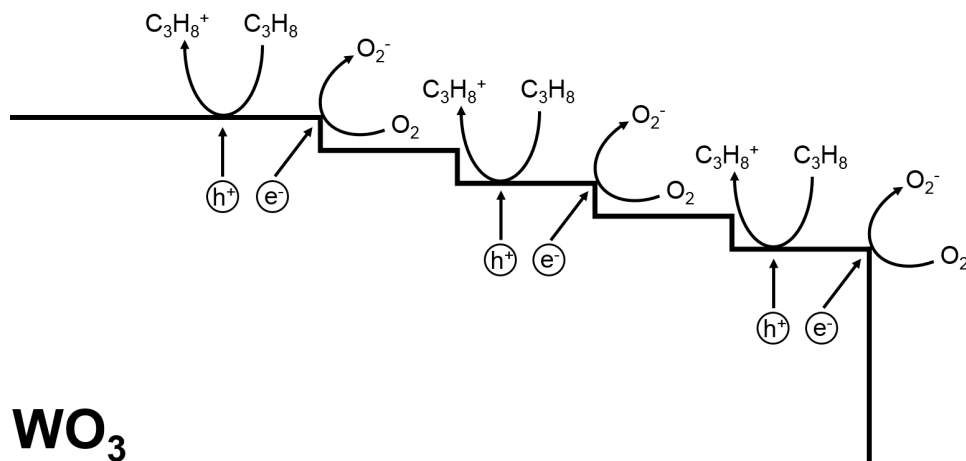


In equation 7.4 the propane is directly oxidized, whereas the formation of OH• radicals through hydroxyl oxidation (equation 7.5) will result in the indirect oxidation of propane through these radicals. Theoretically, for WO₃, single-electron reduction of O₂ is not possible due to the unfavorable position of the conduction band.^[17] Rather, the following multi-electron reductions could occur:



Noteworthy is that there might be a possibility that the H₂O₂ present could form OH• radicals as well through additional photocatalytic reduction,^[18] which could contribute to the oxidation of propane as well. Abe *et al.* have hypothesized that the deposition of Pt on WO₃ will increase the photocatalytic activity due to the Pt particles acting as an electron beacon and hence making multi-electron reduction reactions more feasible.^[17] Therefore, an increase in photocatalytic reaction rate would be expected when Pt is loaded on WO₃.

Now, in our case, we do observe photocatalytic oxidation of propane in the absence of Pt. Two explanations arise: i) multi-electron reductions are taking place on the WO₃ nanoplates even in the absence of Pt or ii) there are sites present on the plate-like WO₃ which have sufficient reductive power after all to reduce O₂ through single-electron reduction. We hypothesize that one of these two phenomena is possible considering the step-wise structure at the edges of the WO₃, as we have evidenced before by atomic force microscopy (Figure 7.5).^[34] In the first case, it could be that electrons migrate favorably towards the tips of the steps, where the multi-electron reduction takes place. In the second case, when single-electron reduction becomes possible, this has to be due to a shift of the conduction band edge to a more negative potential. Considering the fact that these shifts have been observed for different WO₃ facets before,^[7] it might be that single-electron reduction of oxygen becomes possible on the tips of the steps on the WO₃ edge. The grooves or a part of the flat basal plane near the steps could in both cases be used for the oxidation reaction, similar to what Kato *et al.* observed for La:NaTaO₃.^[37] No matter which explanation is used, oxygen needs to adsorb on the tips of the steps before it can be reduced, and propane needs to adsorb on the grooves/flat surfaces near the steps before being oxidized.



WO₃

Figure 7.5. Schematic of propane oxidation at the edge of an unloaded WO₃ nanoplate. Note that the propane oxidation depicted could be the result of both direct and indirect oxidation (via respectively holes and hydroxyl radicals). Also note that oxygen reduction is depicted here through single-electron reduction, while a possibility exists that it can also occur through multi-electron reduction.

When photodeposition of platinum takes place, the platinum will mainly be deposited on the edges/side facets due to adsorption effects, as we have discussed in Chapter 6.^[34] We have demonstrated that the favored sorption of the Pt complexes is likely induced by the steps on the edges of the WO₃ nanoplates. This means that Pt deposition will take place at these steps as well, both for PtO/Pt(OH)₂ and for Pt⁰. Let us first consider what happens when PtO (or Pt(OH)₂) is deposited on these steps (Figure 7.6a). In this case, the PtO particles will start to block both the tips and the grooves of the steps, preventing the adsorption of respectively oxygen and propane. The electrons normally used at the tips have nowhere to go. The only possible pathway is recombination with holes. Blocking of the grooves by the metal oxide particles will prevent holes from being used for propane oxidation. Even when there is some surface left for the oxidation of propane, the holes will be forced to recombine with the electrons and therefore hardly any photocatalytic activity will be observed.

The mechanism becomes different when metallic Pt is present rather than PtO/Pt(OH)₂ (Figure 7.6b). Now, the electrons can migrate into the cocatalytic nanoparticles, and (multi-electron induced) oxygen activation can take place at the surface of the Pt particles. Still, the particles are blocking grooves, and thus blocking sites where normally propane adsorption and oxidation could take place. There will still be some sites left however for propane to adsorb upon. As the holes will now

not be forced to recombine with electrons, they can be used for the oxidation of propane (possibly via hydroxyls). Thus, photocatalytic activity will be observed, all be it lower than when no Pt is present.

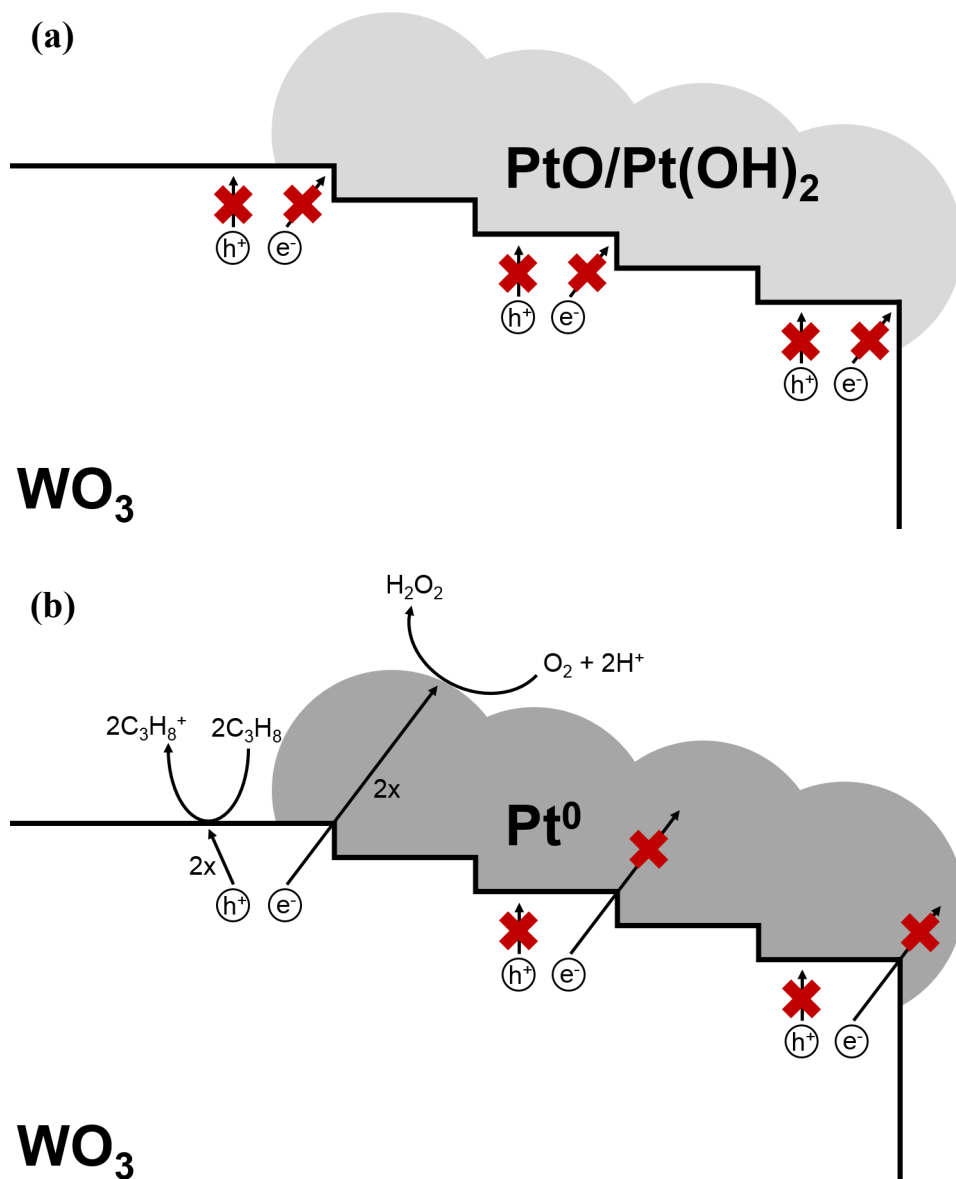


Figure 7.6. Schematic of propane oxidation at the edge of (a) a PtO/Pt(OH)_2 -loaded WO_3 nanoplate and (b) a Pt^0 -loaded WO_3 nanoplate.

A question which remains unanswered until now is why Pt/WO₃-200 slowly becomes more photocatalytically active over multiple runs, but ‘resets’ itself to lower activity values when the sample is not used in a photocatalytic experiment for some time. A possible explanation might be that propane adsorption sites are initially blocked by another compound, and that this compound is slowly removed over multiple photocatalytic runs. However, when the sample is not used for some time, this particular compound adsorbs once more on the propane oxidation sites. The only possible compound which could fulfill these requirements is water. To some extent, water vapor is present inside the gas flows used in the reaction cell. This water will adsorb on sites where propane oxidation could occur as well. There, the water needs to be oxidized to hydroxyl radicals first. As the hydroxyl radicals can react with propane adsorbed nearby, slowly more sites will become available where propane adsorption can take place, and thus the photocatalytic activity will increase. When the photocatalytic measurements stop and the remaining propane will desorb from their sites on WO₃, water will slowly adsorb again on these sites. This hypothesis is strengthened by our observations when flushing with either nitrogen or nitrogen and oxygen takes place between two measurements (Figure 7.4). In both gas flows, water vapor must have been present, which must have adsorbed on the WO₃, resetting the activity values of the WO₃ nanoplates.

If water vapor is present on the surface and oxidation of it might open up sites for propane to adsorb upon, we hypothesize that pre-illumination should have an effect on the activation behavior of WO₃ as well. We observe in Figure 7.4 that when 24 hours of flushing with N₂ or a combination of N₂ and O₂ is followed by 3 hours of LED illumination, the deactivation of the WO₃ takes place as well. However, now the WO₃ activates much faster and reaches its steady state value already after 3 photocatalytic runs. It seems that pre-illumination has a very beneficial effect on activating the WO₃. A possible explanation might be that hydroxyl radicals have formed during the pre-illumination on the surface. These hydroxyl species are still blocking sites where propane adsorption normally can take place. However, due to the reactive nature of the radicals, they can easily react with propane adsorbed nearby, and thus ‘cleaning’ of the surface occurs fast. Without illumination, this cleaning will take considerably longer as there will be no reactive hydroxyl radicals yet: the water first needs to be oxidized before this occurs.

To perform oxidation of water vapor to hydroxyl radicals, a corresponding reduction reaction is required as well, which would normally be the reduction of oxygen. Remarkably, the faster reactivation also occurs when flushing takes place in the absence of oxygen in the pre-illumination studies. An explanation could be that the

reactor itself is not 100% air-tight, leading to mild diffusion of oxygen inside the reactor. Indeed, when we monitor the photocatalytic activity as a function of oxygen concentration, we observe photocatalytic activity even at very low amounts of oxygen (Figure A7.2). Another possibility might be that the tungsten oxide is reducing itself during the photocatalysis measurements. Future Raman studies will be required to verify this.

7.4 Conclusions

We have studied the photodeposition of platinum on WO_3 nanoplates, the latter being synthesized by microwave hydrothermal synthesis at temperatures of 150 °C, 200 °C and 250 °C. Considerably less Pt has been deposited on the WO_3 -150 surface than on the WO_3 -200 and WO_3 -250 surfaces, which can be ascribed to a lower photocatalytic activity of WO_3 -150 due to hydrate groups being present. For Pt/ WO_3 -200 and Pt/ WO_3 -250, structure-directed photodeposition occurs, as we have observed previously in Chapter 6.^[34] Drastic differences are observed in the oxidation state of as-deposited Pt: the dominant oxidation state for Pt/ WO_3 -150 and surprisingly Pt/ WO_3 -250 is Pt^{II} , whereas the dominant oxidation state of Pt/ WO_3 -200 is Pt^0 . The presence of Pt^{II} in the form of either PtO or $\text{Pt}(\text{OH})_2$ turns out to destroy the propane photo-oxidation capabilities of the WO_3 nanoplates, likely because the platinum particles are blocking both oxidation and reduction sites. The presence of Pt^0 also has a negative effect on WO_3 -200, but not as drastic as PtO/ $\text{Pt}(\text{OH})_2$ for Pt/ WO_3 -150 and Pt/ WO_3 -250. Contrary to PtO/ $\text{Pt}(\text{OH})_2$, Pt^0 serves as reduction cocatalyst, providing sufficient reduction sites. However, the Pt will still block oxidation sites, causing the lower activity. Over multiple photocatalysis runs, Pt/ WO_3 -200 becomes more active. This is attributed to the remaining sites suited for propane oxidation being poisoned by water. When illumination starts, the water is oxidized, creating hydroxyl radicals. These hydroxyl radicals can react with propane adsorbed nearby. Hence, ‘cleaning’ of sites where water is adsorbed will occur and more sites will become available for the propane to adsorb upon. The speed of this cleaning process can be intensified by employing pre-illumination of the sample. When the sample is not exposed to illumination, re-poisoning by water might occur once more, ‘resetting’ the activity of Pt/ WO_3 -200 to lower values. The results in this chapter make clear that no beneficial effect in photocatalytic propane oxidation has been observed in the structure-directed photodeposition of Pt on WO_3 nanoplates, opposed to common believe that this should lead to increased activities.

7.5 Bibliography

- [1] Zhao, J.; Yang, X.; *Photocatalytic oxidation for indoor air purification: a literature review*. Building and Environment **2003**, 38, 645-654.
- [2] Mo, J.; Zhang, Y.; Xu, Q.; Lamson, J. J.; Zhao, R.; *Photocatalytic purification of volatile organic compounds in indoor air: a literature review*. Atmospheric Environment **2009**, 43, 2229-2246.
- [3] Tseng, T. K.; Lin, Y. S.; Chen, Y. J.; Chu, H.; *A review of photocatalysts prepared by sol-gel method for VOCs removal*. International Journal of Molecular Sciences **2010**, 11, 2336-2361.
- [4] Zheng, H.; Ou, J. Z.; Strano, M. S.; Kaner, R. B.; Mitchell, A.; Kalantar-Zadeh, K.; *Nanostructured tungsten oxide - properties, synthesis, and applications*. Advanced Functional Materials **2011**, 21, 2175-2196.
- [5] Huang, Z. F.; Song, J.; Pan, L.; Zhang, X.; Wang, L.; Zou, J. J.; *Tungsten oxides for photocatalysis, electrochemistry, and phototherapy*. Advanced Materials **2015**, 27, 5309-5327.
- [6] Kumar, S. G.; Rao, K. S. R. K.; *Tungsten-based nanomaterials (WO_3 & Bi_2WO_6): modifications related to charge carrier transfer mechanisms and photocatalytic applications*. Applied Surface Science **2015**, 355, 939-958.
- [7] Xie, Y. P.; Liu, G.; Yin, L.; Cheng, H. M.; *Crystal facet-dependent photocatalytic oxidation and reduction reactivity of monoclinic WO_3 for solar energy conversion*. Journal of Materials Chemistry **2012**, 22, 6746-6751.
- [8] Amano, F.; Ishinaga, E.; Yamakata, A.; *Effect of particle size on the photocatalytic activity of WO_3 particles for water oxidation*. Journal of Physical Chemistry C **2013**, 117, 22584-22590.
- [9] Xin, G.; Guo, W.; Ma, T.; *Effect of annealing temperature on the photocatalytic activity of WO_3 for O_2 evolution*. Applied Surface Science **2009**, 256, 165-169.
- [10] Kato, H.; Hori, M.; Konta, R.; Shimodaira, Y.; Kudo, A.; *Construction of Z-scheme type heterogeneous photocatalysis systems for water splitting into H_2 and O_2 under visible light irradiation*. Chemistry Letters **2004**, 33, 1348-1349.
- [11] Sánchez-Martínez, D.; Martínez-De La Cruz, A.; López-Cuéllar, E.; *Synthesis of WO_3 nanoparticles by citric acid-assisted precipitation and evaluation of their photocatalytic properties*. Materials Research Bulletin **2013**, 48, 691-697.
- [12] Hernandez-Uresti, D. B.; Sánchez-Martínez, D.; Martínez-De La Cruz, A.; Sepúlveda-Guzmán, S.; Torres-Martínez, L. M.; *Characterization and photocatalytic properties of hexagonal and monoclinic WO_3 prepared via microwave-assisted hydrothermal synthesis*. Ceramics International **2014**, 40, 4767-4775.
- [13] Arai, T.; Yanagida, M.; Konishi, Y.; Ikura, A.; Iwasaki, Y.; Sugihara, H.; Sayama, K.; *The enhancement of WO_3 -catalyzed photodegradation of*

- organic substances utilizing the redox cycle of copper ions*. Applied Catalysis B: Environmental **2008**, 84, 42-47.
- [14] Hayat, K.; Gondal, M. A.; Khaled, M. M.; Yamani, Z. H.; Ahmed, S.; *Laser induced photocatalytic degradation of hazardous dye (Safranin-O) using self synthesized nanocrystalline WO₃*. Journal of Hazardous Materials **2011**, 186, 1226-1233.
- [15] Ma, S. S. K.; Maeda, K.; Abe, R.; Domen, K.; *Visible-light-driven nonsacrificial water oxidation over tungsten trioxide powder modified with two different cocatalysts*. Energy and Environmental Science **2012**, 5, 8390-8397.
- [16] Sayama, K.; Mukasa, K.; Abe, R.; Abe, Y.; Arakawa, H.; *A new photocatalytic water splitting system under visible light irradiation mimicking a Z-scheme mechanism in photosynthesis*. Journal of Photochemistry and Photobiology A: Chemistry **2002**, 148, 71-77.
- [17] Abe, R.; Takami, H.; Murakami, N.; Ohtani, B.; *Pristine simple oxides as visible light driven photocatalysts: highly efficient decomposition of organic compounds over platinum-loaded tungsten oxide*. Journal of the American Chemical Society **2008**, 130, 7780-7781.
- [18] Kim, J.; Lee, C. W.; Choi, W.; *Platinized WO₃ as an environmental photocatalyst that generates OH radicals under visible light*. Environmental Science and Technology **2010**, 44, 6849-6854.
- [19] Tomita, O.; Abe, R.; Ohtani, B.; *Direct synthesis of phenol from benzene over platinum-loaded tungsten(VI) oxide photocatalysts with water and molecular oxygen*. Chemistry Letters **2011**, 40, 1405-1407.
- [20] Tomita, O.; Ohtani, B.; Abe, R.; *Highly selective phenol production from benzene on a platinum-loaded tungsten oxide photocatalyst with water and molecular oxygen: selective oxidation of water by holes for generating hydroxyl radical as the predominant source of the hydroxyl group*. Catalysis Science and Technology **2014**, 4, 3850-3860.
- [21] Shiraishi, Y.; Sugano, Y.; Ichikawa, S.; Hirai, T.; *Visible light-induced partial oxidation of cyclohexane on WO₃ loaded with Pt nanoparticles*. Catalysis Science and Technology **2012**, 2, 400-405.
- [22] Chen, D.; Ye, J.; *Hierarchical WO₃ hollow shells: dendrite, sphere, dumbbell, and their photocatalytic properties*. Advanced Functional Materials **2008**, 18, 1922-1928.
- [23] Miyauchi, M.; Nukui, Y.; Atarashi, D.; Sakai, E.; *Selective growth of n-type nanoparticles on p-type semiconductors for Z-scheme photocatalysis*. ACS Applied Materials and Interfaces **2013**, 5, 9770-9776.
- [24] Sayama, K.; Hayashi, H.; Arai, T.; Yanagida, M.; Gunji, T.; Sugihara, H.; *Highly active WO₃ semiconductor photocatalyst prepared from amorphous peroxy-tungstic acid for the degradation of various organic compounds*. Applied Catalysis B: Environmental **2010**, 94, 150-157.

- [25] Arai, T.; Horiguchi, M.; Yanagida, M.; Gunji, T.; Sugihara, H.; Sayama, K.; *Reaction mechanism and activity of WO₃-catalyzed photodegradation of organic substances promoted by a CuO cocatalyst*. Journal of Physical Chemistry C **2009**, 113, 6602-6609.
- [26] Gunji, T.; Tsuda, T.; Jeevagan, A. J.; Hashimoto, M.; Tanabe, T.; Kaneko, S.; Miyauchi, M.; Saravanan, G.; Abe, H.; Matsumoto, F.; *Visible light induced decomposition of organic compounds on WO₃ loaded PtPb co-catalysts*. Catalysis Communications **2014**, 56, 96-100.
- [27] Zhao, Z. G.; Miyauchi, M.; *Shape modulation of tungstic acid and tungsten oxide hollow structures*. Journal of Physical Chemistry C **2009**, 113, 6539-6546.
- [28] Arai, T.; Yanagida, M.; Konishi, Y.; Iwasaki, Y.; Sugihara, H.; Sayama, K.; *Promotion effect of CuO co-catalyst on WO₃-catalyzed photodegradation of organic substances*. Catalysis Communications **2008**, 9, 1254-1258.
- [29] Wicaksana, Y.; Liu, S.; Scott, J.; Amal, R.; *Tungsten trioxide as a visible light photocatalyst for volatile organic carbon removal*. Molecules **2014**, 19, 17747-17762.
- [30] Romão, J. S.; Hamdy, M. S.; Mul, G.; Baltrusaitis, J.; *Photocatalytic decomposition of cortisone acetate in aqueous solution*. Journal of Hazardous Materials **2015**, 282, 208-215.
- [31] Fraters, B. D.; Amrollahi, R.; Mul, G.; *How Pt nanoparticles affect TiO₂-induced gas-phase photocatalytic oxidation reactions*. Journal of Catalysis **2015**, 324, 119-126.
- [32] Chanjuan, X.; Zhengshi, C.; Qinglin, L.; Zhensheng, J.; *Effects of H⁺, Cl⁻ and CH₃COOH on the photocatalytic conversion of PtCl₆²⁻ in aqueous TiO₂ dispersion*. Journal of Photochemistry and Photobiology, A: Chemistry **1995**, 87, 249-255.
- [33] Jin, Z.; Chen, Z.; Li, Q.; Xi, C.; Zheng, X.; *On the conditions and mechanism of PtO₂ formation in the photoinduced conversion of H₂PtCl₆*. Journal of Photochemistry and Photobiology, A: Chemistry **1994**, 81, 177-182.
- [34] Wenderich, K.; Klaassen, A.; Siretanu, I.; Mugele, F.; Mul, G.; *Sorption-determined deposition of platinum on well-defined platelike WO₃*. Angewandte Chemie - International Edition **2014**, 53, 12476-12479.
- [35] Li, R.; Zhang, F.; Wang, D.; Yang, J.; Li, M.; Zhu, J.; Zhou, X.; Han, H.; Li, C.; *Spatial separation of photogenerated electrons and holes among {010} and {110} crystal facets of BiVO₄*. Nature Communications **2013**, 4.
- [36] Li, R.; Han, H.; Zhang, F.; Wang, D.; Li, C.; *Highly efficient photocatalysts constructed by rational assembly of dual-cocatalysts separately on different facets of BiVO₄*. Energy and Environmental Science **2014**, 7, 1369-1376.
- [37] Kato, H.; Asakura, K.; Kudo, A.; *Highly efficient water splitting into H₂ and O₂ over lanthanum-doped NaTaO₃ photocatalysts with high crystallinity and surface nanostructure*. Journal of the American Chemical Society **2003**, 125, 3082-3089.

7.6 Appendix

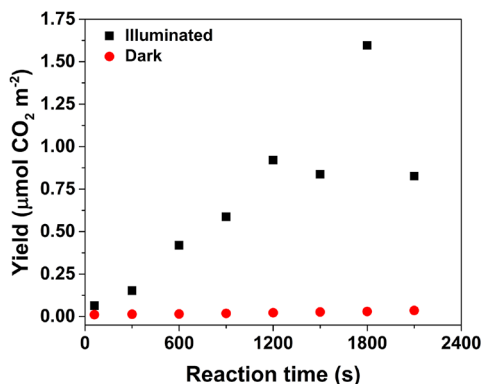


Figure A7.1. Photocatalytic CO₂ production yields from propane oxidation over Pt/WO₃-200 using different illumination times. The measurements correspond with sample 1, cycle 1, as depicted in Figure 7.3b, and have been measured at random. Due to the activation nature of Pt/WO₃-200, a large error is observed at higher reaction times, making comparison of the data difficult.

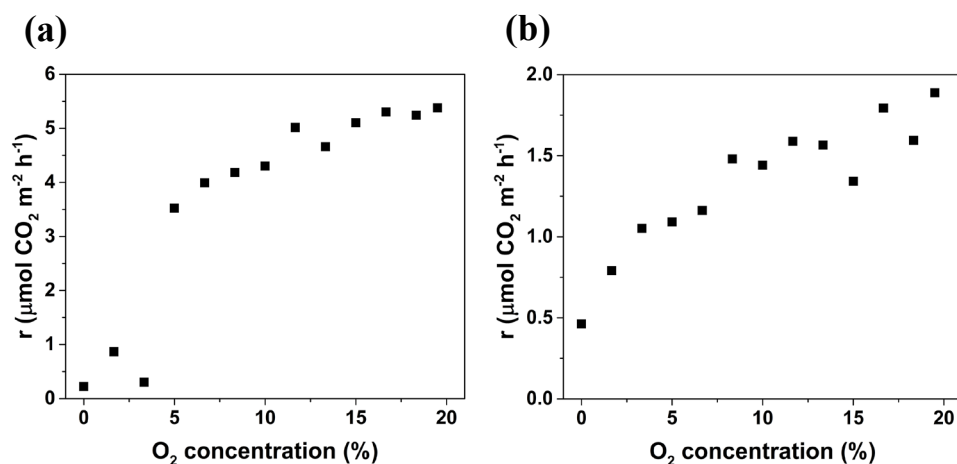


Figure A7.2. Photocatalytic CO₂ production rates from propane oxidation over (a) WO₃-200 and (b) Pt/WO₃-200 using different oxygen concentrations. Both measurements were preceded by a set of multiple runs to achieve a steady state in the amount of CO₂ formed per run. Remarkably, increasing O₂ concentration above the saturation point (2.5% O₂) still results in an increase in photocatalytic activity.

Chapter 8

Outlook

In this thesis, three concepts have been discussed in detail: crystal facet engineering of plate-like tungsten oxide (WO_3), photodeposition of platinum (Pt) on commercial WO_3 and finally structure-directed photodeposition of Pt on the WO_3 nanoplates. In this chapter, I will briefly reflect on the research performed and discuss how as-obtained results can be used in future applications.

8.1 Crystal facet engineering

8.1.1 Crystal facet engineering of WO_3 nanoplates

A large part of the work performed in this thesis has been devoted to engineering monoclinic WO_3 nanoplates with a dominant $\{002\}$ facet. In literature it has been discussed that the presence of the $\{002\}$ facet could be beneficial for specific photocatalytic applications, as this facet will exhibit the highest surface energy of the low-index WO_3 facets.^[1-3] However, the results of experiments discussed in Chapter 6 imply that the photoreduction of platinum is actually occurring on the edges/small facets of the WO_3 nanoplates due to sorption effects. In Chapter 7 it was also implied that for the photo-oxidation of propane, both photocatalytic reduction and oxidation reactions are occurring at the edges of the WO_3 nanoplates. In other words, the photocatalytic reactions seem to be occurring on defects of the plate-like WO_3 . For a WO_3 particle exhibiting low-index facets, it could of course be that the $\{002\}$ facet has the highest surface energy and therefore can theoretically exhibit the most reductive power. However, if chemical compounds such as oxygen are not even able to adsorb on these facets, no reduction can take place at all. In such a case, continuation of engineering WO_3 particles with a dominant exposure of the $\{002\}$ facet does not make sense. In Chapter 3 we have also observed that the WO_3 nanoplates have a considerably lower activity than commercial WO_3 in photocatalytic Orange II sodium salt degradation, raising once more the question if the dominant presence of the $\{002\}$ facet is beneficial for WO_3 at all.

To confirm once and for all whether the presence of $\{002\}$ facets is beneficial or not, studies in photocatalytic propane oxidation described in this thesis should be expanded by comparing the photocatalytic activities of WO_3 nanoplates with commercial WO_3 . Also, it could be very rewarding to perform *in situ* studies to verify the events happening at the different crystal surfaces in various photocatalytic activity measurements. Examples of techniques which can be used are Raman spectroscopy, Fourier transform infrared spectroscopy (FTIR) and atomic force microscopy (AFM).

8.1.2 Crystal facet engineering on a broader perspective

Although no huge beneficial advantage of synthesizing WO_3 nanoplates has been observed in this thesis, this does not mean that the field of crystal facet engineering in general should be given up. Results have been promising for e.g. TiO_2 ^[4-6] and BiVO_4 ,^[7, 8] and even for WO_3 it has been demonstrated that the synthesis of high-index facets could be rewarding as well.^[1] However, it should always be kept in mind that no matter how high the reductive power of a facet is, it should be able to provide sufficient sites for chemical compounds to adsorb upon. I strongly suggest that crystal facet engineering studies are expanded with the earlier mentioned *in situ* studies to get a complete picture on the role of facets in photocatalysis.

8.2 Photodeposition

8.2.1 Photodeposition of platinum on WO_3

As discussed in Chapter 2, multiple studies have demonstrated the importance of photodepositing platinum on tungsten oxide, which will result in increased photocatalytic activities. Therefore it is surprising that the amount of fundamental research done in this field is very limited. We have discussed that properties such as dispersion, particle size and oxidation state of cocatalytic nanoparticles deposited on a semiconductor can be controlled by changing photodeposition parameters, such as the pH or the sacrificial agent used. To the best of our knowledge, hardly any studies exist for Pt/WO_3 where such relationships are verified. There is still a broad spectrum left where research can be performed to find the optimal photodeposition conditions for platinum on WO_3 . Of course, studying the influence of pH will be difficult due to the instability of WO_3 at high pH values, but studying the role of for instance the type of sacrificial agent used, might still be very rewarding in controlling the particle size and dispersion of the Pt deposited.

8.2.2 Future usage of photodeposition

It is my firm believe that research on photodeposition should be continued. In its own way, the technique symbolizes how photocatalysis should be incorporated in commercial applications in the future: it is green and cheap. Properties such as oxidation state and size of the particles deposited can be easily controlled by varying the pH and the type of sacrificial agent used (if it is needed at all). Nevertheless, there is still room for improvement in photodeposition studies. One of the most important points is that the reduction cocatalysts used in photocatalysis are often very expensive noble metals, such as gold, silver and especially platinum.

Alternatives need to be found which can compete in performance with these cocatalysts. For instance, palladium could be a good alternative to investigate instead of platinum.^[9] Recently, a review paper of Ran and co-workers discussed in detail which earth-abundant cocatalysts could be used for photocatalytic water splitting.^[10] Although the focus of this review paper is not on photodeposition, it could still form a good basis for finding alternative cocatalysts. Aside from looking at different cocatalysts, photodeposition studies can be expanded by looking at *in situ* photodeposition.^[11-14] The advantage of this technique is that it can provide information on what chemical compounds are formed during the deposition process.

One final thing I would like to emphasize is that carefulness should be employed when different cocatalyst deposition methods are compared in literature. In what research has been published, the photocatalytic activities of such prepared materials are investigated. This leads authors to conclude that one of the deposition techniques is better suited to prepare highly active photocatalytic systems than the other deposition technique(s). This comparison is not always totally fair. Frequently no full characterization of the as-deposited cocatalytic particles is included, whereas the particles could be different in for example oxidation state or size. Before any conclusions may be drawn which technique is most suited to gain high photocatalytic activities, authors should be completely sure that the properties of as-deposited particles are (almost) identical.

8.3 Structure-directed photodeposition

In this thesis, we have studied structure-directed photodeposition of platinum on tungsten oxide. The favored positioning of platinum particles on the edges/subordinate facets of the WO_3 was attributed to sorption phenomena. Clearly adsorption can play a very large role in structure-directed photodeposition. The studies described here can be largely expanded by investigating if these adsorption phenomena also occur when the Pt precursor is cationic. Actually, we tried this already by employing $[\text{Pt}(\text{NH}_3)_4]^{2+}$ as a precursor. Alas, no Pt was photodeposited on the surface of the WO_3 in this case. Another option might be to perform photoreduction of another metal, where the metal precursor is cationic (such as Pd^{2+} in PdCl_2 ^[9]). Aside from photoreduction, also structure-directed photo-oxidation could be studied using the WO_3 nanoplates, preferably by using both cationic and anionic species. The influence of adsorption can be verified once more in such a case.

According to the theory of structure-directed photodeposition, reduction cocatalysts should be deposited at sites where electrons migrate to.^[8, 15, 16] It has been claimed that enhanced photocatalytic activities will be observed in such a case.^[8, 16] In Chapter 7 however, photodeposition of platinum on plate-like WO₃ turned out to be detrimental in photocatalytic propane oxidation, likely due to the platinum particles blocking oxidation sites. It would be interesting to see what happens if the amount of platinum deposited is decreased. The amount of blockage will decrease due to either less or smaller Pt particles being present on the WO₃ surface. There could be some sort of tipping point where the platinum will start to act beneficially instead of detrimentally. Aside from testing Pt/WO₃ nanoplates in photocatalytic propane oxidation, Pt-loaded commercial WO₃ should also be tested in this field. Here, it is expected that after photodeposition of Pt more than sufficient sites are still available for propane oxidation. Hence, an increase in photocatalytic activity is expected.

The possible presence of strong sorption phenomena of specific sites is something which needs to be taken into account by other researchers who study structure-directed photodeposition as well. When strong adsorption effects occur on specific locations of the photocatalyst, photodeposition cannot be used anymore as a probe to verify what the most reductive and oxidative sites are of the material. However, even when structure-directed photodeposition is the result of adsorption, this does not necessarily mean that no light-induced charge separation is present at all inside the photocatalytic material. To investigate if the latter phenomenon occurs, it might be useful to work with a technique where no photodeposition is required to probe charge separation inside a semiconductor crystal. Atomic force microscopy (AFM) might provide a solution here. In Chapter 6, we have looked at differences in intrinsic surface charge between different sites on WO₃ nanoplates. However, all AFM experiments were done in dark conditions. Continued AFM studies might provide answers if a difference in intrinsic surface charges will be observed when the plate-like WO₃ is exposed to illumination. One could hypothesize for instance that migration of electrons towards the edges could take place due to the presence of a positive charge, whereas the negative charge at the basal plane results in the attraction of holes. In such a case, one would expect to observe an increase in negativity at the edges and an increase in positivity at the basal plane.

I think photodeposition holds much promise in future applications of (photo)catalysis. Therefore, studies on photodeposition should be continued. Theoretically, structure-directed photodeposition could result in highly photocatalytic systems. However, the possible presence of sorption phenomena, both

in photodeposition and in subsequent testing of the newly obtained photocatalytic systems, should never be ignored.

8.4 Bibliography

- [1] Zheng, J. Y.; Haider, Z.; Van, T. K.; Pawar, A. U.; Kang, M. J.; Kim, C. W.; Kang, Y. S.; *Tuning of the crystal engineering and photoelectrochemical properties of crystalline tungsten oxide for optoelectronic device applications*. CrystEngComm **2015**, 17, 6070-6093.
- [2] Xie, Y. P.; Liu, G.; Yin, L.; Cheng, H. M.; *Crystal facet-dependent photocatalytic oxidation and reduction reactivity of monoclinic WO₃ for solar energy conversion*. Journal of Materials Chemistry **2012**, 22, 6746-6751.
- [3] Zheng, J. Y.; Song, G.; Hong, J.; Van, T. K.; Pawar, A. U.; Kim, D. Y.; Kim, C. W.; Haider, Z.; Kang, Y. S.; *Facile fabrication of WO₃ nanoplates thin films with dominant crystal facet of (002) for water splitting*. Crystal Growth and Design **2014**, 14, 6057-6066.
- [4] Liu, G.; Yu, J. C.; Lu, G. Q.; Cheng, H. M.; *Crystal facet engineering of semiconductor photocatalysts: motivations, advances and unique properties*. Chemical Communications **2011**, 47, 6763-6783.
- [5] Dozzi, M. V.; Selli, E.; *Specific facets-dominated anatase TiO₂: fluorine-mediated synthesis and photoactivity*. Catalysts **2013**, 3, 455-485.
- [6] Chen, W.; Kuang, Q.; Wang, Q.; Xie, Z.; *Engineering a high energy surface of anatase TiO₂ crystals towards enhanced performance for energy conversion and environmental applications*. RSC Advances **2015**, 5, 20396-20409.
- [7] Wang, D.; Jiang, H.; Zong, X.; Xu, Q.; Ma, Y.; Li, G.; Li, C.; *Crystal facet dependence of water oxidation on BiVO₄ sheets under visible light irradiation*. Chemistry - A European Journal **2011**, 17, 1275-1282.
- [8] Li, R.; Zhang, F.; Wang, D.; Yang, J.; Li, M.; Zhu, J.; Zhou, X.; Han, H.; Li, C.; *Spatial separation of photogenerated electrons and holes among {010} and {110} crystal facets of BiVO₄*. Nature Communications **2013**, 4.
- [9] Sakai, Y.; Shimanaka, A.; Shioi, M.; Kato, S.; Satokawa, S.; Kojima, T.; Yamasaki, A.; *Fabrication of high-sensitivity palladium loaded tungsten trioxide photocatalyst by photodeposit method*. Catalysis Today **2015**, 241, 2-7.
- [10] Ran, J.; Zhang, J.; Yu, J.; Jaroniec, M.; Qiao, S. Z.; *Earth-abundant cocatalysts for semiconductor-based photocatalytic water splitting*. Chemical Society Reviews **2014**, 43, 7787-7812.
- [11] Busser, G. W.; Mei, B.; Muhler, M.; *Optimizing the deposition of hydrogen evolution sites on suspended semiconductor particles using on-line photocatalytic reforming of aqueous methanol solutions*. ChemSusChem **2012**, 5, 2200-2206.

-
- [12] Rufus, I. B.; Viswanathan, B.; Ramakrishnan, V.; Kuriacose, J. C.; *Cadmium sulfide with iridium sulfide and platinum sulfide deposits as a photocatalyst for the decomposition of aqueous sulfide*. Journal of Photochemistry and Photobiology, A: Chemistry **1995**, 91, 63-66.
- [13] Chen, X.; Chen, W.; Gao, H.; Yang, Y.; Shangguan, W.; *In situ photodeposition of NiO_x on CdS for hydrogen production under visible light: enhanced activity by controlling solution environment*. Applied Catalysis B: Environmental **2014**, 152-153, 68-72.
- [14] Jiang, X.; Fu, X.; Zhang, L.; Meng, S.; Chen, S.; *Photocatalytic reforming of glycerol for H₂ evolution on Pt/TiO₂: fundamental understanding the effect of co-catalyst Pt and the Pt deposition route*. Journal of Materials Chemistry A **2015**, 3, 2271-2282.
- [15] Ohno, T.; Sarukawa, K.; Matsumura, M.; *Crystal faces of rutile and anatase TiO₂ particles and their roles in photocatalytic reactions*. New Journal of Chemistry **2002**, 26, 1167-1170.
- [16] Li, R.; Han, H.; Zhang, F.; Wang, D.; Li, C.; *Highly efficient photocatalysts constructed by rational assembly of dual-cocatalysts separately on different facets of BiVO₄*. Energy and Environmental Science **2014**, 7, 1369-1376.

Summary

In this thesis, structure-directed photodeposition of platinum (Pt) on tungsten oxide (WO_3) nanoplates is described, both considering fundamental aspects, as well as usefulness for applications in photocatalytic propane oxidation. Before such studies are described, the concepts of crystal facet engineering of WO_3 nanoplates and photodeposition of platinum on commercial WO_3 are explained. In **Chapter 1**, the most important theoretical concepts of the thesis are discussed. Most importantly, the promise of tungsten oxide, cocatalytic nanoparticles and crystal facet engineering in heterogeneous photocatalysis are dealt with.

A very detailed review on photodeposition is provided in **Chapter 2**. The concept of photodeposition is discussed, as well as why this technique can be considered promising. First, important studies in the photodeposition of several metals on titanium dioxide (TiO_2) are discussed (with an emphasis on platinum), as well as the photodeposition of silver (Ag) on zinc oxide (ZnO). It is demonstrated that photodeposition parameters such as pH, de-aeration or the presence of a sacrificial agent can play an important role in the photodeposition rate and the resulting size, dispersion and oxidation state of the nanoparticles deposited. Considering the scope of this thesis, a special emphasis in Chapter 2 is given on the literature available discussing photodeposition of Pt on WO_3 , although photodeposition of other materials on WO_3 is also touched upon. The concept of structure-directed photodeposition is then discussed in detail. This theory advocates that photoreduction of particles will mainly occur on the most reductive facet of a photocatalytic material, and photo-oxidation will mainly occur on the most oxidative facet. Ultimately, this concept can be exploited to obtain highly active photocatalytic systems. Finally, points for improvement in photodeposition studies are described in this chapter.

Descriptions of crystal facet engineering studies on WO_3 particles follow in subsequent chapters. In **Chapter 3**, the synthesis of WO_3 with plate-like morphology through a hydrothermal synthesis method is described. A solution containing sodium tungstate, hydrochloric acid and the capping agent citric acid was treated at temperatures of 120 °C and 170 °C in a sealed autoclave. The synthesis temperature turned out to be crucial for the phase composition of WO_3 : at 120 °C, both monoclinic WO_3 and orthorhombic $\text{WO}_3 \cdot \text{H}_2\text{O}$ were detected; at 170 °C, monoclinic WO_3 was the dominant crystal phase, although some $\text{WO}_3 \cdot 0.33\text{H}_2\text{O}$ was present as well. TGA experiments demonstrated that the hydrate in $\text{WO}_3 \cdot \text{H}_2\text{O}$ can be removed at temperatures in the range of 150-250 °C. After treatment at 250 °C, both samples were compared on morphology, surface area and photocatalytic (Fe^{3+} -assisted) dye

degradation. A hydrothermal synthesis temperature of 120 °C yields poorly defined particles, whereas synthesis at 170 °C results in well-defined WO₃ particles. The particles synthesized at 120 °C expose larger surface areas and show better photocatalytic activities in Fe³⁺-assisted Orange II sodium salt degradation, implying that the facets exposed on the well-defined WO₃ particles are not suited for Fe³⁺ adsorption. Furthermore, it is shown in this chapter that the presence of WO₃ · H₂O has a negative effect on photocatalytic activity.

To gain a better understanding of crystal phase transitions during the growth of monoclinic WO₃ nanoplates, additional hydrothermal synthesis experiments combined with *in situ* Raman spectroscopy were performed, as described in **Chapter 4**. The results imply that initially WO₃ · 2H₂O is formed when the tungstate solution is acidified to pH ≤ 1. When temperatures are elevated to 70 °C and 150 °C, transformation of WO₃ · 2H₂O to WO₃ · H₂O and of WO₃ · H₂O to monoclinic WO₃ takes place respectively. Withdrawal of samples from the autoclave during the hydrothermal synthesis allows additional analysis by X-ray diffraction. It is demonstrated that traces of WO₃ · 0.33H₂O are formed as well during the formation of monoclinic WO₃. Sample withdrawal also allows scanning electron microscopy analysis on the growth of well-defined WO₃ nanoplates over time. The studies in Chapter 4 were largely expanded by employing microwave-assisted hydrothermal synthesis, where the crystal structure and morphology of WO₃ were studied as a function of pH and synthesis temperature. It can be concluded that to induce the formation of monoclinic WO₃, the pH should be underneath a tipping point. The pH should at least be 1 or lower. The formation of hydrates inside the crystal lattice can be prevented when the temperature is sufficiently high. The samples synthesized at pH = 0.5 were investigated for i) Brunauer–Emmett–Teller surface area, ii) the amount of defects present and iii) photocatalytic activity in gaseous propane oxidation under visible light illumination. The most important conclusion of the latter studies is that the presence of WO₃ · H₂O is confirmed to be detrimental for the photocatalytic activity. The influence of the amount of defects does not seem to be prominent though.

Photodeposition studies of Pt on commercial WO₃ are described in **Chapter 5**. The influence of the sacrificial agent methanol was investigated in detail. The photodeposition kinetics as well as the oxidation state of platinum were carefully monitored after synthesis in the presence or absence of methanol. When methanol is used as an oxidation reagent, all platinum in the solution is deposited in a metallic state on the WO₃ surface, in the form of large clusters of particles. In the absence of

methanol, not all platinum can be deposited on the WO_3 . Platinum is then found on the surface as highly dispersed nanoparticles in an oxidized state. Remarkably, strong chemisorption effects are observed prior to illumination, especially when methanol is employed. The inability of WO_3 to reduce Pt to a metallic state in the absence of methanol is ascribed to favored back-oxidation of Pt^0 to Pt^{II} over water oxidation. The absence of full photodeposition is attributed to light-induced dissolution of the Pt^{II} species during photodeposition. Indeed, additional illumination experiments in a H_2SO_4 solution confirmed the instability of PtO/Pt(OH)_2 on the WO_3 surface. The Pt^{II} species can be converted to Pt^0 when hydrogenation is employed. Additional photodeposition experiments on such hydrogenated samples in the absence of methanol confirmed that back-oxidation of metallic Pt^0 species can occur, leading to a redistribution of Pt particles on the WO_3 surface. This back-oxidation is not observed when additional photodeposition takes place in the presence of methanol.

The results in Chapter 5 make clear that i) the dispersion and oxidation state of platinum photodeposited on tungsten oxide can be carefully controlled by the potential usage of methanol or, if needed, hydrogenation, and ii) that carefulness should be employed when Pt/WO_3 systems are used in photocatalysis. In the latter case, oxidation of Pt^0 might occur when this is the favored oxidation reaction as compared to the aimed photocatalytic oxidation process.

Structure-directed photodeposition studies of Pt on WO_3 nanoplates (as synthesized in Chapter 3) are described in **Chapter 6**. Pt particles are found on the edges/subordinate facets of the plate-like WO_3 . Additional impregnation and aqueous atomic force microscopy (AFM) studies demonstrated that this is likely due to sorption effects rather than light-induced charge separation. In the case of impregnation, Pt particles are found as well on the edges/small facets. An intrinsic positive charge is found along the edges when AFM is employed, whereas the basal plane exhibits a negative charge. It is concluded that the anionic Pt precursor $[\text{PtCl}_6]^{2-}$ must have adsorbed on the positive sites of the WO_3 nanoplates before being reduced.

After obtaining a fundamental understanding of structure-directed photodeposition of Pt on WO_3 nanoplates, the photocatalytic activity of such samples was finally tested in propane oxidation. This is described in **Chapter 7**. WO_3 samples were prepared through microwave-assisted hydrothermal synthesis, at a pH of 0.5 and temperatures of 150 °C, 200 °C and 250 °C, as described in Chapter 4. Again, the presence of hydrates in a WO_3 sample (synthesized at 150 °C) turned out to have

negative consequences in a photocatalytic process: considerably less Pt was photodeposited in such case. The Pt found on the surface was in a Pt^{II} state rather than in a Pt⁰ state. Surprisingly, Pt was also mainly present in a Pt^{II} state on WO₃ nanoplates synthesized at 250 °C, whereas Pt⁰ was the dominant state for plate-like WO₃ obtained at 200 °C. In photocatalytic propane oxidation, the presence of Pt, especially Pt^{II} species, has negative consequences for the activity. It is considered likely that the Pt particles are blocking both reduction and oxidation sites on the WO₃ nanoparticles. The cocatalytic Pt⁰ particles will still provide reduction sites though, and therefore some photocatalytic activity is still observed when Pt⁰ is the dominant oxidation state. PtO/Pt(OH)₂ particles do not exhibit these new reduction sites however, and hence a very low photocatalytic activity is observed when these particles are present. An interesting feature of the Pt⁰/WO₃ sample is that the sample becomes more active over multiple photocatalytic runs. This is attributed to water groups initially blocking propane oxidation sites. Illumination results ultimately in the removal of such water through photo-oxidation, creating hydroxyl radicals which can react with propane adsorbed nearby. This opens up more sites where propane adsorption and oxidation can take place. Indeed, it was demonstrated that pre-illumination of the Pt⁰/WO₃ sample prior to photocatalytic measurements results in faster activation kinetics than when no pre-illumination is employed. When the sample is left idle in the dark, ‘resetting’ of the activity of the Pt⁰/WO₃ takes place, likely due to re-adsorption of water on the propane oxidation sites. The results in Chapter 7 demonstrate that structure-directed photodeposition of Pt on WO₃ nanoplates does not have a beneficial effect on the activity in photocatalytic propane oxidation.

This thesis ends with an outlook described in **Chapter 8**. Results obtained in this thesis are briefly reflected upon and suggestions for future studies are provided based on those reflections.

Samenvatting

In dit proefschrift wordt structuurgerichte fotodepositie van platina (Pt) op wolframoxide (WO_3 -)nanoplaatjes beschreven, met het oog op zowel fundamentele aspecten als de bruikbaarheid voor toepassingen in fotokatalytische propaanoxidatie. Voordat zulke studies worden behandeld, worden de concepten van kristal facet ontwikkeling van WO_3 -nanoplaatjes en fotodepositie van platina op commerciële WO_3 uiteengezet. In **hoofdstuk 1** worden de belangrijkste theoretische concepten van het proefschrift beschreven, met uitzondering van fotodepositie. Onder andere de belofte van wolframoxide, co-katalytische nanodeeltjes en kristal facet structurering in heterogene fotokatalyse worden besproken.

Een zeer gedetailleerd literatuuroverzicht betreffende fotodepositie wordt verstrekt in **hoofdstuk 2**. Het begrip fotodepositie wordt besproken, evenals waarom deze techniek als veelbelovend kan worden beschouwd. Eerst worden belangrijke studies in de fotodepositie van verscheidene metalen op titaandioxide (TiO_2) besproken (met een nadruk op platina), evenals de fotodepositie van zilver (Ag) op zinkoxide (ZnO). Er wordt aangetoond dat fotodepositieparameters zoals pH, ontluchting of de aanwezigheid van een efficiënte electrondonor een belangrijke rol kunnen spelen in de fotodepositiesnelheid, en dien ten gevolge in de grootte, dispersie en oxidatietoestand van de afgezette nanodeeltjes. In het kader van dit proefschrift wordt in hoofdstuk 2 extra nadruk gelegd op het samenvatten van de beschikbare literatuur over de fotodepositie van Pt op WO_3 , hoewel fotodepositie van andere materialen op WO_3 ook wordt behandeld. Het begrip structuurgerichte fotodepositie wordt vervolgens uitvoerig besproken. Deze theorie pleit er voor dat fotoreductie van deeltjes voornamelijk zal plaatsvinden op het meest reducerende facet van een fotokatalytisch materiaal, en dat foto-oxidatie vooral zal plaatsvinden op het meest oxidatieve facet. Uiteindelijk kan dit concept benut worden om zeer actieve fotokatalytische systemen te krijgen. Tot slot worden punten voor verbetering in fotodepositie-onderzoek beschreven.

Na de theoretische uiteenzetting volgen beschrijvingen van de synthese van WO_3 -deeltjes met specifieke oppervlaktestructuur in **hoofdstuk 3**. De synthese van WO_3 met plaatachtige morfologie door middel van een hydrothermale synthesesmethode wordt beschreven. Daartoe werd een oplossing van natriumwolframaat, zoutzuur en het afdekkingsmiddel citroenzuur behandeld bij temperaturen van 120 °C en 170 °C in een afgesloten autoclaaf. De syntheses temperatuur bleek cruciaal te zijn voor de aanwezigheid van hydraten in WO_3 : bij 120 °C werden zowel monoklien WO_3 als orthorombisch $\text{WO}_3 \cdot \text{H}_2\text{O}$ gedetecteerd in het kristalrooster; bij 170 °C was monoklien WO_3 de dominante kristalfase, hoewel enige $\text{WO}_3 \cdot 0.33\text{H}_2\text{O}$ ook

aanwezig was. TGA experimenten toonden aan dat de hydraten in $\text{WO}_3 \cdot \text{H}_2\text{O}$ verwijderd kunnen worden bij temperaturen in het bereik van 150-250 °C. Na behandeling op 250 °C werden beide monsters vergeleken op morfologie, het specifieke oppervlak en fotokatalytische (Fe^{3+} -geassisteerde) kleurstofdegradatie. Een hydrothermale synthesesettemperatuur van 120 °C levert slecht gedefinieerde deeltjes op, maar synthese op 170 °C resulteert in goed gedefinieerde WO_3 -deeltjes. De deeltjes gesynthetiseerd bij 120 °C laten grotere specifieke oppervlaktes zien, net als betere fotokatalytische activiteiten in Fe^{3+} -geassisteerde Orange II natriumzoutdegradatie. Dit impliceert dat de op de goed gedefinieerde WO_3 -deeltjes geëxposeerde facetten niet geschikt zijn voor Fe^{3+} -adsorptie. Verder wordt in dit hoofdstuk aangetoond dat de aanwezigheid van $\text{WO}_3 \cdot \text{H}_2\text{O}$ een negatief effect heeft op de fotokatalytische activiteit.

Extra hydrothermale synthese-experimenten werden uitgevoerd in combinatie met *in situ* Ramanspectroscopie om een beter begrip te krijgen van kristalfase-overgangen tijdens de groei van monokliene WO_3 -nanoplaatjes. Dit wordt beschreven in **hoofdstuk 4**. De resultaten impliceren dat aanvankelijk $\text{WO}_3 \cdot 2\text{H}_2\text{O}$ wordt gevormd als de wolframaatoplossing wordt aangezuurd tot $\text{pH} \leq 1$. Transformatie van $\text{WO}_3 \cdot 2\text{H}_2\text{O}$ naar $\text{WO}_3 \cdot \text{H}_2\text{O}$ en van $\text{WO}_3 \cdot \text{H}_2\text{O}$ naar monoklien WO_3 vindt plaats als de temperaturen worden verhoogd naar respectievelijk 70 °C en 150 °C. Het nemen van monsters uit de autoclaaf tijdens de hydrothermale synthese maakt het uitvoeren van aanvullende röntgendiffractie-analyse mogelijk. Hiermee wordt aangetoond dat sporen van $\text{WO}_3 \cdot 0.33\text{H}_2\text{O}$ ook gevormd worden tijdens de formatie van monoklien WO_3 . Monsteropname maakt ook rasterelektronenmicroscopie-analyse van de groei van goed gedefinieerde WO_3 -nanoplaatjes in de loop van de tijd mogelijk. De studies in hoofdstuk 4 werden ruimschoots uitgebreid door de toepassing van microgolf-geassisteerde hydrothermale synthese. Hierbij werden de kristalstructuur en de morfologie van WO_3 bestudeerd als functie van pH en synthesesettemperatuur. Geconcludeerd kan worden dat voor de formatie van monoklien WO_3 , de pH onder een omslagpunt moet liggen. Hier dient de pH ten minste 1 of lager te zijn. De vorming van hydraten binnen het kristalrooster kan worden voorkomen wanneer de temperatuur voldoende hoog is. De monsters gesynthetiseerd bij $\text{pH} = 0,5$ werden onderzocht op het Brunauer-Emmett-Teller specifieke oppervlak, de hoeveelheid aanwezige defecten en de fotokatalytische activiteit in gasvormige propaanoxidatie onder zichtbaar licht. De belangrijkste conclusie van laatstgenoemde studies is dat de aanwezigheid van $\text{WO}_3 \cdot \text{H}_2\text{O}$ nadelig is voor de fotokatalytische activiteit. De invloed van de hoeveelheid defecten lijkt echter niet prominent te zijn.

Fotodepositiestudies van Pt op commerciële WO₃ worden beschreven in **hoofdstuk 5**. De invloed van de electrondonor methanol werd in detail onderzocht. Zowel de fotodepositiekinetiek als de oxidatietoestand van het platina werden zorgvuldig gevolgd in de aan- en afwezigheid van methanol. Al het platina in de oplossing wordt afgezet in een metallische toestand op het WO₃-oppervlak in de vorm van grote clusters van deeltjes als methanol wordt gebruikt. Bij afwezigheid van methanol kan niet alle platina afgezet worden op WO₃. Platina wordt dan gevonden op het oppervlak als zeer gedispergeerde nanodeeltjes in een geoxideerde toestand. Opmerkelijk genoeg worden sterke chemisorptie-effecten van de [PtCl₆]²⁻-precursor waargenomen voordat belichting begint, vooral wanneer methanol wordt gebruikt. Het onvermogen van WO₃ om Pt te reduceren naar een metallische toestand bij afwezigheid van methanol wordt toegeschreven aan een terugoxidatie van Pt⁰ naar Pt^{II}, wat een eenvoudigere oxidatiereactie is dan de oxidatie van water. Het ontbreken van volledige fotodepositie wordt toegeschreven aan het lichtgeïnduceerde oplossen van Pt^{II}-oxides tijdens fotodepositie. Extra illuminatie-experimenten in een H₂SO₄-oplossing bevestigden de instabiliteit van PtO/Pt(OH)₂ op het WO₃-oppervlak. De Pt^{II}-oxides kunnen worden omgezet naar Pt⁰ wanneer hydrogenatie wordt toegepast. Extra fotodepositie-experimenten op zulke gehydrogeneerde monsters in de afwezigheid van methanol bevestigden dat terugoxidatie van metallische Pt⁰-soorten kan plaatsvinden. Dit leidt tot een herverdeling van Pt-deeltjes op het WO₃-oppervlak. Deze terugoxidatie wordt niet waargenomen als aanvullende fotodepositie plaatsvindt in de aanwezigheid van methanol.

De resultaten in hoofdstuk 5 maken duidelijk dat i) de dispersie en oxidatietoestand van foto-afgezet platina op wolframoxide nauwkeurig kan worden geregeld door het mogelijke gebruik van methanol of, indien nodig, hydrogenatie en ii) dat zorgvuldigheid moet worden toegepast wanneer Pt/WO₃-systemen gebruikt worden in fotokatalyse. In het laatste geval kan oxidatie van Pt⁰ optreden wanneer dit de preferente oxidatiereactie is in vergelijking met het fotokatalytische oxidatieproces.

Structuurgerichte fotodepositiestudies van Pt op WO₃-nanoplaatjes (zoals gesynthetiseerd in hoofdstuk 3) worden beschreven in **hoofdstuk 6**. Pt-deeltjes worden aangetroffen op de randen/ondergeschikte facetten van het plaatachtige WO₃. Extra impregnatie en waterige atoomkrachtmicroscopie (AFM) studies toonden aan dat dit waarschijnlijk het gevolg is van adsorptie-effecten in plaats van lichtgeïnduceerde ladingsscheiding. Ook bij impregnatie worden Pt-deeltjes op de randen/kleine facetten gevonden. Een intrinsiek positieve lading wordt gevonden langs de randen wanneer AFM wordt toegepast, terwijl het basisvlak een negatieve

lading vertoont. Geconcludeerd wordt dat de anionische Pt-precursor $[\text{PtCl}_6]^{2-}$ op de positieve plaatsen van de WO_3 -nanoplaatjes geadsorbeerd moet zijn voordat fotongeïnduceerde reductie plaatsvindt.

Na het verkrijgen van een fundamenteel begrip van structuurgerichte fotodepositie van Pt op WO_3 -nanoplaatjes werd de fotokatalytische activiteit van zulke monsters uiteindelijk getest in propaanoxidatie. Dit wordt beschreven in **hoofdstuk 7**. De hier toegepaste WO_3 -monsters werden bereid door middel van microgolf-geassisteerde hydrothermale synthese, zoals beschreven in hoofdstuk 4 bij een pH van 0,5 en een temperatuur van 150 °C, 200 °C en 250 °C. Opnieuw bleek de aanwezigheid van hydraten in een WO_3 -monster (gesynthetiseerd op 150 °C) negatieve gevolgen te hebben op een fotokatalytisch proces: aanzienlijk minder Pt was afgezet op dit substraat. Pt op het oppervlak was in een Pt^{II} -toestand in plaats van in een Pt^0 -toestand. Verrassend genoeg was Pt ook voornamelijk aanwezig in een Pt^{II} -toestand op WO_3 -nanoplaatjes gesynthetiseerd bij 250 °C, terwijl Pt^0 de dominante toestand was voor plaatvormige WO_3 verkregen bij 200 °C. In fotokatalytische propaanoxidatie heeft de aanwezigheid van Pt, en vooral Pt^{II} -oxides, negatieve gevolgen voor de activiteit. Het wordt waarschijnlijk geacht dat de Pt-deeltjes zowel reductie- als oxidatieplekken op de WO_3 -nanodeeltjes blokkeren. De co-katalytische Pt^0 -deeltjes zullen echter nog steeds reductieactiviteit bieden. Daarom wordt enige fotokatalytische activiteit nog steeds waargenomen als Pt^0 de dominante oxidatietoestand is. $\text{PtO}/\text{Pt}(\text{OH})_2$ -deeltjes hebben deze nieuwe reductieplekken echter niet en dus wordt een zeer lage fotokatalytische activiteit geobserveerd wanneer deze deeltjes aanwezig zijn. Een interessante eigenschap van het Pt^0/WO_3 -monster is dat het monster actiever wordt gedurende meerdere fotokatalytische runs. Dit wordt toegeschreven aan watergroepen die aanvankelijk propaanoxidatieplekken blokkeren. Belichting resulteert uiteindelijk in de verwijdering van dit water door middel van foto-oxidatie. Hierdoor worden hydroxylradicalen gecreëerd die kunnen reageren met nabij geadsorbeerd propaan. Als gevolg hiervan komen meer plekken beschikbaar waar propaanadsorptie en -oxidatie kan plaatsvinden. Er werd aangetoond dat pre-illuminatie van het Pt^0/WO_3 -monster voor de fotokatalytische metingen resulteert in snellere activeringskinetiek dan wanneer er geen pre-illuminatie wordt toegepast. Wanneer het monster een tijd ongebruikt in het donker wordt achtergelaten, is de activiteit vergelijkbaar met ongebruikt Pt^0/WO_3 , waarschijnlijk door readsorptie van water op de propaanoxidatieplekken. De resultaten in hoofdstuk 7 demonstreren dat structuurgerichte fotodepositie van Pt op WO_3 -nanoplaatjes geen gunstig effect heeft op de activiteit in fotokatalytische propaanoxidatie.

Dit proefschrift wordt afgesloten met een vooruitblik beschreven in **hoofdstuk 8**. De resultaten verkregen in dit proefschrift worden kort geëvalueerd en suggesties voor toekomstige studies worden verstrekt op basis van deze evaluatie.

Acknowledgements

De afgelopen vier jaar heb ik met bijzonder veel plezier gewerkt in de Photocatalytic Synthesis Group aan mijn PhD project. Voor mij stond de promotie centraal voor fascinerende wetenschap en erg leuke mensen om mee samen te werken. Ik wil alle mensen bedanken die op de een of andere manier bijgedragen hebben aan dit positieve gevoel. Allereerst wil ik beginnen met mensen in de vakgroep te bedanken. Ik heb veel mensen zien komen en gaan, maar iedereen heeft wel op een manier een impressie op me achtergelaten. Michel, kletsen met jou was altijd erg gezellig, zowel binnen als buiten werktijd. Ook nu nog drink ik wel eens een biertje met jou en je partner Carola, wat ik er graag in zou willen houden! Bindikt, ook jij heel erg bedankt voor de vele leuke gesprekken die we gevoerd hebben. Toen jij de vakgroep verliet werd het een stuk stiller. Kai, we have been desk mates for only a short time, but that time was great! I could have a lot of fun with you, and I am very thankful for that. Another person with whom I could share many funny moments was Recep. Thank you for that! Alexander, danke für unsere Gespräche um Deutsch und Niederländisch zu lernen. Sie brachten sehr viel Spaß. Om dan maar naar het Nederlands over te schakelen: ook wil ik je van harte bedanken voor je hulp bij het ontwerpen van de voorkant. Joana, thank you for introducing our group to Portugese culture and wine. I really enjoyed travelling to Portugal and attending your wedding. Sun-Young, I will always remember the happiness you brought to the lab and the trip to Korea. Thanks! Rezvaneh, thank you for giving me good advice on several things during the PhD, as well as sharing Iranian culture with us. Vera, Robert and Ronald, I am sure you can carry on the good atmosphere in the group for the next four years: you have convinced me of that. Yuxi and Alexandre, although you are here for only a year, it is really nice to have met you. Zheng, Khalid, Ajin, Marcel, Rafal, Xenia, Hamdy, Jan-Niklas, Nesha, Mehrzad, Jonas, Yang, Chieh-Chao, Engin, Rob, Yi, Yan, Hendra, Gideon, Vic, Xiaolin and also all the bachelor students I have seen during my PhD: you all contributed one way or another to bringing my PhD to a fruitful end, be it with scientific explanations or just coziness, which I am grateful for.

Tijdens een PhD is één van de verantwoordelijkheden het begeleiden van bachelor studenten. Ook ik heb er in totaal vier mogen begeleiden. Edo, door jouw harde werklust en enthousiasme was het erg leuk om met jou te kijken naar kobalt-wolframaten. Shinwoo, in a continuation of Edo's work, you looked at photocatalytic activities of different tungstates. It was fun to work with you as well. In een totaal ander soort project heb jij, Joep, gekeken naar het coaten van fotokatalysatoren op plafondplaatjes. Het was fascinerend om te zien hoe je dit project zelfstandig en enthousiast naar een goed einde hebt weten te brengen. Het zal je vast deugd doen

om te lezen dat dit een veld is waar meer onderzoek in plaats gaat vinden binnen PCS. Bob, op het moment dat ik dit schrijf moet jij nog beginnen met je bachelor-opdracht en op het moment dat ik dit proefschrift verdedig ben jij nog druk bezig met je eigen project. Jij gaat verder waar Joep gebleven was met het onderzoeken van fotokatalytische coatings op plafondplaten. Ik heb er alle vertrouwen in dat dit leuke resultaten gaat opleveren! Naast deze bachelor-studenten heb ik ook nog samengewerkt met Lars en Ruben. Lars, jij bent begonnen met kijken naar de fundamentele aspecten van fotodepositie. Daarmee heb je eigenlijk de eerste opzet gegeven van een onderzoek waar uiteindelijk hoofdstuk 5 uit kwam rollen. Ruben, door een tijdje het synthetiseren van WO₃ nanoplaatjes over te nemen heb je voor mij de handen vrijgemaakt om andere dingen te kunnen doen.

De laatste mensen binnen mijn vakgroep die ik wil bedanken zijn de drie personen die aan de basis stonden van alles wat mogelijk was tijdens mijn promotietraject. Allereerst wil ik jou van harte bedanken, Lidy. Niet alleen ben je simpelweg een fantastische secretaresse, ook jouw vaardigheden in het organiseren van conferenties, het helpen met allerlei aspecten (groot of klein), je harde werklust en toch parallel tijd hebben voor sociaal leuke zaken zijn bewonderenswaardig. Je brengt vaak structurering waar nodig en je weet altijd de juiste weg te vinden in het netwerk van bureaucratie indien er iets moet gebeuren. Ook de PCS trip naar Berlijn organiseren vond ik erg leuk om met jou te doen. Robert, ik betwijfel of er zonder jou wel een goed functionerend lab in de PCS groep zou staan. Jouw technische inzicht en resultaatgerichte denken zorgen ervoor dat nieuwe apparatuur in no-time aan de praat is binnen de groep. Ook weet je altijd erg snel problemen bij apparatuur te verhelpen door op de juiste plekken te zoeken. Daarnaast ben je gewoon een ontzettend gezellige vent.

Als allerlaatste wil ik jou bedanken Guido. Vier jaar geleden ben ik als technisch natuurkundige jouw vakgroep binnengestapt, die verbonden is aan chemische technologie. Omdat ik op dat punt toch relatief ver van het veld afstond, was het voor ons beiden een gok wat de toekomst zou opleveren. Nu weet ik dat het voor mij één van de beste beslissingen in mijn leven is geweest. Sinds dag 1 heb ik me thuis gevoeld in het topic van fotokatalyse, en voor mijn gevoel heb ik de achterstallige kennis redelijk makkelijk kunnen overbruggen. Ook heb ik genoten van het onderdeel zijn van de vakgroep PCS. Dit alles heb jij toch maar mooi mogelijk gemaakt. Ik ken je niet anders dan iemand die keihard werkt, maar parallel toch altijd tijd probeert vrij te maken voor mensen die een (wetenschappelijk) probleem hebben. Ik heb altijd genoten van onze intensieve discussies, waarbij de tijd heel snel

voorbij vloog. Ook het promotietraject zelf is op die manier voorbij gevlogen. Nogmaals, hartstikke bedankt hiervoor!

Of course, there have also been people outside of the PCS group I have been collaborating with. Inside the University of Twente, I owe a big thank you to Aram, Igor and Frieder from the PCF group. The AFM studies described in Chapter 6 really have added value to this thesis. Also a big thank you goes to Johannes, Anne and Annette from the Fritz Haber Institute in Berlin. I had the pleasure to work for a few weeks at your institute, and afterwards we continued research on crystal facet engineering of WO_3 . The results are described in Chapter 4 in this thesis. From the FHI I would also like to thank Jasmin Allan for performing XRD measurements, Frank Girgsdies for his help in analyzing XRD patterns, Gisela Weinberg for making HR-SEM images and Maïke Hashagen for performing BET surface area measurements. Boudewijn, ik wil jou ook heel erg bedanken. Ik heb een redelijke tijd bij jou de deur platgelopen om ICP metingen te kunnen doen. Daar is uiteindelijk in de vorm van hoofdstuk 5 een erg mooi hoofdstuk uitgekomen. Rico, Mark en Gerard, ik geloof dat ik bijna een vaste klant was bij jullie TEM/SEM/XPS apparatuur. Jullie hulp en kennis hebben gigantisch geholpen met het tot stand brengen van dit proefschrift. Dank jullie wel daarvoor! Ook wil ik Erna en Tom bedanken voor hun hulp bij TGA metingen en Karin voor haar hulp bij BET surface area metingen. Lastly, I would like to thank the people in my graduation committee: Paolo Fornasiero, Annette Trunschke, Petra de Jongh, Gertjan Koster and Frieder Mugele. Thank you for making time to read my thesis and travel to Enschede for my defense.

Natuurlijk zijn er ook buiten mijn werk om mensen geweest die de laatste vier jaar bijgedragen hebben aan een succesvol promotietraject. Ook privé zijn vrienden en familie natuurlijk hartstikke belangrijk, en de mensen die op de één of andere manier bijgedragen hebben zou ik hier graag willen bedanken. Laat ik allereerst beginnen mijn paranimfen te bedanken: Josey en Tom. Josey, wij zijn al sinds 2008 enorm goede vrienden van elkaar, waar de vriendschap altijd centraal staat voor een hoop lol, onzin en heel veel films, maar ook voor serieuze zaken wanneer één van ons ergens mee in de maag zit. In 2014 heb ik getuige mogen zijn bij de bruiloft van jou en Manuela, waar je een fantastische partner aan hebt. Tom, ook met jou heb ik sinds 2008 een enorm sterke vriendschap, waarin bijzonder veel ruimte is voor complete onzin. Regelmatig stond je bij me voor de deur tijdens de PhD om koffie te drinken. Hoewel ik vaak erg druk was, waren de keren dat we koffie dronken altijd erg gezellig. Ook bij jou kan ik vaak mijn hart luchten over dingen (en andersom). Jelle en Jaco, ook jullie wil ik heel erg bedanken voor de erg goede vriendschap die we al

jaren hebben. Ik ken jullie al sinds mijn allereerste jaar op de universiteit. Met name onze passie voor muziek zorgt voor veel leuke muziekquizen. Hopelijk kunnen we er binnenkort weer eens eentje doen. Pim, Harmen en Carla, met jullie ging ik elke woensdag altijd lunchen, en af en toe pakten we ook wel eens een filmpje of gewoon een avondje ontspanning. Heerlijk, ik stel voor dat we dat erin houden. Pim, ik wil jou daarnaast ook nog bedanken voor je ideeën voor de cover van deze thesis: die hebben uiteindelijk enorm bijgedragen aan het verkrijgen van een leuke cover. Sean, Jesse en Jeffrey, ook met jullie ging ik wel eens gezellig daghappen; laten we dat ook op korte termijn weer eens een keer doen met Tom erbij. Joachim, hoewel je na Michel waarschijnlijk de persoon bent die het meeste zeurt dat ik meer bier zou moeten drinken, geniet ik altijd erg van de avonden waar ik met jou en Tom een biertje kan pakken. Ook mijn dispuut, Πίθηκος ἀμάρτανος, wil ik bedanken. Hoewel ik nog maar relatief weinig op de dispuutavonden ben geweest de afgelopen vier jaar, waren de avonden die ik wel ben geweest altijd erg gezellig en voelde ik me 100% thuis. Ook de weekenden weg met jullie zijn altijd erg gezellig.

Als laatste wil ik mijn ouders bedanken. Ik ken jullie niet anders dan heel warme, liefdevolle mensen, die altijd het beste voor hebben met anderen. Jullie bieden altijd steun wanneer dat nodig is en ook jullie interesse in mijn werk heb ik altijd enorm gewaardeerd. Dank jullie wel!

List of publications

Journal articles

- [1] Wenderich, K.; Klaassen, A.; Siretanu, I.; Mugele, F. and Mul, G.; *Sorption-determined deposition of platinum on well-defined platelike WO₃*. *Angewandte Chemie - International Edition* **2014**, 53, 12476-12479
- [2] Wenderich, K.; Noack, J.; Kärger, A.; Trunschke, A. and Mul, G.; *Phase transformations in citric acid-assisted hydrothermal growth of WO₃ and implications for photocatalytic performance*. Submitted to *Inorganic Chemistry*.
- [3] Wenderich, K.; Romão, J. S. and Mul, G.; *Principles, mechanism, and applications of photodeposition in (photo)catalysis: a review*. Accepted for submission in *Chemical Reviews*.
- [4] Wenderich, K.; Han, K. and Mul, G.; *Photodeposition mechanism of platinum on tungsten oxide and its corresponding stability upon aqueous phase illumination*. In preparation.
- [5] Wenderich, K. *et al.*; *Photocatalytic propane oxidation over platinum-loaded tungsten oxide nanoplates*. In preparation.
- [6] Amrollahi, R.; Wenderich, K. and Mul, G.; *Selective (photo)catalytic oxidation of ethanol to acetaldehyde by Pt/WO₃*. Submitted to *ACS Applied Materials & Interfaces*.

Oral presentations

- [1] Wenderich, K.; Klaassen, A.; Siretanu, I.; Mugele, F.; Mul, G.; *Towards understanding structure-directed photodeposition of Pt on WO₃ with well-defined facets*. Solar Fuels NRSC-C workshop, Utrecht, The Netherlands, **2014**
- [2] Wenderich, K.; Mul, G.; *Hydrothermal synthesis of hydrate-free cuboid-like monoclinic WO₃*. Presentation during guest research at the Reactivity Group of the Inorganic Chemistry Department at the Fritz-Haber-Institut der Max-Planck-Gesellschaft, Berlin, Germany, **2014**

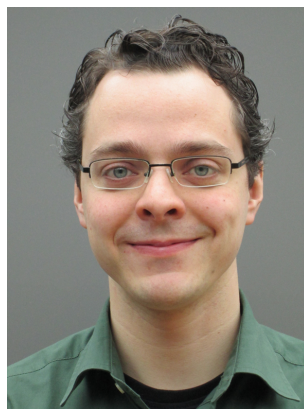
- [3] Wenderich, K.; Mul, G.; *Structure-directed photodeposition of Pt on WO₃ with well-defined facets*. Visit to the chair of Prof. Hermenegildo García at the Universidad Politécnica de Valencia, Valencia, Spain, **2014**
- [4] Wenderich, K.; Mul, G.; *Structure-directed photodeposition of Pt on WO₃ with well-defined facets*. International Conference on Surface Engineering (ICSE 2013), Busan, South-Korea, **2013**
- [5] Wenderich, K.; Mul, G.; *Steering electrons and holes in the right direction*. MESA+ day, Enschede, The Netherlands, **2013**
- [6] Wenderich, K.; Mul, G.; *Photodeposition of Pt on WO₃ with well-defined facets*. The Netherlands' Catalysis and Chemistry Conference (NCCC), Noordwijkerhout, The Netherlands, **2013**
- [7] Wenderich, K.; Mul, G.; *Steering electrons and holes in the right direction*. Solar Fuels Symposium, Eindhoven, The Netherlands, **2012**
- [8] Wenderich, K.; Mul, G.; *Steering electrons and holes in the right direction*. Recent developments in catalysis and energy science workshop, Berlin, Germany, **2012**

Poster presentations (first author only)

- [1] Wenderich, K.; Klaassen, A.; Siretanu, I.; Mugele, F.; Mul, G.; *Structure-directed, sorption-driven photodeposition of Pt on platelike WO₃*. 1st International Solar Fuels Conference (ISF-1), Uppsala, Sweden, **2015**
- [2] Wenderich, K.; Noack, J.; Kärger, A.; Trunschke, A.; Mul, G.; *In situ monitoring of hydrothermal growth of platelike WO₃*. ISF-1 Young, Uppsala, Sweden, **2015**
- [3] Wenderich, K.; Noack, J.; Kärger, A.; Trunschke, A.; Mul, G.; *In situ monitoring of hydrothermal growth of platelike WO₃*. The Netherlands' Catalysis and Chemistry Conference (NCCC), Noordwijkerhout, The Netherlands, **2015**
- [4] Wenderich, K.; Klaassen, A.; Siretanu, I.; Mugele, F.; Mul, G.; *Structure-directed photodeposition of Pt on WO₃: light- or adsorption-induced?* The Netherlands' Catalysis and Chemistry Conference (NCCC), Noordwijkerhout, The Netherlands, **2014**
- [5] Wenderich, K.; Mul, G.; *Photodeposition of Pt on well-defined cubic/plate-like WO₃*. Summer School 'Catalysis for Sustainability', Kerkrade, The Netherlands, **2013**

Curriculum Vitae

Kasper Wenderich was born on November 11th 1987 in Hengelo (Overijssel) in The Netherlands. He obtained his BSc degree in Applied Physics in 2009 at the University of Twente in Enschede, The Netherlands. At the same university, Kasper received in 2011 his MSc degree as well in Applied Physics (Optics & Biophysics track) in the Nanobiophysics Group. The title of his master thesis was *'Building of a single-emitter fluorescence excitation spectroscopy setup and testing its performance using verification samples'*. Afterwards, he started his PhD at the Photocatalytic Synthesis Group, also at the University of Twente. For four years, he has worked on the concepts of crystal facet engineering of tungsten oxide, photodeposition of platinum on commercial tungsten oxide and the structure-directed photodeposition of platinum on tungsten oxide. The research performed is described in this thesis.



PROPOSITIONS

accompanying the thesis

Photodeposition of platinum nanoparticles on well-defined tungsten oxide: controlling oxidation state, particle size and geometrical distribution

Kasper Wenderich

1. Studies on structure-directed photodeposition without verification of adsorption effects (*e.g.* by impregnation) are incomplete (Chapter 2 and 6).
2. Many researchers wrongly advocate that photodeposition results in doping of a material (Chapter 2).
3. Thermodynamic stabilities of crystal phases should be taken into account before drawing conclusions on the formation of the dominant crystal phase of a material (Chapter 3).
4. Chemical engineering is the art of creating and controlling desired chemicals. Applied physics is the art of making optimal use of the laws of nature. Chemical engineering and applied physics combined is the art of changing the world.
5. Slowing down slows down global warming.
6. Without wavelength variations life would be monotonous.
7. Reporting on successes will result in science evolution. Reporting on both successes and failures could unchain science revolution.
8. Supportive colleagues are significantly more important than equipment to achieve success in science.

STELLINGEN

behorende bij het proefschrift

Photodeposition of platinum nanoparticles on well-defined tungsten oxide: controlling oxidation state, particle size and geometrical distribution

Kasper Wenderich

1. Studies met betrekking tot structuurgerichte fotodepositie zonder verificatie van adsorptie-effecten (bijvoorbeeld door impregnatie) zijn incompleet (hoofdstuk 2 en 6).
2. Veel wetenschappers pleiten ten onrechte dat fotodepositie resulteert in het doteren van een materiaal (hoofdstuk 2).
3. Er moet rekening worden gehouden met de thermodynamische stabiliteit van kristalfases voordat conclusies getrokken kunnen worden over de formatie van de dominante kristalfase van een materiaal (hoofdstuk 3).
4. Chemische technologie is de kunst van het creëren en controleren van gewenste chemicaliën. Technische natuurkunde is de kunst van het optimaal gebruik maken van de natuurwetten. Chemische technologie en technische natuurkunde combineren is de kunst van het veranderen van de wereld.
5. Rustiger aan doen remt de opwarming van de aarde.
6. Zonder golflengtevariëaties zou het leven monotoon zijn.
7. Verslaggeving van successen resulteert in wetenschappelijke evolutie. Verslaggeving van zowel successen als mislukkingen kan wetenschappelijke revolutie ontketenen.
8. Behulpzame collega's zijn aanzienlijk belangrijker dan apparatuur om successen in wetenschap te behalen.

ISBN: 978-90-365-4058-2

